Reinforced Sintered Cancellous Bovine Bone as a Potential Bone Replacement Material

A thesis submitted in fulfilment of the requirements for the degree of Doctor of Philosophy at the University of Waikato

by
Dougal Frazer Laird

THE UNIVERSITY OF
WAIKATO
Te Whare Wānanga o Waikato

2010

Abstract

This research was undertaken in order to investigate the possibilities of transforming a widely available waste bone resource into a viable human bone replacement biomaterial. Large quantities of bovine bone are available as a resource in New Zealand due to the presence of an extensive meat industry. Cancellous bone was harvested from within the condyle regions of bovine femoral bone by cutting with either band saw or lapidary saw. Portions of cut cancellous bovine bone were significantly defatted and partially deproteinated through repeated autoclaving. The material was then sintered at 1000°C for 3 hours to give a pristine white sintered cancellous bovine bone (SCBB) material, that although weakened in comparison to its original form, retained the porous trabecular architecture of the original cancellous bone. This material was characterised by means of Fourier transform infrared (FT-IR) spectroscopy and powder X-ray diffraction (XRD), while also being subjected to a washing experiment in distilled water with pH monitoring to show that the material was hydroxyapatite (HAp) ($Ca_{10}(PO_4)_6(OH)_2$) with small quantities of CaO. Scanning Electron Microscopy (SEM) showed that the SCBB material had retained its macroporous architecture, with higher magnification micrographs revealing a microporosity with channels through crystallites of the HAp of approximately 500 – 700 nm in diameter.

Organic infiltrating solutions were prepared by dissolving chitosan in hydrochloric acid in addition to calcium phosphate, such as HAp or $CaHPO_4$, to act as a mineral reinforcing material. Due to the limited solubility of HAp, the maximum concentration that could be achieved involving a 50 : 50 w/w combination of chitosan and HAp was 6 g L^{-1} for both materials in ~ 0.1 mol L^{-1} HCl. ε-Polycaprolactone (PCL) dissolved in tetrahydrofuran (THF) was also trialled as an infiltrating solution, with concentrations up to 14 % w / v dissolved in the THF. Solutions were infiltrated into the porous SCBB material by means of vacuum, vacuum and pressure or a pressure only method. The extent of penetration of the infiltrate into the SCBB was

followed by labelling the chitosan molecule with the fluorophore, Fluorescein Isothiocyanate (FITC) and then examining the infiltrated SCBB by fluorescence microscopy. After infiltration into the SCBB material, chitosan and mineral reinforcing were precipitated by an increase in pH. Several methods for increasing solution pH were trialled, including; the addition of urea into the infiltrating solution with subsequent thermal hydrolysis, the catalysis of urea by urease, and treatment with ammonia gas. By products and excess ammonia were shown to be able to be removed from the infiltrated SCBB by repeated washing in water and buffer solution.

Mechanical testing on the infiltrated SCBB material was carried out by compression testing on an Instron materials testing instrument. Due to the inherent variability in the density and strength of the starting SCBB material, a statistical approach was required. Multiple samples were used and values for ultimate stress, modulus and a modified toughness measurement obtained from the mechanical testing for non-infiltrated SCBB samples were compared against infiltrated samples. SCBB samples infiltrated with a chitosan / $CaHPO_4$ infiltrate displayed an improvement in ultimate stress, while samples infiltrated with PCL showed an overall increase in modulus. Finally, biocompatibility of the SCBB samples infiltrated with chitosan based infiltrates was tested using L929 fibroblast cell culture testing and a Hen's Egg Test - Chorioallantoic Membrane (HET-CAM) test. Materials with low cytotoxic response were produced when sufficient washing and buffer treatment was employed after infiltration.

This research proved that SCBB could be successfully infiltrated with an organic / mineral composite matrix, which was capable of modifying the mechanical properties of the SCBB, while displaying positive biocompatibility potential.

Acknowledgements

Firstly, I would like to thank my supervisor, Dr. Michael Mucalo, for his support and patience during the course of this research. I am extremely grateful. I would also like to thank my co-supervisor Dr. George Dias at the University of Otago for his hospitality and help during the biocompatibility testing stage of this research. Likewise, I would like to thank my third supervisor, Professor Bill Henderson, for his useful research suggestions and appraisal of written work. In addition, I would like to thank Associate Professor Alan Langdon, Professor Brian Nicholson, Associate Professor Lyndsay Main and Associate Professor Merilyn Manley-Harris for help, ideas and encouragement during the course of this research. Furthermore, I would like to thank all of the staff in the chemistry department of the University of Waikato, including; Annie Barker, Jannine Rhodes, Pat Gread, Amu Upreti, Corry Decker, Jenny Stockdill, Steve Cameron and Jacqui MacKenzie. For the supply and initial preparation of the cancellous bone material, I would like to thank management and staff of the butchery department at New World Supermarket (Cambridge Road, Hamilton, New Zealand) as well as the management and staff of the butchery at Pak ' N ' Save (Mill Street, Hamilton, New Zealand). Finally, I would like to thank my family and friends for supporting me through this sometimes-challenging period. I would also like to thank Grant Mathieson for his demonstration as to why certain chemists should not be allowed access to scalpels and liquid nitrogen.

Table of Contents

List of Figures

List of Tables

List of Terms and Abbreviations

ACP	amorphous calcium phosphate
BHT	butylated hydroxytoluene
BSE	Bovine Spongiform Encephalitis
CAD	computer aided design
CAM	chorioallantoic membrane
CaP	calcium phosphate
DMF	dimethylformamide
DMSO	dimethyl sulfoxide
EDTA	ethylenediaminetetraacetic acid
EDX	energy-dispersive X-ray spectroscopy
FCS	Foetal Calf Serum
FITC	fluorescein isothiocyanate
FT-IR	Fourier transform infrared
HAp	hydroxyapatite
HET-CAM	Hen’s Egg Test - Chorioallantoic Membrane
HMDACS	hexamethylene 1,6-di(aminocarboxysulfonate)
IR	infrared
ISO	International Organization for Standardization
MEM	Minimum Essential Medium
Micro-CT	desktop X-ray micro-CT (computer tomography)
Micro-MRI	micro magnetic resonance imaging
PBS	phosphate buffered saline solution
PCL	polycaprolactone
PE	polyethylene
PGA	polyglycolide
PLA	polyactide
PMMA	poly(methyl methacrylate)
SCBB	sintered cancellous bovine bone

SEM	scanning electron micrograph (microscopy)
SEM-EPMA	scanning electron microscope-electron probe microanalysis
TBC	True Bone Ceramics
TCP	tricalcium phosphate
TEOS	tetraethyl orthosilicate
THF	tetrahydrofuran
UHMWPE	ultra high molecular weight polyethylene
UV – Vis	ultraviolet - visible
XRD	X-ray diffraction

CHAPTER ONE

1 Introduction

1.1 Use of bone replacement materials

The search for the optimum bone repair or replacement material has continued since Dreesman's early work in 1892 looking at the suitability of calcium sulfate (plaster of Paris) as a bone replacement material [1]. Subsequent to this, many advances have been made in bone replacement technology, however several key issues remain. One of those issues is availability; autograft implants, which are portions of bone taken from patients themselves (often from the ilium) are known as the 'gold standard' of bone replacement material within the medical profession, and accordingly provide excellent biocompatibility. In general, however there is little tissue redundancy within organisms, which limits the availability of such material. Therefore, access to autograft material is difficult, with its availability tending to be inversely proportional to its utility. Furthermore, morbidity at the site of removal is a known complication occurring in 10-25 % of cases, with patients who have undergone bone excision for transplantation at times reporting considerable and prolonged pain, displaying signs of nerve damage and suffering from infection at the site of removal [2-4]. In view of these facts, it is apparent that autografting is not a complete solution to satisfy the medical demand for bone replacement material.

The use of allografts is one solution to the problem of material availability. Allografts are harvested from another member of the same species (from people in this case) and are therefore in a more plentiful supply (e.g. they may be obtained from a "bone bank"). However, their use has the potential of introducing other complications, the most concerning of which is disease transfer [5]. In addition to this, the presence of

organic material in the form of protein or fat in allografts raises the possibility of eliciting antigenic immune responses after implantation into the host [5, 6]. A means of minimising such immunological problems is to use a synthetic material devoid of biological substance. Synthetic materials, for example ceramics, are relatively simple to manufacture, and due to modern processing techniques, can be manufactured to consistent chemical, physical and mechanical properties [7]. However, challenges remain in the ability to match precisely all properties particular to certain bone types found in specific body locations. There remain also some biocompatibility issues with the use of ceramics due to micro-structures and chemical compositions present in synthetic materials, that are foreign to biological systems [8].

An additional limitation associated with the production of a synthetic bone replacement material is the difficulty in developing a process, which allows the simultaneous creation of the required porosity, internal architecture, and micro topography in order to minimise the body's rejection processes and maximise bio-incorporation. These parameters must often be traded off against each other to obtain the best compromise in chemical, physical and mechanical properties. By contrast, material of biological origin has been fine-tuned through millions of years of evolution to exist and function in a biological environment, and accordingly tends to possess appropriate properties. Hence, it is advantageous to use such material where possible.

1.2 Sintered bone as bone replacement material

Sintered bone is a material that although no longer an example of functional tissue, maintains the trabecular architecture characteristic of bone matrix material. This inherent bone like structure represents a first step along the developmental path towards a successful bone replacement material. Sintered bone is composed predominantly of hydroxyapatite (HAp), which is a phase of calcium phosphate that studies have shown the body will accept and resorb [9]. There is some controversy over this assertion, with some authors reporting that osteoclasts (cells responsible for

the resorption of the mineral constituent of bone) are not capable of resorbing HAp (synthetic or from sintered bone), while other studies have shown the opposite to be true. Other studies have shown that physiochemical properties of the HAp such as grain size, sintering temperature and surface roughness are important variables in determining whether HAp is or is not bio-resorbable [10].

The mineral constituent in living bone tissue is a carbonated apatite, with the sintering process leading to a decomposition of the carbonate constituent to release $CO_{2(g)}$ and leave $CaO_{(s)}$ as a residue [11]. Barralet *et al*. observed a rapid loss of carbonate from synthetically produced 5.8 % wt carbonate apatites over 30 minutes of heating at 1000°C, despite the fact that samples were heated in an atmosphere of CO_2 [12]. Similarly, elemental analysis of the sintered bone produced by Foster showed a calcium to phosphorus mole ratio of 2.10 to 1.00, a finding, which in combination with the fact that the powdered material raised the pH of deionised water, led Foster to hypothesise that CaO had indeed been produced by the sintering process [13].

Sintered bovine bone has a porous architecture that allows the migration of cells into the centre of the material, a process that is expected to increase the rate of bone cell colonisation and implant resorption. The processes of bone formation on the surface of the material in this fashion is known as osteoconduction [14]. An *in vitro* study of a commercially available sintered bovine bone product, True Bone Ceramics (TBC), using osteoblast cells by Matsumoto *et al.*, showed the material promoted proliferation and differentiation of these bone cells [15]. Meanwhile, Minamide *et al.* performed an *in vivo* experiment showing that TBC was an effective bone replacement material, when used in spinal fusion operations on the vertebra of pigs. The authors used autologous bone that was harvested from the iliac crest as a comparison to the TBC, and the same operation performed on another group of pigs. A control was created on another group of animals, by surgically exposing the spine with subsequent surgical closure without implantation. After 3 and 6 months pigs were sacrificed and spinal fusion was shown through radiographic, histological and biomechanical testing to be successful on all pigs with the sintered bone or

autologous implant. The authors noted that the sintered bone material "adjusted" to the stiffness of the host bone, which they suggested was particularly important in spinal surgery, where other harder implants have been seen to "sink" into the host bone. This deleterious effect is particularly detrimental when patients suffer from bone weakening conditions such as osteoporosis. New bone matrix was seen to be growing into the pores of the sintered bone implant, and no growth of soft tissue between the sintered bone implant and existing bone was seen, indicating compatibility [16]. This study showed that sintered bone is both biocompatible and osteoconductive, as it is readily incorporated by the body displaying a natural tendency to assimilate.

1.3 New Zealand bovine bone as a resource

The New Zealand meat industry is one of the country's largest exporters. By-products from the slaughtering process make up 55 % of the weight of the animal, a quarter of which is bone. At present this material is utilised largely as a low added value fertiliser [17]. The potential exists for New Zealand bone to be considered as a raw material source for medical applications. New Zealand-sourced products also benefit from a favourable commercially-marketed image based on its perceived pristine environment. An additional advantage for New Zealand sourced bone is that as of yet, there have been no reported incidences of Bovine Spongiform Encephalitis (BSE) in New Zealand cattle populations [18]. This is important, as whenever material is transferred from animal to human for *in vivo* use, of primary concern is always the absolute elimination of any possibility of disease-transfer. With this in mind, the complete lack of BSE in New Zealand cattle populations represents a significant promotional advantage over bone from other regions such as Europe, America or Japan.

1.4 Previous work at the University of Waikato

Mucalo, Johnson and Foster [13, 17-20] at the University of Waikato, New Zealand have developed processing techniques to take raw cancellous bovine bone with an idea to producing biocompatible bone replacement material . Johnson was involved in the bulk of the early work that focused on converting waste bovine bone into a usable biomaterial. He stated that the desired characteristics of bone implants were that they should be biocompatible, osteoconductive, of defined strength and of a pristine white colour. Physical appearance was important in ensuring end user acceptance and approval for surgical application.

Johnson also noted that in order for an implant to promote osteoconduction it should possess pores to allow the migration of osteoclasts into the material, and that the matrix material with such characteristics was the cancellous bone located at either end of the bovine femoral shaft. The rounded prominences at either end of the bone are known collectively as condyles, and at one end is the femoral head where the femur attaches to the hip, and at the other end are the lateral and medial condyles forming the femoral component of the knee joint [21]. Both locations contain cancellous bone, but the bulk of the cancellous bone is found at the knee joint.

A sectioning method for harvesting cancellous bone was developed by Johnson, in which cancellous bone was cut away from the shaft of the femur by band saw as close as possible to the condyle. Two methods of removing cancellous bone from the condyles were trialled. One was to bore with a bench press drill, and the other was to use a band saw to cut 25 mm^2 thick sections through the condyle region containing cancellous bone. The bone was pre-frozen at -35°C which helped to prevent overheating and leaching of blood through the matrix, which was seen to occur when the bone thawed. This was also found to prevent heat-induced gelatinisation of proteinaceous material that tended to seal the pores.

Cut blocks were stored in the freezer at -30°C until required. Several physical and chemical methods were employed by Johnson in an attempt to de-fat and de-

proteinate the bone. A major processing step in most of these systems was to pressure cook the bone in water at 15 psi (above atmospheric pressure) in a standard household pressure cooker (autoclave). This removed a large portion of the fat and a significant portion of the protein and other organic matter from the bones. In work expanding on Johnson's, Foster introduced the step of sintering the autoclaved bone samples at 1000°C to remove all remaining structural (collagenous-based) organic material [13]. Although production of sintered bone in this or in a similar manner is not new worldwide, its production was to provide for this group a conceptual catalyst in taking sintered bone and reinforcing it with a non-proteinaceous material to yield a reinforced, guaranteed BSE-free bone replacement material.

1.5 Purpose and objectives

Bovine bone in New Zealand represents a massive resource of xenogeneic bone material available for human use. Bovine bone has been used directly or in modified form before as a xenograft with some success [4, 22-24]. In a simplified sense, bone is a micro / nano scale composite of calcium phosphate (hydroxyapatite) and protein. A normal constituent of this in all mammals is a protein known as a prion protein (PrP), which in rare cases may convert for unknown reasons to a misfolded variant called PrP^{Sc}. This is believed to be the infectious agent responsible for the transfer of the degenerative disease causing cell death in the brain of cattle with mad cow disease, or of patients with the human variant Creutzfeldt-Jakob Disease (vCJD). PrP^{Sc} itself is not believed to be the neurotoxic agent responsible for the death of cells, with the exact nature of the agent not yet known [25]. As an organic compound however, the activity of PrP^{Sc} can be degraded by heat, with temperatures between 160 – 200 °C being effective in achieving very high, but not complete, prion activity deactivation [26, 27]. In fact, a study on the effects of heat treatment on hamster scrapie agent (a prion) showed that this agent was still capable of transmitting disease after being heated to 600°C for 5 to 15 minutes, however at 1000°C no activity was detected [28]. Unmodified bovine bone has been used previously as a surgical implant in humans [29], but incorporation by the body appeared limited and the risk

of disease transfer would appear to mitigate any advantages. Regardless, a sintering temperature of 1000°C and time of 3 hours employed by Foster is sufficient to guarantee the complete destruction of PrP^{Sc} material if it were present in the bovine bone raw material.

However, a disadvantage of the sintering process is that there is a marked reduction in strength in the end material when compared to original bone. Discussions between Dr. Michael Mucalo and Dr. George Dias (from Otago University) led to the concept of utilising the natural porosity of sintered bone to infiltrate a reinforcing material into the sintered bone to mitigate this weakness. The concept was to use a non-proteinaceous material in order to eliminate the risk of disease transfer, such as cellulose derived from plants, or chitosan, a glucosamine polymer derived from the shells of marine organisms such as shrimp, crab and squid. This and successive discussions set the platform from which this present research was launched at the University of Waikato.

Therefore, the general aim of this project was:

- To examine the possibilities and limitations of infiltrating organic macromolecular compounds into sintered bone to yield a material with improved mechanical properties, while, at a minimum, maintaining the biocompatibility qualities inherent to sintered bone. The ultimate aim was to create a bio-implant that has superior mechanical properties and enhanced biocompatibility to that of unmodified sintered bone.

Progressive aims to accomplish the main goal were:

- To adapt and improve on the methodologies for the production of sintered cancellous bovine bone (SCBB) samples developed by Foster, to enable the generation of the number of samples required to satisfy the statistical requirements for mechanical testing on what are innately variable samples.

- To generate sintered bone samples of consistent physical dimensions appropriate for the purposes of infiltration and mechanical testing.
- To identify possible infiltrating materials that satisfied the following criteria:
    - Biocompatible and biodegradable *in vivo.*
    - Possessing a degree of mechanical strength.
    - Able to be solubilised or converted to a liquid (or a gas) facilitating transportation into the sintered bone matrix.
    - Able to be immobilised or cured within the sintered bone matrix without blocking the macropores, which are important to allow the inward migration of bone reforming cells.
- To examine existing infiltration techniques to ascertain what was physically and chemically possible with current methods, and from this develop techniques that could be applied to this project.
- Depending on the nature of the infiltrated material, to apply current knowledge or develop new knowledge, in order to achieve immobilisation of the infiltrate within the sintered bone material, while also ensuring the resultant material was free of toxic by-products in cases where these were generated during the infiltration or immobilisation processes.
- To develop mechanical testing methods to evaluate changes in the physical properties of the infiltrated sintered bone in comparison to the starting material, while simultaneously incorporating and accommodating for the natural variation inherent in the starting material.
- To test the biocompatibility of the infiltrated sintered bone samples using standard biocompatibility tests such as a cell culture cytotoxicity evaluation with L929 mouse fibroblast cells and a tissue irritation test such as the Hen's Egg Test – Chorioallantoic Membrane (HET-CAM)

CHAPTER TWO

2 Literature review

2.1 Introduction

Bone is a highly complex, specialised biological composite capable of adapting to the many and varied stresses imposed upon it by the body. In order to manufacture a substitute bone material with the level of adaptation in form to function presented in bone several features must be examined. Firstly, the basic structure of bone and processes responsible for the construction and maintenance of this structure should be examined, followed by the physical and mechanical properties resulting from such architecture. The composition and properties of sintered bovine bone must be investigated and then compared to those of natural bone. For comparison, an appraisal of the characteristics and limitations of the range of biomaterials already available on the market today should be made. After which, an examination of materials with the potential to act as infiltrates capable of enhancing the mechanical and biocompatibility properties of sintered bone should be made.

2.2 Bone

2.2.1 Structure and composition of human bone

The human skeleton is a complex array of individual bones each with its own particular structure and composition depending on its specific form and function. These bones are subcategorised according to their respective shapes, denoted with terms such as “long bones”, “short bones”, “flat bones” and “irregular bones” [21]. Irrespective of outward appearance, every bone consists in varying proportions, of two basic osseous tissue types, cortical bone and cancellous bone. Comprising 80 %

of the bone tissue in the human body, cortical bone is a dense, highly mineralised [30] form of bone located on the surface of a complete bone, where it serves a biomechanical, structural, and protective role. By contrast, cancellous bone is macroscopically porous consisting of an interconnected array of rods or curved plates, and while also serving a structural role like cortical bone (but within the middle of the bone), its main function revolves around mineral homeostasis [31].

Solid bone material is a composite predominantly of hydroxyapatite (HAp) and collagen, with HAp comprising *ca.* two-thirds by weight of the bone and collagen fibre making up *ca.* one-third by weight. In fact, it is more accurate to say that the mineral component of human bone is "carbonated hydroxyapatite" because of the tendency of CO_3^{2-} to substitute for OH^- and PO_4^{3-}, with the existence of hydroxyl groups being possible theoretically but difficult to detect [32]. Carbonate increases the solubility of the apatite crystal [33], with levels in the crystal lattice commonly between 2 and 7.4 wt %, the variation of which is largely dependent on age [34, 35]. Although collagen is extremely strong under tensile stress, under compression it collapses and yields. However, with the addition of the hard but brittle HAp crystals, which nucleate and grow on the collagen framework, an extremely strong, slightly flexible, and shatter resistant material, comparable and often superior to the best synthetic materials results [21].

2.2.2 Cellular processes within bone – laying down of new bone and resorption

Far from a being a simple composite of protein and mineral, bone is a living tissue containing living cells fed by a vascular system. There are four cell types found within bone of which the mature bone cell (the osteocyte) predominates. Osteocytes exist within cavities known as lacunae surrounded by bone matrix, with narrow passageways called canaliculi allowing the passage of cytoplasmic extensions between adjacent cells, which in turn facilitate the transfer of nutrients and hormones from cell to cell. Osteoblasts, originally produced from osteoprogenitor stem cells, are immature osteocytes that produce new bone matrix. In the initial stages of bone

formation, osteoblasts secrete the unmineralized protein constituent of the bone matrix to from what is known as the osteoid. The formation of this matrix precedes mineralization by approximately 15 days at which time the osteoblasts induce mineralisation by elevating local concentrations of calcium and phosphate to the point of precipitation. When the osteoblast is completely surrounded by new bone matrix it has matured into an osteocyte. In cortical bone, osteocyte orientation and bone deposition processes lead to the formation of concentric lamellae of bone tissue surrounding a central vascular canal known as the Haversian canal, all of which is collectively referred to as an osteon. The fourth cell type in bone is the osteoclast, whose origin is completely independent of the other three cell forms, being derived from circulating macrophages. The osteoclast is a multinucleated giant cell which secretes acids and proteolytic enzymes capable of breaking down and dissolving bone mineral and protein respectively [21, 31].

2.2.3 Physical and mechanical properties of bone

Bone is a dynamic, adaptable tissue whose mechanical properties are dependent upon the environment in which it finds itself. A human femur can withstand forces up to 10-15 times greater than those exerted by body weight, so long as those forces are applied along the shaft of the bone [21]. This uniaxial strength is due to the parallel alignment of osteons along the principal weight bearing axis within the shaft of the femur bone. Fracture occurs with less force, when that force is applied perpendicular to the alignment of osteons rather than parallel. This property is termed anisotropy, and is the response of bone to the disparity of axial stresses placed upon it within its environment, which is both an evolutionary and “real time” adaptation. The term “real time” is used because bone responds to stresses by building more bone in areas of increased stress; for example, body builders will show increased bone mass, in comparison with the general population due to the increased stress they place on their bones. This is particularly evident in the bony ridges where muscles connect to bone [21].

Elastic modulus is a measure of a material's stiffness, with human cortical bone showing values up to 17.4 GPa in the longitudinal direction. As another illustration of bone's anisotropy, elastic modulus values in the transverse direction exhibit lower values in the region of 9.6 GPa. As a means of comparison, respective bovine values for the same parameters have been measured as 20.4 and 11.7 GPa. A means of measuring elastic moduli microscopically across the surface of osteons was developed by Ascenzi and Bonucci, who accomplished this by cutting cylinders of osteons and applying dead loads while measuring the deformation by means of a microwave extensometer. Hardness measurements have also been made on cortical bone with different authors reporting values varying from 0.285 GPa to 0.614 GPa for tests carried out on osteon material [30].

The mechanical properties of cancellous bone can be difficult to measure accurately and reproducibly, due to the inherent variability in structure and density. However, several strategies have been employed to accommodate this variability. In one technique, individual trabeculae, which are the fine bony struts or beams forming the porous structure of cancellous bone, were extracted from cancellous bone and subjected to uniaxial stress to induce buckling. With the aid of the Euler equation, which describes the elastic buckling of a beam, and at the same time incorporating geometric variables of the trabeculae, an average modulus of 11 GPa was calculated. Some micro-tensile tests on individual trabeculae have also yielded similar modulus values, although other tests have shown values an order of magnitude lower than 11 GPa. This observation emphasises the difficulty in obtaining consistent values between studies on cancellous matrices [30].

Micro-bending experiments, which can be conducted as three point or four point bending experiments, on single trabecula tended to yield lower modulus values (i.e. 5-8 GPa) than that reported in the above research. However, when the same bending methods were employed on cortical bone, values 20-30 % lower for cancellous bone in comparison to that cortical bone were consistently obtained [30]. This result showed reproducibility within this experimental method, if not a consistency with other experimental data.

The advent of advanced 3D imaging techniques, such as micro-CT and micro-MRI, has enabled the non-destructive imaging of the intricate structure of cancellous bone [36]. This phenomenon, along with the expansion of computing power, has led to the development of complex structural modelling on cancellous bone, which can elucidate the relationship between internal architecture and physical properties [37-39]. A Finite Element-Model may be built up from a scan incorporating complex parameters such as bone volume fraction, anisotropy and connectivity. Comparison of theoretical and empirically obtained data for the modulus of cancellous bone showed r^2 values of 0.89, with modulus values averaging around 6 GPa [30].

Rather than testing the properties of bone within specific highly localised areas, it is often simpler to test the bulk properties of bone, such as strength, toughness or elastic modulus, under either tension or compressive loading. However, because of bone's underlying heterogeneity, data are likely to show large degrees of variation even when taken from ostensibly similar samples. Tensile testing on bone generally involves pre-test machining in order to generate samples of a classic "dog bone" shape, which facilitates gripping by the instrument at either end and presents a thinner section of bone between the points of contact that is subjected to the highest degree of strain. Compared to cancellous bone, cortical bone is a better candidate for this method of testing, because of its relatively homogeneous microstructure which allows the production of small consistent samples. By contrast, cancellous bone samples must be produced with a diameter of at least 5 mm to ensure that sample-created artefacts are not introduced [40].

If undertaken meticulously, tension testing can yield very accurate data in the mechanical testing of bone. However, sample preparation is vital to achieving quality data, a requirement that can be both technically challenging and time consuming. Compression testing by comparison can be carried out on easy to produce shapes of cancellous of bone such as cylinders. The ultimate stress (force / area) is a measure of the maximum stress a sample can withstand before failure, with values for human cancellous bone derived from compression testing varying depending on bone

location and age of the person. Average ultimate stress values for human vertebral cancellous bone have been shown to decline approximately linearly ($r^2 = 0.66$) from *ca.* 4 MPa at the age of 20 to below 1 MPa at 80 years. As an illustration of the contrast in mechanical properties between bones from different locations, the data corresponding to human proximal femoral cancellous bone, show an approximate linear relationship ($r^2 = 0.51$) of ultimate stress from *ca.* 13 MPa at 20 years to *ca.* 6 MPa at 80 years [41].

2.3 Sintered bone, calcium phosphate and hydroxyapatite

As mentioned in section 1.2, the major chemical constituent of sintered bone is hydroxyapatite, which is a phase of calcium phosphate and has the generalised formula $Ca_5(PO_4)_3X$. The formula is often presented with each stoichiometric value doubled to give $Ca_{10}(PO_4)_6X_2$, to denote the unit cell, with X representing anions such as F^-, Cl^-, or OH^- to yield fluorapatite, chlorapatite and hydroxyapatite respectively [42]. These apatite phases themselves belong to a wide range of calcium phosphate phases, many of which are formed and then transformed during bio-mineralisation processes, and are intricately linked through a series of complex reactions controlled by solubility, pH, along with kinetic and thermodynamic considerations [43].

2.3.1 Hydroxyapatite, other important calcium phosphate phases

The term apatite was conceived by mineralogist Werner in the 18th century and is derived from the Greek “apato” which means, “to deceive”; a reference to the frequency with which the mineral was confused with other minerals in earlier times [42]. As the most thermodynamically stable phase of calcium phosphate, hydroxyapatite is often the end result of several complex intermediary reactions involving precipitation and redissolution of various precursor calcium phosphate phases. Hydroxyapatite readily undergoes ion substitution reactions in which cations and anions may replace calcium and phosphate ions respectively in the crystal lattice,

with examples being, Pb^{2+}, Sr^{2+} or Ba^{2+} displacing Ca^{2+} and CO_3^{2-} displacing PO_4^{3-}. Properties of substitutional lability and facility of phase interconversion in the apatite family leads to a highly complex assortment of compounds [42].

Another calcium phosphate phase particularly relevant to biological systems is octacalcium phosphate ($Ca_8H_2(PO_4)_6.5H_2O$). This phase has a very similar crystal structure to hydroxyapatite and accordingly is often seen as a transient intermediate solid phase before the formation of the more thermodynamically stable hydroxyapatite [42]. Tricalcium phosphate (TCP) ($Ca_3(PO_4)_2$) is a phase that exists in several different structural phases (α, β, and γ) and its chemistry is complex, being particularly dependent on reaction conditions. Brushite ($CaHPO_4.2H_2O$) is yet another phase that has been identified as a precursor phase to hydroxyapatite. Amorphous calcium phosphate (ACP) is an important biological phase as it is the first transient precursor phase to form in precipitation reactions from aqueous solutions and ultimately transforms to apatitic phases. Ca / P molar ratios of ACP were initially thought to be invariably 1.5, but subsequent research has produced ACP compounds with molar ratios over a range of 1.33-1.53 [42].

2.3.2 Sintered cancellous bone structure and anisotropy

As stated in section 1.2, sintered cancellous bone maintains a natural trabecular architecture closely resembling that of the bone from which it was produced. The sintering process leads to the removal of organic material, and a fusing of the inorganic constituent into organised crystals of bone mineral, but the interconnecting macroporous structure is preserved [9, 11, 44]. This porosity is important, because although hydroxyapatite has excellent biocompatibility and osteoconductive properties, it is not readily resorbed in a biological system. It has been shown that in a synthetic hydroxyapatite ceramic bone replacement implant with inadequate porosity or inappropriate structure, bioincorporation processes may not progress rapidly enough to yield the homogenous incorporation of the implant into the living bone tissue [45]. It is the inherent bone-like architecture of sintered bone that is believed to be a major factor in its capacity to accommodate vascularisation and the formation of

new bone [44, 46]. However, as Bignon *et al.* explain for artificially created HAp and β-TCP bone substitutes, there is always a trade off between increased porosity, which promotes positive cellular response (macroporosity promotes cell ingression and microporosity facilitates cell adhesion), against mechanical strength [47].

2.3.3 Sintered bone as a bone replacement material; properties *in vivo*

Sintered cancellous bovine bone (SCBB) has been shown to perform its function as a bone replacement material well. As an illustration of this, Taniguchi *et al.* used SCBB, produced according to a method initially developed by Ueno *et al.* (1983), as filler for voids created after the excision of benign tumours in the hand [48]. According to Taniguchi *et al.*, Ueno *et al.* named this material True Bone Ceramics (TBC) as an allusion to the material's bone like structure and ceramic nature. The preparation of this sintered bone involved boiling raw bone for 10 hours, treatment with 1 % H_2O_2/ 1 % NaOH, neutralisation with 1N HCl and then sintering in a stepwise process, with prolonged heating at 600°C for 3 to 5 hours, followed by a 3 hour ramp to 1100°C and holding it at that temperature for 3 hours. 22 patients ranging in age from 9 to 59 had TBC material surgically implanted at the site of tumour removal. No post surgical complications such as infection or fracture were observed. Furthermore, any clinical symptoms such as discomfort, swelling, or restrictive movement in the joints adjacent to affected fingers were not reported. X-ray analysis after 3 months showed the formation of new bone, and after 6 months, incorporation of bone into the implant appeared to be complete, with X-ray-translucent lines of differentiation between implant and bone not detectable [48].

With the goal to investigate the biocompatibility of sintered bone on a more cellular level, an immunohistochemical study was undertaken by Hashizume *et al.* using TBC implanted in the femur of Japanese white rabbits. The implant and surrounding tissue was harvested postoperatively at 1, 2, 3, 4, 6, 8, 12, 24 and 48 weeks, with sub samples being decalcified in order to examine the organic extracellular matrix that had formed while the implant was *in vivo*. After 1 week the pores of the implant material were seen to contain red blood cells and granulation tissue (blood vessels

and fibroblasts). The make up of the extracellular matrix within the implant up to two weeks post surgery was found to contain collagen types I and III, with type I becoming predominant at week three and exclusive thereafter. As osteoblasts produce multiple collagen types before maturity and solely type I at maturity, this was taken as positive indication that cells were maturing within the implant [44].

In addition to collagen I and III, fibronectin was detected after the first week of implantation. Fibronectin is a protein which is known to be involved in cell attachment processes and stromal cell differentiation. After initially being deposited as a fine network throughout the pores of the implant material, fibronectin was adsorbed onto the surface of the TBC material and continued to be adsorbed over subsequent weeks. Other sub samples were left with the mineral constituent intact in order to measure calcium and phosphorus levels across the sample by scanning electron microscope-electron probe microanalysis (SEM-EPMA). High concentrations of Ca and P were seen at the implant / bone interface, which is believed to be necessary for the formation of a strong bond between implant and the adjacent bone. Conversely, fibrous tissue was not seen at the interface between implant and bone tissue, which was another positive indication of compatibility. In the course of the report the authors made reference to the work of Kurihara *et al.* who used osteoblasts with calcifying capacity and tested materials against these cells looking for degrees of cytophilicity (having an affinity for cells) and calcification. Kurihara *et al.* concluded that the "detailed surface structure" of TBC offered a superior substrate for cell adhesion, differentiation and proliferation to that of synthetic hydroxyapatite and tricalcium phosphate. Ultimately, Hashizume *et al.* themselves concluded that TBC possessed the bioactivity required to allow the generation of new bone within the pores of the TBC material when implanted into a bone defect [44].

Other bovine bone derived inorganic material has also been shown to give positive results upon implantation. Baslé *et al.* reported that a bovine derived hydroxyapatite (BONAP) promoted greater osteo-regeneration in rabbits over a period of two weeks

than a 40 % TCP : 60 % HAp synthetic mix [49]. This finding was somewhat mirrored by Artzi *et al.*, who reported that the "inorganic bovine bone" Bio-Oss (Geistlich Biomaterials, Switzerland) showed greater osteoconductivity and took longer to resorb than β-TCP in a canine model [50].

Ultimately, there is still debate as to whether sintered bone represents a resorbable implant material. Variations in results exist with some researchers reporting remnants of implanted material remaining for years, while others studies show degradation by osteoclast activity. This discrepancy may in part be due to differences in the animal models (pig versus dog for example), and also the locations in which the materials were implanted. There is compelling evidence that areas subjected to high mechanical forces (for example, locations in the mandible), which tend to be areas of high bone remodelling, are regions conducive to sintered bone resorption [51].

2.4 Implant materials and reinforcing materials

For an exogenous material implanted into a living organism to be successful it must possess properties allowing it to resist or deflect specifically evolved physiological mechanisms to remove exogenous material from the body. According to Hench and Wilson (1993), there are four general tissue responses to an implant material. In the worst case, the implant is toxic, often due to the leaching of substances from within the material into the surrounding tissues, which have a toxicological effect on these tissues, and which can spread via the vascular system throughout the entire body causing systemic damage. Alternatively, the implant can be biologically inert, in which case there is no tissue damage, but in response to the presence of the implant, the body forms a non-adherent fibrous capsule around the implant partitioning it off from the rest of body [8], see section 2.5.1.

A bioactive implant however has the capacity to interact biologically with the surrounding tissue to form bonds mimicking interactions that occur between purely biological tissues. These interface regions are dynamic and are continually reformed

as are those found between adjacent biological tissues. Finally, there are implants that are sufficiently soluble to be dissolved in body fluids, or they may be broken down by enzymatic processes or digested by macrophage activity to be incorporated fully into the biological processes of the host. The success of this type of implant therefore is not only conditional of the low toxicity of the original material, but also on its metabolites [8].

2.5 Host reactions to common biomaterials

2.5.1 Generalized host reactions to biomaterials

The implantation of a biomaterial into a host is invariably accompanied by a damaging of the surrounding tissue, which in combination with subsequent foreign body reactions, leads to a highly complicated series of biological processes. In order to examine all possible processes, the following account describes the series of events that transpire following the implantation of a non-resorbable foreign body into a host. Implants that are absorbed and/or biodegraded rapidly, or have specific reactivities complementary to the host's biological processes, may respond differently [52]. Additionally, it should be noted that these responses do not necessarily occur in a strictly chronological order but often overlap.

Immediately following the injury caused by implantation, blood flows into the affected area leading to an interaction between the implant material and blood. The blood, fluid and protein that fill the space created by the introduction of the biomaterial form what is known as the provisional matrix. This consists of fibrin (a protein responsible for the coagulation of blood), activated platelets, inflammatory cells and endothelial cells [52]. Provisional matrix formation is generally complete in minutes or hours, depending on the site of implantation, after introduction of the biomaterial. The aforementioned process represents the onset of the inflammatory response, which is followed by the acute inflammatory phase that can last for minutes, hours or days, and is characterised by the migration of neutrophils and other white cells (leukocytes) to the site of implantation. The purpose of this influx of

neutrophils and macrophages is the phagocytosis of micro-organisms and foreign materials, a process that is usually thwarted by the unfavourable size disparity between leukocyte and biomaterial. This can lead to "frustrated phagocytosis" whereby the failed engulfment of the biomaterial leads to the release of leukocyte products, such as enzymes designed to break down the material. It has been shown that when a foreign material is identified as phagocytosable by the body the amount of enzyme released is dependent on the size of the foreign material, with larger particulates eliciting a greater quantity of enzyme. However, if the material is in a non-phagocytosable form such as in a film the inflammatory response may be completely different. Typically, the acute inflammatory phase does not last for more than one week [52].

Commonly, a chronic phase of inflammation follows the acute phase, which tends to show greater histological variation than the acute phase. A proliferation of blood vessels and connective tissues are characteristic of the chronic inflammatory phase, as well as the presence of macrophages, monocytes (large single nucleus white blood cells) and lymphocytes (B-cells, T-cells, amongst others). In addition to the physical and chemical properties of the biomaterial, infection or physical movement of the biomaterial can lead to chronic inflammation. However, if the biomaterial is well accepted, this chronic phase is generally short-lived [52].

Wound healing processes initiate the formation of granulation tissue within 1 day of biomaterial implantation. So named because of its soft granular appearance, this tissue is the result of the proliferation of fibroblasts and vascular endothelial cells, and accordingly is characterised histologically by the evidence of fibroblasts and of the proliferation of new blood vessels. The fibroblasts are active in synthesizing collagen and proteoglycans which can ultimately lead to the formation of a fibrous capsule. It is possible during the previous phases to see also a foreign-body reaction in which monocytes and macrophages fuse to form foreign-body giant cells, in an attempt to phagocytose the implant material. Ultimately, foreign-body giant cells along with macrophages may be seen on the surface of the implant material during its

entire life. However, a fibrous capsule is usually laid down over the surface separating the foreign-body reaction from the surrounding tissue. With or without a foreign-body response, the usual end process of wound healing around a biomaterial is the formation of a fibrous capsule [52].

2.5.2 Selected biomaterial material properties and specific host reactions

Metals

There is a range of material types that are used as biomaterials each suited to specific purposes and each with their own advantages and disadvantages. Metals have been used for a wide range of purposes including intricate devices such as vascular stents and catheter guide wires, but more so in structural support systems within orthopaedics and dentistry. This can be on a smaller scale, such as in the form of wires, plates and screws [53], or as complete joint replacement systems such as in total hip and knee replacements [54]. Metals excel in this role because of their excellent structural properties. When employed as a biomaterial, metals are normally combined as alloys, because most elemental metals have poor anticorrosion properties. Stainless steels with levels of chromium, nickel and molybdenum have superior corrosion resistance over the earlier developed vanadium steels which are no longer used. Cobalt / chromium alloys have excellent corrosion resistance, with strength properties able to be customised by adjusting manufacturing processing and the addition of supplementary alloy metals such as nickel and molybdenum. However, problems can arise due to wear and/or corrosion with the release of toxic metal ions or toxic particulates into the body, raising concerns over the long term biocompatibility of some metal implants [53]. Conversely, titanium and titanium alloys (often with aluminium) have high strength and are lightweight, while also forming a highly thermodynamically stable and biologically compatible TiO_2 surface layer between implant and surrounding tissue [55].

Polymeric compounds

Polymeric materials represent a completely different class of materials from metals, with a wide variation of physical and chemical properties, and a corresponding wide range of functions for which they can be employed. Polymethylmethacrylate has very good biocompatibility characteristics, and has been used extensively in biomedical applications such as cement in joint prostheses, in contact lenses and implantable ocular lenses amongst others. Polyethylene exists in several different forms with straight chained or branched molecular structures, which are generally classified by their density. Ultra High Molecular Weight Polyethylene (UHMWPE) has sufficient strength and appropriate wear characteristics to be used for orthopaedic load bearing applications such as acetabular cup (socket of the hipbone that receives the head of the femur) [56]. Nevertheless, wear particles are seen to detach from such implants, to be subsequently phagocytised and to be taken into the lysomes within cells such as neutrophils, monocytes and macrophages [57]. In some cases, an implant will in this way cause death to such inflammatory cells, with the subsequent release of lysosomal enzymes causing destruction to surrounding tissue. A means of overcoming this problem is the use of a biodegradable polymer such as polylactide (PLA) [58], polyglycolide (PGA) [59] or polycaprolactone (PCL) amongst several others. PLA is a polyester that degrades *in vivo* through a non-specific hydrolysis reaction at the ester bond to yield the metabolically familiar lactic acid produced during anaerobic activity. Although also a polyester, PGA by contrast degrades through a combination of a non-specific hydrolysis reaction and an enzymatic cleaving of the ester bond to form glycolic acid which is metabolised or directly excreted from the body [56].

The initial interaction between host blood, body fluids, tissue and the biomaterial surface itself appears to be fundamental to determining the ultimate success of the implant. Research involving polymeric biomaterials has centred on altering the surface chemistry or physical properties of the surface, often as a gradient across an area of a material, and then evaluating how biological molecules, cells or tissue interact. A chemogradient can be created on a polymer surface by progressive oxidation across a polymer's surface, leading to the prevalence of particular

functional groups at different locations. In turn, this affects the wettability of the material surface, which has been shown to influence the adsorption of serum proteins such as fibronectin and vitronectin. Cell culture evidence shows that cells such as fibroblasts and endothelial cells exhibit maximal adherence, growth and migration behaviours on areas corresponding to the similar wettability [56]. For example, Lee *et al.* demonstrated with a low density polyethylene (PE) oxidised to give a chemogradient, that the maximum protein adsorption, cell adhesion and cell growth for Chinese hamster ovary, fibroblast, and endothelial cells occurred at a water contact angle of ca. 60°, when presented a surface ranging from ca. 40 – 90° [60].

Ceramics

Due to their strong ionic bonding ceramic materials tend to exhibit high strength and hardness, but low ductility. Ionic bonds are non-directional in nature and require high energy to break, so they generally show a high degree of chemical insolubility and resistance to mechanical wear [57]. Ceramic biomaterials may be categorised as either biologically inert or active in nature depending on their interaction with the host. Aluminium oxide (alumina, Al_2O_3) and zirconium dioxide (zirconia, ZrO_2) are examples of ceramics that are bioinert, as illustrated by their lack of bonding reaction when placed in contact with bone. Both alumina and zirconia exhibit high strength, stability and high wear resistance, which makes them ideal for a range of surgical and dental load bearing applications, in particular hip joint replacement balls [61].

In contrast to bioinert ceramics, bioactive ceramics show properties such as the capacity to bond with bone and being able to degrade *in vivo*. In fact, degradation is considered to be an important prerequisite for bone bonding, and is recognised as occurring in two ways, either as a solid/liquid dissolution process, or as a function of cell processes, for example, phagocytosis. HAp and TCP are classic examples of bioactive ceramics both showing good biocompatibility, however only TCP has been shown consistently to degrade by processes of dissolution *in vivo*, a difference that may be attributed to the differences in solubility as shown by their respective pK_{sp} values of ca. 30 for TCP and ca. 120 for HAp. *In vitro* cell culture studies have shown

that human bone cells are capable of ingesting both TCP and HAp granules, and that osteoclasts are capable of dissolving HAp, but *in vivo* studies on the degradation of HAp have shown large variations in results. The results of one study indicated that the biodegradability of marine coral derived HAp was dependent on the site of implantation, with material implanted in the high load-bearing region of the mandible showing significant levels of degradation, when compared to material implanted in cortical bone of the radius, and cancellous bone of the tibia. Authors of another study involving highly porous HAp reported that it was mechanical collapse and cellular ingestion of fine particles released from the surface of the material that facilitated degradation. Highlighting the variation in HAp degradation, another study resulted in a porous HAp implant showing no degradation after 3.5 years [62]. From this collection of research, it would appear that common favourable features promoting the degradation of HAp are high porosity, and the capacity of the material to degrade as fine particles.

2.6 Potential organic infiltrating materials for sintered bone

To be a suitable candidate as a reinforcing material certain property characteristics were preferable. A material needed to be readily available and preferably comparatively cheap in order to complement the advantage of the SCBB with its ready supply and relative inexpensive. In addition to being biocompatible and biodegradable, the material had to be soluble, so that it could be delivered into the interior of the SCBB material. Both of the following described materials meet these criteria, with the exception of ε-polycaprolactone (PCL) in regard to expense [63].

2.6.1 *ε*-Polycaprolactone (PCL)

PCL is a linear aliphatic polyester commonly manufactured by the ring opening polymerisation reaction of ε-caprolactone under the influence of heat and a catalyst such as stannous octanoate, as shown in Figure 2-1 opposite [64]. The PCL polymer

molecules pack together to form a thermoplastic (liquid at higher temperatures cooling to a solid) with a relatively low melting temperature ca. 60°C and a low glass transition (T_g) temperature of -60°C [65]. In addition, the polymer is ductile, possessing moderate strength (ca. 15 MPa – tensile strength) and low Young's modulus (ca. 335 MPa) [66, 67]. The strength value is similar to that seen in bone but the Young's modulus value is approximately ¼ of that seen in many human bone samples. Research has been carried out to investigate combining PCL with inorganic solids to produce composite materials with improved mechanical properties. Calandrelli *et al.* manufactured PCL and HAp composites of up to 20 % HAp by premixing the materials and then screw extruding at 100°C. Ultimate stresses of up 35 MPa were achieved with 10 : 90 HAp to PCL samples, and Young's Modulus values of up to 479 MPa were achieved with 20 : 80 HAp to PCL samples. Biocompatibility testing of the composites showed positive results with superior cell adhesion and proliferation responses to that of pure PCL [67]. Although not intended for biological use, Kai *et al.* showed in a similar manner that graphite oxide could be combined with PCL to yield materials of higher tensile yield stress and Young's modulus values [66].

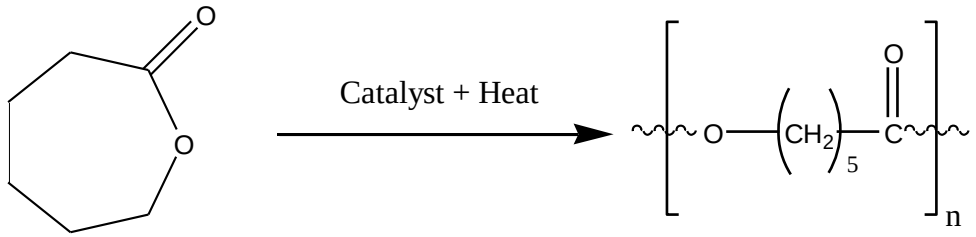

ε-Caprolactone PolyCaprolactone

Figure 2-1 – Basic reaction scheme of the polymerisation of *ε*-caprolactone to polycaprolactone.

General biodegradability has been confirmed in PCL by fungal and soil burial studies with some microorganisms even being capable of utilizing PCL as a food supply [68]. Specific *in vivo* biodegradability of PCL has been confirmed using isotope labelling experiments with carbon-14 and tritium showing that sub-dermally implanted PCL was degraded, and removed from the body to yield only ε-hydroxycaproic acid and water [64]. Initial *in vivo* degradation is comparatively slow for molecular weights

above ~ Mw 5000 with Sun *et al.* showing a designed PCL drug release implant still present in rats after 2 years. By contrast, with low molecular weight tritium-labelled PCL (~ Mw 3000) implanted subcutaneously, an accumulative 92 % of the radioactive tracer was seen to be excreted after 135 days [69].

The reason for PCL's biodegradability is the susceptibility of the ester bond to undergo hydrolytic scission in aqueous media, and as a result, degradation is seen to occur both in biological systems as well as simple aqueous systems. Furthermore, the reaction is autocatalytic with the cleavage of each ester bond producing chain terminal carboxylic acid groups capable of catalysing additional hydrolysis reactions. The initial mode of degradation involves preferential scission of polymer chains in regions of greater amorphousness, causing an overall increase in crystallinity as newly formed shorter polymer chains recrystallise. Gradually, smaller polymer particles or oligomers break away and diffuse out of the bulk material, a process that eventually leads to the complete breakdown of the material. *In vivo*, the basic degradation process described above is accompanied by a concomitant "surface erosion" process caused by enzymatically enhanced ester bond hydrolysis [64, 65]. In an experiment confirming the activity of biologically available enzymes on PCL, Chen *et al.* reported an increase in degradation rate for particles of PCL (ca. 13.4 μm diameter) in the presence of lipase in pH 7.4 phosphate buffered saline solution (PBS) over that of PBS alone. After 5 weeks a 24 % decrease in molecular weight was noted for particles in the presence of lipase and 11 % for particles in without lipase [70].

Interest has been shown in using PCL as a craniofacial bone substitute material by Gough *et al.* with encouraging results seen in cell culture tests using human craniofacial osteoblasts. The polymer was prepared using a cationic polymerisation reaction using a boron trifluoride catalyst and a post-treatment designed at reducing residual catalyst. The nature of the polymerisation reaction also allowed greater control over molecular weight, which in turn allowed a greater control of rate of biodegradation. Cells were seen to attach and proliferate on the surface of the PCL material, with Collagen-I production being observed from 5 days up until the end of

the experiment at 28 days. Additionally, mineralization of the extracellular matrix due to osteoblast activity was seen to occur, leading to the conclusion that PCL has potential as a craniofacial implant.

If PCL were to be infiltrated into sintered bone, whose architecture includes both macro and micro porous HAp structures, one can visualise the resultant combination as a composite between PCL and HAp similar in concept to some of the materials outlined above. Therefore, the potential exists for a synergistic enhancement of each individual material's properties, leading to the production of a composite material superior in mechanical and biocompatibility properties from those of the starting materials themselves. In theory, the infiltration of PCL into sintered bone could be achieved by initially melting the material, and then forcing it into the porous structure by a vacuum / release process, pressure or a combination of both. Alternatively, PCL is soluble in a range of organic solvents including tetrahydrofuran (THF) and dimethylformamide (DMF) [65, 66], which may be used to carry the material into the sintered bone and the carrier solvent subsequently evaporated off. These properties and those discussed above highlight PCL as a material possessing properties favourable for processing, and with the potential to produce an improved material over that of sintered bone.

2.6.2 Chitosan

Chitosan is a polysaccharide bio-copolymer containing the monomer units N-acetylglucosamine (2-acetamido-2-deoxy-*β*-D-glucopyranose) and glucosamine (2-amino-2-deoxy-*β*-D-glucopyranose) both bonded via β(1→4) glycoside linkages. The chitosan polymer is derived from chitin, which is a naturally occurring structural polymer found in some insects, fungi, annelids, molluscs, coelenterata and crustaceans [71, 72], with the bulk of the commercially available chitin being sourced from the crustaceans krill, crayfish and crab [72, 73]. Chitosan is produced by the base catalysed partial N-deacetylation of chitin leaving the copolymer, a process which is commonly carried out heterogeneously, and which leads to a block-wise distribution of N-acetylglucosamine and glucosamine monomer units (see Figure 2-2

below) [74]. Other methods have been developed to allow the homogeneous deacetylation of chitin to chitosan, which results in the production of chitosan with randomly distributed monomer-units. The respective characteristic IR frequencies of the each monomer units have enabled the development a number of IR methods for determining the degree of deacetylation in chitosan molecules [75-77]. Unlike chitin, chitosan is soluble in water when combined with certain acids such as acetic, lactic and hydrochloric amongst others. The acids act to protonate the amino group on glucosamine monomer-units yielding a soluble salt. However, sequences of adjacent acetylated monomer-units, as in polymers with block-wise distribution of monomer-units can lead to pockets of hydrophobicity, which in turn, are believed to be the cause of chitosan's tendency to form aggregates in solution [78].

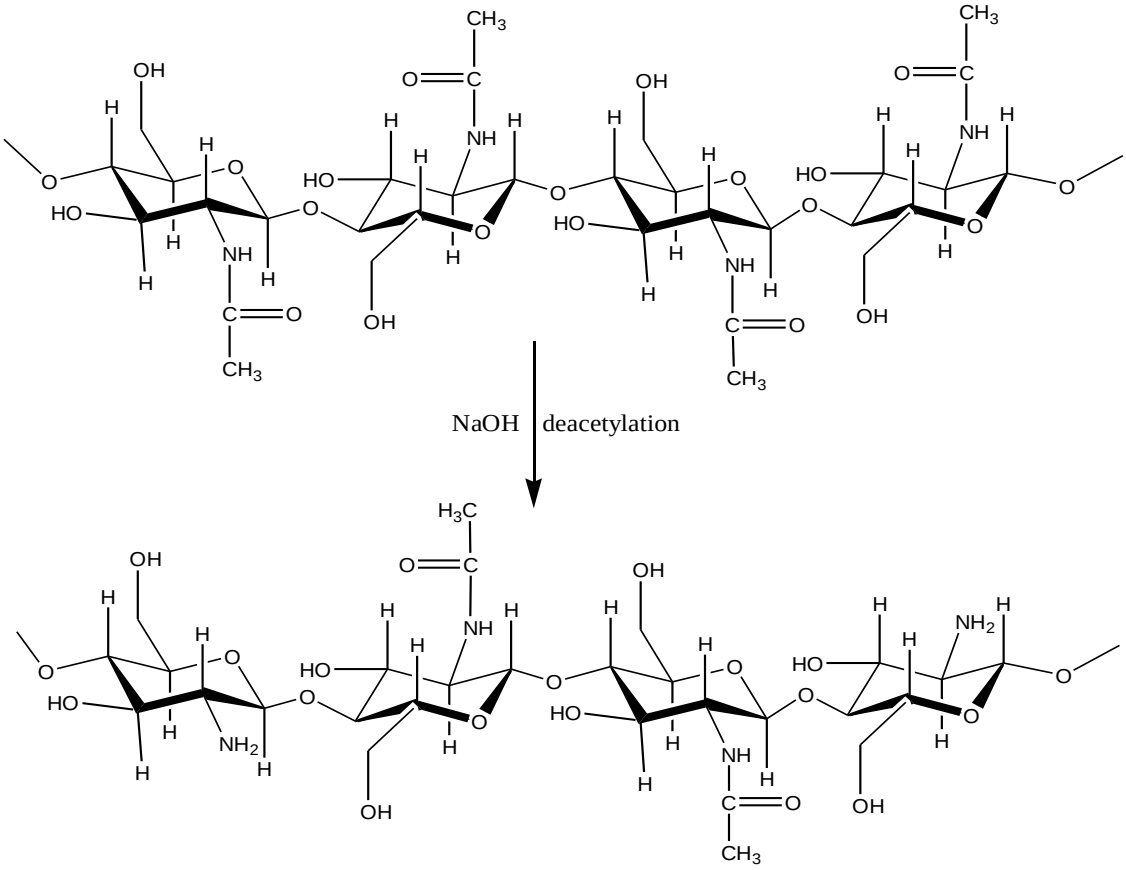

Figure 2-2 – Structural diagram showing the partial deacetylation reaction of chitin to form chitosan.

Physical and mechanical properties

The mechanical properties of chitosan have been shown to vary significantly, depending on whether the material is tested in dry or wet conditions. This is illustrated by Cheng *et al.*'s research showing a Young's modulus value for a chitosan film of ca. 1250 MPa under dry conditions, and the same material exhibiting ca. 6 MPa under wet conditions [79]. Zhang *et al.* stated that chitosan is a "mechanically weak" material [80], which is a relative concept with Mi *et al.* reporting tensile testing results showing ultimate stress values of ca. 38 MPa for chitosan (not stated, but presumably in dry conditions) [81]. This compares to tensile testing results for cancellous bovine bone (stronger than human) showing yield stress values between ca. 10-20 MPa [82].

Many studies have been undertaken to investigate combining chitosan with an inorganic material such as HAp [83-85], or incorporating other organic compounds through covalent or ionic cross-linking to design materials more suited to particular biological applications [86-89]. Ito *et al.* studied the combination of chitosan with hydroxyapatite to produce a membrane for periodontal applications. A composite was manufactured by physically mixing solid hydroxyapatite with a chitosan sol, produced by mixing chitosan with malonic acid in physiologic salt solution. Various ratios of hydroxyapatite to chitosan were produced, with the ratio of 4 : 11 producing the highest hardness and tensile strength values [90]. Matsuda *et al.* produced fibres of chitosan / calcium phosphate by injecting a stream of chitosan dissolved in acetic acid combined with H_3PO_4 into a solution of $Ca(OH)_2$. Depending on conditions, the inorganic phase was shown to be either HAp or a low crystalline mix of HAp and brushite [91]. In a separate study, Hu *et al.* produced a composite material of chitosan and hydroxyapatite through a co-precipitation process from an acidified solution (acetic acid) of chitosan, $Ca(NO_3)_2$ and KH_2PO_4 [92]. XRD patterns of the materials confirmed that the inorganic component of the composite was the hydroxyapatite phase of calcium phosphate, while mechanical tests yielded bending strengths and modulus values of 86 MPa and 3.4 GPa respectively. These values were greater than values in chitosan / hydroxyapatite composites produced from mechanical blending

methods, and 2 to 3 times greater than poly(methyl methacrylate) (PMMA) and bone cement.

The incorporation of hydroxyapatite in the chitosan also had the effect of reducing the quantity of water that the material absorbed. It was shown that after 24 hours of soaking in water, composites of 100 g chitosan / 5 g hydroxyapatite composition absorbed 10 % less water than chitosan alone, and composites of 100 g chitosan / 10 g hydroxyapatite absorbed 17 % less water than chitosan. As penetration of water into chitosan is accompanied by a reduction in mechanical properties [93], the ability to reduce water absorption was seen as a means of maintaining mechanical strength of a bioimplant material.

Another means of altering the properties of chitosan is cross-linking, which can reduce its hydrophilicity and susceptibility to enzymatic degradation [94]. The presence of the amine functionality on the glucosamine polymer subunit provides reactive sites along the polymer chain at which reactions to other molecules may be induced, as shown by Ramos *et al.* who reacted chitosan with a vinyl acrylate modified dextrin [95]. More standard cross-linking reactions can also be employed with a range of agents already having been trialled, including ethylene glycol diglycidyl, glutaraldehyde [81, 93], as well as hexamethylene 1,6-di(aminocarboxysulfonate) (HMDACS) to give blocked diisocyanate crosslinked chitosan membranes [96]. However, these chemicals are highly cytotoxic, reducing their suitability in the production of materials destined for *in vivo* use. By contrast, genipin is a natural crosslinking agent, being the aglycone of genipinoside derived from a traditional Chinese medicine, Gardeniae Fructus (gardenia fruit). In addition, genipin has been shown to be 5,000-10,000-fold less cytotoxic than glutaraldehyde [97], while also displaying anti-inflammatory properties [98]. In a comparative study between genipin and glutaraldehyde cross-linked chitosan, the genipin cross-linked material showed lower swelling characteristics, greater ultimate tensile strength (for samples treated with lower concentrations of cross-linker), and lower strain at fracture values [81].

Biodegradation and Biocompatibility

A number of studies have been undertaken to investigate the biocompatibility of chitosan, chitosan derivatives and chitosan composites [80, 84, 99-106]. *In vivo* chitosan is degraded predominantly by the action of macrophages, which release the enzymes lysozyme and human chitinase. These enzymes catalyse the hydrolysis of the glycoside bond, with lysozyme appearing to act at the site of acetylated residues. There is also some evidence of limited proteolytic enzyme activity, and other non-specific enzymatic activity on chitosan by such enzymes as lipase.

The rate of chitosan degradation has been found to be proportional to the degree of deacetylation, with more highly deacetylated chitosans being less susceptible to enzymatic attack; this is to a large degree due to the greater crystallinity that is associated with such deacetylated chitosans. Research as shown that chitosan above 85 % deacetylation may take up to 3 months to degrade *in vivo*. The result of the aforementioned degradative processes is the cleaving of long chitosan polymer chains into oligomer fractions, which in turn activate macrophages to produce higher levels of lysozyme, human chitinase and N-acetyl-β-D-glucosaminidase. The presence of these enzymes ultimately leads to the complete de-polymerisation of chitosan to its monomers. The monomers are subsequently phosphorylated, and, along with chitooligmers, actively interact with the metabolism of the host promoting healing processes [107, 108].

In a test of biocompatibility, with respect to the use of chitosan in skin wound healing, Howling *et al.* (2001) reported a study into the effects of chitin and chitosan of different degrees of deacetylation and polymerisation on the proliferation of human dermal fibroblasts and keratinocytes *in vitro* [105]. It was found that chitosans with a high level of deacetylation (89 %) stimulated fibroblast proliferation to a greater extent than their less deacetylated (37 %) counterparts. In addition, the degree of deacetylation appeared to have a greater significance on the level of fibroblast proliferation than did the molecular mass of the polymer. The effect of chitosan on keratinocytes also appeared to be dependent on the degree of deacetylation, but in

contrast to fibroblasts, more deacetylated chitosan samples inhibited keratinocyte proliferation. Interest has also been shown in using chitosan and chitosan composite materials as three dimensional tissue engineering scaffolds [80], particularly for bone tissue regeneration. Jiang *et al.* cited chitosan's excellent biocompatibility, biodegradability, antimicrobial and antifungal properties as reasons for use, and went on to produce microspheres of chitosan for use in 3D-scaffolds of high compressive modulus and good osteoconductivity [109].

In an *in vivo* study, Van de Vord *et al.* investigated the biocompatibility of a chitosan scaffold in mice [102]. Chitosan samples were prepared as millimetre scale hollow tubes with an internal diameter of 1.5 mm and an external diameter of 2.5 mm then surgically implanted into mice in two locations, subcutaneously (SC) and intraperitoneally (IP). Mice were euthanised at 1, 2, 4, 8 and 12 weeks with immune response being evaluated showing a very low incidence of chitosan-specific reactions, and no evidence of antibodies binding to chitosan. In addition, no pathological inflammation was seen at sites of implantation; however, a large number of neutrophils were seen to be drawn into the implant region. These macrophage cells are usually associated with the acute phase of inflammation, however tests showed that they were not in an activated state, and other signs of cardinal inflammation such as erythema and edema were not present. Chemotactic attraction of neutrophils to chitosan has been reported in previous studies, and may be linked to specific interactions between neutrophil receptors and the chitosan molecule or its oligomers.

A fibrous capsule containing a large number of neutrophils was seen to form initially around the implants, but reduced in thickness along with the number of neutrophils over time. This capsule remained highly cellular at all times, confirming the absence of an adverse foreign body response. Tissue overgrowth and vascularisation were apparent on all implants examined at later time points, in spite of which, no signs of chitosan degradation were apparent. However, the chitosan used in this study was 92 % deacetylated, and therefore likely to possess a high degree of crystallinity,

accounting for its slow rate of degradation. In this study, chitosan was shown to retain structural integrity for at least 3 months *in vivo*.

2.7 Research plan

The present chapter has outlined the background surrounding the compounds, components and concepts necessary to construct a novel bone replacement bio-implant. Prior to commencing research, a research approach was devised with the goal of producing a medically useful bone replacement material.

1. An initial priority was to determine the dimensions of SCBB samples suitable for compression testing, as this technique was intended to be the fundamental means of measuring changes in mechanical properties from non- infiltrated to infiltrated samples.
2. Once the appropriate dimension of the sintered cancellous bovine bone sample was established, a method of rapidly producing many similar samples had to be developed, in order to provide sufficient samples for statistical analysis. This method would be developed bearing in mind the potential of the process to be scaled up in subsequent commercial projects.
3. Efficient and reproducible means of infiltrating chitosan and PCL into the SCBB samples and then immobilising or setting those compounds needed to be developed. Particular consideration would be paid to minimising the introduction of cytotoxic compounds, and if the presence of cytotoxic compounds within the materials was found to be unavoidable, a guaranteed means of neutralising or eliminating these compounds would be necessary.
4. Continuous appraisal of the feasibility of producing this product commercially had to be maintained at all stages throughout the research with particular attention paid to:
   4.1. Feasibility of scaled up production
   4.2. Feasibility of commercial production
   4.3. Ability to guarantee consistency of product

4.4. Cost considerations of the processing techniques, materials and chemicals used in the process of manufacture
4.5. Physical appearance of the end product
4.6. Utility of product
4.7. Shelf life of the product

5. It would be necessary to carry out strength testing on the samples to evaluate the effect that the infiltrate had on the strength of the material.
6. Natural bone exhibits variation in physical properties from bone type to bone type, and from location to location within that bone, and this aspect was likely to be mirrored in sintered bone. Therefore, a statistical method would need to be developed to accommodate this inherent natural variation in the starting material.
7. Biocompatibility testing also had to be conducted on the sintered bone / organic composite materials to evaluate its suitability for use *in vivo*.

CHAPTER THREE

3 Processing and SCBB preparation

3.1 Introduction

This chapter describes the process by which cancellous bovine bone was harvested from waste cow bone, and processed to give sintered cancellous bovine bone (SCBB) samples ready for infiltration with a reinforcing material. This process included cutting the raw material by saw into suitable sizes, autoclaving these pieces in water to remove fat and protein and then sintering at 1000°C. In addition to this, characterisation of the SCBB material was undertaken by pycnometry, IR, powder XRD and SEM.

3.2 Materials

The bone used in this study originated from the cancellous bone found within the femur of cattle slaughtered for the supply of meat to the New Zealand market. The breed of animal was not ascertained for each sample of bone; however, the same collection of femoral bones were used for each individual experiment. Bones were stored at -10°C until required at the University of Waikato for lapidary saw sample preparation. Otherwise, bone was cut by band saw into sections at a supermarket packed in plastic wrapping and then transferred to the freezer until required.

An Allegro Supercut SAW by W. Latham & Co., N.S.W. lapidary saw with a 2 mm diamond toothed saw, commonly used to cut hard mineral was used to cut cancellous bone into regular shapes as shown later in Figure 3-1. This saw has the capacity to spray cooling water onto the circulating saw blade in order to minimise friction-

induced heating at the cutting surface. A standard butchery band-saw was employed to cut bone condyles into sections approximately 20 mm thick.

A Hawkins domestic pressure cooker (autoclave) with a 7 L capacity was used in the gross fat and protein removal process, and heated by placing on top of a laboratory hot plate. Cylindrical samples of autoclaved bone were produced by drilling with a 16 mm internal diameter Blu-Mol hole cutter bit secured in Tool DP-208B drill press set at a rpm rate of 1200. Autoclaved bone was sintered in a Tetlow muffle furnace within alumina crucibles manufactured by Nikkato Corporation (Japan). Sintered bone cylinders were reshaped by a power-grinding tool (angle grinder) with grinding disk.

3.3 Methods

3.3.1 Bone cutting

Femoral bones were cut initially in half at the medial point between opposing condyles to provide greater ease of handling. Figure 3-1 opposite shows the lapidary saw with half a bovine femoral bone sitting on the sliding bench. Lengths of bone were held by hand against the right angle frame of the sliding saw bench and pushed through the saw. Cancellous bone sections of varying thicknesses were cut from the condyles as required, while a constant flow of cooling water was sprayed on either side of the saw to prevent friction induced heating. According to requirements, sections of cancellous bone were also cut into cubes or other angular shapes.

Figure 3-1 – Photograph of lapidary saw with bovine femoral bone.

Sections of bone for the production of compression testing samples were cut by butchery band saw. These sections were produced by cutting frozen bovine femur bones perpendicular to the primary femoral axis against a width guide set to 20 mm. Bone was cut while frozen to minimize heat induced pore blockage as described by Foster and Johnson mentioned above in section 1.4.

3.3.2 Autoclaving

A sufficient quantity of cut bone sections or bone pieces were placed in a 7 L capacity stainless steel Hawkins domestic pressure cooker (autoclave) to the point at which they half filled the vessel (approximately 1 kg of bone). Water was added to the vessel until the bone was covered by at least 2 cm of water. With the pressure lid secured, the autoclave was set atop a hotplate, which was set to full heat. Once the autoclave began to vent steam (commonly after 1 – 1½ hours), heat was reduced and the autoclave allowed to "cook" for 2 hours. Thereafter, heating was discontinued, the

autoclave was dismantled and the extracted liquid was decanted off the bone pieces. Fresh water was added to cover the bone and the procedure repeated. This complete procedure was performed in triplicate for all processed bone specimens.

3.3.3 Coring autoclaved sections of bone

Autoclaved sections of bone, which had been dried overnight in an oven at 50°C, were placed on a Tool DP-208B drill press platform. A 16 mm internal diameter Blu-Mol hole cutter bit was secured in the drill chuck and the drill set to a revolution rate of 1200 rpm. Gentle pressure was exerted through the drill press onto the hole cutter attachment to bore slowly through each section of cancellous bone to give a cylindrically shaped "dowel" of cancellous bone.

3.3.4 Sintering autoclaved bone

Pieces of autoclaved bone formed into specific shapes, whether angular shapes or cylindrical, were placed in a 280 mL cup shaped alumina crucible manufactured by Nikkato Corporation (Japan) for sintering. A Tetlow muffle furnace was set at 1000°C and full power was applied to heat the samples to the set temperature. No ramping protocol was used, but the increase in temperature against time was recorded, and once 1000°C had been reached, this temperature was maintained for 3 hours. The furnace was then switched off and allowed to cool overnight with the bone samples contained within.

3.3.5 Shaping SCBB

A powered grinding tool (angle grinder) was mounted on a stand in a fume cupboard, so that the grinding wheel was orientated vertically. Samples were held by hand and pressed lightly against the grinding wheel to square the surface.

3.4 Characterization

3.4.1 Pycnometry

Calculation of void volume within the SCBB was performed on a Quantachrome Instruments Ultrapycnometer 1000 running with nitrogen gas at 18 psi. 5 SCBB samples were dried in a 100°C oven for three days, then moved to a desiccator containing self indicating silica gel, and the desiccator was evacuated while the SCBB samples were allowed to cool. Once cool, samples were weighed, physical dimensions measured (length and diameter) by digital calliper, and the samples were returned to the desiccator, which was re-evacuated. The pycnometer was calibrated according to the protocol given in the instructions using the provided standard volumetric sphere. Once calibrated, a sample was introduced into the sample chamber, and the instrument programmed to run a total of eight repetitions. The last three measurements were averaged to give a value for volume and density for the sample. Percentage void volume was calculated according to Equation 1 below where V_{pycn} = volume of the SCBB sample calculated by the pycnometer and V_{bulk} = bulk volume of the SCBB sample.

Equation 1

$$\%V_v = \frac{V_{pycn} - V_{bulk}}{V_{bulk}} \; x \; 100\,\%$$

Each of the five samples was run in the same manner on the pycnometer, with values for density and volume calculated for each, which in turn enabled the calculation of percentage void volume for each.

3.4.2 Scanning Electron Microscopy (SEM)

A Hitachi S-4700 SEM running at 10 - 20 kV for images and 20 kV for energy-dispersive X-ray spectroscopy (EDX) analysis was employed. Samples were prepared by scraping a small quantity of SCBB particles off the SCBB surface from the area of interest by scalpel onto a strip of double-sided carbon tape mounted on a SEM sample

stub. For SEM analysis the sample was plasma coated with Pt / Pd, while samples intended for EDX analysis were not coated.

3.4.3 Powder X-Ray Diffraction (XRD)

Finely ground SCBB samples were run on a Philips X'Pert MPD X-ray diffractometer and data were collected through the X'Pert Data Collector (version 2.0b) software. The following parameters were used to analyse the SCBB samples; Cu anode, wavelengths K-Alpha$_1$ = 1.540598 Å and K-Alpha$_2$ = 1.544426 Å, monochromator PW3123/10 for Cu scan range 12 – 80 degrees 2θ, scan step size 0.02 degrees 2θ, divergence slit 0.5 mm, receiving slit 0.8 mm. The PANalytical X-Pert Highscore database was used to compare XRD patterns and characterise samples.

3.4.4 FT-IR

IR spectra were obtained on a Digilab FTS-40 Fourier transform spectrometer at 4 cm^{-1} resolution over the range 4000 – 400 cm^{-1}, and later on a PerkinElmer Spectrum-400 spectrometer with Spectrum V. 6.3.1. software. Samples were prepared by grinding approximately 20 mg of sample with approximately 200 mg dry KBr.

3.4.5 Evaluation of surface alkalinity of SCBB

Small sub-samples (~ 0.2 g) of standard 10 mm height x 10 mm diameter SCBB samples were prepared by shaving a thin cross-section off the standard cylinder shape with a scalpel. Individual samples were placed in 100 mL distilled water at 20°C and stirred gently with a magnetic stirrer, so to cause a flow of water of the sample, but not sufficient to induce movement of the sample. pH measurements were recorded each minute.

3.4.6 Reduction of surface alkalinity

Repeated washing in distilled water

A 0.8 g SCBB sample was placed in 200 mL distilled water and the water stirred gently by magnetic stir bar, so that the water flow was not sufficient to move the sample. pH was recorded every 15 minutes for 1 hour, after which the water was replaced with fresh distilled water, and the procedure repeated. In total, this 1 hour "washing" procedure was repeated 4 times. A value for the number of moles of $OH^-_{(aq)}$ dissolved in the washing water per gram of SCBB sample was estimated from the pH of the solution, the relationship of K_w to $[OH^-]$ and $[H^+]$, and weight of the sample.

Washing in carbonated water

$CO_{2(g)}$ was dissolved in distilled water through the use of a commercially available carbonated drink maker (Soda Stream). The initial pH of the $CO_{2(aq)}$ produced and used in the experiments was between 4.0 – 4.2. A SCBB sample that weighed 1.136 g was placed in 200 mL of the slowing effervescing $CO_{2(aq)}$, which was slowly stirred with a magnetic stirrer while pH was monitored. Stirring was continued for 1 hour, the $CO_{2(g)}$ was replaced with fresh $CO_{2(aq)}$ and stirring continued for another hour.

Autoclaving

Five pre-weighed SCBB samples approximately 0.2 g in weight were placed on a stainless steel grill platform within a Hawkins autoclave containing 0.5 L boiling distilled water. Samples were autoclaved for 30 minutes, and then removed to cool and dry. The surface alkalinity of autoclaved samples were compared to 6 non-autoclaved samples (~ 0.2 g) by placing each sample individually in 100 mL distilled water for 1 hour while stirring gently and recording pH. pH measurements for the 100 mL of washing water used were then converted to moles of $OH^-_{(aq)}$ in the 100 mL solution per gram of washed sample.

3.5 Results and Discussion

3.5.1 Lapidary saw

It was found that the lapidary saw blade could be eased slowly through a femoral condoyle of approximately 10 - 15 centimetres in diameter in approximately 10 - 20 minutes. However, after an initial groove had be cut into the bone, it was vital that attention be paid to maintaining the precise square orientation of the condyle with respect to the saw blade, otherwise friction-induced jamming and heating would ensue. Johnson stated that the occurrence of high temperatures during cutting was undesirable, as the surface pores of the cancellous bone became blocked, probably because of heat induced gelatinisation of the bone protein [17]. Foster suggested that this in turn would reduce the effectiveness of subsequent defatting and deproteination processes via autoclaving [13].

Nevertheless, Foster demonstrated that 25 mm thick sections, transverse to the shaft of the femur, could be produced successfully by cutting femoral bones with a lapidary saw [13]. In order to achieve this, Foster described clamping lengths of bone in place on the lapidary saw before each section was cut. Firmly securing bone to the apparatus would be an ideal means of minimising jamming and controlling the width of sectioning precisely, while also presenting the potential to develop a semi-automated sectioning process. Attempts to clamp bone to the apparatus were however unsuccessful because of the irregular shape of bone and its inherent “slippery” nature. Therefore, hand held only cutting was ultimately successful, which allowed for the production of highly regular prisms and cubes nonetheless, as shown opposite in Figure 3-2. Such shapes may be more useful when applied as implant materials, but for mechanical testing, literature sources recommended that cylindrical shapes were more suited [40]. In addition, it was ascertained at a later stage during the course of this research, that cylindrical shapes with consistent dimensions were easier to mass-produce. The lapidary saw method of producing samples was still regarded as being useful in producing samples of specific shapes, and could be improved by securing

bone to the apparatus, which could be achieved by screwing securing pins into the bone material itself.

Figure 3-2 – Various shapes and sizes of raw cancellous bone prepared by lapidary saw.

3.5.2 Band saw

Sections of raw bone that were produced varied in size and shape depending on the area from which they were cut, but typically appeared as shown in Figure 3-3. Variations in width through the sections were slight (~ 17 – 23 mm) despite the relatively rapid and imprecise production method, in addition to which each cross section required only 2 - 5 seconds to produce. As is apparent from the image below, remnants of meat and fat were present on the surface of the section. Although the surfaces of the cut section are seen to be flat in this image, autoclaving often revealed areas that were entirely composed of fatty tissue, which when removed left cavities in the surface as shown later in Figure 3-6.

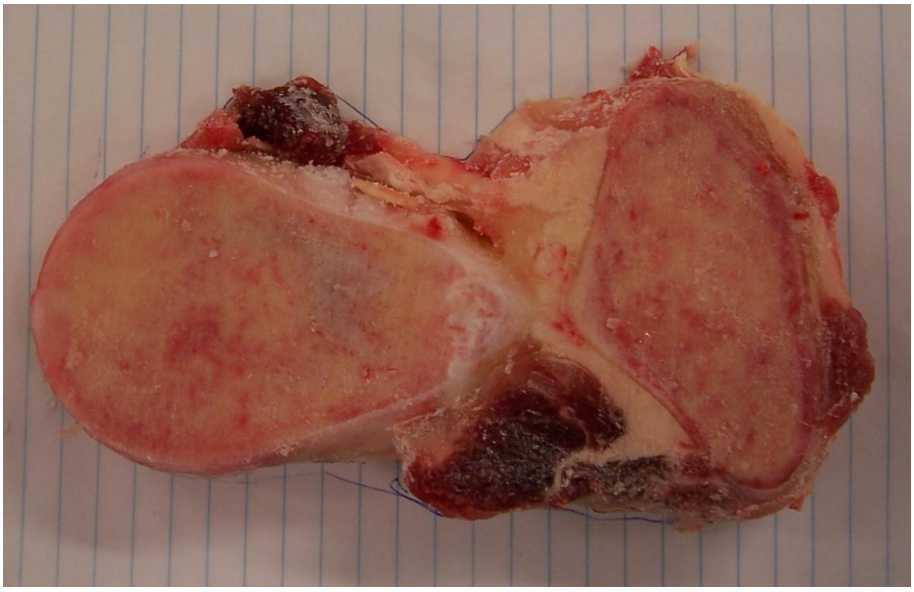

Figure 3-3 - Section of bovine femoral condyle cut by band saw showing remnant portions of meat and fat on the surface.

3.5.3 Autoclaving

A yellow fatty liquid was seen to float on the surface of the water in the autoclave vessel above the sections of bone after the first 2 hour cycle of autoclaving. After all liquid (fatty and aqueous) had been decanted off from above the bone sections into a beaker, clear gelatinous material was seen to form at the bottom of the aqueous portion upon cooling. The same gelatinous material was seen to coat the surface of the bone sections when cooled to room temperature. Figure 3-4 opposite shows the molten yellow fatty liquid floating on top of the extracted autoclaving water in a 3 litre beaker after the second 2 hour cycle of autoclaving. By the third and final autoclaving step, the amount of fat and protein extracted from the bone sections had been reduced considerably to approximately 20 mL of fatty liquid per 1 kg of bone, while no obvious gelatinous material was apparent.

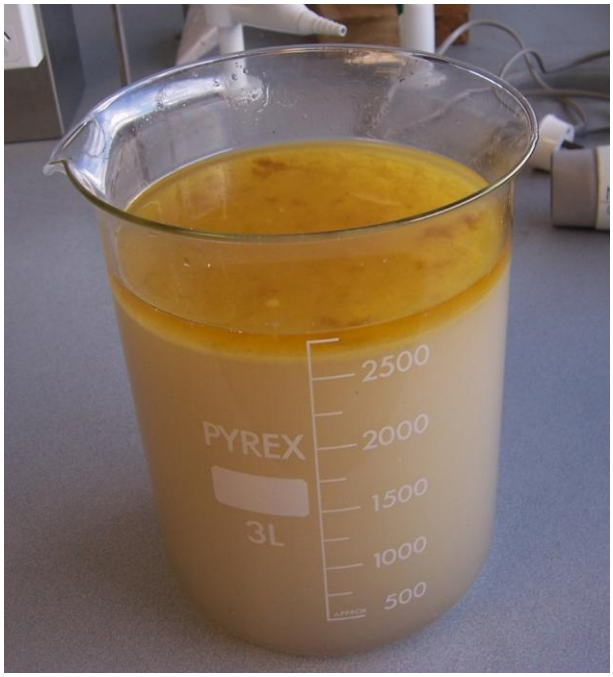

Figure 3-4 – Photograph of fatty liquid floating on top of water removed from autoclaving cancellous bone samples.

Autoclaved samples had an off white to yellow colouration as seen below in Figure 3-5, which shows regular shaped samples prepared by lapidary saw. Also apparent was the porosity and the variation in pore size in the cancellous bone, which was revealed after the removal of fat and protein.

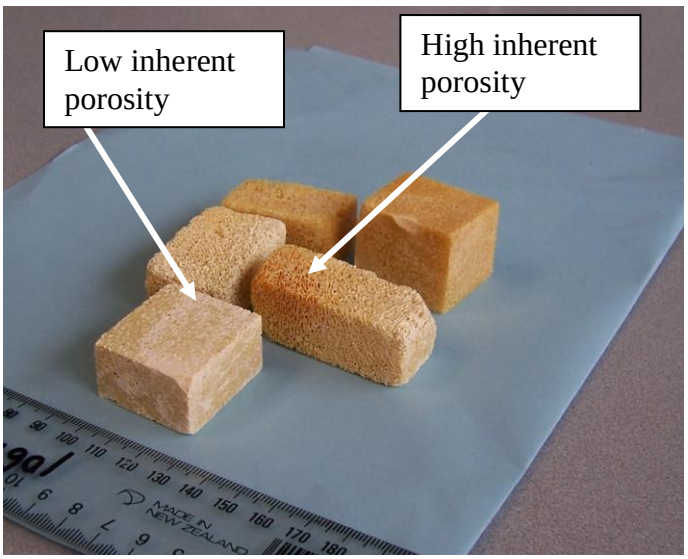

Figure 3-5 - Cancellous bovine bone cut by lapidary saw and after autoclaving for a total of 6 hours, cf. SCBB in Figure 3-9.

Sections of bone cut by band saw after three repetitions of autoclaving appeared as shown in Figure 3-6 below. As can be seen, many different shapes and sizes were generated during the sectioning process, with the autoclaving process revealing cavities and regions of low density within each section.

Figure 3-6 - Autoclaved cross-sections of femoral condyle cut by band saw.

Coring sections

The gradual application of manual pressure on the drill press (shown opposite in Figure 3-7) onto the hole cutter attachment allowed cores (cylindrically shaped "dowels") of cancellous bone to be cut from sections of cancellous bone, as shown in Figure 3-8. Depending on the shape and size of each section, 1 to 10 samples per section were produced in this manner.

Figure 3-7 – Photograph of section of dried autoclaved bovine bone after being cored with Blu-Mol hole cutter.

Figure 3-8 – Photograph of 'dowels' of autoclaved cancellous bovine bone generated by coring into sections of cancellous bone as shown above in Figure 3-7.

3.5.4 Sintering cancellous bovine bone

Approximately 60 g of autoclaved bone proved to be the maximum weight possible per sintering run. Quantities larger than this generated excessive smoke, which created a safety risk. After sintering, the SCBB appeared as a pristine white material as shown in Figure 3-9 and Figure 3-10 below. Figure 3-10 shows the result of sintered cores extracted from autoclaved condyle sections shown in Figure 3-8.

Figure 3-9 – SCBB sintered at 1000°C for 3 hours, cf. the original autoclaved samples in Figure 3-5.

Figure 3-10 - Cylindrically shaped SCBB generated through autoclaving, coring and sintering processes.

The final shape of the SCBB samples ready for mechanical testing is shown below in Figure 3-11. This shape was produced by grinding the ends of the samples as seen in Figure 3-10.

Figure 3-11 – Photograph of SCBB samples after having ends ground square.

3.5.5 Pycnometer

The results of volume calculations derived from the pycnometry experiment were plotted against apparent density values for the respective samples resulting in the plot presented in Figure 3-12 over the page. The plot was expanded to incorporate both the x- and y-intercepts in order to facilitate extrapolation. A large r-squared value of 0.96 indicated a strong correlation between % void volume and apparent density, showing the expected decline in % void volume with increasing apparent density. Y-error bars on the data were derived from the variation in the pycnometer output and x-error bars from weighing and dimension measurement error. The y-intercept of 98 % void volume was close to the theoretical 100 % void volume for a sample possessing a hypothetical apparent density value of 0, and when the graph was extrapolated to 0 % void volume (i.e. completely solid sample with no porosity) a density value for the

HAp material of 3.35 g / mL resulted. Considering the error inherent in the experiment, as represented by the maximum and minimum slope on the plot, this value is similar to that of literature values for stoichiometric HAp of 3.16 g / mL [110].

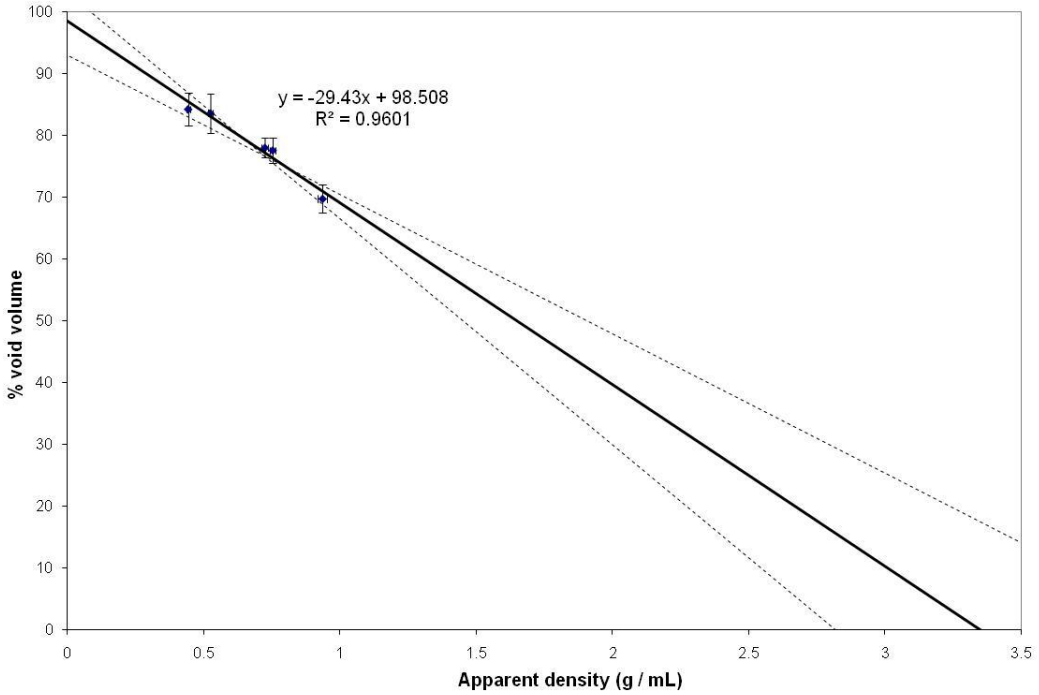

Figure 3-12 – Plot of % void volume in SCBB against apparent density from values obtained by pycnometer.

3.5.6 SEM

The results of SEM imaging confirmed the relationship seen in the pycnometry experiment, which was that samples of low apparent density displayed greater porosity and samples with higher apparent density lower porosity. This is evident when examining Figure 3-13, which shows a denser material commonly described in literature as having a plate-like morphology, and Figure 3-14 which represents a more open structure possessing a rod-like morphology [111]. The macroporous nature of

the materials is apparent with pores ranging in size from approximately 300 μm to 1000 μm.

SEM imaging also confirmed that the material retained a macroporous architecture characteristic of the raw bone starting material. In addition, an elaborate structure was revealed as can be seen in Figure 3-13, where smaller holes (or channels) approximately 25 – 75 μm in diameter were seen to lie on the surface of the material within the larger macropores. The larger holes were possibly the remnants of arteries and blood vessels that had been burnt out during the sintering process, while the smaller holes could have been the remnants of lacunae, which are cavities, in which osteocytes reside in living bone, see section 2.2.2. SEM images generated by Gao *et al.* of bone sintered at 1120°C for 3 hours showed similar characteristics [112].

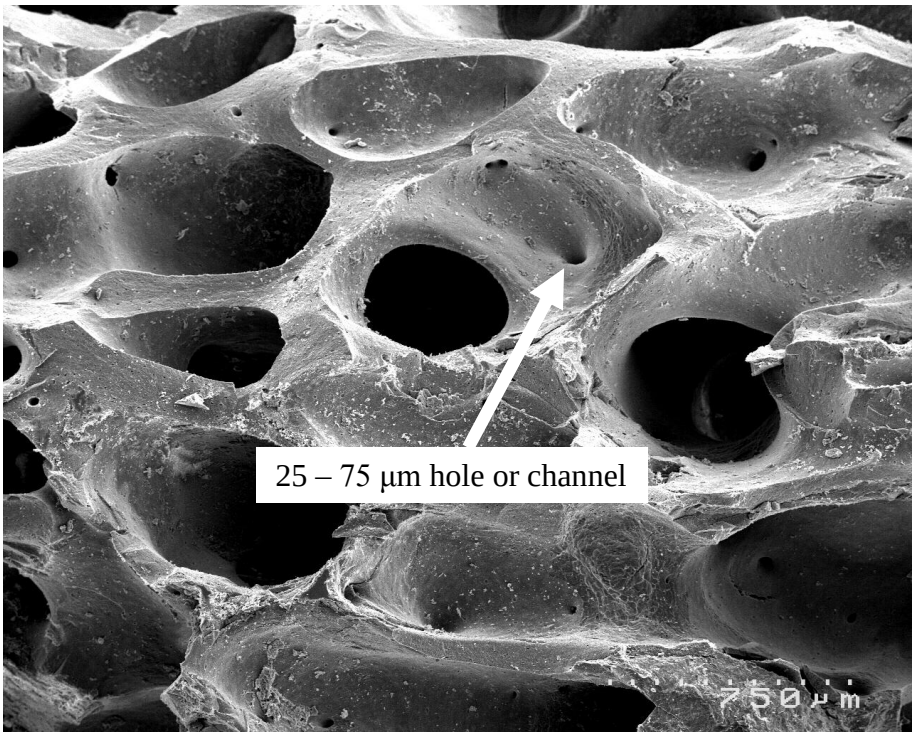

Figure 3-13 - SEM of a comparatively denser SCBB material showing macropores, smaller cavities and exhibiting plate-like morphology.

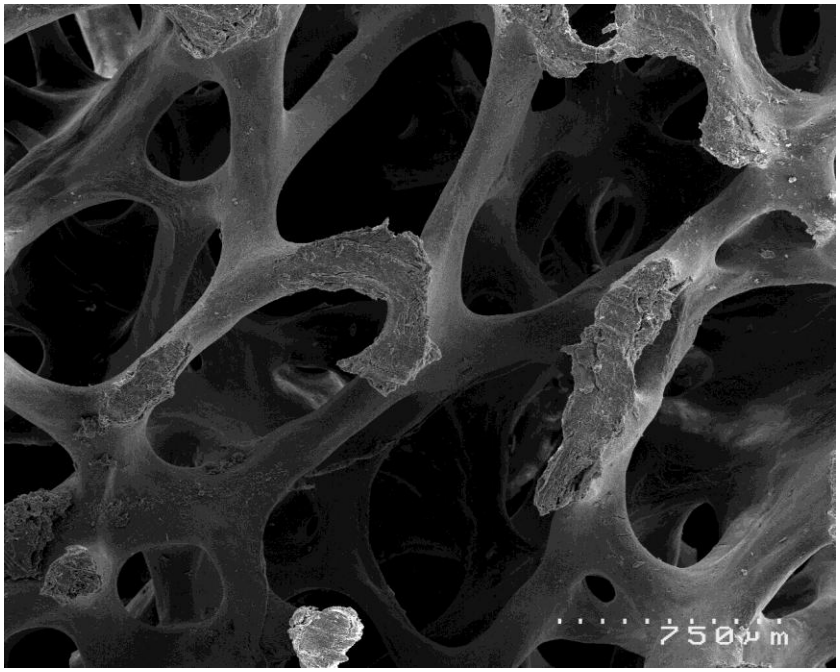

Figure 3-14 - SEM of a comparatively less dense SCBB exhibiting rod-like morphology.

The complexity of the SCBB was further revealed when viewed under higher magnification, where its microporosity and molten fused appearance was visible as shown in Figure 3-15. This can be seen clearly in the higher magnification SEM of the same sample in Figure 3-16. The SEM images presented are similar to those seen by Rhee *et al.* for sintered bovine bone at 1000°C. These authors investigated the effect of three sintering temperatures, 600°C, 800°C and 1000°C on the chemical and structural properties of bovine cancellous bone [113]. Rhee *et al.* found that material sintered for 3 hours at 600°C contained small apatite granules comparable in size to those found in natural bone, but when the material was sintered at 1000°C for three hours, granule size was close to 20 times greater. Meanwhile, Joschek *et al.* reported in a study involving the examination of the commercially available sintered bovine bone product, Endobon, that while apatite crystals in natural bone were of the dimensions 20-40 x 20-40 x 2.5-5 nm, those in Endobon ranged from 1 to 7 μm [11]. This would make the crystals in the Endobon approximately 50 to 200 times larger than in natural bone. For the material produced in this research, as seen in Figure 3-16, crystals ranged from approximately 300 nm up to 1-2 μm which are approximately 20 times larger than the natural bone apatite dimensions in agreement

with Rhee *et al.*'s findings. Unfortunately, materials with greater crystallinity (generally those that have been sintered at higher temperature) have been shown to be less resorbable by osteoclasts [2]. However, this disadvantage must be balanced against the imperative, that the possibility of the presence of a disease be completely eliminated (see section 1.5 - prions in bone).

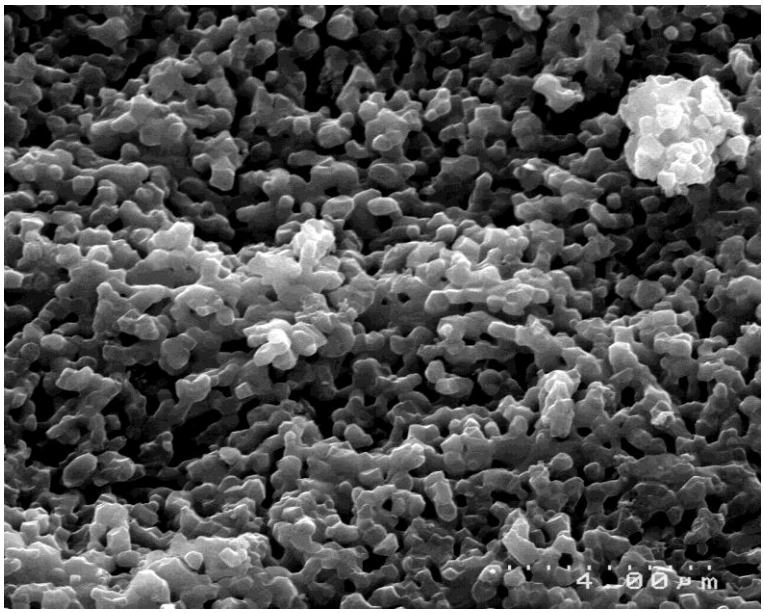

Figure 3-15 – SEM of the surface of a fractured piece of SCBB revealing the morphology and microporosity of the material.

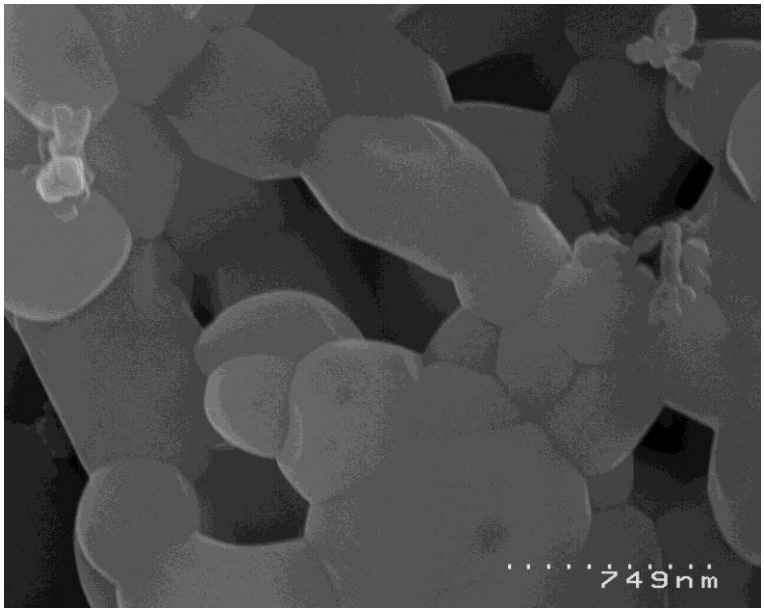

Figure 3-16 – Highly magnified SEM image of SCBB showing molten appearance of crystallites.

3.5.7 XRD

Powder XRD analysis on the SCBB correlated to the hydroxyapatite phase of calcium phosphate. This is shown below in Figure 3-17 with most peaks in the powder XRD pattern accounted for by hydroxyapatite except for small peaks at 37° 2θ and 54° 2θ. Figure 3-18 illustrates that these peaks can be accounted for by the presence of CaO. However, another SCBB sample shown in Figure 3-19 showed a complete absence of this peak indicating either an absence of CaO, an inconsistency of composition or the presence of amorphous material.

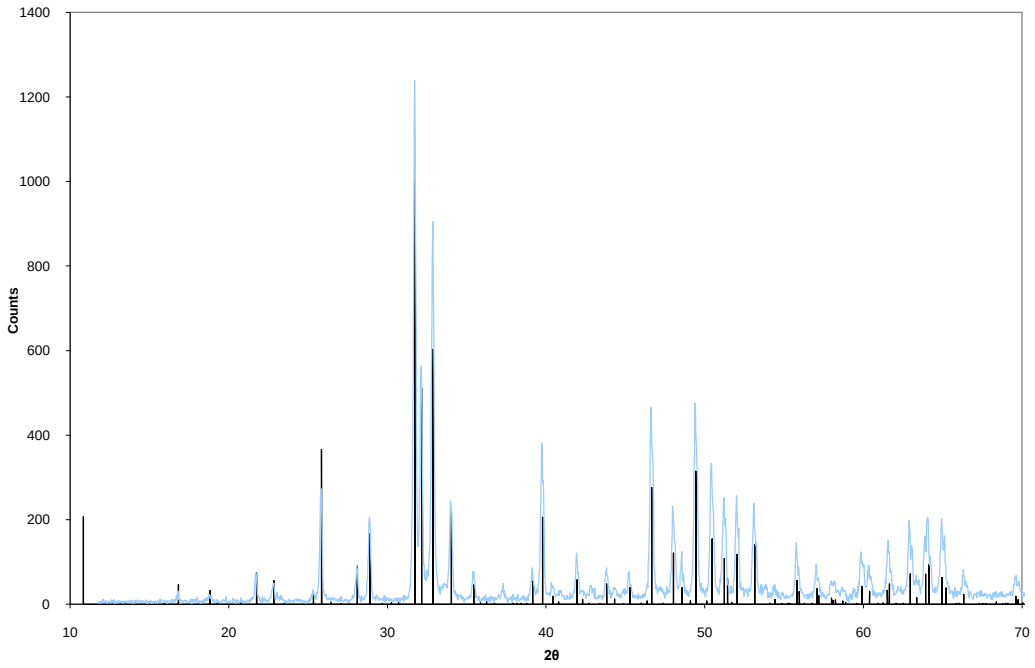

Figure 3-17 - Powder XRD pattern of sintered bone with Hydroxyapatite, syn. 89-4405 pattern superimposed.

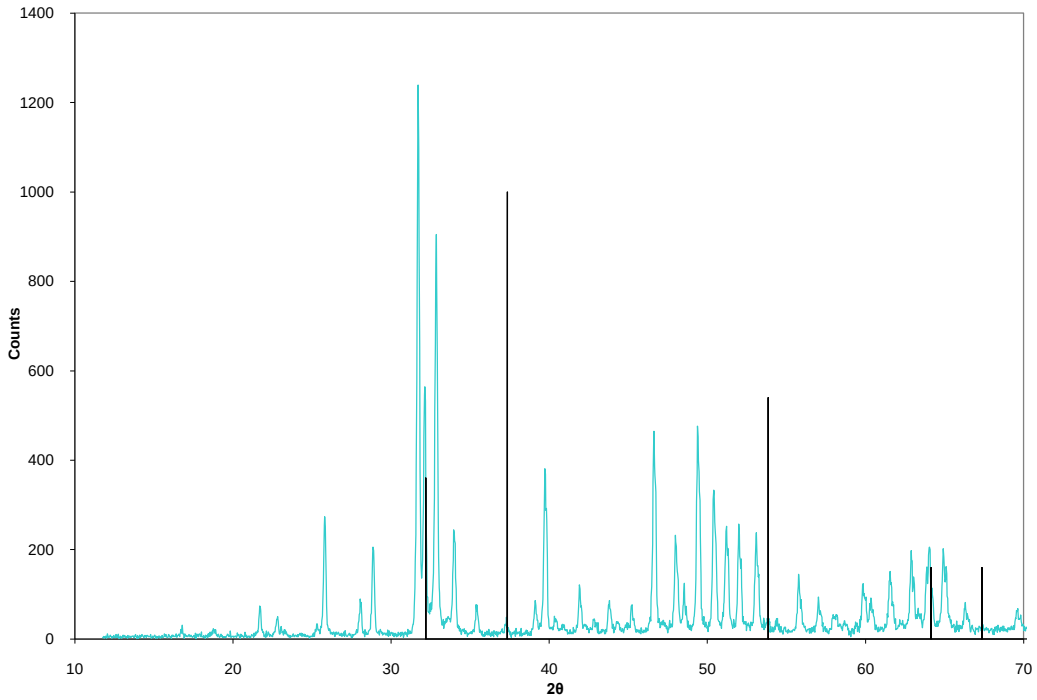

Figure 3-18 - Powder XRD pattern of SCBB with CaO, Lime syn., 37-1497 pattern showing the presence of CaO as indicated by a small peak at 37° 2θ.

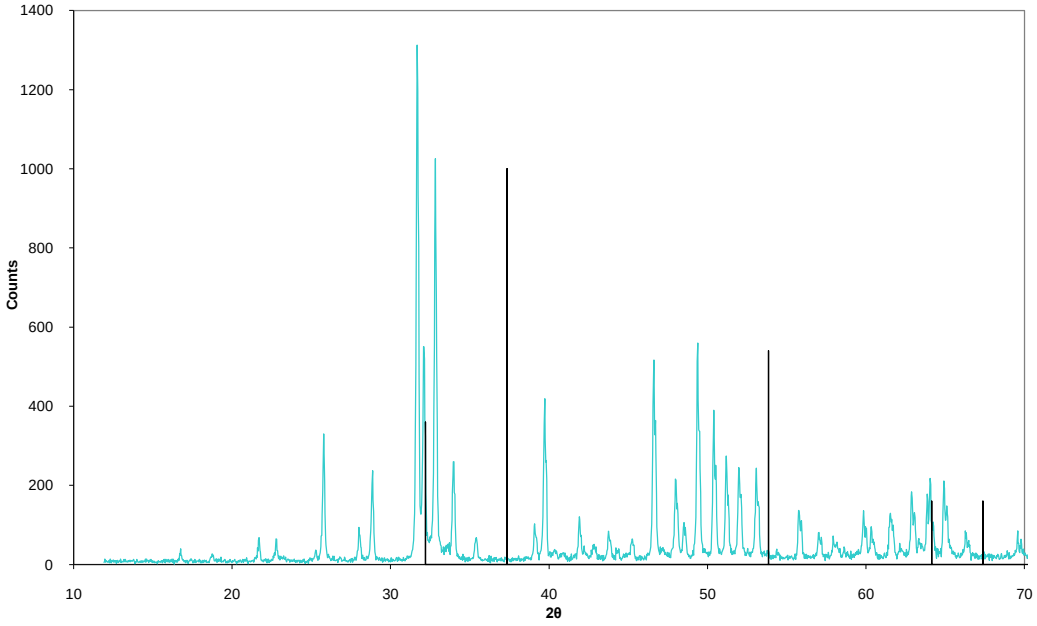

Figure 3-19 - Powder XRD pattern of SCBB with CaO, Lime syn., 37-1497 pattern showing no indication of CaO as indicated by an absence of a peak at 37° 2Theta.

Apart from the evidence of a small quantity of CaO, XRD spectra showed the SCBB material to be a single phase of hydroxyapatite. By contrast, Herliansyah *et al.*

reported that XRD patterns of bovine bone sintered at 900°C for 2 hours in air showed the material to be a single phase of HAp with high crystallinity without secondary phases such as CaO or TCP [114]. Rodrigues *et al.* however reported the presence of both CaO and $Ca(OH)_2$ in XRD analysis on sintered bovine bone material that had been produced by chemically treating raw cortical bone with hypochlorite, hydroxide and peroxide and then sintering at 1100°C for 3 hours [115]. In another study, Barralet *et al.* investigated the decomposition characteristics of synthetic carbonated hydroxyapatites and found no XRD evidence for the presence of CaO up to 1500°C. However, they attributed the lack of CaO to the relatively rapid heating profile of their experiment (30°C min^{-1}) and the time dependent nature of the decomposition of carbonated hydroxyapatite [12].

3.5.8 IR

IR was employed as a further means of characterising the SCBB material. For comparison, an IR spectrum was generated initially on the starting material, autoclaved bone. A baseline corrected IR spectrum of the autoclaved bone after 3 repetitions of 2-hour autoclaving procedures is shown in Figure 3-20 on page 57. The broad peak at 3449 cm^{-1} was assigned to the O-H stretch of water indicating the presence of water in the sample. Peaks at 2924 cm^{-1} and 2854 cm^{-1} were attributed to C-H stretching associated with the presence of fatty material remaining in the cancellous bone. Peaks between 1385 cm^{-1} and 1745 cm^{-1} were assigned to organic material present in the cancellous bone, although there may also have been a contribution here from CO_3^{2-} originating from the mineral constituent present in the sample. The peak at 1745 cm^{-1} is consistent with that of the carbonyl stretch for a monomeric aliphatic fatty acid commonly found at around 1750 cm^{-1} [116]. Broad peaks at 1657 cm^{-1} and 1454 cm^{-1} were assigned to the Amide I and Amide II bands associated with proteinaceous material collagen [117]. The peak at 1039 cm^{-1} and its shoulder at approximately 1093 cm^{-1} was assigned to v_3 modes of PO_4^{3-} [118]. Peaks at 603 $cm^{-1}$and 565 cm^{-1} were assigned to the v_4 modes of PO_4^{3-} and also appear in the spectrum of SCBB shown in Figure 3-21.

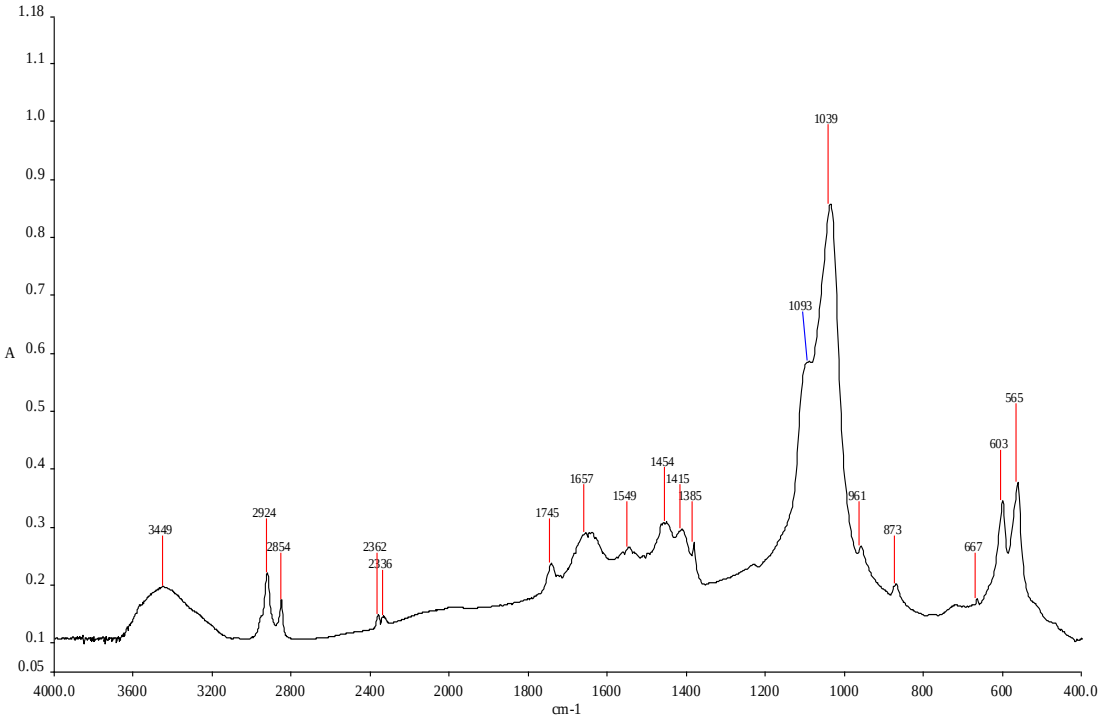

Figure 3-20 - IR spectrum of autoclaved bone (baseline corrected).

Figure 3-21 shows an IR spectrum of SCBB which demonstrated less complexity in comparison to the IR spectrum of autoclaved bone. Significantly, there was no obvious peak at 1745 cm^{-1} in the SCBB, which would have indicated the presence of an aliphatic fatty acid carbonyl stretch. Pronounced peaks at 571 cm^{-1} and 602 cm^{-1} were assigned to the v_4 vibration (bending) modes of the PO_4^{3-} ion, with adjacent peak at 632 cm^{-1} assigned to the librational mode of OH within the hydroxyapatite lattice. The peak at 962 cm^{-1} was assigned to the v_1 mode of PO_4^{3-} and the peaks at 1048 and 1089 to the v_3 (P-O stretching) modes of PO_4^{3-}. The very sharp peak at 3574 cm^{-1} was assigned to the O-H stretch of the OH group in the hydroxyapatite lattice. The results of IR pointed to the absence of organic material in the SCBB, however this must be considered under the caveat that the detection limit for IR is commonly only 1 - 0.01 % [119].

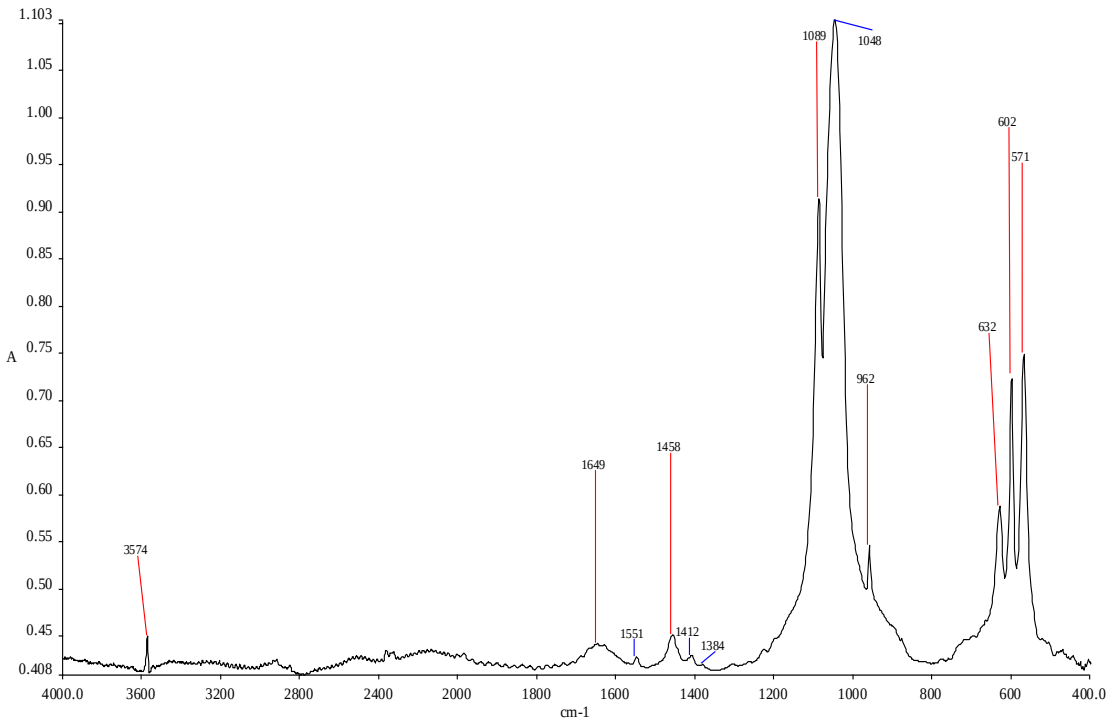

Figure 3-21 – IR spectrum of SCBB (baseline corrected).

Figure 3-22 shows a magnified view of the region 1750 – 1300 cm^{-1} where peaks at 1412 cm^{-1}, 1458 cm^{-1}, and 1551 cm^{-1} suggested the presence of CO_3^{2-} in the material. Peaks at 1458 cm^{-1} and 1551 cm^{-1} may be assigned to v_{3a} and v_{3b} modes respectively of type A carbonate substituted hydroxyapatite, where as peaks at 1412 cm^{-1} and 1458 cm^{-1} again may be assigned to the v_{3a} and v_{3b} modes of type B carbonate substituted hydroxyapatite. Type A substitution refers to the replacement of OH^- ions for CO_3^{2-} ions, whereas type B substitution involves the replacement of PO_4^{3-} ions for CO_3^{2-} ions. Both carbonate substitutions should also show peaks at 877 cm^{-1} and 872 cm^{-1} for type A and type B substitutions respectively, which may be seen as a slight shoulder on the dominate peak of 1048 cm^{-1} above in Figure 3-21 [115, 120-123].

The appearance of carbonate in sintered bone is not unusual and has been reported by other authors [11, 113-115]. Its loss is temperature dependent with Rhee *et al.* reporting IR peaks corresponding to CO_3^{2-} decreasing in size in samples sintered for 3 hours at 600 with respect to samples sintered at 800°C, whereas at 1000°C a carbonate signal IR was not seen. Loss of carbonate during sintering is also time

dependent as discussed further in the XRD section 3.5.7. As the SCBB samples used for this IR analysis were stored open to the atmosphere for days or weeks after being produced, it is possible that $CO_{2(g)}$ from the atmosphere was also reincorporated into the lattice, or perhaps reacting with CaO (or $Ca(OH)_2$) produced during sintering.

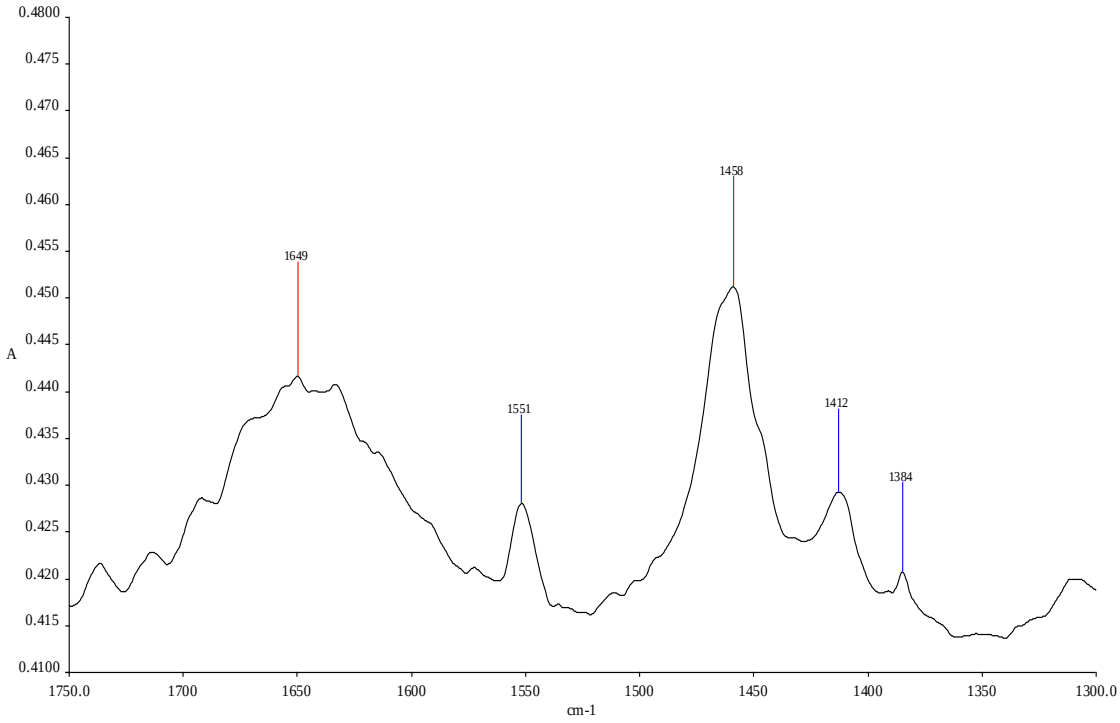

Figure 3-22 – IR spectrum of SCBB in the region 1750 – 1300 cm^{-1}.

3.5.9 SCBB Surface alkalinity

As presented above in the powder XRD analysis, there was evidence that the SCBB contained CaO. If the $CaO_{(s)}$ was available to react with water to give $Ca(OH)_{2(aq)}$ an increase in pH would indicate this. pH measurements of stirred distilled water in which SCBB samples were placed showed a trend of increasing pH over time, particularly within the first 30 minutes of washing, and then a general levelling off of pH, as shown over the page in Figure 3-23.

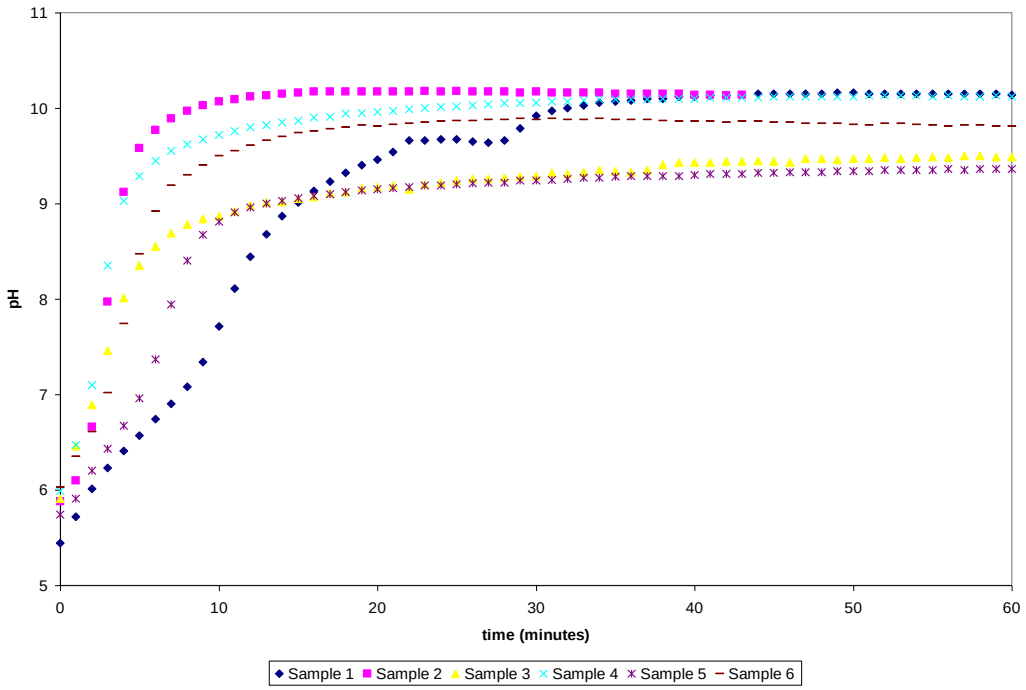

Figure 3-23 - Increase in pH of 100 mL distilled water against time per ~ 0.2 g sample.

A maximum pH of 10.2 was observed for one sample, and when this pH value was converted to concentration of OH^- in water, a value of 1.4 x 10^{-4} mol L^{-1} was obtained. The solubility product of $Ca(OH)_2$ is $K_{sp}(Ca(OH)_2)$ = 5.02 x 10^{-6} (at 25°C) [124], and so an estimation of the molar solubility of $Ca(OH)_2$ can be made as shown in Appendix A. When comparing the OH^- concentration in the 100 mL washing solution (1.4 x 10^{-4} mol L^{-1}) against that of the theoretical maximum for $Ca(OH)_2$ at saturation (3.24 x 10^{-2} mol L^{-1}), it was apparent that the levelling off of pH (and therefore $[OH^-]$) was not caused by a saturation of the solution by $Ca(OH)_2$.

Repeated washing to remove alkalinity

When SCBB was repeatedly washed for 1 hour in fresh distilled water, a reduction in soluble alkaline material on the surface of the SCBB was seen with each successive wash. A decrease from the end of the first 1 hour wash to the end of the 4th wash from approximately 1.2 x 10^{-4} to 5.0 x 10^{-7} mol. OH^- / g sample in the washing water was observed. This simple washing technique was found to be an effective way of

reducing soluble alkaline material present on the surface of the SCBB, as shown below in Figure 3-24.

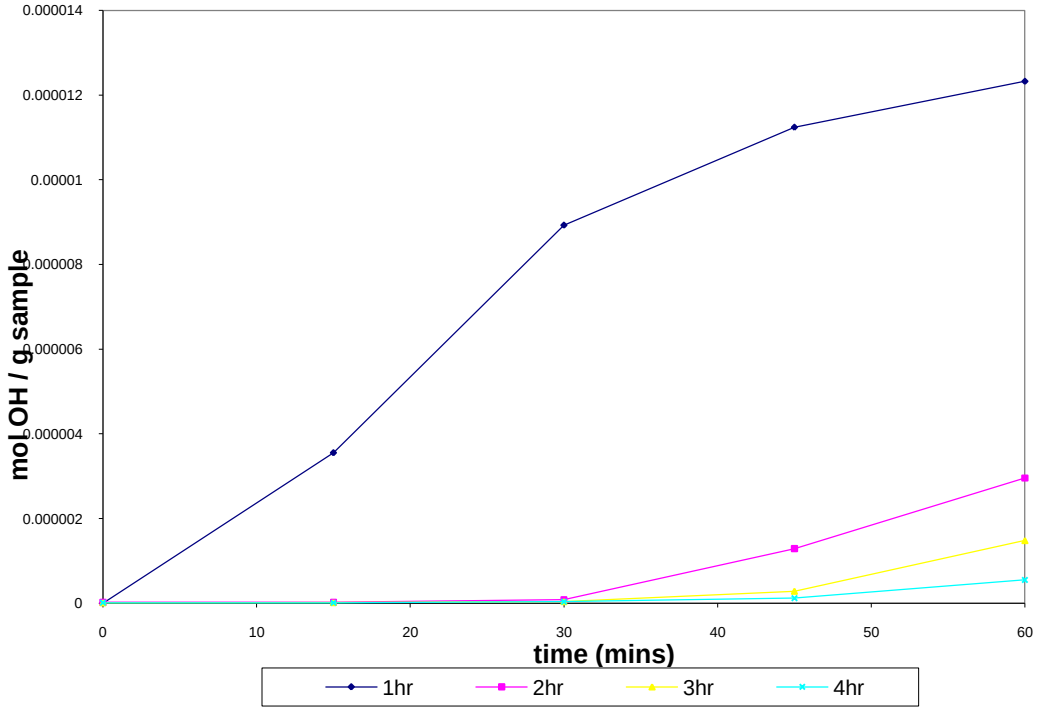

Figure 3-24 – Mol OH^- / gram of sample in washing water against time per wash cycle.

Washing SCBB in $CO_{2(aq)}$

Washing in distilled water was observed to reduce the surface alkalinity of the SCBB material. Washing in $CO_{2(g)}$ was seen as a means to increase the rate and/or effectiveness of this process. At the moment of contact between SCBB samples and $CO_{2(aq)}$ rapid effervescence was observed. As can be seen in Figure 3-25, the number of moles of OH^- per grams of SCBB rose little but steadily for the 1st wash in $CO_{2(aq)}$ and less for the 2nd wash in $CO_{2(aq)}$. A subsequent wash in distilled water however showed an increase in the number of moles of OH^- per grams of SCBB (pH of 8.3 after 60 minutes) indicating the continued presence of soluble alkaline material, after washing in $CO_{2(aq)}$.

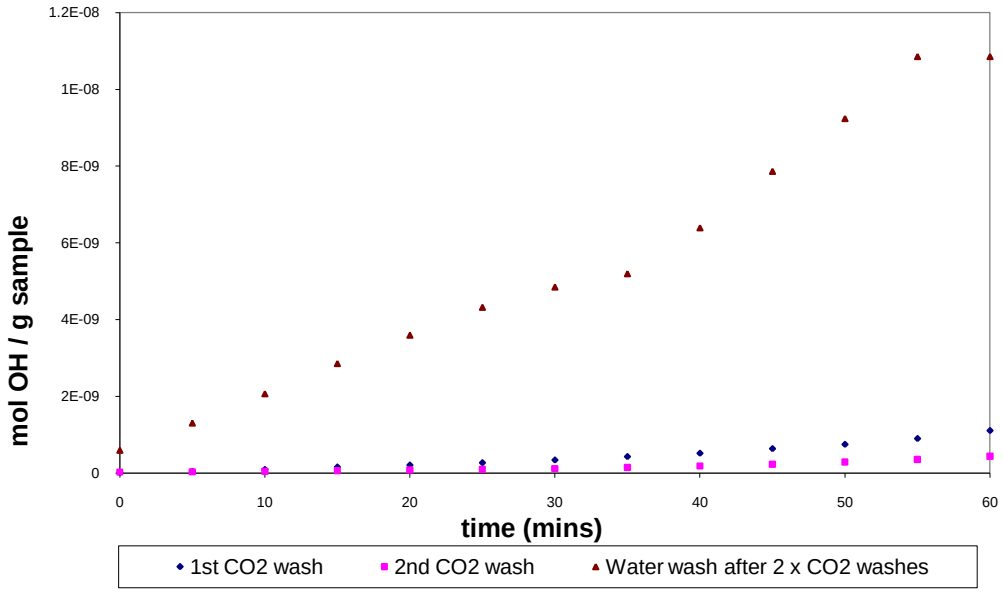

Figure 3-25 – Mol OH^- / g sample in washing solution with time for sintered bone samples washed twice in 200 mL carbonated water and then washed in 200 mL distilled water.

However, it should be noted that these values for mol OH^- / g sample are low in comparison to the distilled water wash values. This can be seen by comparing the data "Water wash after 2 x CO_2 washes" above in Figure 3-25, and equivalent data in Figure 3-26 below. This shows the increased effectivenesss of $CO_{2(aq)}$ washes in comparison to distilled water washes alone.

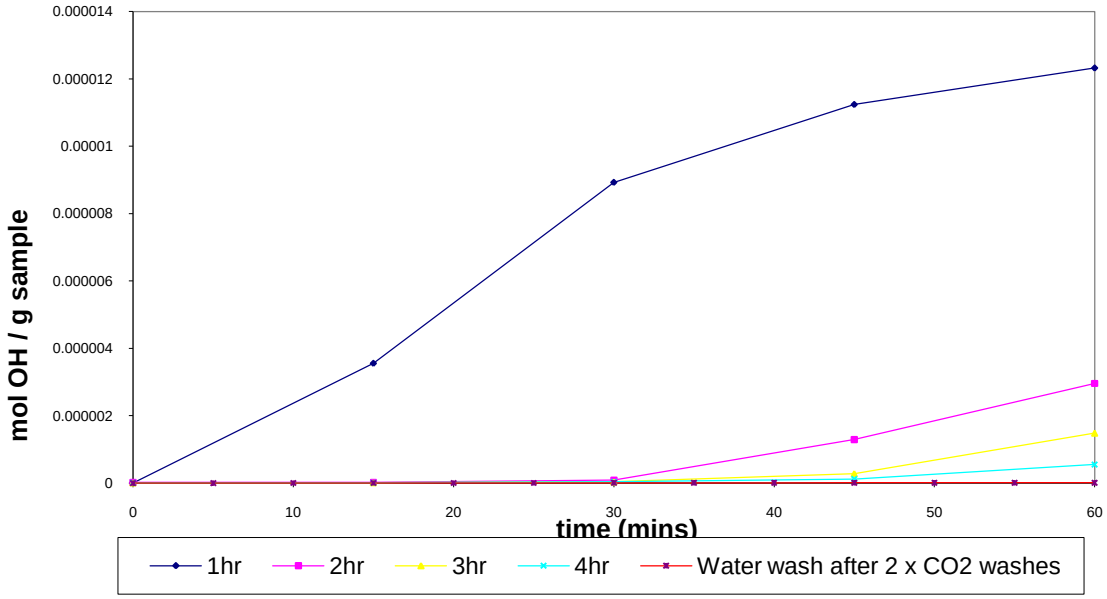

Figure 3-26 – Graph showing number of moles of OH^- in distilled washing water per gram of SCBB sample, as shown in Figure 3-24 above, combined with the number of moles of OH^- in washing water per gram of SCBB sample for a sample having been washed twice in $CO_{2(aq)}$.

Autoclaving SCBB as a means of reducing surface alkaline material

Repeated washing of SCBB with distilled water or washing in $CO_{2(aq)}$ were effective means of reducing surface alkalinity, but their repetitive nature made them time consuming processes. Therefore, as an alternative method the concept of autoclaving SCBB samples to remove surface alkalinity was trialled. The results of autoclaving SCBB are illustrated below in Figure 3-27 with autoclaved samples (samples 7-11, **red** data points) plotted on the same graph as non-autoclaved samples (samples 1-6, **blue** data points).

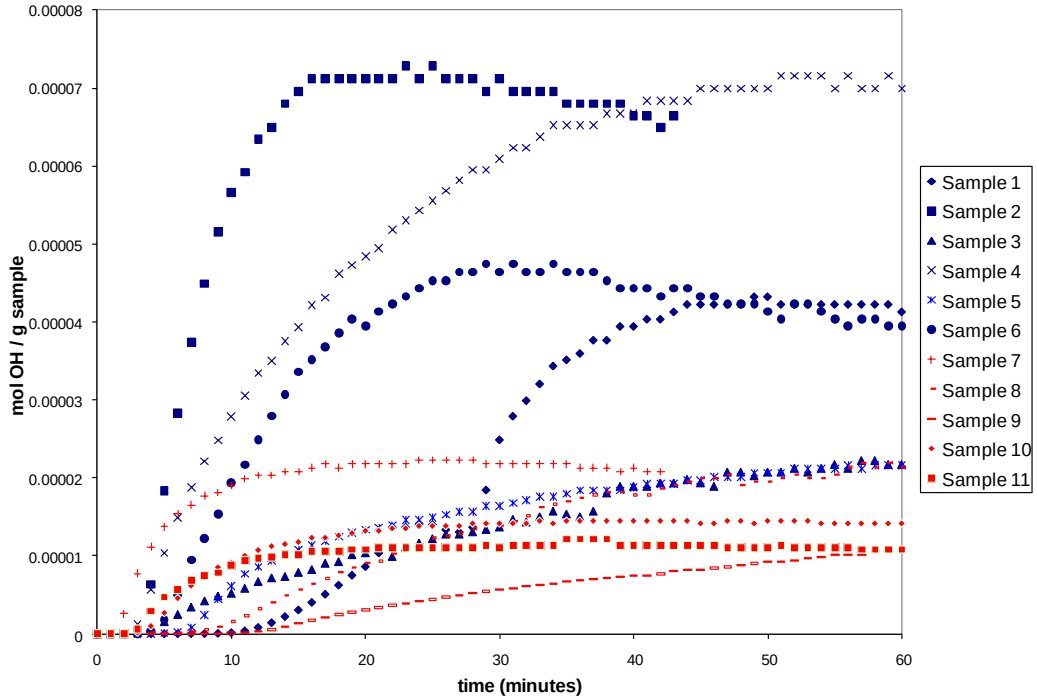

Figure 3-27 – Mol OH^- in 100 mL washing water / weight of sample against time for SCBB samples. SCBB samples 1-6 not autoclaved, SCBB samples 7-11 autoclaved.

These data show that a large variation in mol of OH^- / g sample existed after 60 minutes of washing between different samples (1-6) that had not been autoclaved. Most importantly, it was also apparent that non-autoclaved SCBB samples exhibited a higher level of available alkalinity to the washing water on average than autoclaved SCBB samples, as summarised in Figure 3-28 where error bars displayed are equivalent to 1 standard deviation.

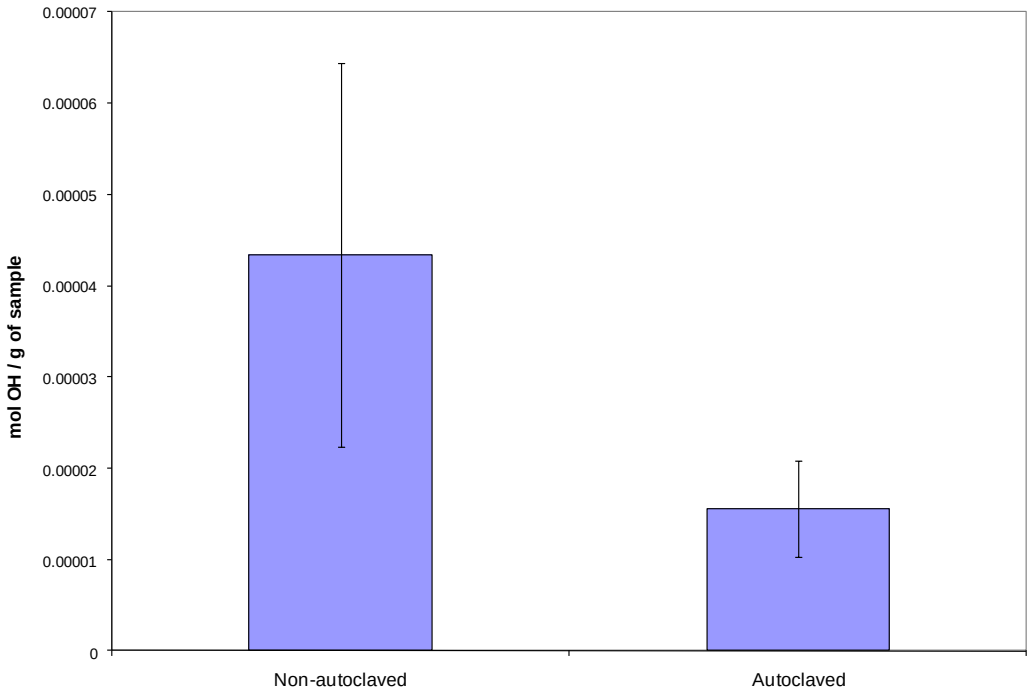

Figure 3-28 – Average mol OH^- in 100 mL washing water / gram of sample corresponding to autoclave treatment, or non autoclave. Error bars equal 1 standard deviation for the respective samples.

The autoclave method for removing alkalinity from SCBB samples proved to be effective especially when considering the short period of implementation (30 minutes), yielding samples with consistent (smaller standard deviation compared to non-autoclaved sintered bone) and generally lower levels of OH^- than non-autoclaved SCBB. However, the process of washing in distilled water allowed constant pH monitoring, making it a more informative method during experimentation, and with that, a preferred method. Nevertheless, it is believed that this result does not preclude the autoclaving method from having the potential to be useful in a commercial context.

3.6 Conclusion

Ultimately, two methods of cutting raw cancellous bovine bone into shapes were employed. The lapidary saw method was suitable for cutting bone into precise angular shapes, while the band saw method provided a rapid method for the mass production of samples with appropriate dimensions for experimental work.

Autoclaving proved to be effective in removing fat and protein from the cut pieces of bone, with sintering at 1000°C for 3 hours removing the remaining organic material. The SCBB material was shown by pycnometry and SEM to vary in both porosity and density from sample to sample, while also retaining the trabecular architecture of the original bone. XRD showed the SCBB material to consist predominantly of hydroxyapatite while also confirming the presence of CaO in the SCBB material seen by other researchers. The presence of a soluble alkaline material was established by washing in distilled water, and this was seen to be reduced by repeated washes in distilled water, or in the weak acid, $CO_{2(aq)}$.

CHAPTER FOUR

4 Infiltrating Solutions and Infiltration Methodology

4.1 Introduction

When developing an infiltrating liquid, the choice of components is dependent on the solubility and the physical properties necessary to allow the solution to penetrate into the desired regions within the SCBB. Chitosan containing solutions described in the following sections were developed with these considerations in mind. The concentration of solutes in infiltrating solutions containing calcium phosphate was largely dependent on their solubility in combination with chitosan. A summary table of the infiltration solutions displaying their constituents and sample name is presented at the end of section 4.3.8 in this methods chapter. Immobilisation of chitosan infiltrate materials where mentioned, if not otherwise stated, was performed by exposure to $NH_{3(g)}$ as described in section 5.3.3.

4.2 Materials

Materials were used as received and included: BDH Analar 36 % w / w HCl; Fluka low viscous chitosan; Fluka "hydroxylapatite", Assay ≥ 90 %; BDH Laboratory Reagents Calcium hydrogen orthophosphate ($CaHPO_4$) Min assay (ex calcium) 95 %; Aldrich Polycaprolactone, FW 114.1, mp 60 C, d1.145 Typical Mn 10,000 (GPC) Typical Mw 14,000, Tg = -60.0 C; BDH Tetrahydrofuran (THF); Wako Pure Chemicals, Osaka, Japan, Genipin.

4.3 Methods

4.3.1 Chitosan in hydrochloric acid (chitosonium chloride)

To prepare 10 g L^{-1} (1 % w / v) chitosan in HCl, 2.5 g of Fluka "low viscosity" chitosan was placed in a beaker (equipped with a mechanical stirrer) containing 230 mL of distilled water and rapidly stirred. A calibrated pH electrode was positioned and clamped in the stirred liquid to monitor pH. Approximately 2 mL of concentrated HCl was placed in a pre-weighed glass vial with lid and then weighed. While the chitosan and water were stirred vigorously, conc. HCl was added drop wise while the degree of chitosan dissolution was visually monitored along with the pH of the solution. When all chitosan had dissolved, addition of HCl was ceased and the volume of water made up to 250 ml. The weight of conc. HCl added to the solution was calculated by weighing the remaining conc. HCl in the vial and taking the difference from the starting weight. If the pH of the resultant solution was found to be < 4, it was adjusted to above pH 4 by dropwise addition of 0.1 mol L^{-1} NaOH solution.

4.3.2 Preparation of chitosan / HAp (or $CaHPO_4$) in hydrochloric acid

230 mL distilled water was placed in a 500 mL beaker and stirred rapidly. A calibrated pH electrode was introduced into the stirred water and clamped in position. 1.5 g HAp (6 g L^{-1}) was introduced in one addition into the stirred distilled water. Conc. HCl was added drop-wise to the stirred mixture until all HAp had dissolved. The pH at this point was commonly between 1 and 2. Next, 1.5 g Fluka low viscosity chitosan (6 g L^{-1}) was introduced slowly to the rapidly stirred solution with strict monitoring of the pH. When pH approached 3, a drop of conc. HCl was added to reduce pH. When pH had stabilized more chitosan was added. This process was repeated until all chitosan had been added and dissolved. 0.1 mol L^{-1} NaOH was then added drop-wise with rapid stirring to raise pH to the desired value between 4 and 4.5. It was found that this procedure prevented premature precipitation of calcium phosphate during the increase in pH that was otherwise seen to occur with the

addition of chitosan. During the slow dropwise addition of 0.1 mol L^{-1} NaOH into the rapidly stirred solution stringy white strands of material, which were likely to be chitosan, were seen to precipitate at the point of contact. However, these rapidly re-dissolved with continued stirring.

4.3.3 Preparation of chitosan, and chitosan / calcium phosphate suspensions

Solutions of chitosan, or chitosan and a calcium phosphate (HAp or $CaHPO_4$) were prepared similarly to those solutions above in sections 4.3.1 and 4.3.2., except that in some cases solutions were made up to 30 g L^{-1} (3 % w / v) chitosan. To these mechanically stirred solutions, 0.1 mol L^{-1} NaOH solution was added in a dropwise fashion causing uniform precipitation of chitosan, or chitosan and calcium phosphate. pH was monitored throughout with 0.1 mol L^{-1} NaOH solution being added until pH reached 7.4, which is physiological pH. This suspension was either used immediately for infiltration or stored at 4°C until required.

4.3.4 Chitosan solutions with urea

Solutions of chitosan and chitosan / calcium phosphate as prepared in sections 4.3.1 and 4.3.2 above with pH values between 4 and 4.5 were used to prepare solutions in combination with urea. From the weight of acid added to the solutions, the number of moles of acid were calculated, and subsequently, the same number of moles of urea where added to the solution. For example, 0.5080 g of Fluka low viscosity chitosan was sprinkled into 50 mL rapidly stirred distilled water. 0.2926 g conc. HCl was required to dissolve all the chitosan, which equated to 0.002887 mol HCl in 50 mL. Therefore, 0.002887 mol of urea was added to the solution, which equated to 0.1734 g urea. The theoretical stoichiometry required to neutralise the acid using urea is shown in reaction Equation 2 and Equation 3 over the page.

Equation 2 $H_2NCONH_{2(aq)} + H_2O_{(l)} \rightarrow CO_{2(aq)} + 2NH_{3(aq)}$

Equation 3 $NH_{3(aq)} + HCl_{(aq)} \rightarrow NH_4Cl_{(aq)}$

A calculation of a chitosan solution with urea showing concentrations is given in Appendix B.

4.3.5 Chitosan solutions with urea and urease

Solutions of chitosan or chitosan / calcium phosphate containing urea were prepared as described above in section 4.3.4. Urease was prepared for addition to the infiltrating solutions by dissolving in degassed distilled water at the concentration of 3.0 mg urease in 0.5 mL degassed distilled water. This quantity of urease dissolved in water was added to 50 mL chitosan solution containing 0.15 – 0.20 g urea.

4.3.6 Chitosan solutions with genipin as a crosslinker

Two genipin containing infiltrating solutions were prepared. The first was a high genipin composition solution used as an infiltrate in SCBB samples that were later mechanically tested. The other contained less genipin and was used to examine the effectiveness of low concentrations of genipin to immobilise chitosan. The chitosan / $CaHPO_4$ / genipin composite infiltrate material infiltrated into SCBB for mechanical testing (see section 6.2) contained a higher proportion of genipin. Here a chitosan / $CaHPO_4$ in HCl solution was generated according to the method described above in section 4.3.2 and genipin dissolved in EtOH added as described directly above. Weight of each constituent were: chitosan 25 g L^{-1} (2.5 % w / v), $CaHPO_4$ 5 g L^{-1} (0.5 % w / v), and genipin 10 g L^{-1} (1 % w / v).

To prepare 50 mL of 0.05 g L^{-1} (0.5 % genipin to chitosan w / w) solution from a chitosan at 10 g L^{-1} (1 % w / v) solution, 0.0025 g of genipin was weighed into a vial

and then dissolved in a small volume of 95 % EtOH (commonly 0.5 mL). The chitosan solution was placed in a round bottom flask along with boiling chips and attached to a vacuum line with a liquid nitrogen trap in order to evaporate the EtOH out of the solution. This process also served to degas the chitosan solution of oxygen, which was important as oxygen promotes a competing radical initiated self-polymerisation reaction in genipin [125].

4.3.7 Preparation of PCL solutions in THF as a solvent

By contrast to the preparation and manipulation of chitosan solutions, the preparation and use of PCL infiltrating solution was relatively simple. Solutions of PCL in THF were prepared by weighing the desired quantity of Aldrich polycaprolactone (PCL), and dissolving in stirred THF. The THF was sourced from BDH Chemicals, and contained the peroxide formation inhibitor butylated hydroxytoluene (BHT). This inhibitor can be removed by distillation but was not done in this case as this experiment was a conceptual test of infiltration and mechanical strength of the infiltrated SCBB material, and not of biocompatibility. If the concept of infiltrating PCL into SCBB was to be carried further to the point of implantation, it would be preferable to use BHT free THF.

As an example of the preparation of a 14 % w / v PCL in THF solution, 7.010 g PCL was added to 50 mL of rapidly stirred THF in a 200 mL beaker. PCL dissolved rapidly to produce a solution of higher viscosity than the neat solvent, which was stored in a fridge at 4°C until required.

4.3.8 Nomenclature of infiltrating solutions

Table 1 – Summary of infiltrate solutions prepared and the concentration of their constituents

Material	**Sample name**	**Constituents**	**pH**
chitosan (1 % w / v) in hydrochloric acid (chitosonium chloride)	Infil-1	10 g L^{-1} chitosan, HCl	4.0 - 4.5
chitosan / HAp in hydrochloric acid	Infil-2	6 g L^{-1} chitosan, 6 g L^{-1} HAp, HCl	4.0 - 4.5
chitosan / $CaHPO_4$ in hydrochloric acid	Infil-3	10 g L^{-1} chitosan, 6 g L^{-1} $CaHPO_4$, HCl	4.0 - 4.5
chitosan / $CaHPO_4$ in hydrochloric acid	Infil-4	25 g L^{-1} chitosan, 5 g L^{-1} $CaHPO_4$, HCl	4.0 - 4.5
chitosan suspension	Infil-5	10 - 30 g L^{-1} chitosan, HCl	7.4
chitosan / calcium phosphate suspension	Infil-6	6 g L^{-1} chitosan, 6 g L^{-1} HAp, HCl	7.4
chitosan solutions with urea	Infil-7	Infil-1, Infil-2 and Infil-3 with 1.7 g L^{-1} urea	4.0 - 4.5
chitosan solutions with urea and urease	Infil-8	Infil-6 with 50 mg L^{-1} urease	4.0 - 4.5
chitosan with genipin as a crosslinker (low concentration)	Infil-10	Infil-1, Infil-2, or Infil-3 with 0.05 g L^{-1} genipin	4.0 - 4.5
chitosan with genipin as a crosslinker (high concentration)	Infil-11	Infil-4 with 10 g L^{-1} genipin	4.0 - 4.5
PCL in THF	Infil-12	100 g L^{-1} PCL	n/a
PCL in THF	Infil-13	140 g L^{-1} PCL	n/a

4.3.9 Labelling of chitosan with fluorescein isothiocyanate (FITC)

Fluka low viscous chitosan was labelled with the fluorescent molecule fluorescein isothiocyanate (FITC) based on the method described by Qaqish and Amiji [126]. 2.5 g of chitosan was dissolved in 250 mL water with 1.5030 g concentrated acetic acid (to produce approximately 0.1 mol L^{-1} acetic acid). To this solution was added 250 mL methanol and to this was added 0.0021 g FITC having previously been dissolved in approximately 1 mL methanol. The solution was stirred for 30 minutes and then allowed to stand for two hours. 250 mL 0.1 mol L^{-1} NaOH was added to the solution with stirring to induce precipitation of the solid. The fluorescently labelled chitosan precipitate that formed was filtered over a Buchner funnel and washed with copious quantities of distilled water and allowed to dry. The reaction scheme of this reaction is shown in Figure 4-1 over the page.

To ensure that fluorescence seen after the labelled material had been infiltrated was not due to the presence of unreacted FITC, the FITC labelled chitosan was subjected to a purification procedure before use. 1 g of the FITC labelled chitosan precipitate was redissolved in 100 mL water with 0.7993 g conc. HCl. When all chitosan had been dissolved to form a solution at pH 1.35, 1 mol L^{-1} $NaOH_{(aq)}$ was added until all solid had precipitated at a pH of ~ 9.5. The solid was filtered from the liquid over a Buchner funnel and the liquid collected to be run on a Cary 300 UV-Vis spectrometer to evaluate for the presence of free FITC. The precipitate was subsequently washed 4 times with 100 mL distilled water, once with 100 mL 0.1 mol L^{-1} NaOH and then once again with 100 mL distilled water. The washing liquid was collected each time and analysed on a Cary 300 UV-Vis at 479 nm. Appendix C presents experimental evidence, which demonstrates that fluorescence seen in infiltrated SCBB samples could not be attributed to the presence of free unreacted FITC.

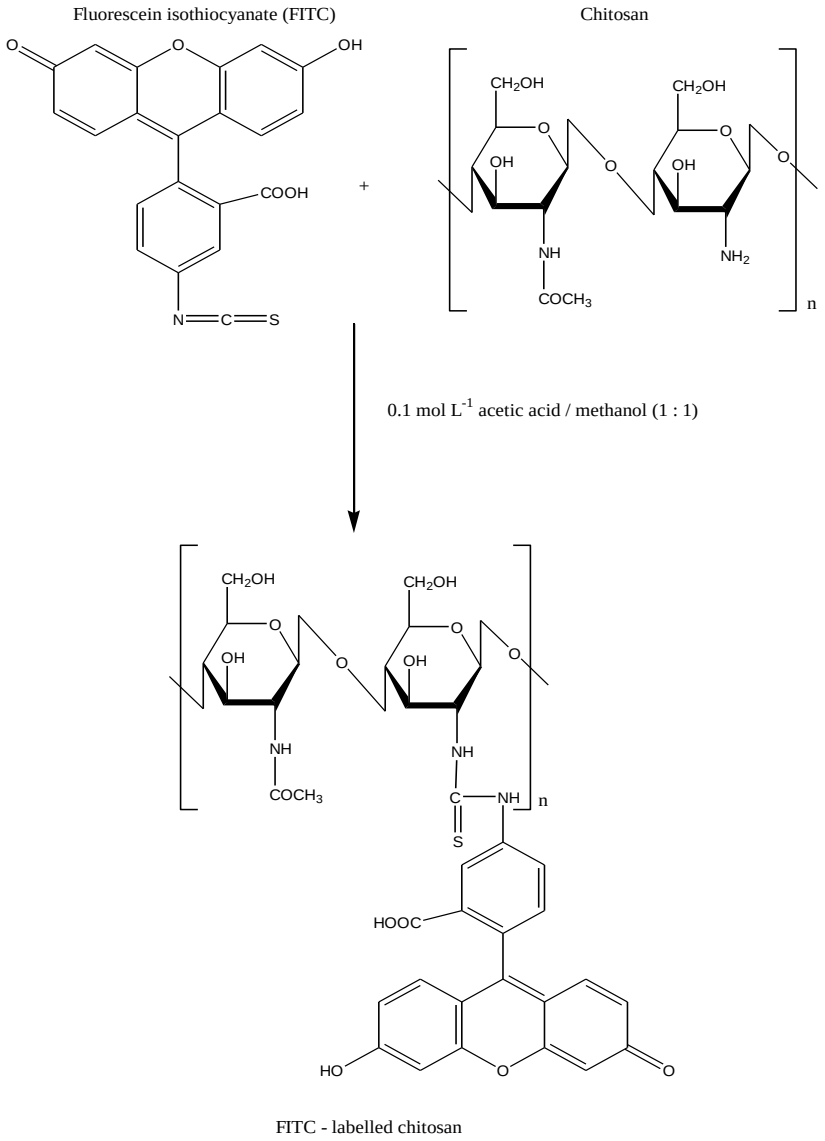

Figure 4-1 – Reaction scheme of the reaction between chitosan and FITC.

4.3.10 Fluorescence microscopy

After infiltration with fluorescently labelled chitosan, samples were prepared by sectioning and then scraping the cut surface of the infiltrated SCBB with a scalpel over a glass microscope slide to collect the small fragments that broke free. Samples were examined on a Leica DML fluorescence microscope running a 50 Watt mercury arc lamp. For fluorescence images, samples were illuminated using a Leica I3 blue filter / reflector system (excitation filter BP 450-490 nm), with a HC PL FLUOTAR 10x / 0.30 objective lens. An initial image showing the position and size of the

fragments was captured by illuminating the sample from above (or below) with an incandescent light source. Digital photographs were taken of all fluorescence images at a 1/5 second exposure time and a digital sensitivity of ISO 1600. Fluorescence intensity and dispersion throughout the SCBB samples was visually compared against examples of samples having been infiltrated with FITC labelled chitosan.

4.4 Infiltration Methods

4.4.1 Vacuum only infiltration

Method A

Cylindrically shaped SCBB samples of the approximate dimensions, 10 mm height x 10 mm diameter, were placed in a vacuum tube with a glass marble placed on top to prevent the samples from floating. An infiltrate solution or suspension was added on top of the SCBB samples in sufficient volume to maintain coverage of the samples after the completion of infiltration, as shown in Figure 4-2. Vacuum produced by a Burkret Heavy Duty vacuum pump was applied through a vacuum line measured by a Thyracont (VD84M) digital Pirani vacuum gauge to produce pressure as low as 0.001 atm. Upon exposure to vacuum, bubbles of gas were seen immediately to expand and evolve from the macropores of the samples. Vacuum was maintained for 10 minutes until a few bubbles were seen occasionally to depart from the samples; the vacuum tube containing the samples was periodically flicked or tapped with a finger to promote the detachment of gas bubbles from within the porous SCBB material. After 10 minutes the vacuum was released slowly allowing the infiltrating solution and the samples to return to atmospheric pressure, which had the effect of forcing the infiltrate into the pores of the SCBB. After a pause of 10-30 seconds, vacuum was reapplied to the infiltrating solution and the samples for another 10 minutes. This process of applying vacuum to the system and releasing was repeated a total of three times over 30 minutes. After the last cycle, the infiltrated SCBB sample was removed by tweezers from the vacuum tube and processed further according to specified goal of the experiment. Depending on the material/s used in the infiltration, this processing

step could be repeated multiple times allowing an accumulation of infiltrate within the SCBB.

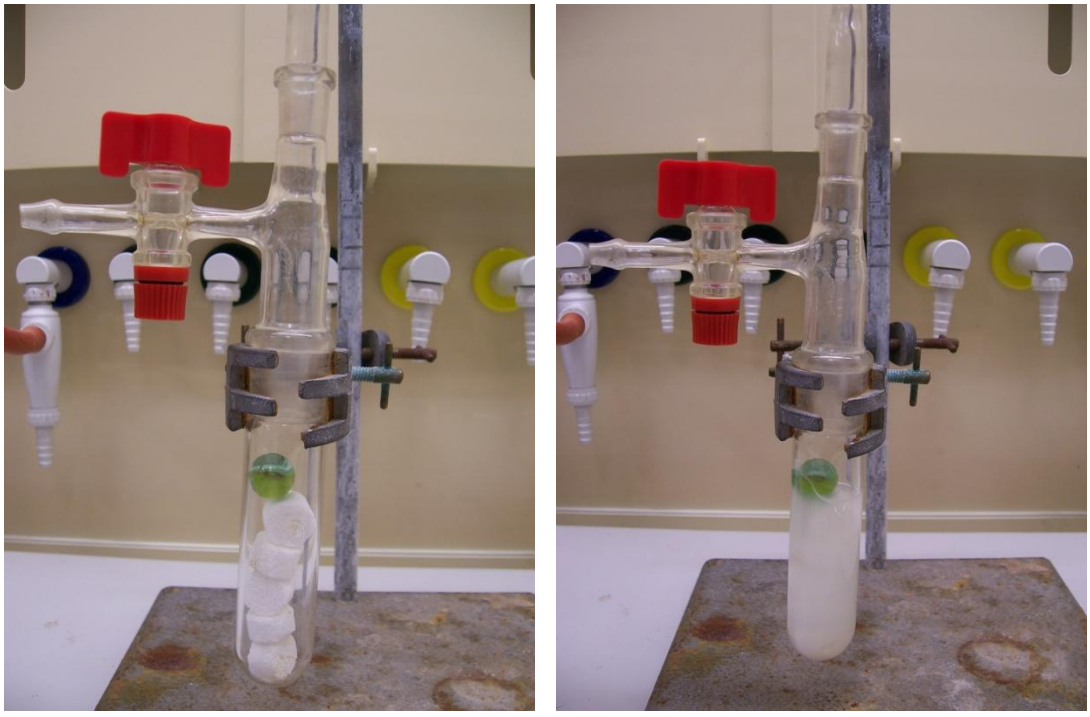

a) b)

Figure 4-2 – Photographs showing infiltration apparatus with a) marble placed on top of SCBB samples preventing them from floating in the infiltrating solution b).

Method B

SCBB samples were placed in a specifically designed and manufactured length of glass vacuum tubing produced to act as an infiltration vessel. The internal diameter of the tube was slightly larger than the diameter of the samples themselves, and a Quikfit attachment at the top of the tube allowed connection to a feed vessel as shown opposite in Figure 4-3. The infiltration feed vessel was constructed with a tube allowing connection to a vacuum pump, with a stopcock to shut off vacuum from the system. Meanwhile, a stopcock between the feed vessel above and infiltration vessel below provided a means of isolating the two vessels for the application of vacuum to the SCBB samples alone. Samples were placed inside the infiltration tube, and vacuum applied via a Burkret Heavy Duty vacuum pump for 2 hours. Towards the end of this 2 hour period, the infiltrating solution was degassed by being placed in a

round bottom flask with boiling chips in the bottom, and subjected to vacuum for *ca.* 15 minutes, until no more bubbles of gas were seen to evolve from the solution.

Before the degassed infiltrating solution was poured into the feed vessel, the stopcock to the vacuum pump was closed and the stopcock to the feed vessel opened returning the infiltration vessel to atmospheric pressure. The stopcock to the feed vessel was then closed and the infiltrating solution poured into the feed vessel, with the stopcock then being opened slightly to allow liquid to flow into the space created by the tube of the stopcock. When the space within the stopcock was full with liquid, it was closed and the stopcock to the vacuum pump reopened. This procedure was undertaken to remove the volume of air within the stopcock, which would have otherwise reduce the vacuum created within the infiltration vessel when the stopcock was opened. Vacuum was allowed to build within the infiltration vessel for 15 minutes and then the stopcock to the vacuum tube was closed and the stopcock to the infiltrating solution immediately opened. The liquid was thus allowed to infiltrate into the SCBB samples, with the apparatus being left in this condition for a further 15 minutes.

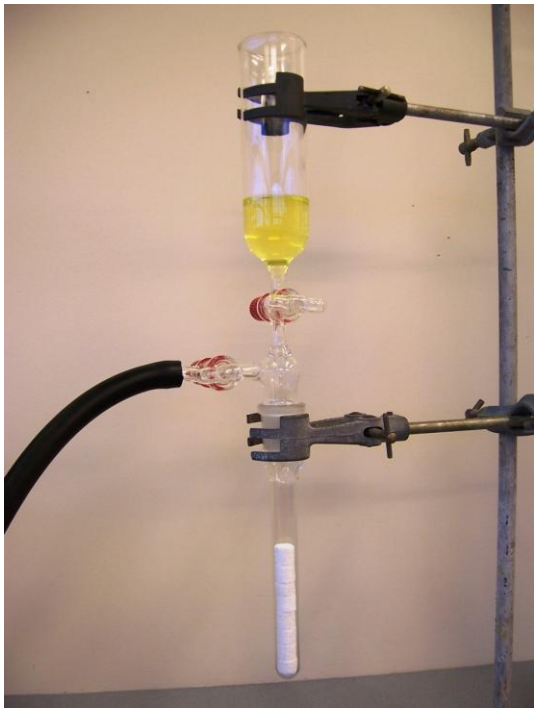

Figure 4-3 - Vacuum vessel containing SCBB samples with feed vessel and connecting vacuum tube positioned above, (Method B).

4.4.2 Vacuum and pressure infiltration

A working concept for a hydrostatic pressure vessel capable of creating and withstanding 200 atm of pressure was developed in cooperation with Nick Jarman of Tamaterau Engineering Ltd., Whangarei, NZ. Once optimised, the design was built by Tamaterau Engineering Ltd and delivered to the University of Waikato, a computer aided design (CAD) image of which is shown below in Figure 4-4. The device was designed and built around the concept of a piston with sealing o-ring inside a cylinder, so that the application of force along the main axis of the piston and cylinder would induce a pressure within the chamber. A release port was built into the design through the piston, which allowed the release of trapped air and excess infiltrating liquid when the piston was inserted into the cylinder. The port was shut off by a Swagelok bleed valve rated to 275 bar pressure at 37°C. Figure 4-5 shows the external appearance of the device.

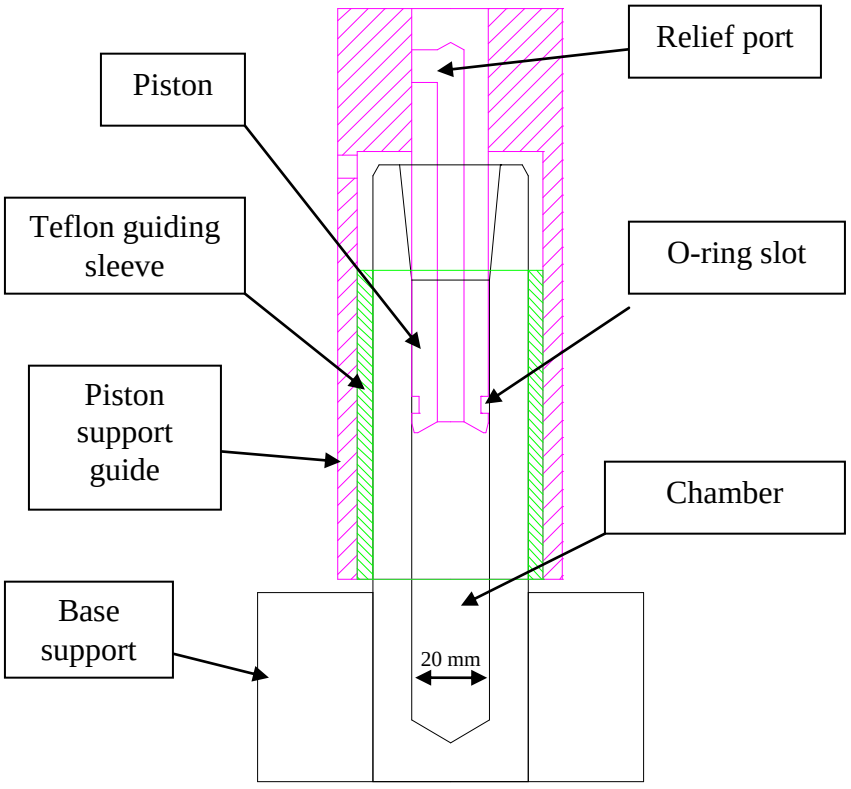

Figure 4-4 – Cut-away view of hydrostatic pressure device.

Figure 4-5 - Hydrostatic pressure vessel rated to 200 atm.

Method of use

Samples were placed into the stainless steel pressure vessel and the feed vessel containing a degassed infiltrate was inserted into the tapered stainless steel pressure vessel as shown in figure 4-6. Vacuum was applied to the pressure vessel through the attached vacuum tubing for 2 hours, the stopcock shut off and then the infiltrate liquid allowed to flow in. The feed vessel was removed and the pressure piston gradually inserted into the pressure vessel, with the valve open allowing air and then infiltrating liquid to escape until the piston was positioned 1 – 2 cm above the top most sample within the pressure vessel. The valve was then shut, at which stage the device was ready. The complete pressure device was then placed under a Lloyd LR 30K Materials Testing Machine and force was applied to induce the required internal pressure as shown in Figure 4-7 over the page.

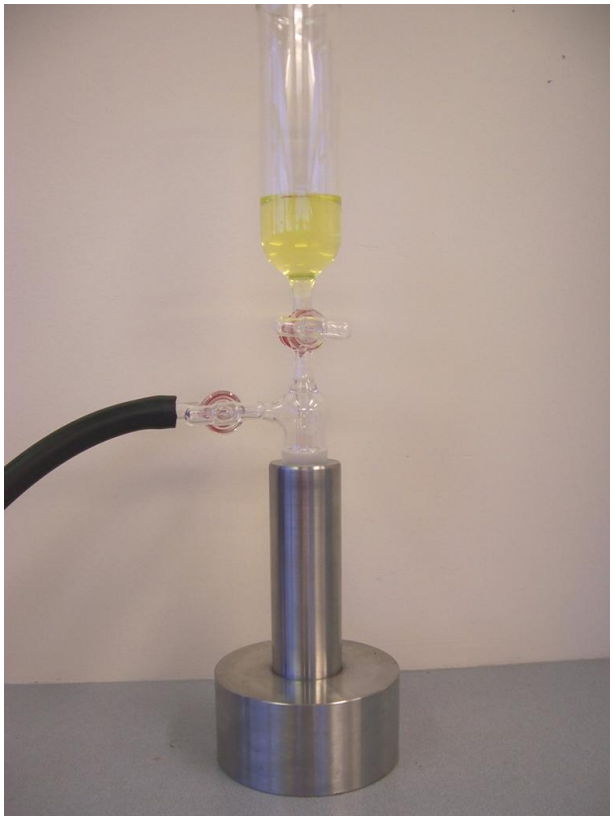

Figure 4-6 - Stainless steel pressure vessel with infiltrate feed vessel inserted above.

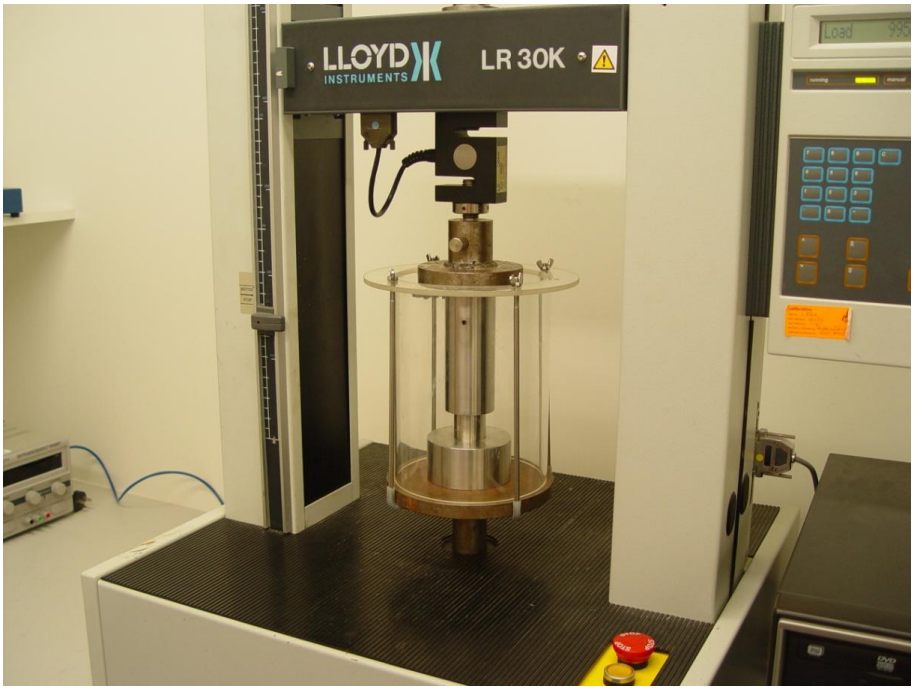

Figure 4-7 - Hydrostatic pressure device positioned between cross-arm and stage on an LR 30K Lloyd Instruments Materials Testing Machine.

The pressure device had an internal diameter of 20 mm, which resulted in the force to internal pressure relationship as shown below in Table 2.

Table 2 –Forces required to be exerted by the Lloyd Materials Testing Machine in order to generate specific pressures within the pressure device.

Force (N)	Pressure (Atm)
32	1
318	10
1592	50
3183	100

Force was exerted on the piston of the pressure device through the Lloyd Materials Testing Instrument and increased in a step-wise fashion, an example of which is shown below in Figure 4-8.

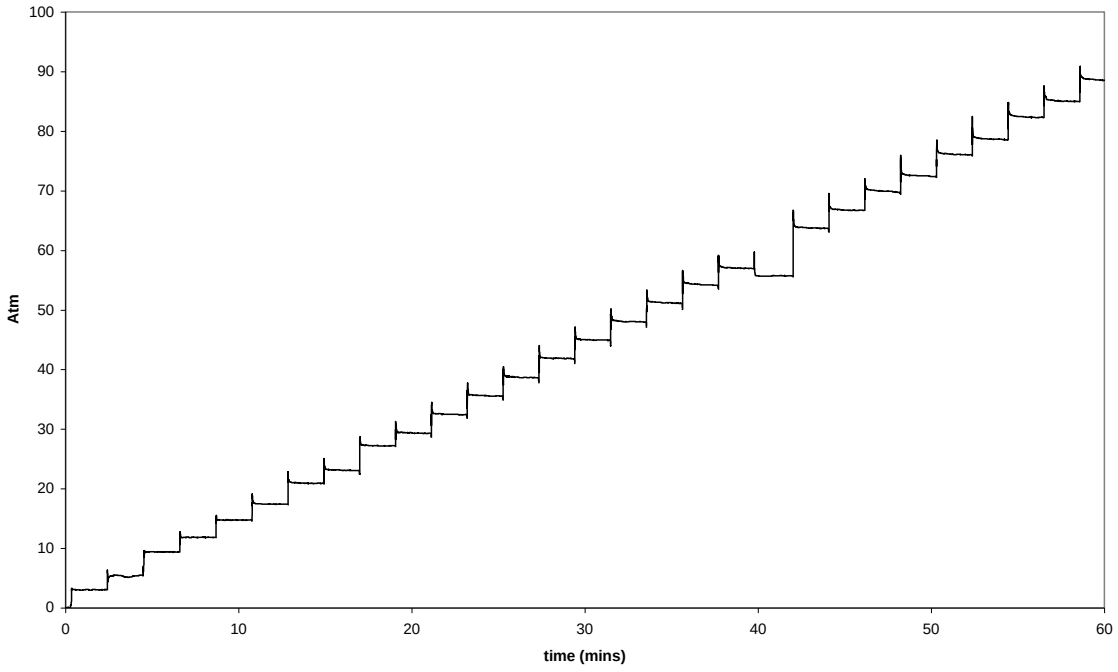

Figure 4-8 – Pressure ramping profile using small increments.

4.4.3 Pressure only infiltration

In pressure only infiltration, vacuum was not employed in the infiltration process. Samples were placed in the pressure vessel and the degassed infiltrate was poured in from above. The piston was inserted and the device was placed in a Lloyd LR 30K Materials Testing Machine as shown in Figure 4-7. Pressures up to ~ 90 atm were induced by subjecting the hydrostatic pressure device to up to 3000 N force.

4.4.4 Infiltration of FITC labelled chitosan / HAp into a pre-infiltrated SCBB sample

An obstacle to infiltrating a material into the microporous structure of the SCBB with repeated infiltration steps was the formation of a layer of infiltrate lying on the surface of the microporous material forming a barrier to further penetration. To examine this problem, a SCBB sample was infiltrated with Infil-3 solution (non-FITC labelled chitosan and HAp in HCl) under vacuum. The sample was then exposed to $NH_{3(g)}$ overnight to immobilise the chitosan and make its re-solubilisation in a subsequent infiltrating solution a slower process than a non-immobilised chitosan infiltrate (which would still be in the chitosonium chloride soluble state). After chitosan immobilisation, the infiltrated SCBB sample was washed in a copious quantity of distilled water (2L) for 42 hours, after which it was allowed to dry on the bench top for several days. Subsequently, the sample was infiltrated under vacuum with FITC labelled chitosan / HAp, allowed to dry and examined under fluorescence microscope, the method of which is described in section 4.3.10.

4.4.5 Infiltration of FITC labelled chitosan/HAp by vacuum and pressure, and pressure alone into pre-infiltrated SCBB.

Samples of SCBB were initially infiltrated under vacuum with degassed Infil-3 solution (6 g L^{-1} chitosan (non FITC labelled)/ 6 g L^{-1} HAp at pH 4.5). Samples were allowed to dry in the open atmosphere for 48 hours causing the infiltrate to deposit but were <u>not</u> treated with $NH_{3(g)}$ to immobilise (cf. section 4.4.4 above). Effectively,

this maintained the infiltrate in a soluble state; at least it maintained the chitosan as chitosonium chloride, which is soluble. The second infiltration was undertaken with degassed FITC labelled chitosan at the standard concentration of 6 g L^{-1} and HAp 6 g L^{-1} in HCl at pH = 4.5. Samples infiltrated under a vacuum / pressure procedure, were subjected to vacuum for 1 hour before the degassed infiltrate liquid was allowed to flow into the porous structure. Samples infiltrated under a pressure only procedure were then added to the pressure vessel containing the degassed infiltrate liquid. All samples were left to stand in the infiltrate liquid for 1 hour before being subjected to pressure ramped at ~ 30 atm for 15 minutes, ~ 60 atm for 15 minutes, then ~ 90 atm for 30 minutes. After being allowed to dry for several days, samples were prepared and examined by fluorescence microscopy.

4.5 Results and Discussion

4.5.1 Infiltration

Samples infiltrated under vacuum alone

When SEM images of samples that had been infiltrated with chitosan solutions under vacuum were inspected, infiltrate material was always observed to have been distributed throughout the entire macroporous structure of the SCBB. The infiltrate was identifiable as a layer of material lying on the surface of the microporous architecture as shown to the right of the SEM image in Figure 4-9. On closer examination of the microporous structure to the left in the image, it was seen that the topography was altered from that of non-infiltrated SCBB microporous structure as shown in Figure 4-10, cf. Figure 3-15 and Figure 4-11. A “blurred” appearance suggested the presence of additional material attributed to be infiltrate, and later proven to be so by fluorescence labelling of the chitosan infiltrate, see section 4.5.5.

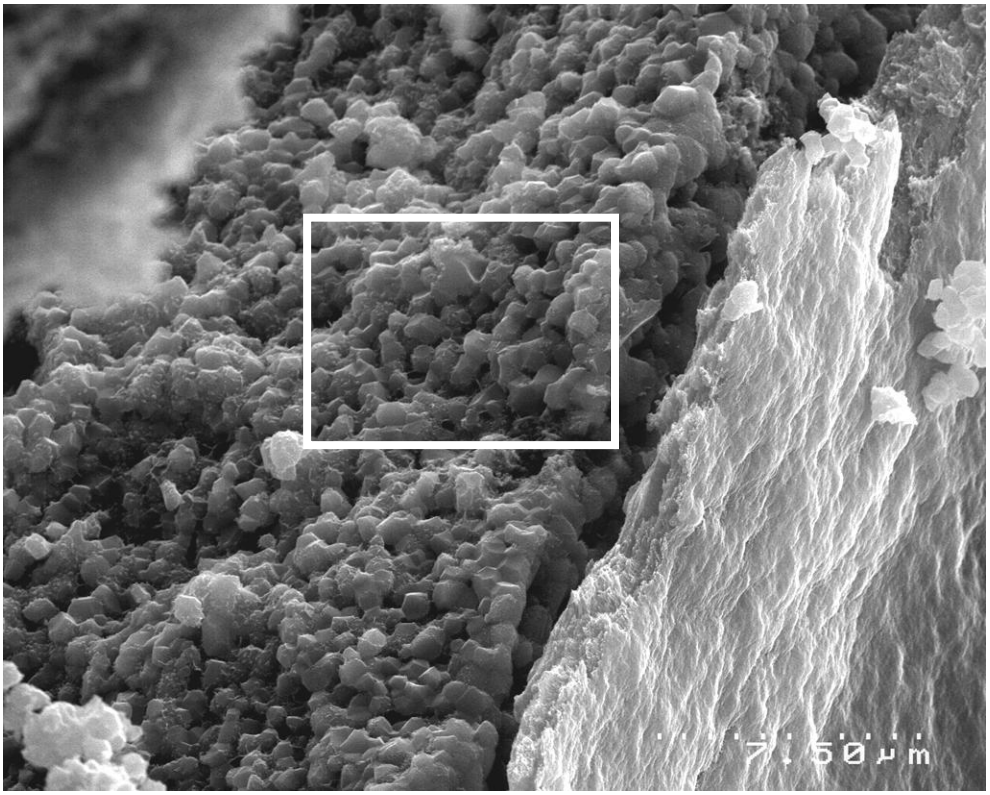

Figure 4-9 – SEM image showing a layer of chitosan / CaP infiltrate on the surface of the microporous structure after infiltration with Infil-4.

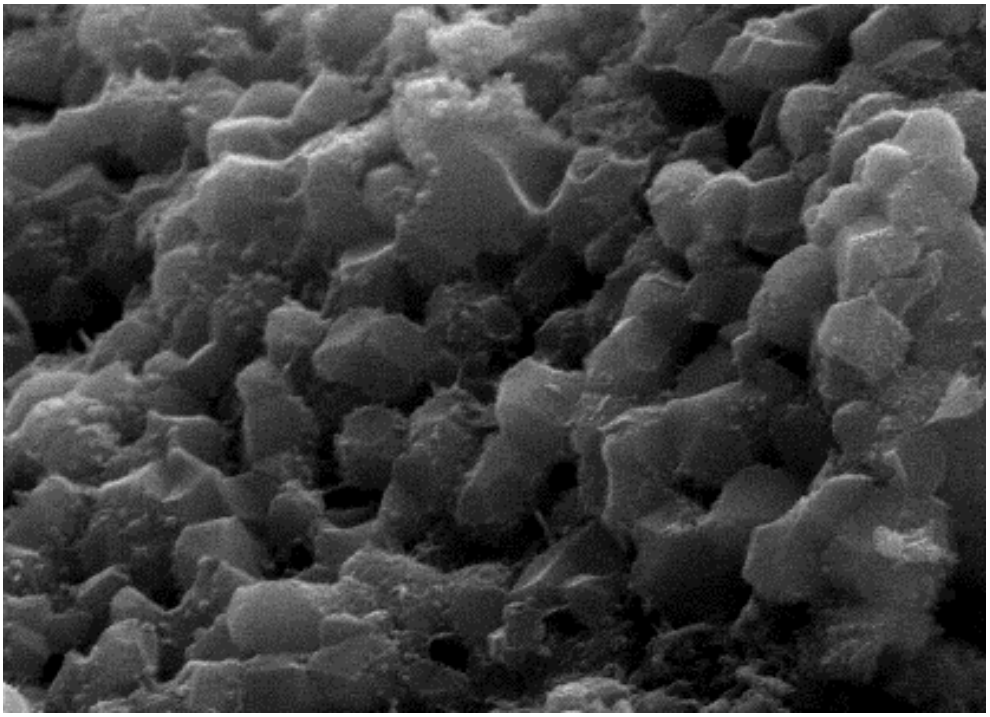

Figure 4-10 – SEM image showing a zoomed in view of the area within by the white box in Figure 4-9 above.

Further exploration of the broken exposed surface of the SCBB microporous structure after infiltration by vacuum alone, showed an inconsistent distribution of the "blurred" appearance throughout the microporous structure, but when it was seen, it was generally near the overlying infiltrate layer, and not deep within the SCBB microporous structure.

The appearance of the infiltrated material in Figure 4-9 and Figure 4-10 contrasted well with SEM images of SCBB samples infiltrated with chitosan suspensions and chitosan / HAp suspensions, which showed no 'foreign' material within the microporous structure of the SCBB. Instead, a layer of infiltrate was seen only to be deposited on the surface of the SCBB microporous structure as shown below in Figure 4-11 and Figure 4-12, which show SCBB infiltrated with Infil-5 and Infil-6 respectively (see Table 1, p. 72).

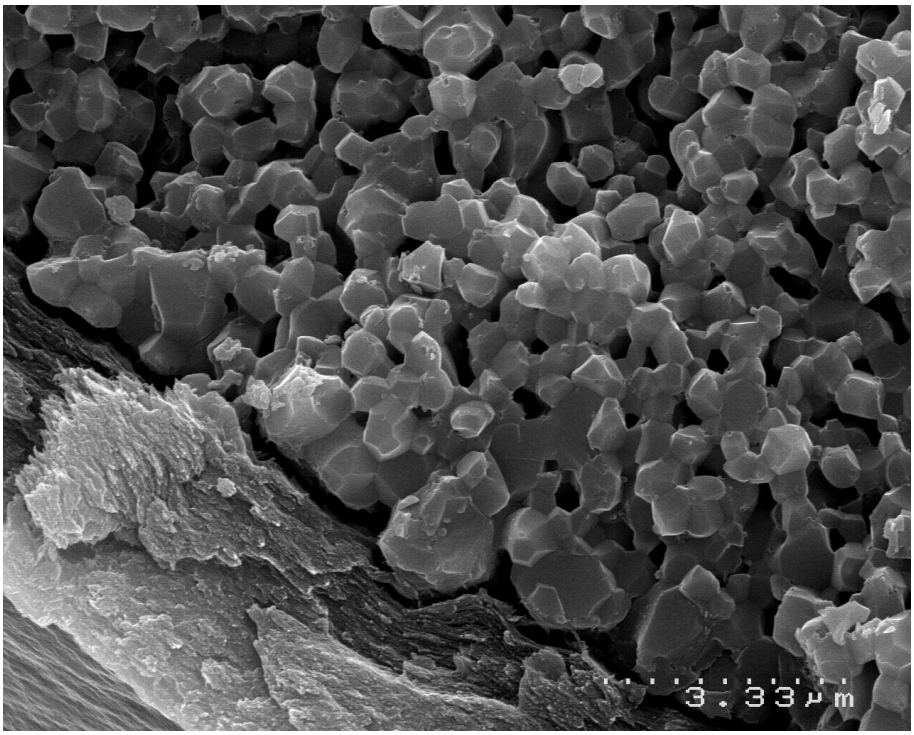

Figure 4-11 – SEM image showing broken exposed surface of SCBB microporous structure after infiltration with Infil-5 (chitosan suspension) under vacuum. No infiltrate material was seen within the microporous structure, cf. Figure 4-9 and Figure 4-10 above.

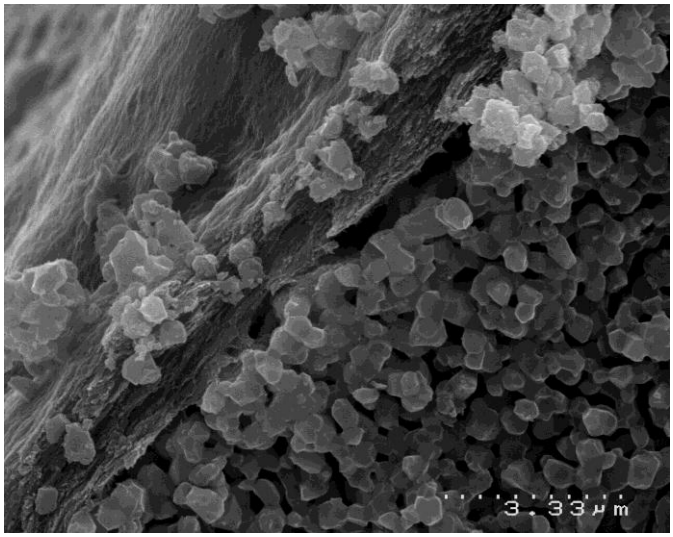

Figure 4-12 - SEM image showing broken exposed surface of SCBB microporous structure after infiltration with Infil-6 (chitosan / HAp suspension) under vacuum. No infiltrate material was seen within the microporous structure, cf. Figure 4-9 and Figure 4-10 above.

SEM images did however reveal that vacuum infiltration was sufficient to distribute chitosan based infiltrates (as solutions or as suspensions) throughout the entire macroporous structure as the layering was observed consistently throughout the SCBB material. This effect is evident below in Figure 4-13, which shows a broken fragment of infiltrated SCBB with the smooth surface of the infiltrate interspersed with areas of bare microporous SCBB revealed as a result of breaking trabeculae during sample preparation.

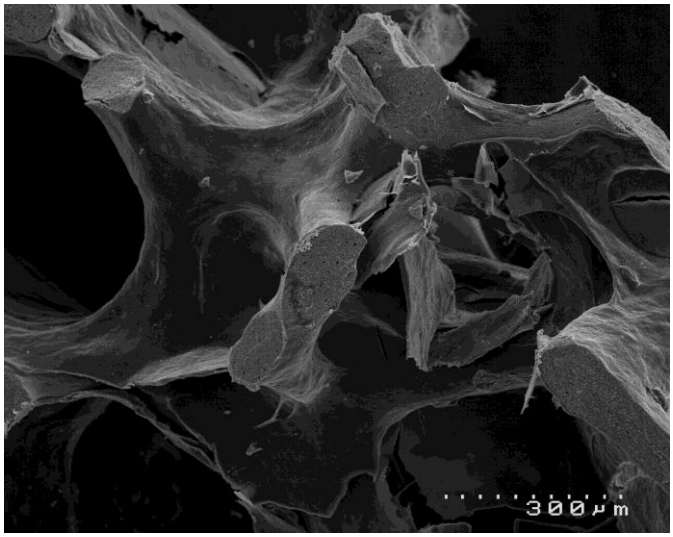

Figure 4-13 – SEM image of a portion of SCBB infiltrated with a suspension of chitosan removed from the centre of a ~ 10 mm diameter x 10 mm height sample showing the smooth infiltrate covering the surface of the material and the exposed microporous structure revealed due to breakage of trabeculae during preparation.

PCL in THF solutions as described in section 4.3.7 were infiltrated only under vacuum as the dangers of pressurising THF were unknown. Initially, attempts were made to infiltrate PCL into SCBB by melting the material and then using vacuum to force the molten material into the SCBB. The neat, molten PCL proved too viscous to penetrate the macropores of the SCBB using this method, and was observed only to cake the outside of the SCBB samples. However, by dissolving PCL in THF, viscosity could be controlled by adjustment of the concentration of PCL in solution. A PCL concentration of 10 % w / v in THF (Infil-12, see p. 72) was able to penetrate the microporous structure of the sintered bone matrix as shown in figure 4-14, as was a 14 % PCL w / v THF solution (Infil-13, see p. 72) as shown in figure 4-15.

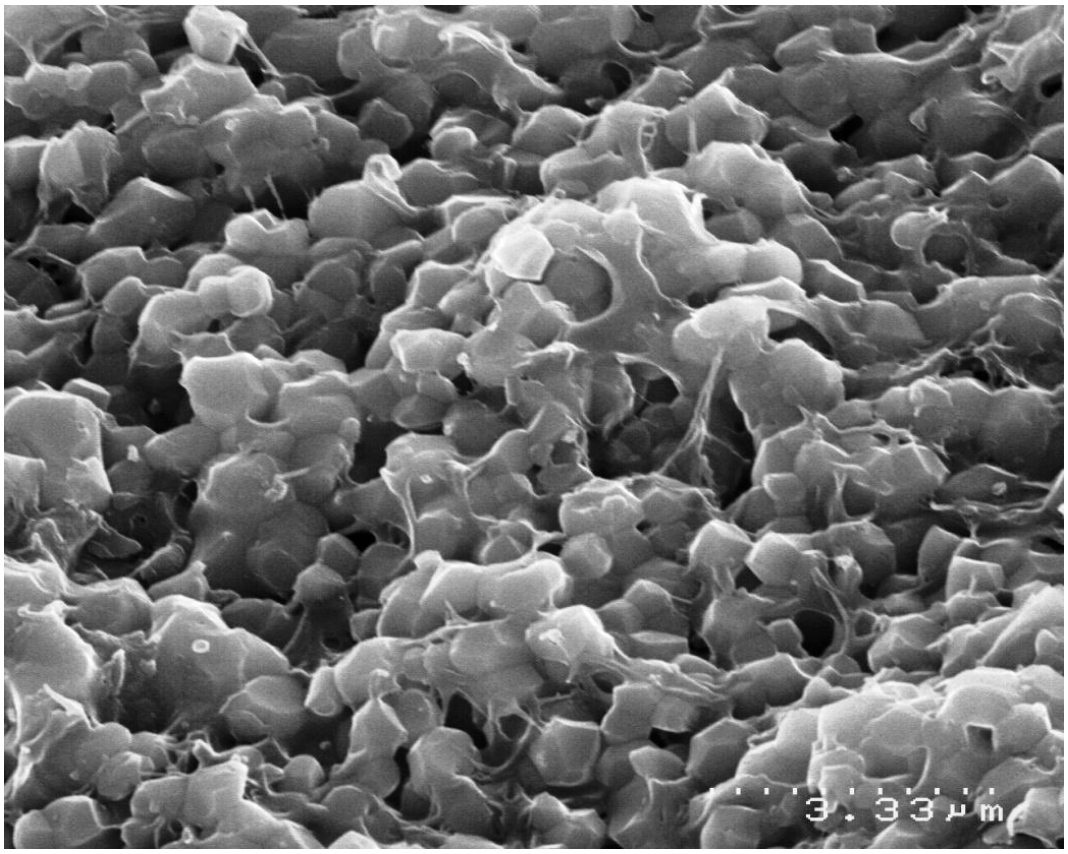

Figure 4-14 - SEM of SCBB infiltrated with 10 % PCL w / v dissolved in THF.

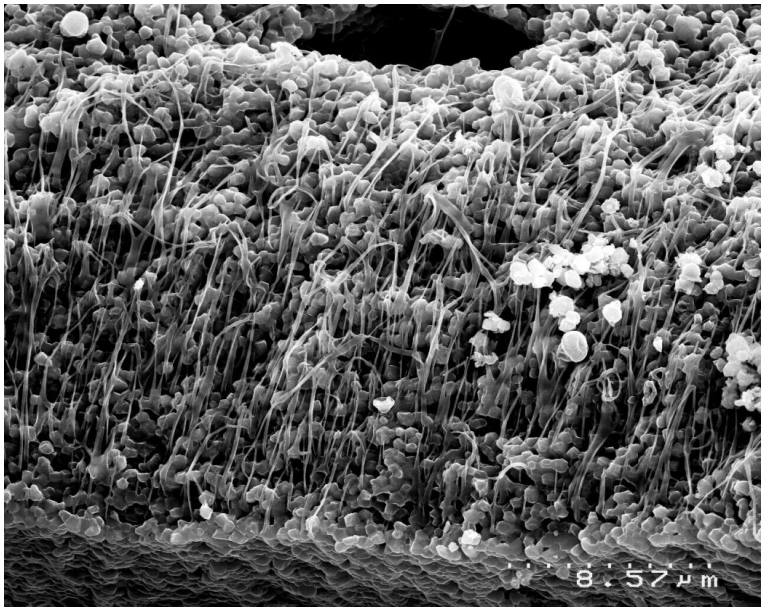

Figure 4-15 - SEM of SCBB infiltrated with 14 % PCL w / v in THF.

When repeated infiltrations were made, multi-layering of PCL on the surface of the macropores of the SCBB occurred. Figure 4-16 shows PCL lying on the surface of the SCBB showing material with a "fibrous" appearance to the right due to mechanical trauma caused by cutting with a scalpel blade at the time of sample preparation.

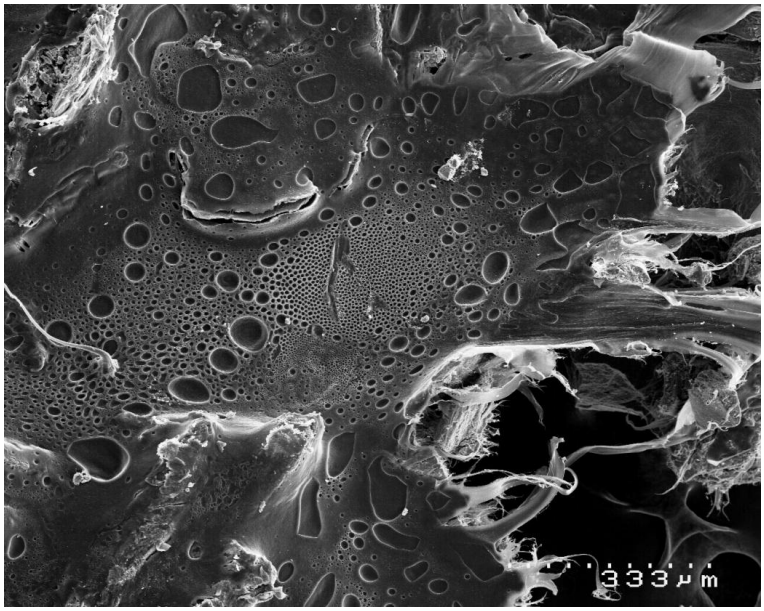

Figure 4-16 - SCBB coated with PCL. Pores in the surface of the PCL may have been formed during solvent evaporation.

IR spectra as shown in figure 4-17 confirmed that PCL was penetrating to the centre of the SCBB. Spectrum a) is SCBB, b) is SCBB infiltrated with PCL and c) is PCL. Spectrum b) was generated from a sample removed from the centre of a piece of PCL infiltrated sintered bone. Clearly visible within the spectrum, which is dominated by phosphate vibrational peaks of sintered bone between 900 – 1100 cm^{-1}, is the peak corresponding to the carbonyl stretching vibration in PCL at 1731 cm^{-1}. The C-H stretching frequencies associated with PCL between 2800–3000 cm^{-1} are also present in the SCBB PCL infiltrated spectrum, of which an image is shown over the page in Figure 4-18.

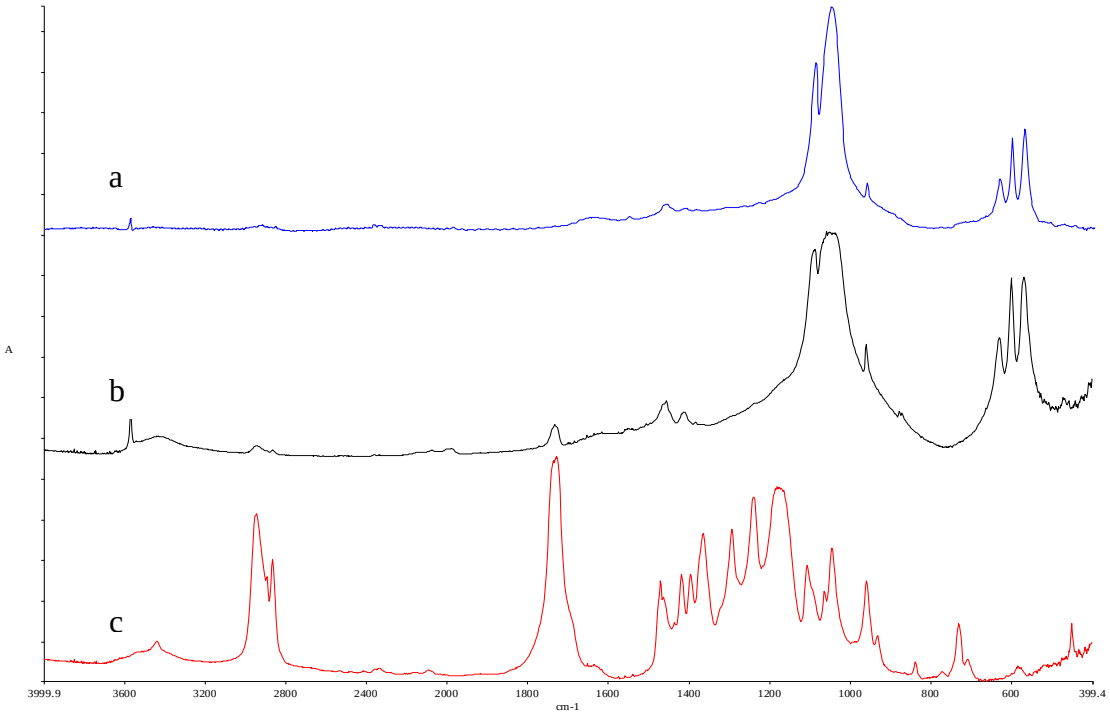

Figure 4-17 - IR spectra from of sintered bone a), sintered bone infiltrated with PCL b) and PCL c).

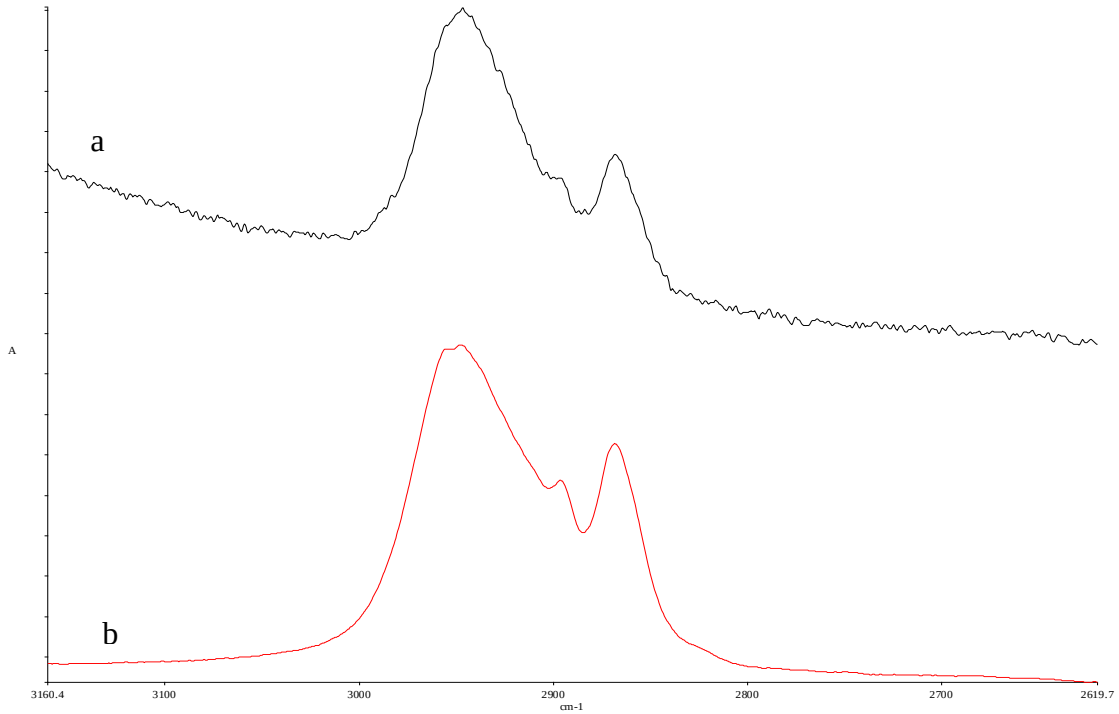

Figure 4-18 - IR spectrum of SCBB infiltrated with PCL a) showing C-H stretching peaks assigned to PCL and PCL b).

A possible limitation to the method of dissolving PCL in THF is that not all the THF may evaporate out of the PCL after deposition. THF is not considered a particularly toxic compound, in its vapour form at least, with Elovaara *et al.* showing rats able to metabolise exposure of up to 2,000 ppm for up to 18 weeks [127]. Nonetheless, for this research it was considered preferable to have as little residue THF in the PCL as possible. Therefore, IR was used to investigate whether a large quantity of THF solvent remained in the PCL deposited within the sintered bone after infiltration and drying. IR is not a particularly sensitive method for such analysis, with a detection limit commonly of 1% [119]; therefore, a more rigorous analysis such as an extraction and chromatography method would be necessary to determine trace levels of THF.

Figure 4-19 opposite shows the IR spectra of THF (with BHT stabiliser) and SCBB. It was apparent that the peak at 1070 cm^{-1} for the THF spectrum corresponding to asymmetric C-O-C stretch for 5-membered cyclic esters [128], unless in significant

concentration, will likely be swamped by the phosphate peaks in sintered bone at 1088 cm^{-1}, or at best appear as a shoulder. The peak at 1459 cm^{-1} also coincides with the 1460 cm^{-1} peak in sintered bone (ν_{3a} type A carbonate substituted hydroxyapatite) making its appearance in sintered bone inconclusive evidence for the presence of THF. This leaves the C-H stretching vibrations at 2861 cm^{-1} and 2977 cm^{-1}, which although also present in the PCL spectrum are at slightly different wavenumbers as can be seen in figure 4-20, and with specific focus on the region 2780 cm^{-1} to 3080 cm^{-1} in figure 4-21. No shoulder was apparent on the peak at 2947 cm^{-1} in the PCL spectrum that would have indicated an overlap with the THF peak at 2978 cm^{-1}. This result does not conclusively preclude the presence of THF in the PCL / SCBB material, but this method did indicate that if it was present it was probably below 1 % w / w in comparison to PCL.

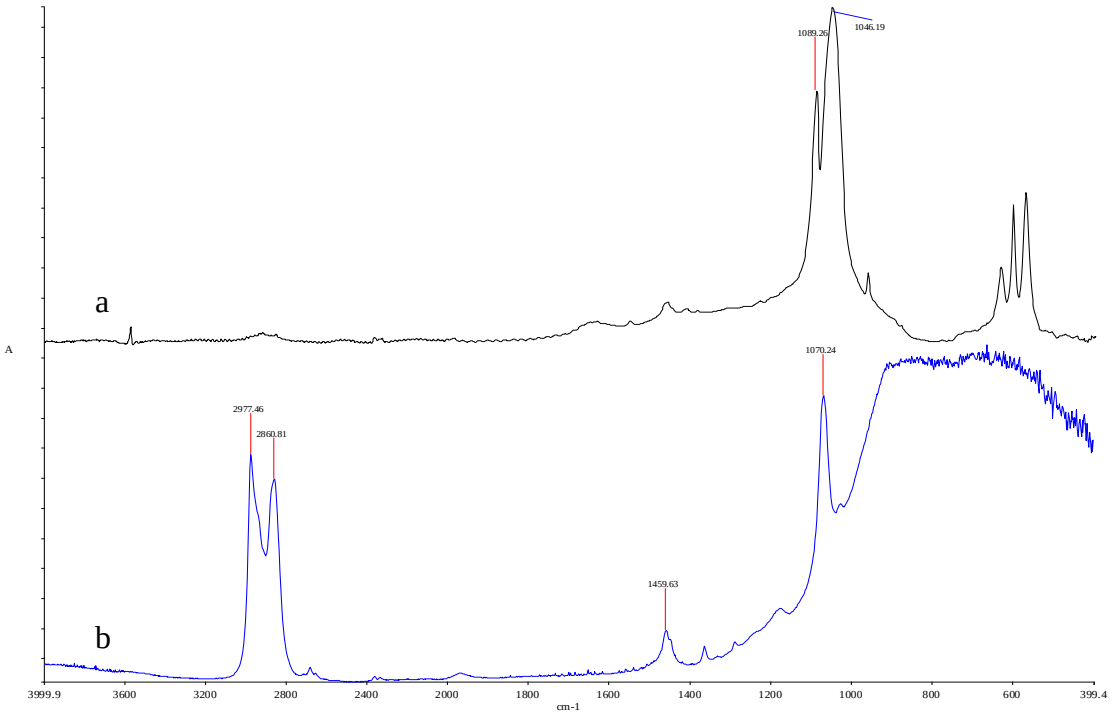

Figure 4-19 - IR spectra of sintered bone a) and THF between CaF_2 disks b).

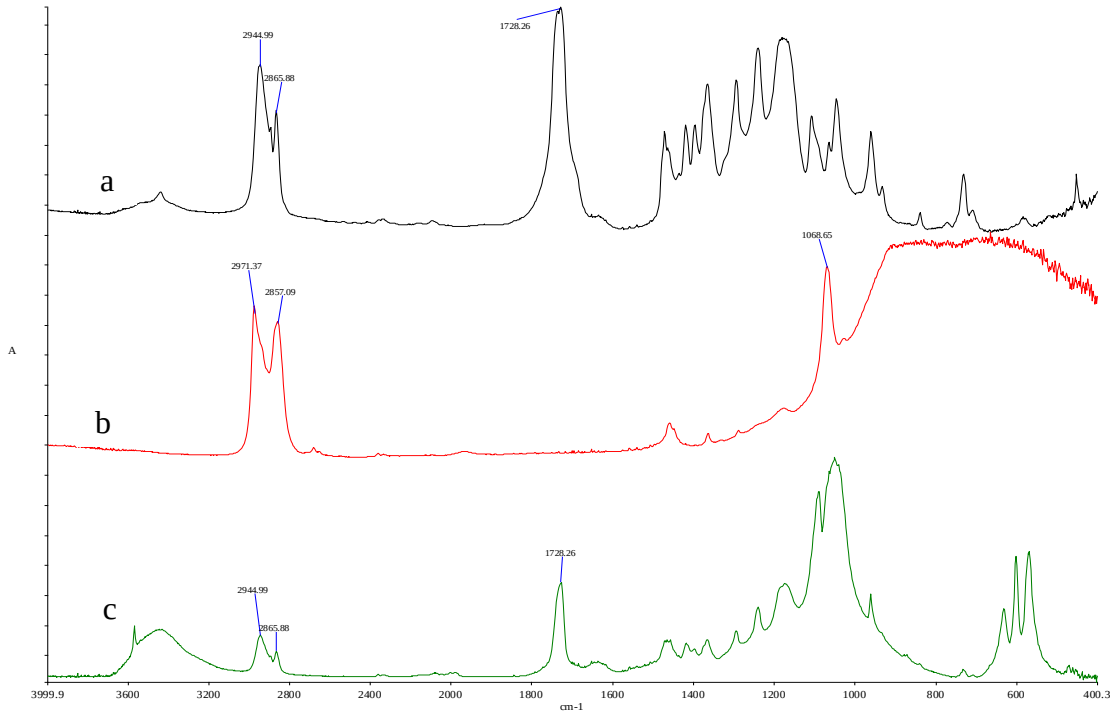

Figure 4-20 - IR spectra of PCL a), THF b) and SCBB infiltrated with PCL c).

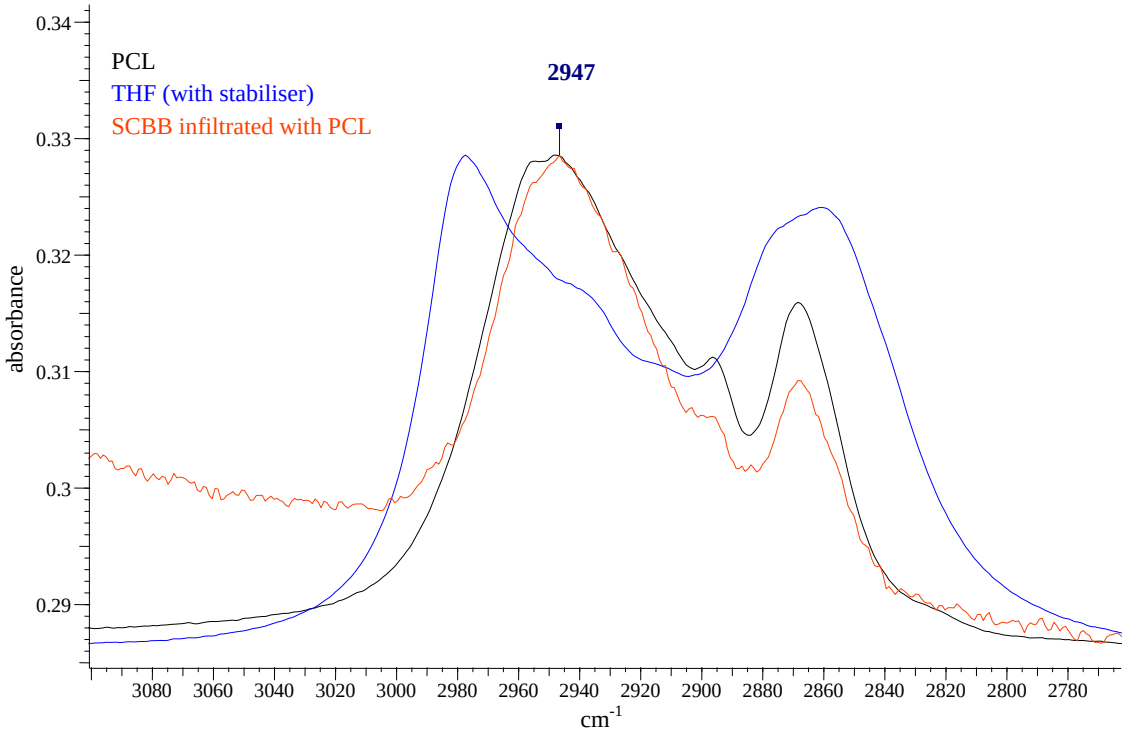

Figure 4-21 - IR spectra of PCL, THF and SCBB infiltrated with PCL dissolved in THF.

Repeated infiltrations were possible using PCL dissolved in THF solutions with an increase in the quantity of PCL deposited within the SCBB being seen after each infiltration as shown below in Figure 4-22. However, SEM images showed no evidence of an increasing quantity of PCL within the microporous structure over that seen in the initial infiltration. This was attributed to the 1st infiltrate acting as a barrier to further penetration by subsequent infiltrating liquids into the microporous structure. Additionally, due to the infiltrate solution not being in a saturated state, it was possible that each infiltration step was leading to the partial dissolution of the previously deposited material. Although each infiltration generally led to an increase in weight, this facet of the infiltration technique must be regarded as inefficiency.

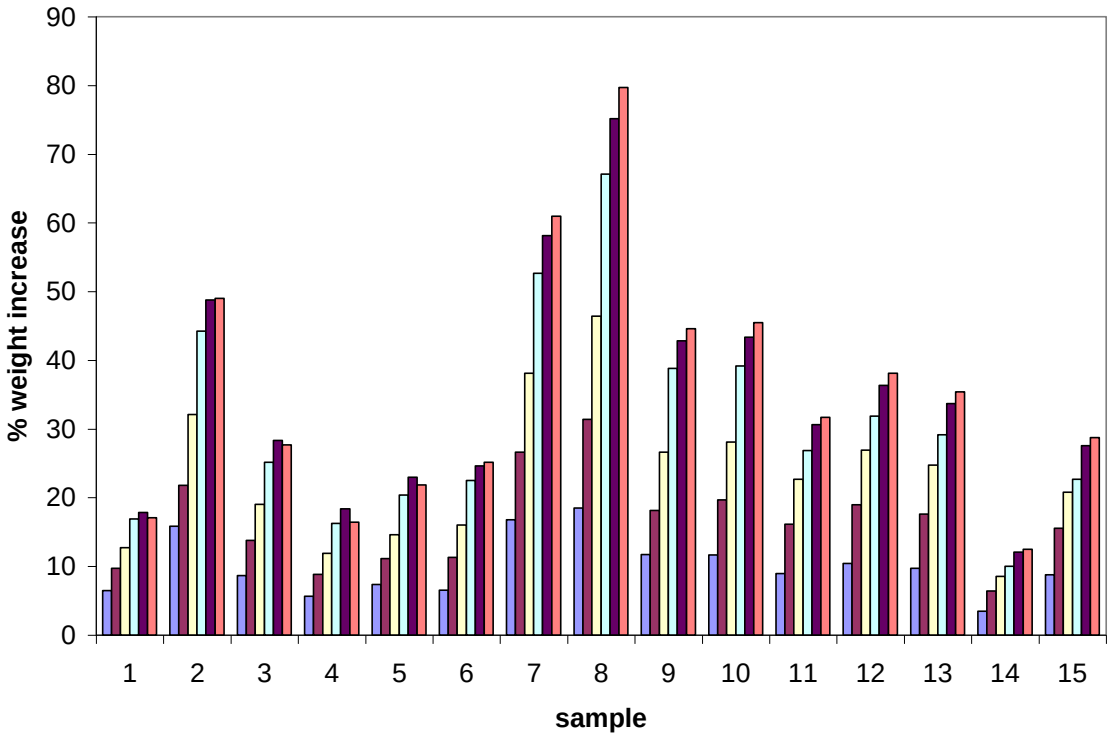

Figure 4-22 - Percentage weight increase per infiltration for 15 samples of PCL in THF (10% w/v).

4.5.2 Iterative infiltration of chitosan / HAp ($CaHPO_4$) into SCBB

Repeated infiltrations of chitosonium chloride / HAp infiltration solutions (Infil-2, Infil-3 and Infil-4, see p. 72) into SCBB samples was undertaken using the vacuum infiltration system described in section 4.4.1 (method B). The pressure infiltration systems described in sections 4.4.2 and 4.4.3 were investigated as a means of infiltrating into the microporous structure, but not routinely used to build up significant quantities of infiltrate within the SCBB macropores. Infiltrates could be immobilised by ammonia gas between each infiltration or as one final step as described in section 5.3.4.

Figure 4-23 below shows a typical percentage weight increase per infiltration for a range of samples of different weights and apparent densities. Initial sample weights, weight increases and bulk volumes are presented in Appendix D. Note that the percentage weight increases per infiltration are less in comparison to the PCL material shown in Figure 4-22.

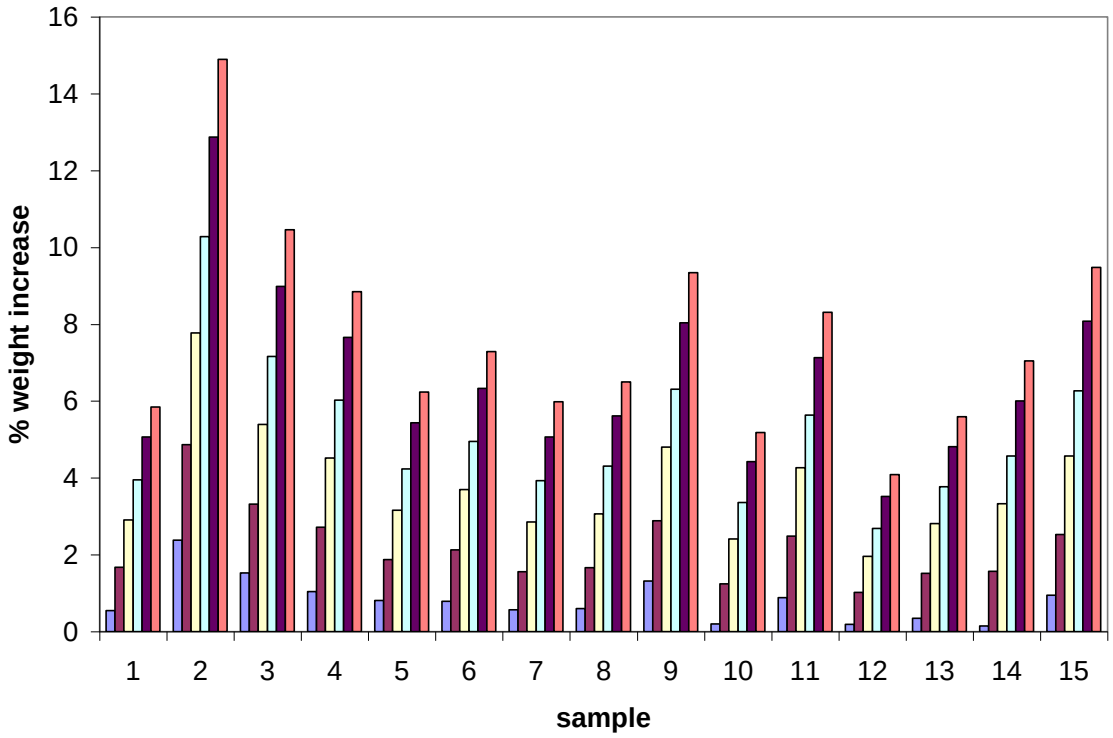

Figure 4-23 – Percentage weight increase per infiltration of chitosonium chloride / $CaHPO_4$ (Infil-3, p. 72).

The column chart above shows some variation in the quantity of infiltrate deposited per infiltration from sample to sample. Consistently, SCBB samples with lower apparent density (i.e. more porous) accommodated more material per infiltration step than samples with higher apparent density. A power type relationship was observed between the initial apparent density of the samples and the percentage weight increase (here, after six infiltrations) as shown below in Figure 4-24.

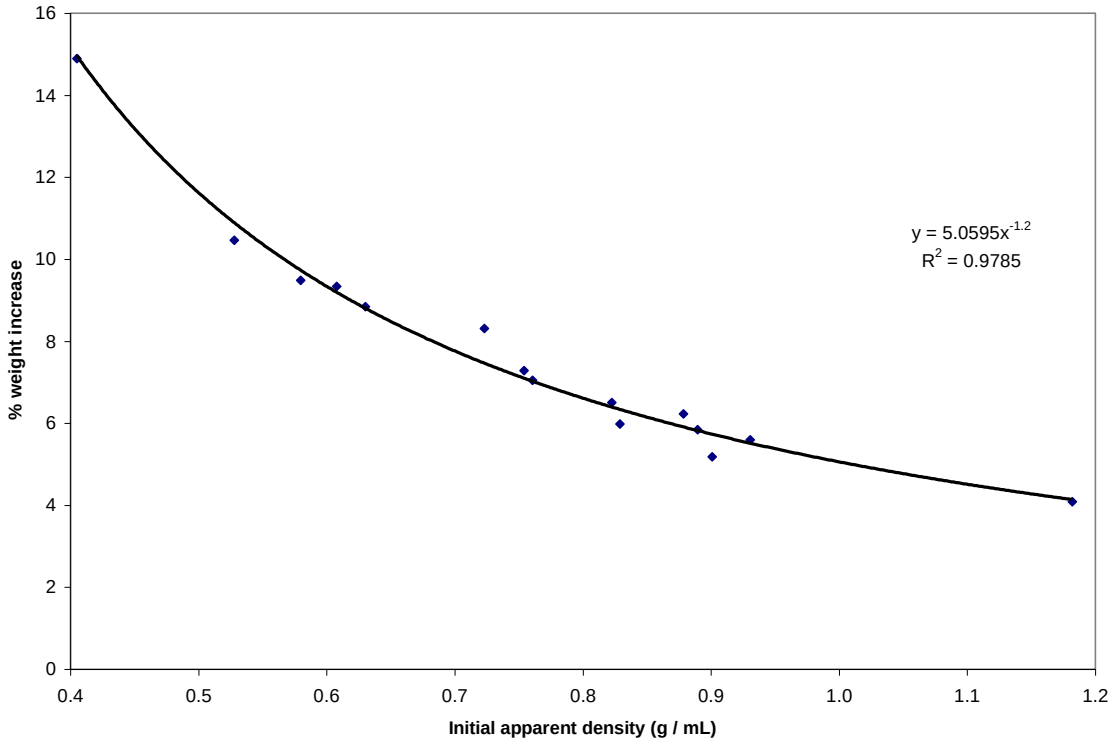

Figure 4-24 – Graph showing the relationship between percentage weight increase and initial apparent density in SCBB samples after 6 infiltration steps with chitosonium chloride / $CaHPO_4$ (Infil-3, p. 72).

4.5.3 SCBB samples infiltrated under vacuum and pressure.

Infiltration of SCBB with chitosan / HAp (Infil-2, p. 72) under vacuum and *then* with application of pressure (using the device described in section 4.4.2) up to ~ 90 atm revealed that the infiltrate material could be deposited consistently and more uniformly throughout the microporous structure of the SCBB material than when using vacuum alone. This is demonstrated from Figure 4-25 to Figure 4-27 where a

consistent distribution of foreign material within the microporous structure of the SCBB was detected after infiltration. In a further experiment, FITC labelling of chitosan confirmed that the material was in fact chitosan as shown in section 4.5.5.

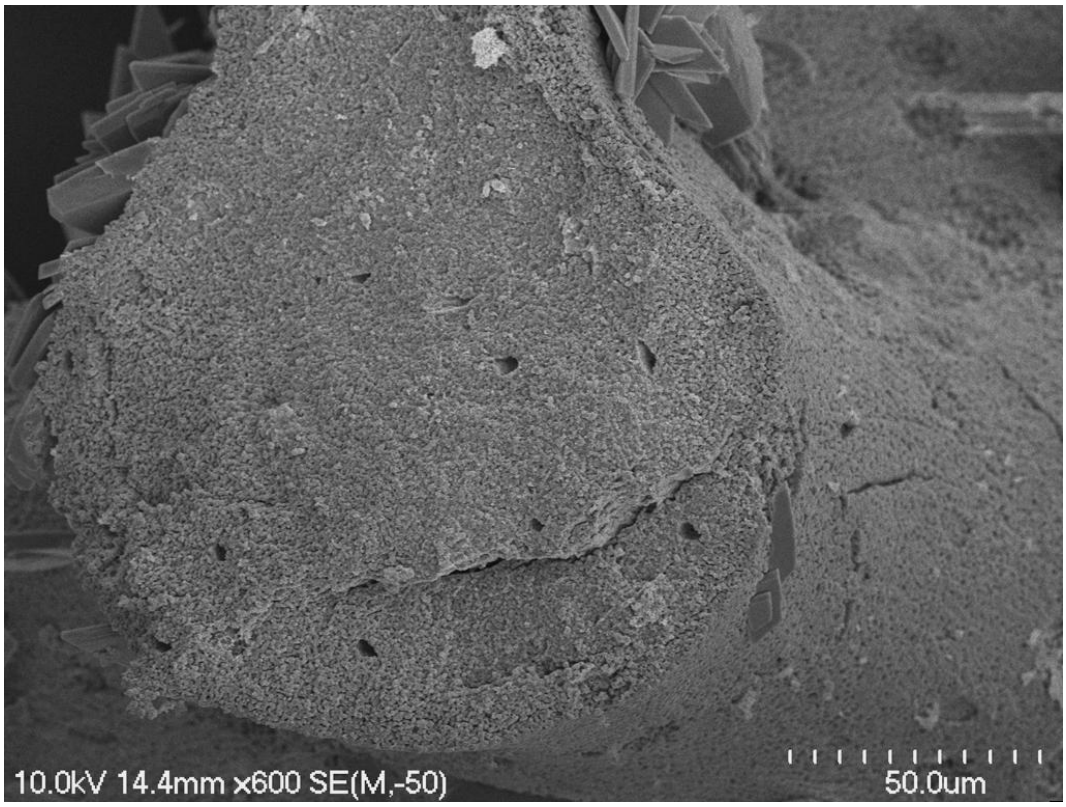

Figure 4-25 – SEM image of a cross-section of trabecular bone after being infiltrated with chitosan / HAp solution (Infil -2) under vacuum and then pressurised to ~ 60 atm for 1 hour.

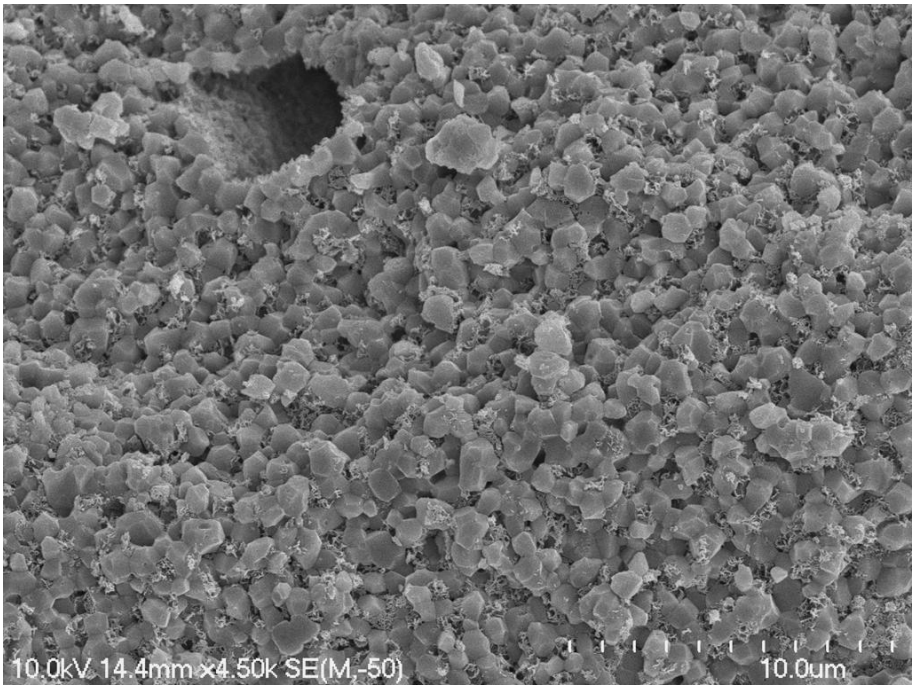

Figure 4-26 - SEM image of a cross-section of trabecular bone after being infiltrated with chitosan / HAp solution (Infil -2) under vacuum and then pressurised to ~ 60 atm for 1 hour. Magnified image of sample shown in Figure 4-25, and revealing foreign material distributed within the pores of microporous structure.

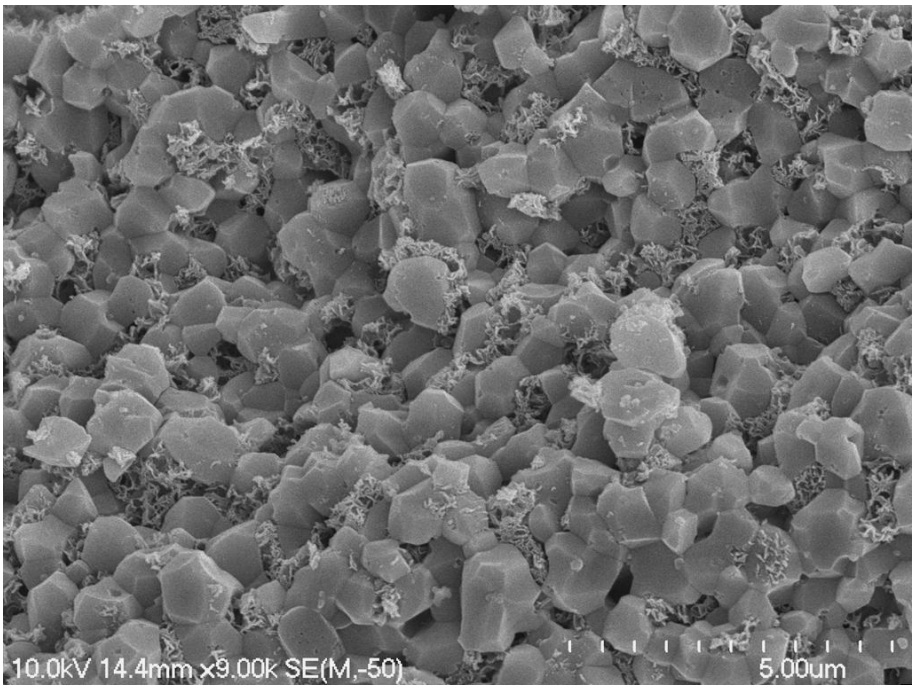

Figure 4-27 - SEM image of a cross-section of trabecular bone after being infiltrated with chitosan / HAp solution (Infil-2) under vacuum and then pressurised to ~ 60 atm for 1 hour. Magnified image of sample as shown in Figure 4-26 above.

When infiltration was carried out on a SCBB sample that had not previously been infiltrated, in other words during the first infiltration, the results of infiltration process using vacuum and pressure, in comparison to pressure alone where indistinguishable with regard in infiltration into the microporous structure. However, as discussed later in section 4.5.5, the outcome was different when a pre-existing layer of infiltrate was present on the surface of the microporous structure. Effectively, this was shown to block the pores to further infiltration, which gradual application of pressure was successful in overcoming. To track the path of the infiltrating material with different infiltrating methods and throughout successive infiltration steps, chitosan was labelled with a fluorescent marker according to the method in section 4.3.9.

Figure 4-28 opposite shows a SCBB sample that has been infiltrated under vacuum and then pressurised to ~ 63 Atm for 1 hour with 6 g L^{-1} FITC labelled chitosan and 6 g L^{-1} HAp (Infil-2). Particularly significant in this image was that all fragments, even the smallest, showed signs of fluorescence. Due to its uniformity of intensity and comprehensive dispersion, this appeared to show complete infiltration into the microporous structure. However, the presence of fluorescence in larger fragments also could be explained in part by the presence of a layer of infiltrate on a portion of the surface of the microporous structure (a portion originally exposed to the macropores of the SCBB). From this, it is feasible that the layer of FITC labelled chitosan could emit fluorescent light into the fragment, which in turn could be reflected through the microporous architecture to give the illusion of the presence of FITC labelled infiltrate throughout the entire fragment. However, it is highly improbable that this phenomenon be reproduced on every fragment, particularly on smaller fragments, where the probability increases that no portion of the fragment was originally a component of the macroporous surface. In addition, a layering effect was seen in a later experiment shown in Figure 4-29, section 4.5.4, where layers of FITC labelled chitosan and non-infiltrated SCBB were easily discernible.

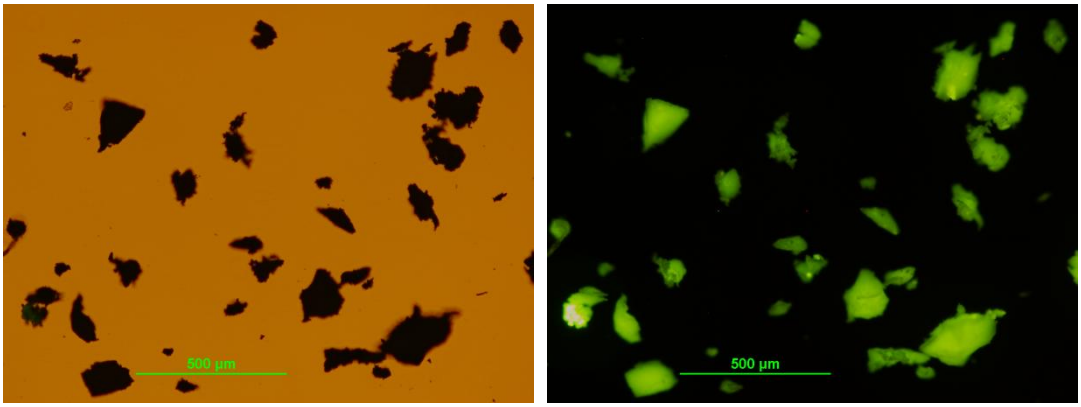

a) Microscope image of SCBB fragments having been infiltrated with FITC labelled chitosan and HAp at 6 g L^{-1} solution (Infil-2), illuminated from below (in this case) by incandescent light. No fluorescence is visible under this system.

b) Fluorescence microscope image of the same sample shown in a) excited by blue light (450-490 nm). All sample fragments showed a degree of fluorescence throughout.

Figure 4-28 – Top lit incandescent and fluorescent microscope images of SCBB having been infiltrated with FITC labelled chitosan and HAp (Infil-2, p. 72) under vacuum, then pressurised at ~ 63 atm.

These results combined gave very strong evidence that fluorescence within the microporous structure was caused by the presence of FITC labelled chitosan, and not free FITC or by an illumination effect through adjacent lying fluorescence.

4.5.4 Infiltration of FITC labelled chitosan / HAp (Infil-2) into a pre-infiltrated SCBB sample

The intent of this experiment was to generate samples with a layer of FITC labelled chitosan lying on top of the microporous matrix, but not within the micropores. This was to provide comparison for an accompanying experiment designed to test whether a second infiltration step could force infiltrate through a previously deposited layer of infiltrate, see section 4.5.5. Under the fluorescence microscope, SCBB sample fragments as shown in Figure 4-29 displayed a fluorescence distribution of varying intensity, with areas of relative high intensity as well as regions of no fluorescence. This pattern was highly indicative of a layering of the infiltrate on the surface of the

microporous architecture, which was in stark contrast to the even dispersion as shown in Figure 4-28.

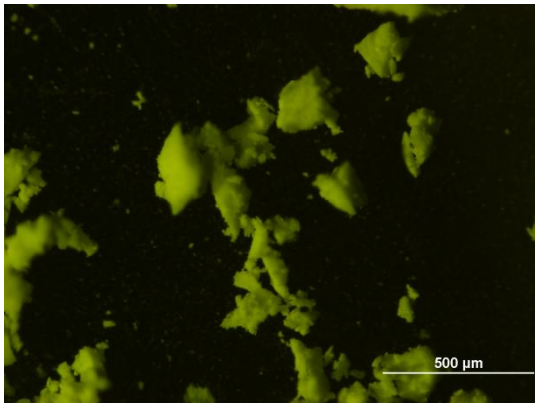

a) Microscope image of SCBB fragments having been infiltrated with chitosan and HAp at 6 g L^{-1} solution (Infil-2), illuminated from above by incandescent light. No fluorescence is visible under this system.

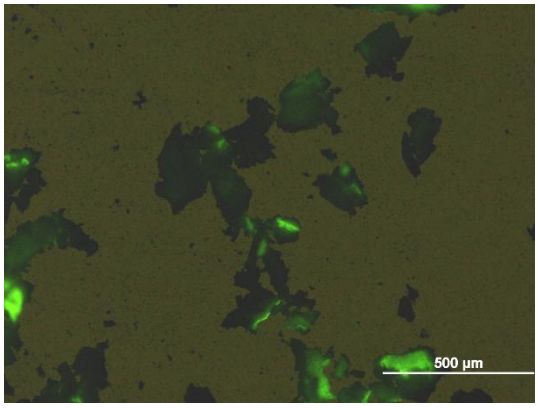

b) Fluorescence microscope image of the same sample shown in a) excited by blue light (450-490 nm). Sample fragments are characterised by areas of fluorescence and areas completely devoid of fluorescence consistent with a layer of fluorescent infiltrate on, but not within, the microporous structure of the original intact SCBB.

Figure 4-29 - Top lit incandescent and fluorescent microscope images of SCBB having been infiltrated initially with non-FITC labelled chitosan and HAp (Infil-2), then infiltrated with FITC labelled chitosan and HAp (Infil-2) under vacuum.

4.5.5 Infiltration of FITC labelled chitosan / HAp (Infil-2) by vacuum and pressure, and pressure alone into pre-infiltrated SCBB

Figure 4-30 opposite shows a series of three incandescently top-lit images (left) accompanied by their fluorescence image (right) as a representative collection of what was observed over the entire sample after using the vacuum and pressure infiltration method. FITC labelled chitosan was distributed throughout the entirety of the original SCBB sample as indicated by the presence of fluorescence in each of the particles. However, fluorescence became increasingly difficult to detect as particle size decreased, to the point where small particles visible in the incandescently top-lit image were not visible in the fluorescence image. This was due possibly to smaller

particles containing less fluorescent material, in turn producing less fluorescent light, therefore making them difficult to detect.

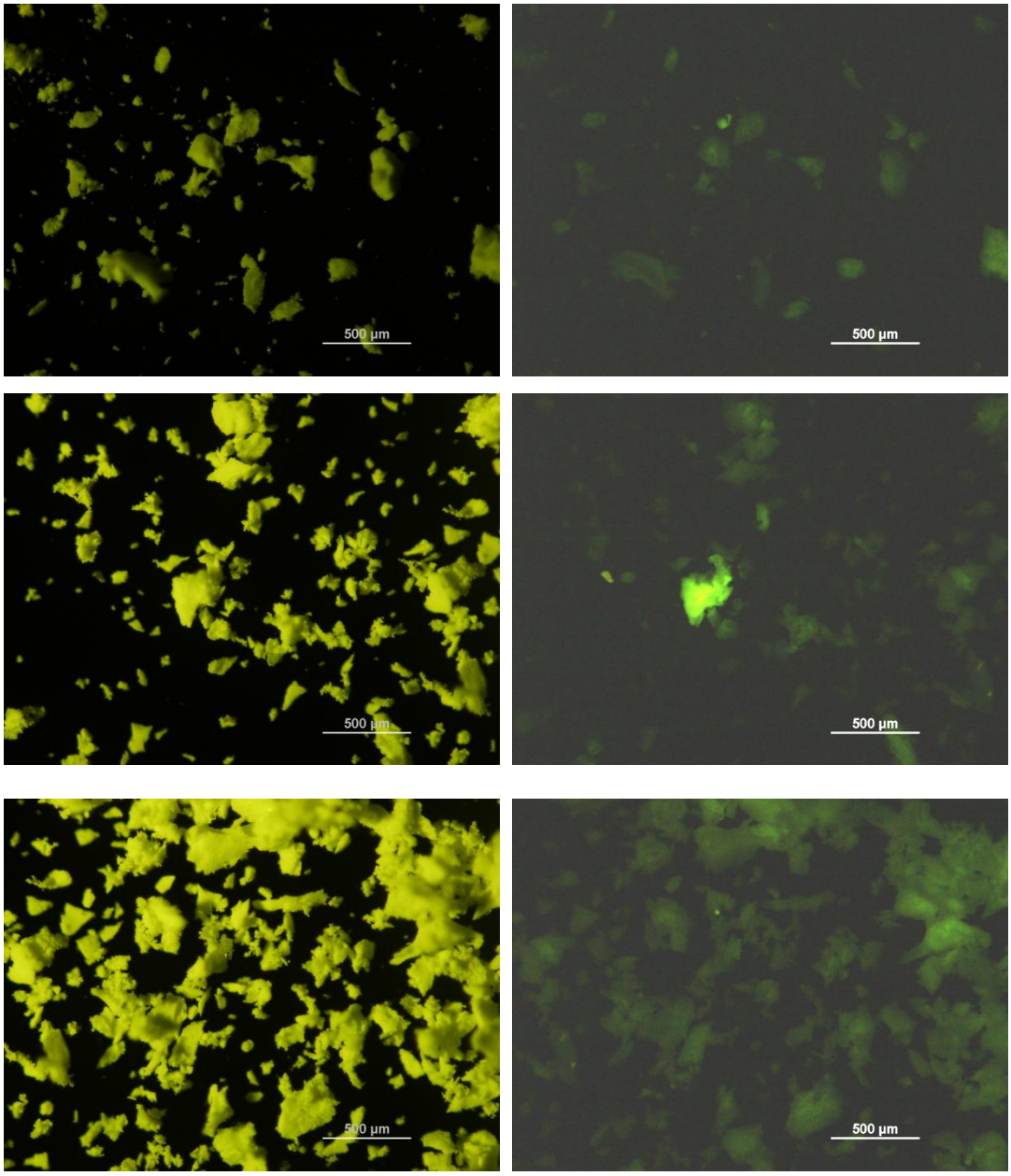

Figure 4-30 – Top lit incandescent images (left) and accompanying fluorescent image (right) of SCBB infiltrated with FITC labelled chitosan / HAp infiltrate (Infil-2) under vacuum and pressure after the sample was originally infiltrated with non labelled chitosan / HAp infiltrate (Infil-2).

Figure 4-31 shows images of particles created from the sample where the second infiltration was under pressure only. In a qualitative comparison, while considering

that all images were produced under identical conditions, with the same level of blue light excitation and with the same detection sensitivity settings, fluorescence images for the pressure only infiltration appeared to show a greater level of intensity and uniformity in comparison to those samples infiltrated by vacuum and pressure shown above.

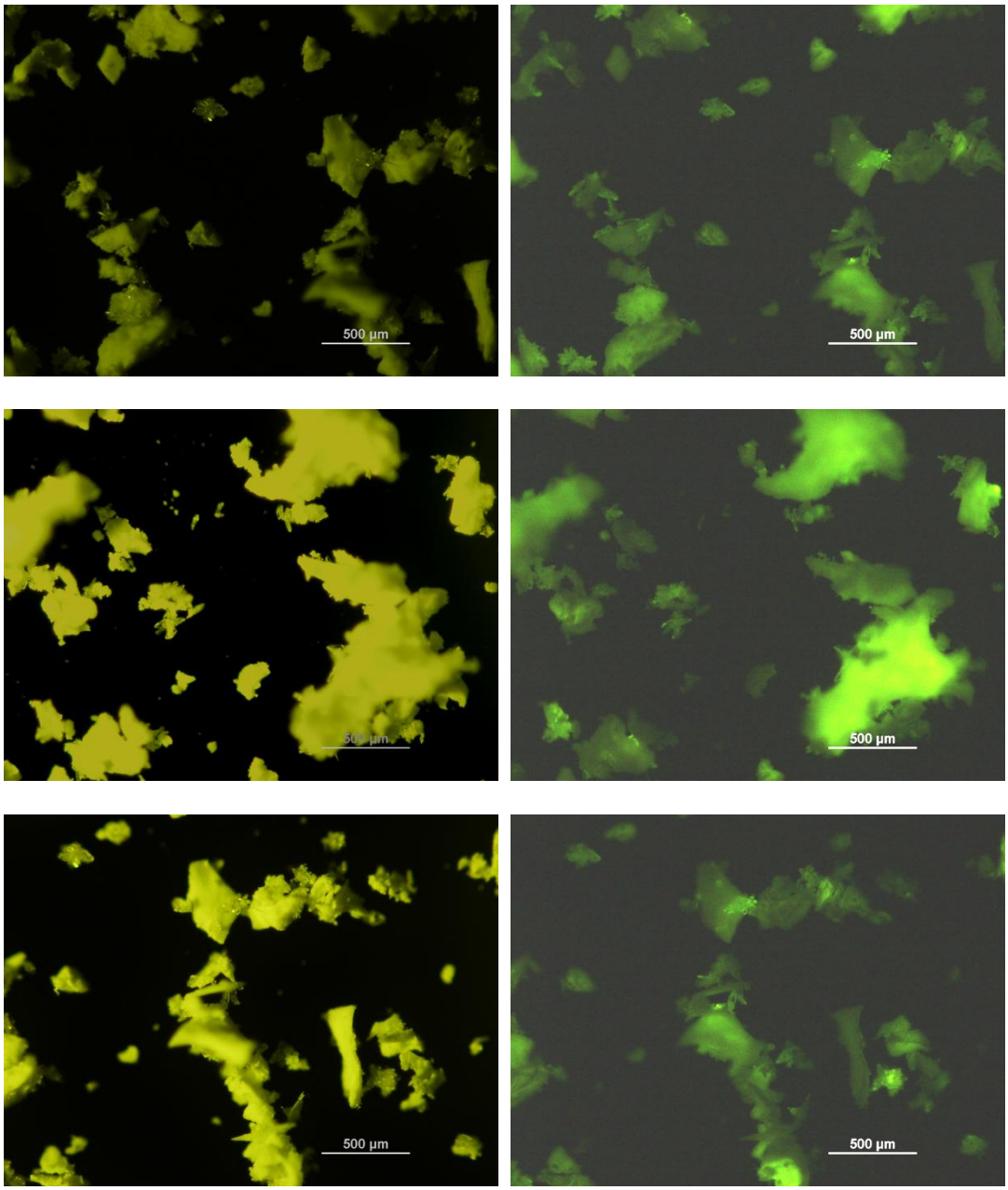

Figure 4-31 –Top lit incandescent images (left) and accompanying fluorescent image (right) of SCBB infiltrated with FITC labelled chitosan / HAp infiltrate (Infil-2) under <u>pressure only</u> after the sample was originally infiltrated with non labelled chitosan / HAp infiltrate.

This series of experiments using FITC labelled chitosan and the purification protocol described in Appendix C, demonstrated that it was highly probable that the fluorescence seen within the small fragments of SCBB (and therefore within the microporous structure) was caused by the presence of FITC labelled chitosan and not unbound FITC. Results as shown in Figure 4-30 and Figure 4-31 led to the conclusion that chitosan / HAp infiltrating solution (Infil-2) could indeed be infiltrated through a pre-existing layer of infiltrate into the microporous structure of the SCBB material by the use of vacuum and pressure, or pressure alone. In addition, from the qualitative data it appeared as though the pressure alone method was superior in facilitating a comprehensive dispersion of the infiltrating material.

The structure of the chitosan molecule in an acidic solution is helicoidal and has been described as a "flexible wormlike chain" due to the electrostatic repulsion of adjacently protonated amine functionalities (especially in chitosan polymers with higher degrees of deacetylation) [78, 129]. However, at higher ionic strength, for example, due to the introduction of a salt into the solution (i.e. dissolved calcium phosphate in this case), a reduction in this "stiffness" results because of shielding between adjacent positive charges [78]. Therefore, it was envisaged that the expected flexible "worm"-like structure of chitosan under these conditions could be forced to penetrate the micropores of the SCBB ranging in size from ~ 200 to 750 nm. Supporting this concept was the fact that chitosan solutions had already been successfully filtered through 0.22 μm (200 nm) filter membranes [78, 130].

In the pressure only infiltration, vacuum was not employed in the infiltration process. Samples were placed in the pressure vessel and the degassed infiltrate was poured in from above. As the infiltrate liquid had been degassed, it was predicted that air trapped within the micropores of the SCBB would dissolve under pressure into the infiltrating liquid, thus allowing the infiltrate to occupy that space. Using Henry's law of partial pressures a calculation was made to estimate the volume of air that could be dissolved in the ~ 30 mL infiltrating solution within the pressure device at different pressures. It should be noted that this calculation assumed that the infiltrating liquid

was capable of dissolving similar volumes of air as pure water. Presented in Appendix F, the calculation showed that at atmospheric pressure approximately 0.57 mL of air could be dissolved in 30 mL water, whereas at 50 atm pressure 28 mL of air (volume equivalent at atmospheric pressure) could be dissolved in 30 mL water at 25°C. The success of this infiltration method therefore relied on dissolving air trapped within the SCBB samples into the degassed infiltrating liquid upon pressurisation, allowing the then dissolved air to diffuse and dissipate into the macropores. In this way, if the moment of pressure release were accompanied by an effervescence of gas, it would not lead to an expulsion of infiltrate from the microporous structure. The results confirmed the viability of using a pressure only infiltration method.

4.6 Conclusion

Several infiltration techniques were trialled over the course of this research, with the simple vacuum method, *Method A,* described above in section 4.4.1 found to be completely adequate for infiltrating material, whether that material be in a solution or as a suspension, into the macroporous structure of the SCBB. All further infiltration methods were investigated with an aim to infiltrating solutions into the microporous structure of the SCBB, with the ultimate aim being to facilitate repeated infiltrations into the microporous structure. A pressure only infiltration method was found to be most effective in enabling repeated infiltrations into the microporous structure of the SCBB.

CHAPTER FIVE

5 Immobilisation and Removal of By-Products

5.1 Introduction

This chapter focuses on the techniques used for the immobilisation of the infiltrated material within the porous SCBB matrix. An infiltration system such as PCL dissolved in THF provides a simple one step means of permanently immobilising the infiltrate material within the SCBB, because after infiltration the solvent evaporates leaving behind the immobilised, insoluble material. However, the chitosan system is more complex, because chitosan is initially dissolved in acid as a means of solubilisation, and in order to render the chitosan (and accompanying material if present) insoluble, the pH of the solution must be raised above approximately 6-7 (depending on the concentration of the solution). This increase in pH can be induced potentially at different stages during the entire infiltration process, as follows: (i) before the material is infiltrated into the SCBB (to create a suspension), (ii) after the solution has been infiltrated into the SCBB but while the infiltrate is still a solution, or (iii) after the solution has been infiltrated and allowed to dry to form a solid mass. Additionally, an increase in the pH of the infiltrating solution may be accomplished in several ways as is described in the following sections including: addition of alkali solution (e.g. $NaOH_{(aq)}$), exposure to ammonia gas, thermal hydrolysis of urea added to the solution, enzymatic decomposition of urea with urease and electrolytically induced migration of basic ions (OH^-, PO_4^{3-}) into a solution of infiltrate within the sintered bone.

5.2 Materials

Latex rubber tubing, Fluka, Urease from Jack beans, Biochemica (1g) Powder, 37.6 U/mg, Made in Switzerland; Andrew Industries, Ammonia liquid, 285g/L, 32% Solution, Porana Road, Takapuna, New Zealand; Aldrich urea 98 % reagent grade.

5.3 Methods

5.3.1 Immobilisation of chitosan within SCBB using latex tubing

SCBB samples that had been infiltrated with chitosan solution were quickly removed from the infiltrating solution with tweezers after each infiltration step and immediately plunged into sufficient 0.1 mol L^{-1} NaOH solution to cover the sample. The sample was left in the NaOH solution for 2 minutes until a layer of precipitated chitosan had formed on the surface of the SCBB sample. The sample was then placed in a length of thin elastic latex tubing (unstretched diameter approximately 3 mm), together with a length of glass tubing as shown in Figure 5-1. This was done by expanding the diameter of a 20 mm length of latex tubing using a commercially available tool known as an Elasticator. The tool is sold commercially for the purpose of applying rubber rings to male lambs for neutering. With the latex expanded, the glass tube, which was designed to act as a reservoir, was inserted into the expanded latex tubing. The infiltrated SCBB sample was then inserted into the other end of the latex tubing as shown in Figure 5-1.

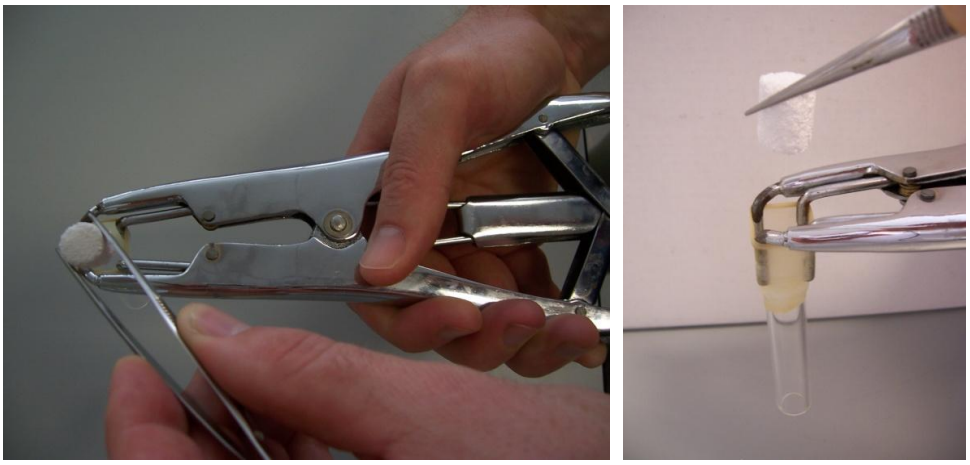

Figure 5-1 – Photographs of the process of placing an infiltrated SCBB sample inside elastic tubing after the tubing has been expanded by Elasticators.

After being clamped as shown in Figure 5-2, a 1 mL volume of 0.1 mol L^{-1} $NaOH_{(aq)}$ was introduced into the glass tube to permeate through the sample. Some samples exhibited no flow of $NaOH_{(aq)}$ with the pressure exerted by 1 mL of liquid, but with the addition 1 or 2 mL more $NaOH_{(aq)}$ flow could be induced.

Figure 5-2 - Neutralisation of chitosan within SCBB by gravity induced flow of 0.1 mol L^{-1} NaOH solution through sample.

A dye tracing experiment was also undertaken in order to evaluate the degree of dispersion of $NaOH_{(aq)}$ within the infiltrated SCBB samples. FITC was dissolved in the 0.1 mol L^{-1} NaOH by placing an excess (~ 5 – 10 mg) in 100 mL and ultrasonicating for 30 minutes. This solution was added 1 mL at a time to make up 3 mL total to the reservoir tubing as described above. After removal from latex tubing and drying, the sample was sectioned parallel to the axis of rotation and across the length of the sample. The freshly exposed surfaced surfaces were presented to a UV light at 254 nm, visually examined and photographed.

5.3.2 Immobilisation of chitosan / calcium phosphate (Infil-4) within SCBB by electric field hydroxide migration

Two half-cells were constructed from glass, one of which is shown in Figure 5-3 below. A semi-permeable membrane (Spectra/Por MWCO: 3,500) was secured to the horizontal tube by the use of a rubber o-ring and elastic bands as shown in Figure 5-4 opposite. A vertical reservoir tube was separated from a horizontal tube by a disk of sintered glass frit to prevent solid moving from the vertical tube into the horizontal tube where it may have contacted the semi-permeable membrane and impeded ion flow.

Figure 5-3 – Photograph of glass tubing making up a half-cell.

A saturated solution of $NaHCO_3$ plus additional solid $NaHCO_3$ was placed in the left hand half-cell and a saturated solution of Na_3PO_4 plus additional solid Na_3PO_4 was placed in the right hand cell as shown in Figure 5-4. A voltage of 12 V from a Topward Electric Instruments Co. Ltd. DC Power Supply (Model: TPS-4000), was

applied across the cells via two carbon electrodes, and the circuit was completed by a sample of Infil-4 (see p. 72) infiltrated SCBB placed in contact with the semi-permeable membranes. The pH indicator, phenolphthalein was added to the infiltrating solution in order to reveal regions of increased pH with colour changes relating to pH (pH 0 - 8.3 colourless, pH 8.3 – 10.0 pink, highly alkaline colourless) [131]. Voltage was applied for 2 hours after which the cylindrical sample was extracted from the apparatus and dissected parallel to the axis of rotation and then laterally.

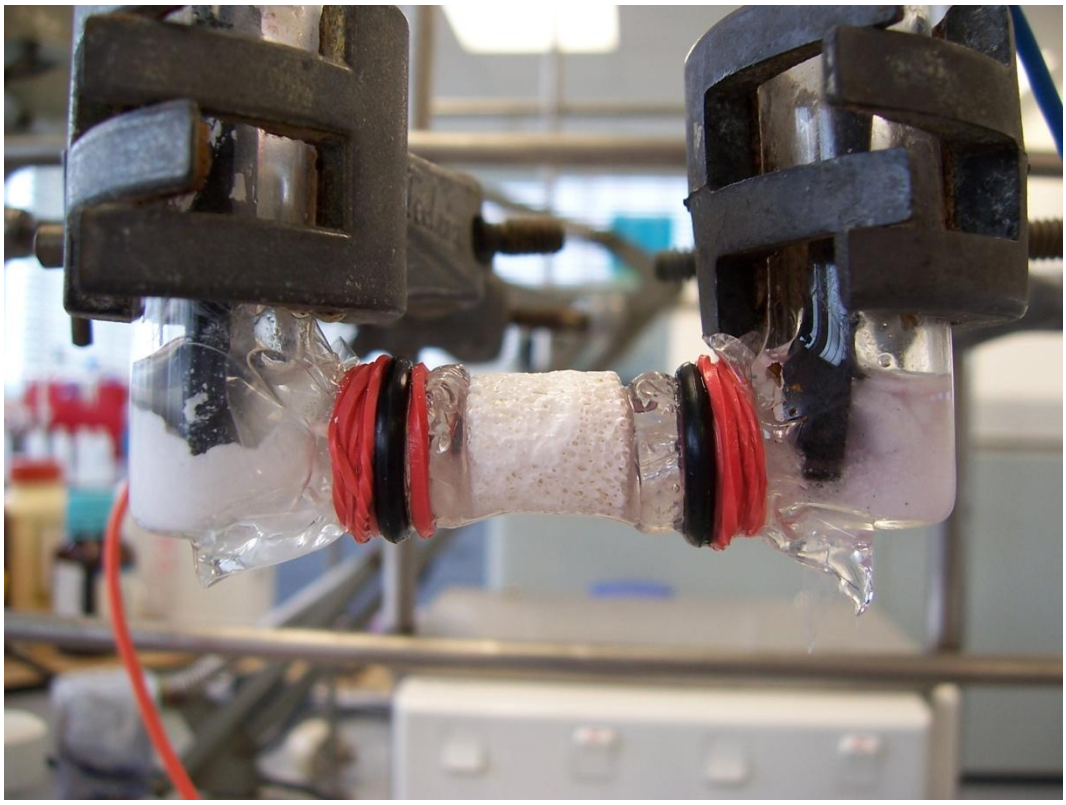

Figure 5-4 - Photograph of SCBB sample infiltrated with chitosonium chloride solution between half-cells separated from conducting solutions by semi-permeable membranes.

A control experiment was also undertaken where all conditions were reproduced except that no voltage was applied for 24 hours.

5.3.3 Immobilisation of liquid infiltrate within SCBB with $NH_3(g)$

After infiltration with a particular chitosan infiltrating solution (Infil-1, Infil-2, Infil-3, Infil-4, Infil-10 or Infil-11, see p. 72), SCBB samples were placed in an enclosed desiccator vessel with a 50 mL beaker containing 30 mL conc. $NH_{3(aq)}$. Samples were left for a minimum of 2 hours, but generally overnight (~ 14 hours) to effect the precipitation of chitosan and CaP[1] (calcium phosphate) if present. To evaluate the efficacy of $NH_{3(g)}$ diffusion into infiltrated SCBB samples, an experiment was conducted on SCBB samples that had been infiltrated with Infil-2 solution (pH 4.20) with the addition of phenolphthalein to show the pathway of $NH_{3(g)}$ permeation into the SCBB cylindrical cores. Infiltrated SCBB samples were placed in a small desiccator next to 30 mL conc. $NH_{3(aq)}$ in a 50 mL beaker, and removed at 5, 15, 30 and 60 minutes. After removal, SCBB samples were dissected halfway along the length of the cylinder to reveal the progress of the $NH_{3(g)}$ as indicated by the phenolphthalein indicator.

5.3.4 Evaluation of the penetration of $NH_{3(g)}$ into solid chitosan / CaP infiltrate

A chitosan / HAp solution prepared by dissolving 2.5 g chitosan and 1 g HAp in 100 mL in $HCl_{(aq)}$ with a pH of ~ 4.5 was poured into 50 mL Falcon tubes, which are plastic tubes with tapered ends. The tubes were then placed upright in a fume-cupboard and left to allow the water to evaporate. The tapered ends of the Falcon tubes dictated that as the water evaporated, the solid was concentrated in the point of the tube yielding a solid "ball" of material of approximately 1.8 g. Some of these solid samples were placed in an enclosed desiccator vessel with a beaker containing 30 mL conc. $NH_{3(l)}$ for 12 hours, after which they were removed and dissected. Small sub-samples were cut from a groove cut along the centre of the cross-section as shown opposite in Figure 5-5, prepared as KBr disks and examined using FT-IR. This was done to trace the penetrability of gaseous ammonia into the solid.

[1] The abbreviation CaP was used to refer to precipitated calcium phosphate rather than HAp or $CaHPO_4$, because of the uncertainty of the phase of the precipitated material.

Figure 5-5 – Photograph of a solid lump of chitosan / CaP composite after being sectioned and sub-samples removed along a central groove.

5.3.5 Immobilisation of chitosan (Infil-1) and chitosan / HAp (Infil-2) through the thermal hydrolysis of urea by pressurised high temperature steam

At elevated temperatures, aqueous urea decomposes due to thermal hydrolysis via an ammonium carbamate intermediate into ammonia and carbon dioxide as shown in Equation 4 and Equation 5 below [132]. This reaction has been successfully used in the past to raise the pH of reaction mixtures [133].

Equation 4 $NH_2CONH_{2(aq)} + H_2O_{(l)} \rightarrow H_2NCOO^-_{(aq)} + NH_4^+{}_{(aq)}$

Equation 5 $NH_4^+{}_{(aq)} + H_2NCOO^-_{(aq)}) \rightarrow CO_{2(g)} + NH_{3(g)}$

Infiltrated SCBB samples were placed on a mesh platform above water level, as represented in Figure 5-6 below. Test solutions of infiltrate in a beaker were placed on the platform in order to track changes in pH over time.

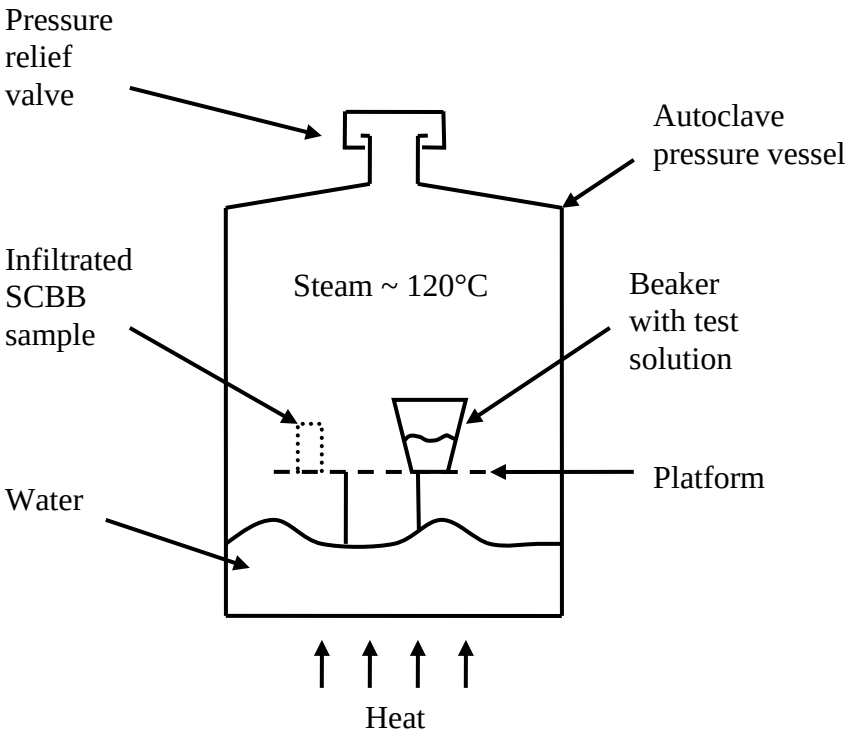

Figure 5-6 – Diagrammatic representation displaying the positioning of components within the autoclave system.

A test experiment was conducted to evaluate the quantity of urea and the time required to effect precipitation of chitosan (and CaP, if present) from chitosonium chloride solutions. Infil-7 solutions were produced from Infil-1 and Infil-2 (see Table 1, p. 72) as described in section 4.3.4. 10 mL of each of these solutions (chitosonium chloride and 10 mL of the chitosonium chloride / HAp + urea) where placed in 50 mL beakers, pH measured of each solution and then placed on a platform within the pressure cooker as shown above in Figure 5-6. The water inside the pressure cooker was pre-heated before the introduction of the beakers, so that after the beakers had been placed inside, operating temperature could be rapidly achieved. The autoclave was removed from heat every hour and the pH of the solutions measured.

Similarly, the urease / urea immobilisation system, of which the preparation is described in section 4.3.5, was investigated by infiltrating solutions into SCBB samples under vacuum and by following the pH of the reaction solution in a beaker. Results are shown in section 5.6.2.

5.4 Removal of immobilisation by-products

5.4.1 Removal of by-products from $NH_{3(g)}$ immobilised chitosan infiltrated within SCBB

Infil-1 infiltrated SCBB samples that had had the chitosan immobilised by exposure to $NH_{3(g)}$ were placed in duplicate in a 3 L beaker with 400 mL distilled water. The water was gently stirred with a magnetic stirrer and pH readings were taken every 15 minutes. After 1 hour of stirring, the infiltrated SCBB samples were removed, a 100 mL sample of the washing water was taken and the surplus water discarded. The beaker was washed with fresh distilled water, filled with 400 mL distilled water and the infiltrated SCBB samples re-introduced.

At the end of the washing process, infiltrated SCBB samples were placed in a clean mortar and crushed to granules with a pestle. Distilled water was then added to the sample and the combination stirred with the pestle used to crush the bone. The mixture was filtered through filter paper into 100 mL volumetric flasks and distilled water was added to make the solutions up to 100 ml. Samples were submitted to a commercial laboratory (Hill Laboratories, Hamilton, New Zealand) and tested for total ammoniacal-N, as a measure of residual ammonia / ammonium, and chloride according to modified standard laboratory methods as described in Appendix G. Through this method, the concentration of ammoniacal-N (NH_3 / NH_4^+) and Cl^- in the washing water, and that remaining within the infiltrated SCBB samples after 1, 2, 3, 4, 5 and 6 x 1 hour washings was measured. pH was also monitored in the washing water to allow calculation of the quantity alkaline substances removed from the samples.

5.5 Results and Discussion

5.5.1 Dye tracing of the path of $NaOH_{(aq)}$ through infiltrated SCBB with FITC

Figure 5-7 below shows the bright yellow coloured FITC molecule in the feed solution, in the SCBB and as waste below in the latex tubing.

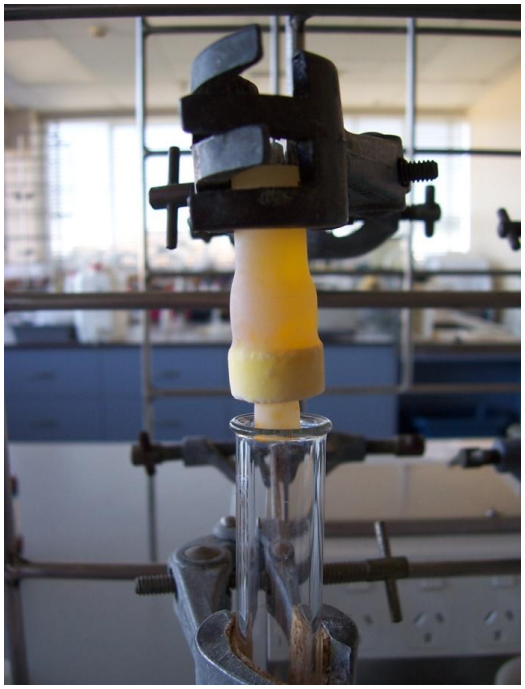

Figure 5-7 - Photograph of SCBB secured within elastic latex tubing with feed tube above containing 0.1 mol L^{-1} NaOH and FITC.

When a total of 3 mL of 0.1 mol L^{-1} NaOH with FITC had passed through the sample, it was extracted from the latex tubing and examined visually as shown in Figure 5-8. The sample was then sectioned parallel to the axis of rotation and across the length of the sample. After the freshly exposed surfaces had been examined visually, these surfaces were presented to a UV light at 254 nm and photographed as shown opposite in Figure 5-9.

Figure 5-8 - Sintered cancellous bone having been infiltrated with chitosan and then the chitosan immobilised with 0.1 mol L^{-1} NaOH containing FITC.

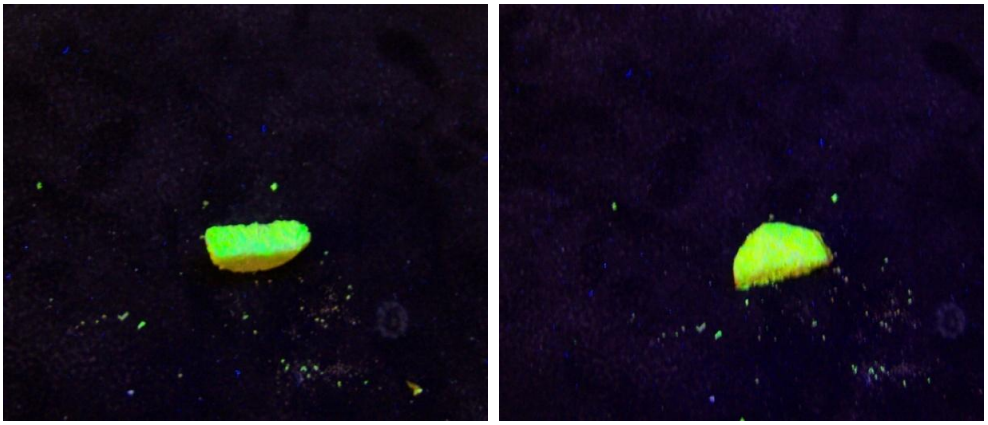

Figure 5-9 – Sectioned piece of sintered cancellous bone having been infiltrated with chitosan, and then the chitosan immobilised with 0.1 mol L^{-1} NaOH containing FITC. Fluorescence was present throughout the sample indicating complete dispersion of FITC.

Due to the low light levels, photographs lacked focus. However, visual inspection under UV light revealed that every sample subjected to the FITC dye treatment contained dye in all regions. This simple method provided an effective means of delivering a neutralising solution to the entire volume of the samples, without displacing the infiltrate within. However, it should be noted, that as the FITC molecule was not actually chemically bound to OH^- ions, its migratory path could not be regarded as a direct means of tracking the path of OH^- movement, but rather a representation of the possible locations a negatively charged species may travel

within the infiltrated sample. The fact that the FITC molecule and anion are many times greater in size than the OH^- ion, and that OH^- diffuses rapidly by a structural diffusion mechanism [134, 135], dispersion of OH^- through the sample is likely to have been as extensive if not more so than FITC.

5.5.2 Immobilisation of Infil-3 solution within SCBB by electric field hydroxide migration

With the apparatus set up as shown in Figure 5-10 voltage was applied, after which gas was seen to evolve immediately from the surface of both of the carbon electrodes. No immediate colour change was apparent on the sample from the photographs, however after 15 minutes a line of pink colouration was seen around the circumference on the surface of the sample at the end closest to the Na_3PO_4 half-cell end. Over the space of 2 hours, this front was seen to move in the direction from the Na_3PO_4 half-cell to the $NaHCO_3$ half-cell. Photographs were taken every 5 minutes as a means of tracking the progress of the "pink front" which indicated a marked change of pH from acidic to basic.

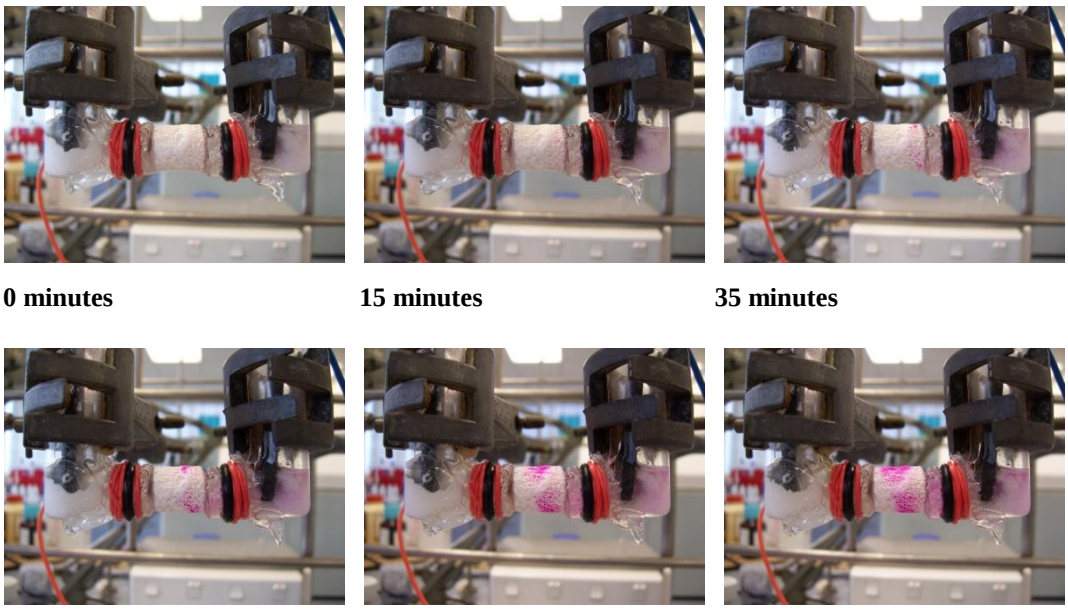

Figure 5-10 – Progress of line of pH change through the chitosan infiltrated SCBB over 115 minutes.

Figure 5-11 below shows a diagrammatic representation of the apparatus and reactions that were proposed to occur causing the migration of anions from the half-cell containing Na_3PO_4 into the chitosan infiltrated SCBB. It was preferable that $PO_4^{3-}{}_{(aq)}$ alone was drawn to the positive electrode as this ion, although basic in nature, was considered more innocuous that OH^-. However, $OH^-{}_{(aq)}$ migrates through a structural diffusion mechanism [135] leading to a coefficient of diffusion larger than other anions, and although it was likely that $PO_4^{3-}{}_{(aq)}$ would also be drawn to the positive electrode, $OH^-{}_{(aq)}$ was predicted to be of more significance. Irrespective of which ion was prevalent, this process was predicted to raise pH within the SCBB leading to precipitation of the chitosan and accompanying acid soluble salt to give an immobilised infiltrate within the SCBB. The reaction at the positive electrode is possibly more accurately represented as $4OH^- \rightarrow H_2O + O_2 + 4e^-$, but both reaction schemes show that the action of the hydrolysis of water is to decrease pH, which is in turn countered by the loss of $CO_{2(g)}$ from the bicarbonate ion.

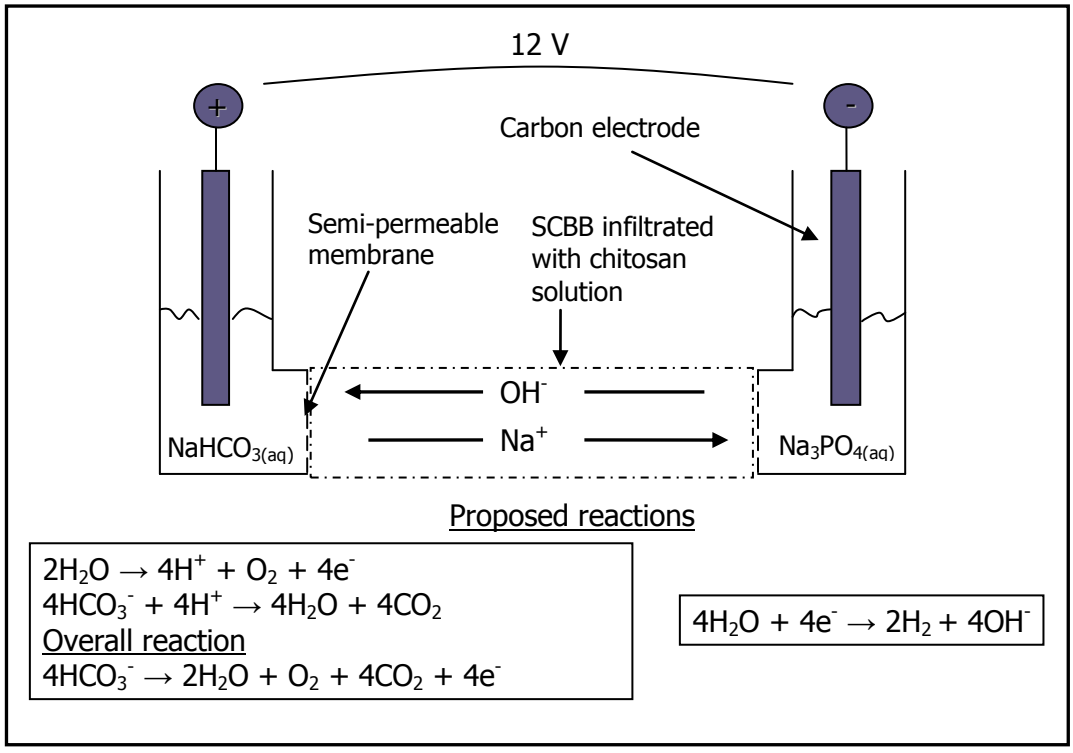

Figure 5-11 - Diagrammatic representation of the electrochemical cell.

Close visual inspection during the experiment revealed that, the pink colouration was apparent within 2 minutes of the voltage being applied at the Na_3PO_4 half-cell end of the infiltrated SCBB sample. However, this was not visible in the early photographs, as it did not possess sufficient intensity to be differentiated against the bright white of the SCBB. Throughout the experiment, there was a lighter pink front that moved slightly ahead of that seen in the photographs above. After dissection, it was apparent that the pink colouration was not dispersed throughout the entire SCBB sample. The most striking absence of colouration was evident at either end of the SCBB sample as shown below in Figure 5-12.

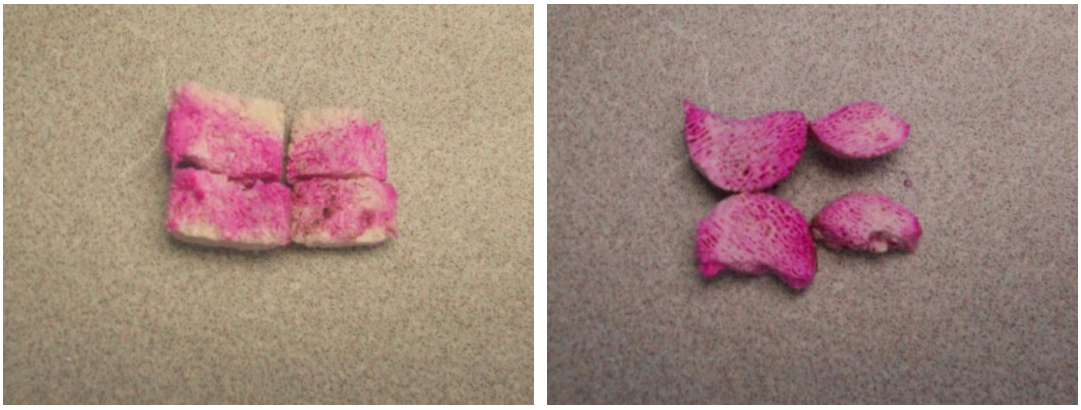

a). SCBB sectioned parallel to axis of rotation showing the pink interior of the sample

b). The same sample showing surfaces created by cutting perpendicularly half way along the axis of rotation.

Figure 5-12 – Photographs of a SCBB sample (~ 10 mm height x 10 mm diameter) having been infiltrated with chitosan and phenolphthalein indicator, and then subjected to an electric field to draw OH^- through the sample.

There are several explanations for why "clear" patches appeared at each end of the SCBB. It is possible that the solution within the SCBB nearest the half-cell generating OH^- became highly alkaline, because the apparatus would have effectively been generating an OH^- gradient, with high levels in the Na_3PO_4 half-cell decreasing in concentration through the sample toward the $NaHCO_3$ half-cell. Phenolphthalein becomes colourless at pH values higher than 12, so the decolouration on the sample end may have been the result of pH values becoming higher than 12 in that area of the sample. Furthermore, phenolphthalein is anionic at pH values higher than 8.2 (when

it turns pink) so that lack of colouration could have been due to the indicator being drawn away from the end of the sample towards the positively charged electrode.

The half cell at the other end of the sample was generating "H^+" (consuming OH^-) from the reactions as shown in Figure 5-11, and if H^+ were able to migrate into the infiltrated SCBB sample would have kept pH low resulting in phenolphthalein remaining colourless. However, with the saturated solution of $NaHCO_3$ and excess $NaHCO_{3(s)}$ all H^+ should have been consumed at the instant of production. An alternative explanation is that the dissolved chitosan, because of its positive charge (chitosonium ion) has been drawn towards the negatively charged electrode leaving only an ionic solution (NaCl) at the $NaHCO_3$ half cell end. Because this solution is in direct contact with saturated $NaHCO_3$ solution through the semi-permeable membrane, the water has been drawn into the $NaHCO_3$ solution due to osmotic differential, leaving bare SCBB behind. See Appendix E for exploration of chitosonium ion migration.

Early on in the development of immobilisation techniques it was recognised that diffusion of ions from an immobilising solution (e.g. NaOH) into the infiltrating solution within the SCBB could be problematic. This was because at the point of contact between infiltrating solution and immobilising solution a precipitate would form, possibly forming a physical barrier that could hinder the continued diffusion of ions. This would be particularly relevant for larger samples, where the extent of immobilisation over time would be governed by Fick's Law of diffusive flux, which states that diffusive flux is proportional to the concentration of the solution divided by the distance travelled. Limitations in diffusion could significantly restrict the ultimate size of the finished product, as large samples could require impracticable lengths of time to effect immobilisation.

Fernandes *et al.* showed that chitosan could be deposited at the surface of an electrode through an induced pH gradient as the result of the electrochemical evolution of hydrogen [136]. This presented an appealing concept for the deposition

of chitosan (and possibly calcium phosphate) within SCBB, if the SCBB could be forced to act as a cathode surface. Although calcium phosphate ceramics such as hydroxyapatite can be polarised [137] to give negatively and positively charged surfaces, they do not conduct significant amounts of current except at elevated temperature (~ 800°C) [138]. However, using a different approach it was proposed to use an electric field to induce the migration of basic anions (OH^-, PO_4^{3-}) through the SCBB infiltrated with chitosan (or chitosan / HAp), thereby accelerating the diffusion process. This would in turn cause the immobilisation of chitosan within the SCBB.

Ultimately, this concept was proven to work in practice on a laboratory scale, although it was unlikely to be practical on a large scale, as the method required time consuming manual manipulation of samples. The technique did however offer one fundamental advantage over other immobilisation techniques, in that the theoretical major by-product was NaCl (conceivably with various levels of Na_3PO_4 and NaOH_. After buffer treatment to attain physiological pH, none of these species would be expected to present a toxicological threat to the human body.

5.5.3 Immobilisation of liquid chitosan infiltrates within SCBB

Figure 5-13 below shows the progression over time of $NH_{3(g)}$ diffusing into the sample made visible by the presence of phenolphthalein. As is apparent from the figure, complete permeation was achieved after 30 minutes of exposure to $NH_{3(g)}$.

5 minutes 15 minutes 30 minutes

Figure 5-13 - Diffusion of NH_3 as seen through sectioned portions of SCBB infiltrated with chitosonium chloride and HAp solution at pH 4.2. Pink colour is due to phenolphthalein indicator.

5.6 Immobilisation of solid chitosonium chloride / CaP with $NH_{3(g)}$

After exposure to $NH_{3(g)}$ no visible change was observed in the chitosonium chloride / CaP solid sample. A section of the IR spectrum (1800 – 900 cm^{-1}) on the solid is shown over the page in Figure 5-14, with spectrum a) showing the material before being treated with ammonia and spectrum b) showing the effect of ammonia treatment. A strong band at 1401 cm^{-1} was seen in the ammonia treated sample which was assigned to the $\nu_4(F_2)$ band of the tetrahedral ammonium ion [139]. Other bands in the region 900-1200 cm^{-1} where largely due to P-O stretching modes of phosphate c.f. IR spectrum of SCBB Figure 3-21, section 3.5.8. While a broad band centred at 1650 cm^{-1} was assigned to a combination of the chitosan carbonyl C=O-NHR at 1651 cm^{-1} for the acetylated amine and the amine NH_2 deformation band at 1590 cm^{-1} [100, 140].

The presence of the IR peak for the tetrahedral ammonium ion was strong evidence that ammonia gas had reacted with protons in the sample to give the ammonium ion, effectively proving that the gas had penetrated the sample. When portions of composite precipitate through the entire sample were analysed under IR, it was seen that ammonia gas had penetrated to the centre of the sample, or ~ 2 – 3 mm. This is shown in Figure 5-15 where IR spectra (a – e) are sub-samples taken from exterior to centre and then to exterior again, so that spectrum c) represents the centre of the solid "ball". All spectra showed the presence of the absorbance band for the ammonium ion showing that ammonia gas had penetrated all the way into the sample, however the lower relative intensity of the ammonium 1401 cm^{-1} peak with respect to adjacent bands in the central spectrum suggested that the centre of the sample had received less exposure to $NH_{3(g)}$ as can be expected.

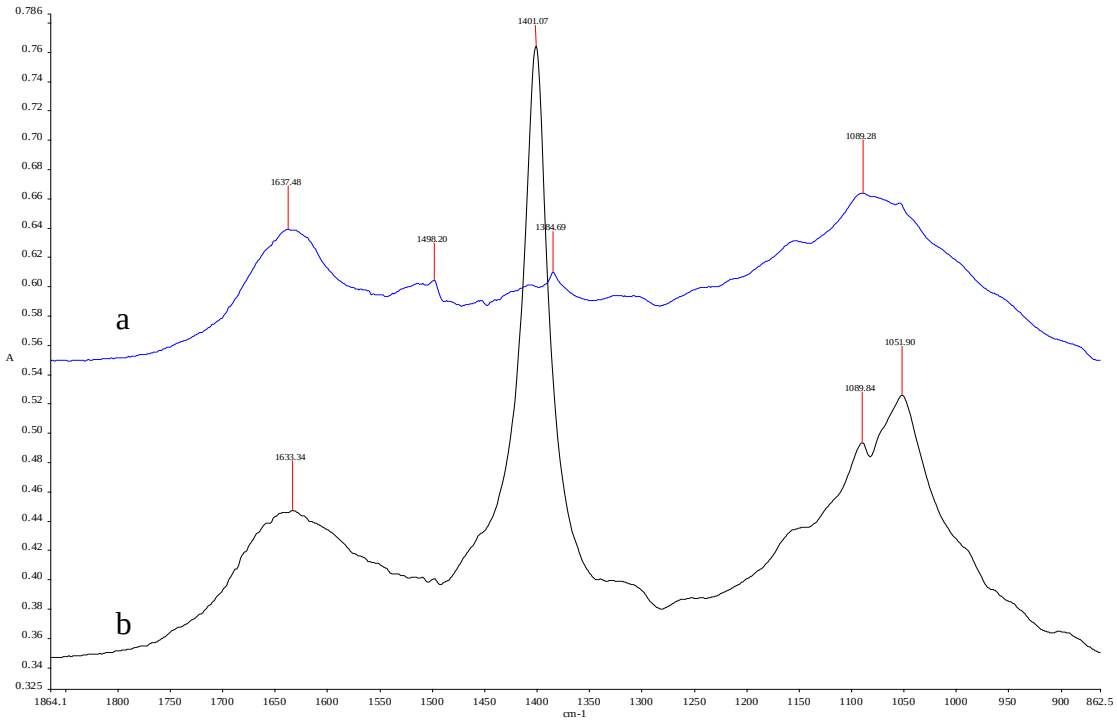

Figure 5-14 – IR spectra of precipitated chitosonium chloride / CaP (a) and the same material after being exposed to $NH_{3(g)}$ for 12 hours (b) showing the strong IR absorbance band for the tetrahedral NH_4^+ ion [139]

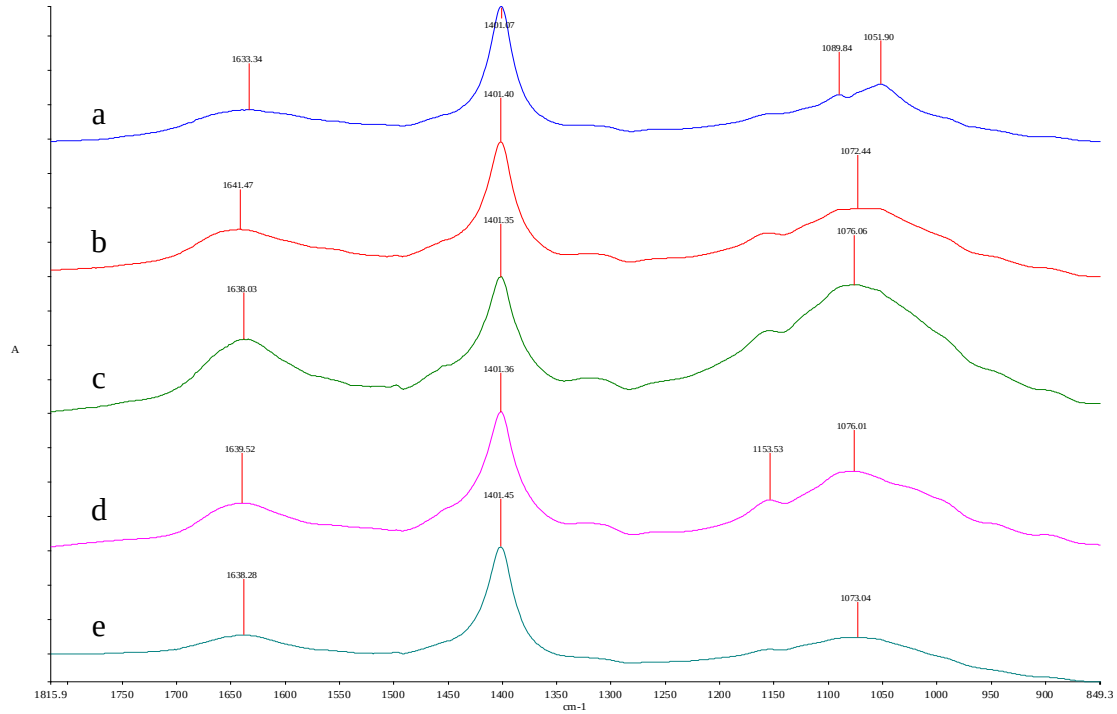

Figure 5-15 – IR spectra representing progressive sampling from surface, through the centre and then to other surface of the $NH_{3(g)}$ treated solid chitosonium chloride / CaP composite.

This experiment proved that the gaseous ammonia molecule was able to diffuse through the solid chitosonium chloride / CaP material, which was important in establishing the feasibility of repetitive infiltrations into SCBB followed by a single immobilisation step.

However, one important property of the solid chitosonium chloride / CaP was also revealed. It was found that if the samples were left to sit for days or weeks after being exposed to $NH_{3(g)}$ without being washed immediately in water, the chitosan infiltrate was seen to revert back to its soluble form. As graphically presented in Figure 5-16, this was believed to be due to the loss of the $NH_{3(g)}$ back to the atmosphere upon sitting. This process would dictate that over time a point would be reached where there was insufficient $NH_{3(g)}$ to maintain the pH above ~ 8 when the solid was exposed to water, hence rendering the material soluble.

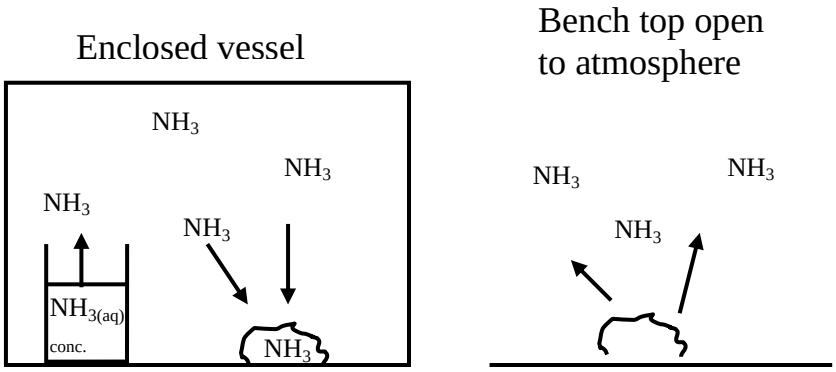

Figure 5-16 - Diagrammatic representation of the loss of NH_3 bound to chitosonium chloride.

Nevertheless, in theory ammonia should still be able to extract a proton from the protonated chitosan amine group, because chitosan is a weaker base than ammonia (pK_b = 6.3 [141], pK_b = 4.75 respectively). However, it is possible that the reaction stalled at the middle stage (and then reversed), because the by-product NH_4Cl was not washed away by water, see Figure 5-17. Therefore, it was essential that soon after exposure to $NH_{3(g)}$, the composite material was washed in distilled water.

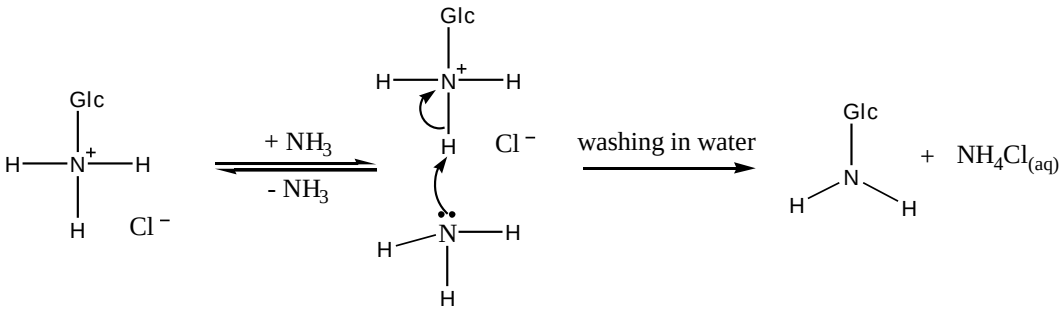

Solid chitosonium chloride

$NH_{3(g)}$ having diffused into the solid

Removal of ammonium chloride by washing in water

Figure 5-17 - Reaction scheme of chitosonium chloride with ammonia gas showing its reversible nature.

5.6.1 Immobilisation of infiltrate solutions by thermal hydrolysis of urea

When SCBB samples infiltrated with Infil-7 (Table 1, p. 72) solutions were heated by steam within an autoclave, chitosan and CaP were seen to precipitate within the material after 1 – 2 hours. This result was more facilely observed in test solutions placed in beakers that accompanied the infiltrated SCBB samples in the autoclave. As Table 3 below shows, heating the solutions in an autoclave was successful in increasing pH. After autoclaving for 1 hour pH had risen to 6.76 in the chitosonium chloride (without HAp), however no chitosan precipitation was apparent with the solution remaining clear. Chitosan has a transition from soluble to insoluble state occurring between pH 6 - 6.5 [142, 143].

Table 3 – Increase in pH with time for chitosonium chloride and chitosonium chloride / HAp solutions in combination with urea heated in an autoclave.

Time (hours)	Chitosonium chloride solution (pH)	Chitosonium chloride / HAp solution (pH)
0	4.52	3.65
1	6.76	6.06
2	7.58	7.32
3	7.75	7.47
4	7.99	7.64

However, a sample of the liquid was taken at this stage and set aside, and found after a few hours of standing to have gelled indicating at least partial chitosan precipitation. In contrast, the chitosan solution containing HAp (with the initial lower pH of 3.65) showed a milky precipitate after 1 hour. Given the observed pH after 1 hour of 6.06, this milky precipitate was probably a calcium phosphate phase.

After two hours in the autoclave, the chitosan only solution had gelled. The pH was measured at 7.58, while at the next two hourly measurement times, pH readings were 7.75 and 7.99 for 3 hours and 4 hours respectively. At both of these times, the sample was observed to have formed a clear gel, but with no cloudiness that would have otherwise indicated the presence of a solid precipitate, as was seen in the preparation of chitosan suspensions, see section 4.3.3.

In the solution containing HAp, after two hours in the autoclave, pH had risen to 7.32 and chitosan precipitation was obvious as characterised by a white precipitate reminiscent of crabmeat. After a further hour pH increased to 7.47 and then finally 7.64 after a total of 4 hours, with a visually noticeable increase in the quantity of chitosan precipitate at each time point. Figure 5-18 below, shows the increase in pH over time for the chitosonium chloride and chitosonium chloride / HAp with urea solutions.

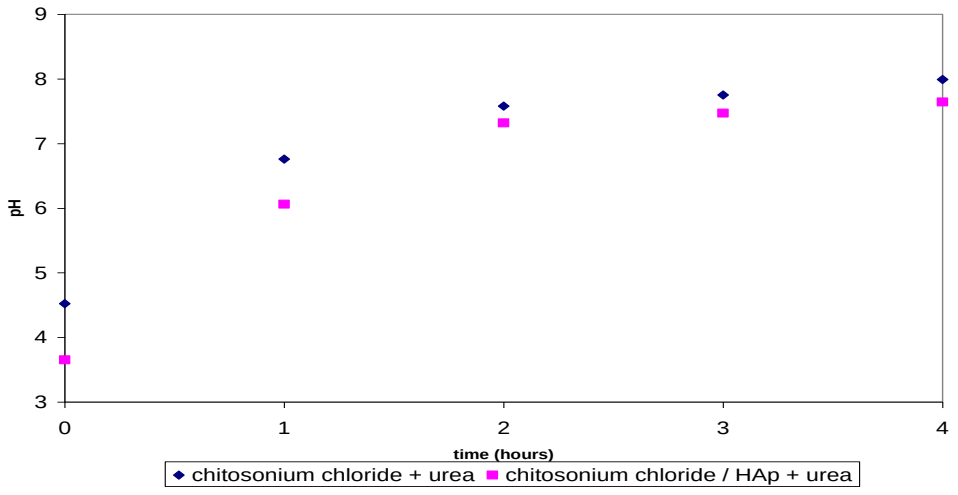

Figure 5-18 pH against time for chitosan solutions in autoclave subjected to 15 psi pressure / high temperature steam (~ 120°C).

Results showed that 2 hours was a sufficient length of time to "immobilise" via precipitation both infiltrating solutions using this method.

IR Spectral Analysis

Urea hydrolyses thermally to give ammonia and carbon dioxide. Carbon dioxide is only partially soluble in water and so is lost rapidly under elevated temperature. This leaves ammonia in solution, as it is more soluble, to react as a base with the acid used to dissolve chitosan. The reaction of ammonia in water with $HCl_{(aq)}$ gives ammonium and chloride ions. Therefore, IR spectra over the period of heating would be expected to show a decrease in signal for urea and an increase for the ammonium ion. Figure 5-19 and Figure 5-20 opposite show the IR spectra for urea and ammonium chloride respectively. The IR spectrum for urea shows two strong and distinctive peaks around 1600 wavenumbers; one at 1624 cm^{-1} corresponds to the antisymmetric (B_1) NH_2 bending mode and the other at 1676 cm^{-1} to the (A_1) ν_{CO} + NH_2 symmetrical bending mode. While the peak at 1155 cm^{-1} was assigned to the NH_2 rocking (B_1) mode, the peak at 1464 cm^{-1} was assigned to the ν_{CN} antisymmetric mode, and the peaks at 3353 and 3440 cm^{-1} were assigned to N-H stretching modes [144].

Ammonium chloride has a relatively simple IR spectrum with strong peaks centred around ~ 3200 corresponding to N-H stretching modes and a strong characteristic peak at 1403 cm^{-1} assigned to the $\nu_4(F_2)$ vibrational mode of the tetrahedral ammonium ion (Nakamoto, 1986) [139]. Using these characteristic IR fundamental peaks of the urea and ammonium chloride, it was possible to monitor the conversion of urea to ammonium ions, which is further explored over the page in Figure 5-21. Here the spectra of urea (a), chitosonium chloride / HAp / urea infiltrate autoclaved for 1 hour (b) and chitosonium chloride / HAp /urea that had not been autoclaved (c) are presented. The IR spectrum confirmed that the ammonium ion was produced in the autoclaved solution as indicated by the presence of a peak at 1401 cm^{-1}, which was absence in the non-autoclaved starting material (c).

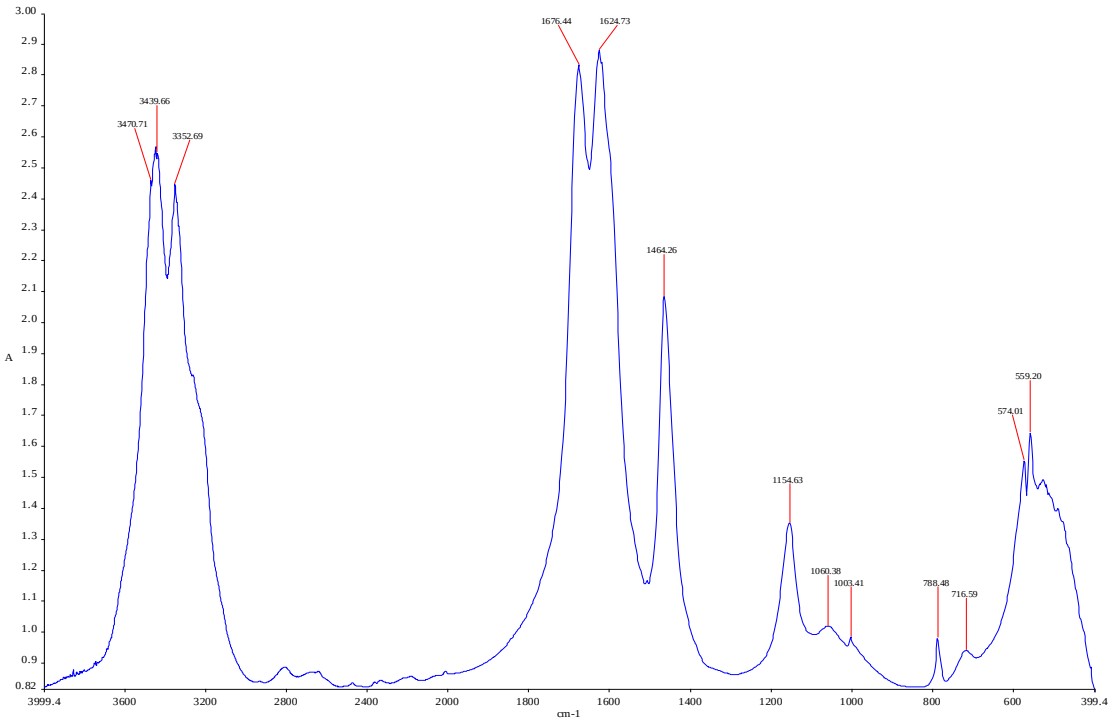

Figure 5-19 IR spectrum of urea as a KBr disk

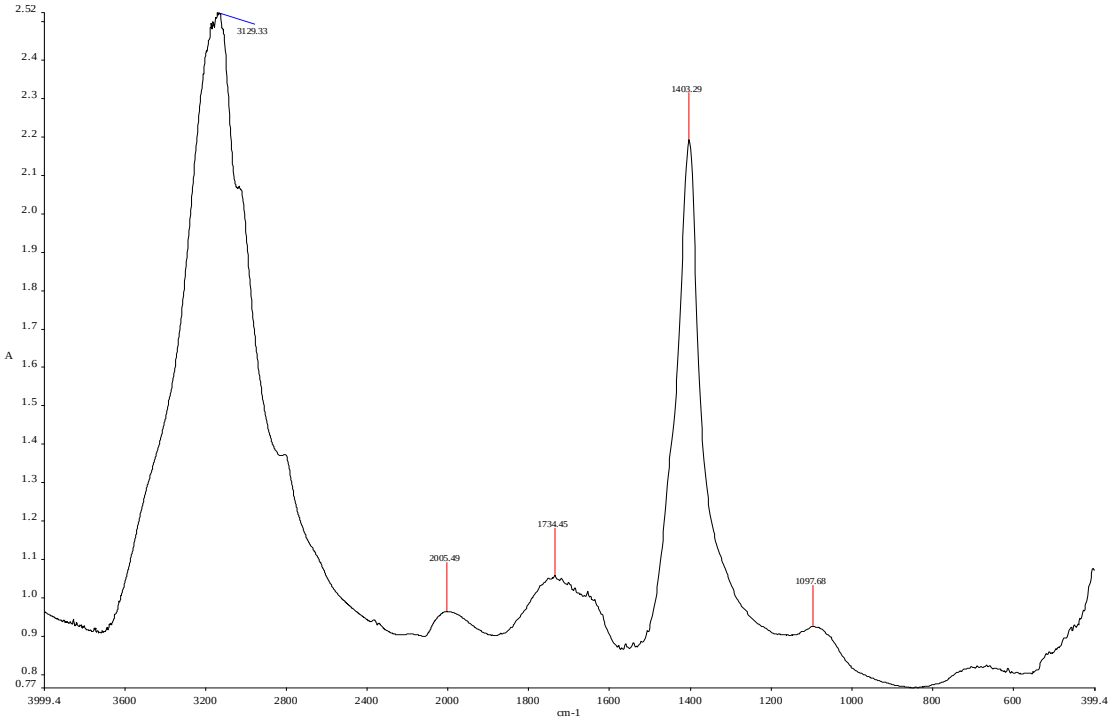

Figure 5-20 IR spectrum of ammonium chloride as a KBr disk

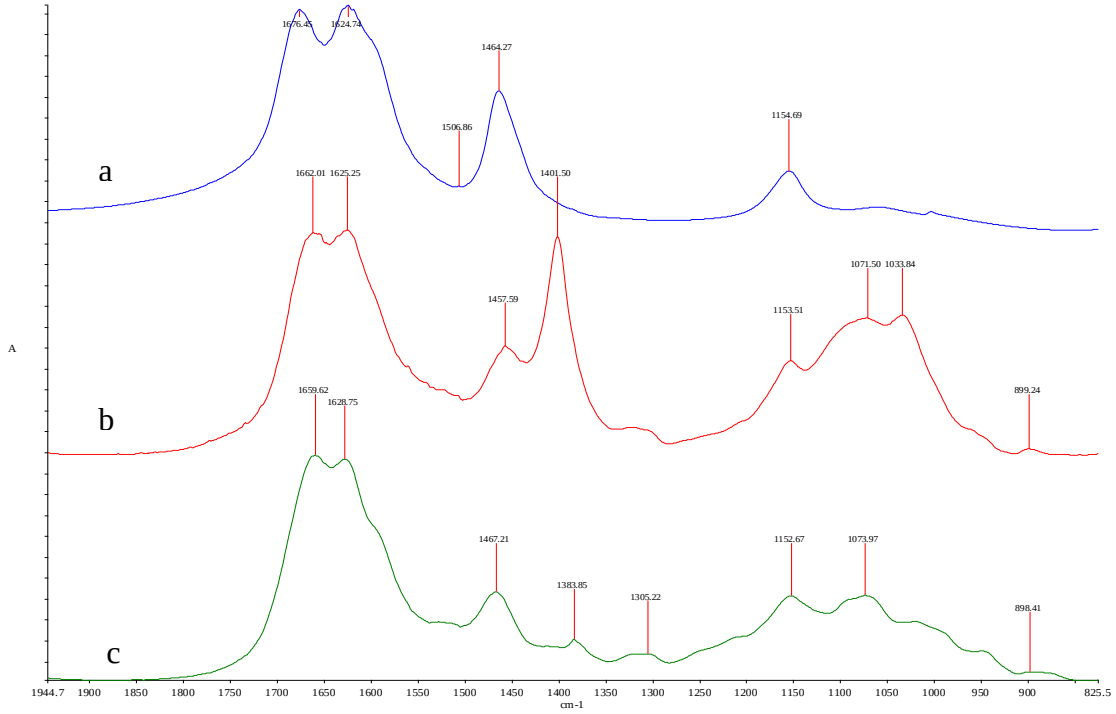

Figure 5-21 – IR spectra of urea a), chitosonium chloride / HAp / urea infiltrate after 1 hour of autoclaving b) and chitosonium chloride / HAp / urea mixture before being autoclaved c).

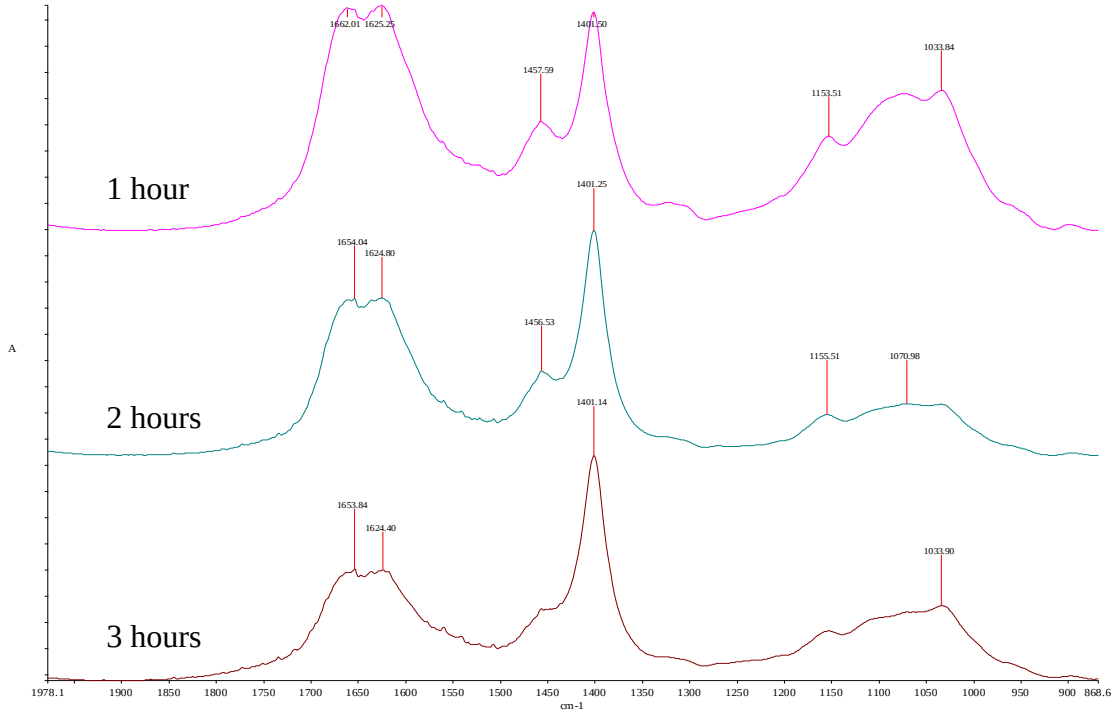

Figure 5-22 IR spectra of chitosonium chloride / urea solutions with respect to time spent in autoclave

Displayed in Figure 5-22 are the IR spectra of the chitosonium chloride / HAp / urea solution with respect to time spent in the autoclave from 1 to 3 hours. The spectra showed that the NH_4^+ peak at 1401 cm^{-1} increased in intensity over 3 hours of autoclaving as expected relative to the two broad peaks centred around 1625 cm^{-1} and 1662 cm^{-1}. These two broad peaks were assigned to a combination of the two distinctive urea peaks at 1624 cm^{-1} (antisymmetric (B_1) NH_2 bending mode) and 1677 cm^{-1} ((A_1) ν_{CO} + NH_2 symmetrical bending mode), and the chitosan carbonyl C=O-NHR band at ~ 1670 cm^{-1} and amine NH_2 band at ~ 1590 cm^{-1} [140].

Ultimately, results from the experiment showed this method of immobilisation using urea promising as a method for the deposition of an infiltrate within the SCBB material. However, there was one overriding concern that the elevated temperatures may lead to a degradation of the chitosan material. As a means of avoiding heating the material, the potential of adding the enzyme urease to the urea containing solutions was investigated.

5.6.2 Immobilisation of infiltrate solutions by urease catalysed decomposition of urea

It was found that 2.5 – 3.0 mg urease per 50 mL chitosan solution containing 0.15 – 0.20 g urea was an adequate weight ratio of urease to urea to result in a pH rise sufficient to cause precipitation over 2 - 5 hours. Urease is active in the catalysis of the urea hydrolysis reaction at pH values as low as pH 3.5 [145], with activity significantly diminishing as pH 8 is approached [146]. This property was regarded as ideal in the production process of the infiltrated SCBB material, as pH 8 is sufficient to cause the precipitation of chitosan and calcium phosphate, while being only slightly above that of physiological pH of 7.4. Figure 5-23 shows a plot of pH against time for Infil-3 (Table 1, p. 72) infiltrating solution with the urea / urease combination.

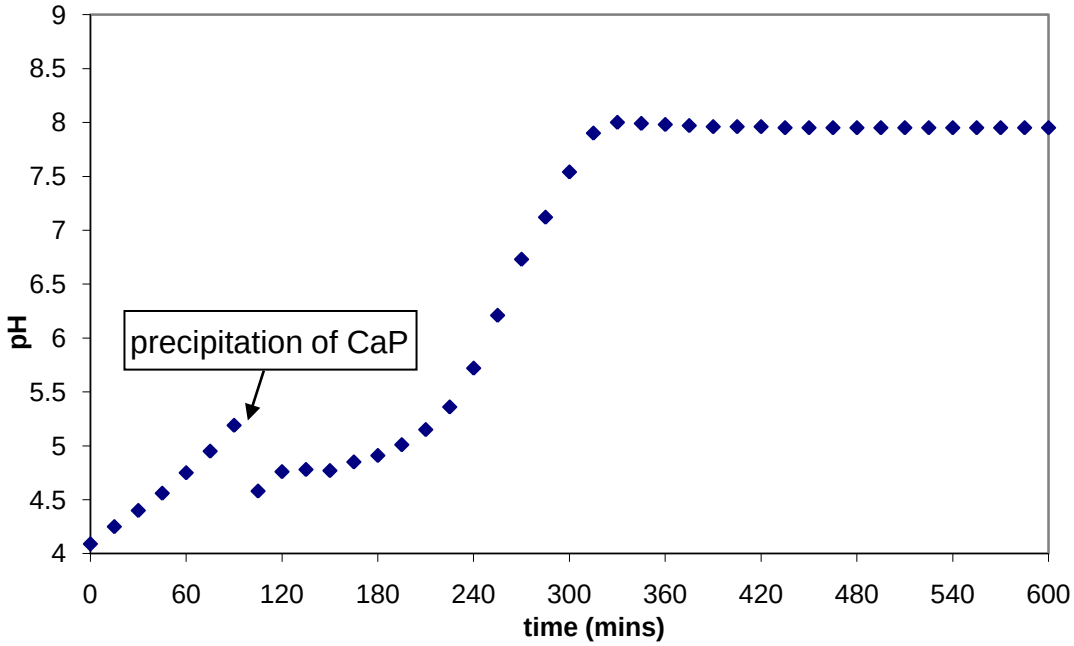

Figure 5-23 – Plot of pH against time for Infil-3 infiltrating solution with urea / urease

This immobilisation system was trialled conceptually, but not carried forward to routine implementation due to concerns about the biocompatibility/safety of urease if it remained as a residue in the SCBB.

5.7 Removal of immobilisation by-products - washing

SCBB samples infiltrated once with Infil-1 solution (Table 1, p. 72) and immobilised as described in section 5.3.3 were used for this experiment. pH readings of water during washing showed a rapid increase immediately after samples were placed in the water during the first wash. The rate of increase in pH after samples were placed in the washing water was seen to decrease as the number of 1-hour long washings increased. pH was used to estimate the concentration of OH^- in the washing water for each of the washing cycles, and is shown in Figure 5-24. The concentration of OH^- in the washing water of the infiltrated samples contrasts well with the non-infiltrated control samples shown in Figure 5-25, which showed only a slight increase in OH^- over the washing period. This increase in OH^- in the washing water was attributed to the dissolution of $Ca(OH)_2$ from the SCBB samples that is believed to have formed during sintering through the thermal decomposition of the carbonated apatite.

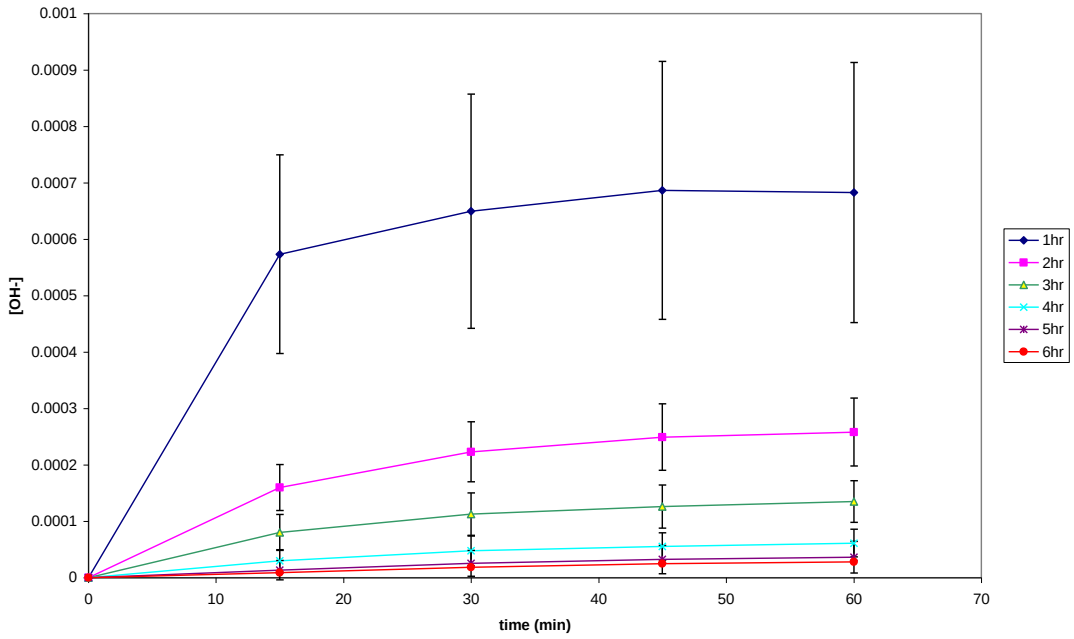

Figure 5-24 - Average concentration of OH^- in washing water for infiltrated and immobilised SCBB samples with time and number of washes. Error bars represent 1 S.D.

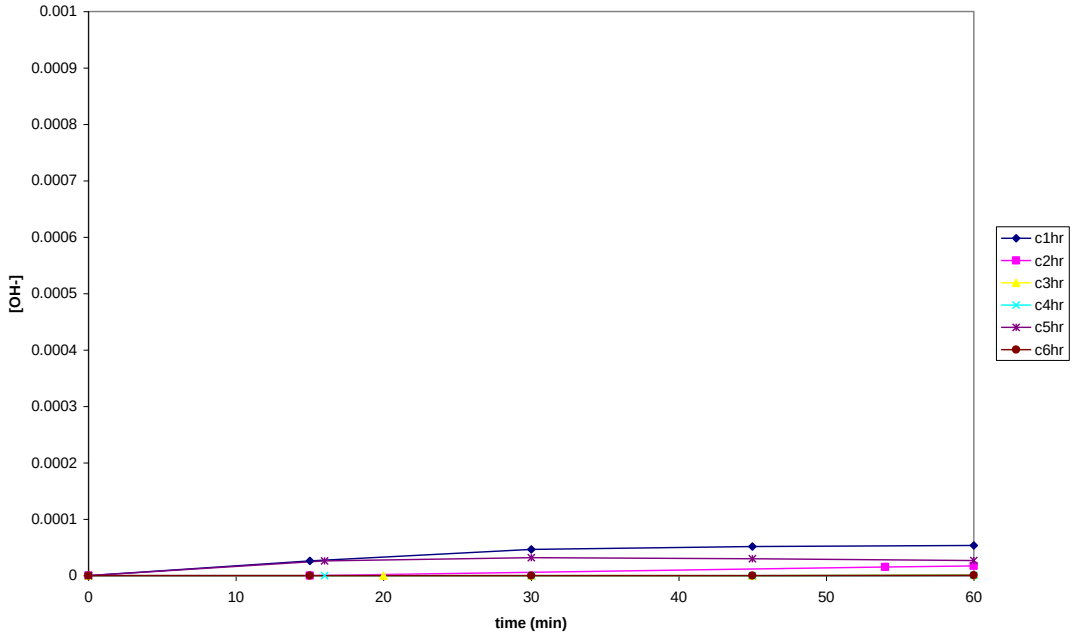

Figure 5-25 - Concentration of OH^- in washing water for control samples (untreated SCBB) with time and number of washes. Y-axis scale is the same as above in Figure 5-24 as a means of comparison.

The concentration of total ammoniacal-N and Cl^- was measured in the washing water, with these species showing an increase in concentration over the 1 hour washing period and a steady decline for each wash cycle as shown below in Figure 5-26 and Figure 5-27.

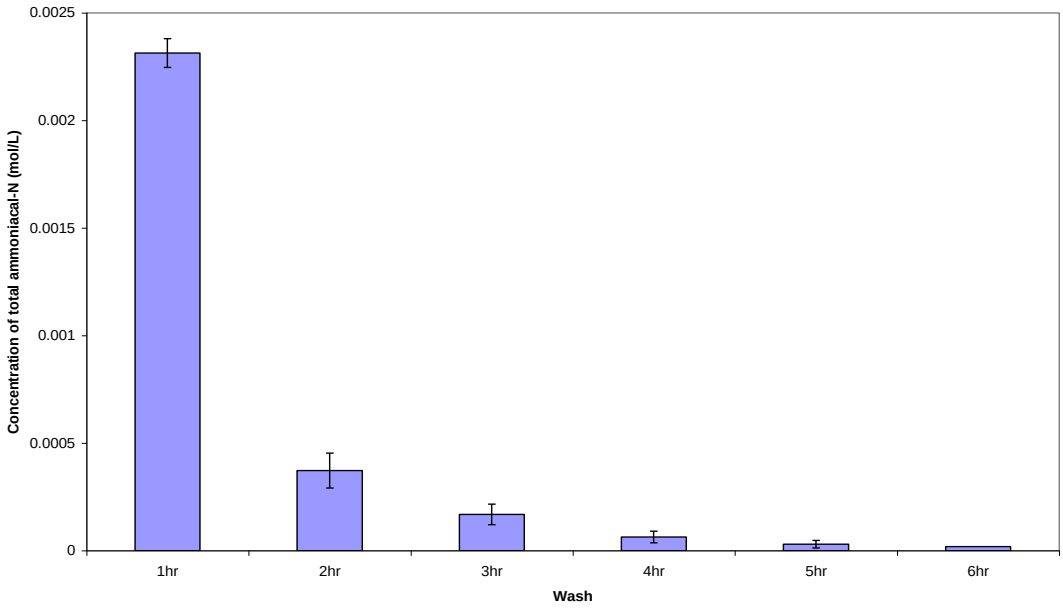

Figure 5-26 - Total ammoniacal-N in washing water for the infiltrated and $NH_{3(g)}$ immobilised samples against hours of washing

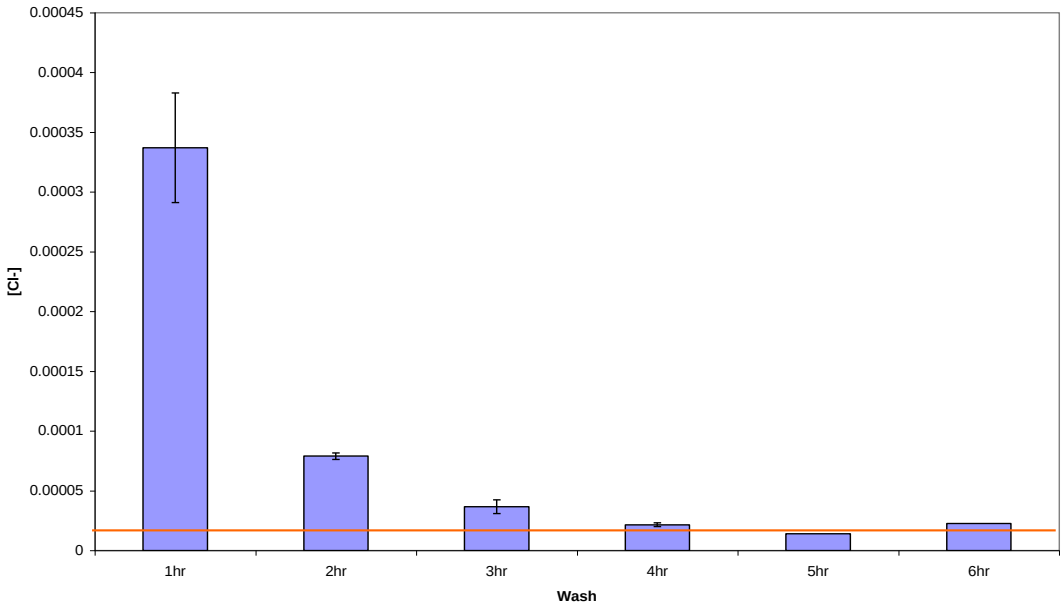

Figure 5-27 - Concentration of Cl^- in washing water for the infiltrated and $NH_{3(g)}$ immobilised samples per wash. Horizontal line represents detection limit for method.

Figure 5-24 shows an increase in OH^- concentration over time per each wash in the washing water, as $NH_{3(aq)}$ was washed out and/or diffused out of the infiltrated samples over time. However, with each successive wash, less $OH^-_{(aq)}$ was seen in the washing water at the end of the 1 hour. Depending on diffusion rates through the samples, this could represent a depletion of $OH^-_{(aq)}$ throughout the entire sample or depletion of $OH^-_{(aq)}$ only in the outer reaches of the sample. It was important to establish that by-product was being removed from throughout the sample, therefore total ammoniacal-N (NH_3 + NH_4^+) and chloride levels within the samples were measured. Although a measurement of OH^- concentration within the sample would also have been useful, it was thought that direct measurement of $OH^-_{(aq)}$ concentration within the sample would be made unreliable by the process of sample preparation, which involved crushing the SCBB material. This could have exposed previously unexposed SCBB particle surfaces to the aqueous environment, surfaces which may have contained CaO formed during the sintering process. This would have led to an over estimation of the OH^- concentration contained within the SCBB samples.

In contrast to the washing water where ammoniacal-N and Cl^- levels were calculated as concentrations, ammoniacal-N and Cl^- levels within the samples were calculated as mol per sample (with each sample being the ~ 10 mm diameter x ~ 10 mm height SCBB cylinder). The values after each 1-hour wash showed a steady decline in levels of both ammoniacal-N and Cl^- as presented in Figure 5-28 and Figure 5-29. 4 x 1-hour washings proved to remove a large percentage of the by-products formed during the immobilisation process with $NH_{3(g)}$. Depending on requirements, 4 x 1-hour washes may be sufficient to remove adequate quantities of by-products, especially if samples are subsequently treated for long time periods with a buffer solution to bring all regions of the interior of the sample to physiological pH. Cl^- and NH_4^+ in low concentrations are not physiologically toxic, with both ions existing naturally in the body. In fact, NH_4Cl solutions are administered intravenously for medicinal purposes with up to 10 grams being administered over 3 hours for treatment of hypochloremic states (abnormally high chloride) and metabolic alkalosis (abnormally high pH) [147]. While Lockwood *et al.* reported the concentration of 'ammonia' (combination

of ammonium and ammonia species) to be between 73 – 113 µmol/L, with an average of 98 µmol/L for healthy individuals [148].

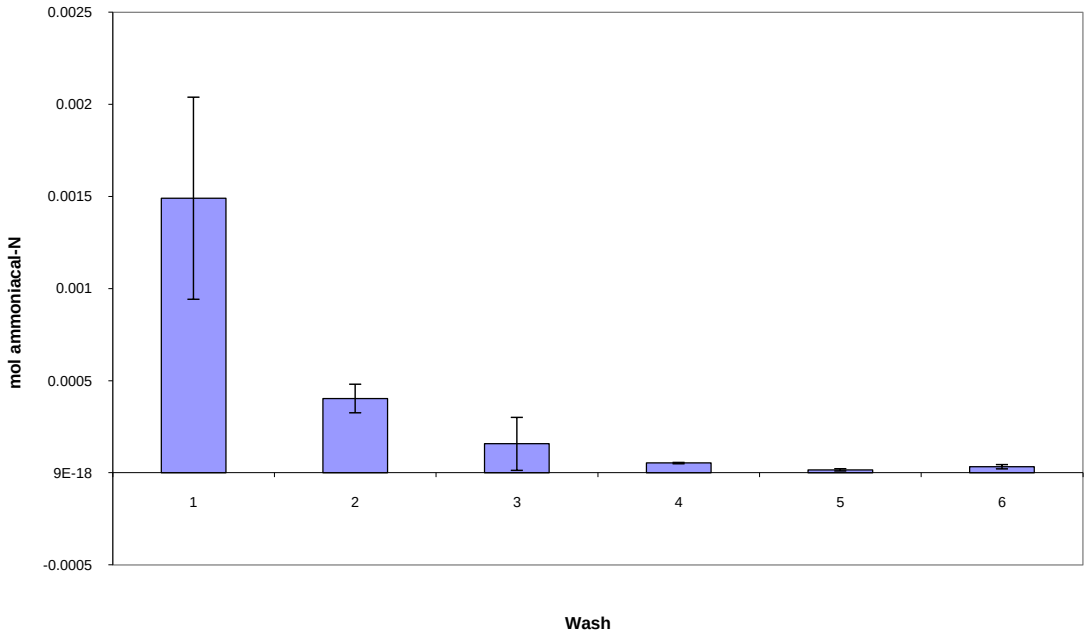

Figure 5-28 - Mol ammoniacal-N per infiltrated and immobilised SCBB sample after being washed for 1 to 6 hours (control levels below detection limit). Error bars represent 1 standard deviation.

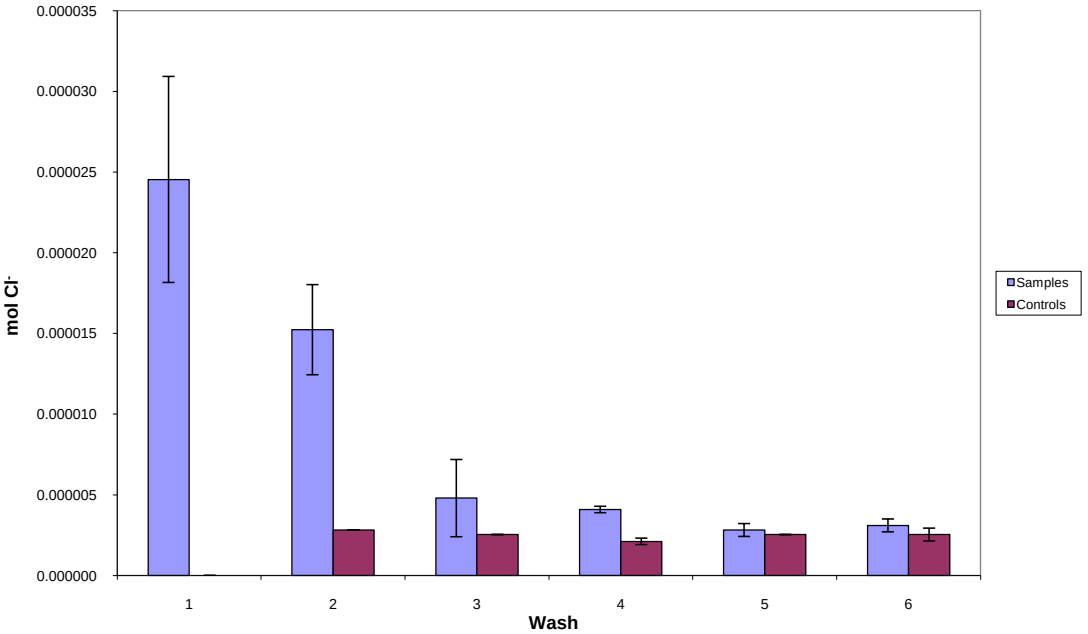

Figure 5-29 - Mol Cl^- per infiltrated and immobilised SCBB sample after being washed for 1 to 6 hours. Controls for the 1-hour wash were below detection limit as was one of the controls for the 2 hour wash. Error bars represent 1 standard deviation.

Results from the washing experiment above enabled the estimation of the residual levels of NH_3 / NH_4^+ and Cl^- within the infiltrated-immobilised SCBB samples after each 1-hour wash in distilled water. This was important, as results from the first biocompatibility cell culture test (Protocol-1 samples) showed that there was a toxicity problem with samples washed 3 times in distilled water and treated with a 50 mM phosphate buffer at pH 7.4 for 15 minutes.

Therefore, a calculation of the residual levels of NH_3 / NH_4^+ and Cl^- was made for samples after 3 x 1-hour washes, which is presented in Appendix H. This calculation showed that after the 3rd 1-hour wash the average $[Cl^-]$ = 0.008 mol L^{-1}, and the average $[NH_3$ / $NH_4^+]$ = 0.26 mol L^{-1}. From these results it was apparent that a significant concentration of $NH_{3(aq)}$ was present in the bone samples after 3 washings. As mentioned above NH_3 / NH_4^+ species are present in normal healthy individuals, but not in the aforementioned concentrations. In fact, when considering cell cultures across a range of cell types, a concentration of NH_3 / NH_4^+ as low as 2 – 3 mmol L^{-1} has been shown to inhibit cell growth, with 5 – 15 mmol L^{-1} shown to cause apoptosis and with concentrations in the vicinity of 50 mmol L^{-1} causing necrosis [149].

A large portion of this NH_3 / NH_4^+ was expected to be lost to the atmosphere upon drying, a process that was not allowed to occur between the 1-hour washes in this experiment. Nevertheless, as the Protocol-1 biocompatibility test showed in section 7.4, 3 washes, subsequent drying and a 15-minute buffer treatment were not sufficient to eliminate toxicity effects. However, toxicity effects were markedly reduced (eliminated in some cases) by soaking samples in phosphate buffered saline (PBS) at pH = 7.4 for 24 hours.

5.8 Conclusion

Several immobilisation systems were trialled in the course of this research. The urea systems, including the thermal hydrolysis of urea and the urea / urease catalysis

combination, were effective in precipitating chitosan and calcium phosphates from infiltrating solutions to give immobilised solids. An added advantage to these systems, was that the end pH of the solutions was near pH = 8 which is close to physiological pH. The "electric field-induced migration of basic ions" system was also successful in raising the pH of the infiltrating solution, and thereby effective in precipitating the dissolved solid infiltrate material. However, this system was complicated and not suited to large-scale application. Ultimately, exposure to ammonia gas was the method routinely employed to raise pH and immobilise infiltrate material. A complementary washing procedure to remove excess ammonia and immobilisation by-products was developed and evaluated for efficacy. This method of washing in distilled water was found to reduce the level of ammonia progressively in the immobilised SCBB samples.

CHAPTER SIX

6 Mechanical Testing

6.1 Introduction

As a bone replacement material, the environment into which the infiltrated SCBB is to be implanted may be subjected to mechanical stresses and physical trauma before the body's healing processes have time to remould and adapt its form to that demanded by site of implantation. Accordingly, it is preferable if the implant, itself, is manufactured to possess physical properties more closely approximating those of the bone material it is to replace than the pure SCBB. Therefore, a goal of this research was to increase the mechanical strength of the SCBB material through the infiltration of a reinforcing material. In order to measure the physical properties of the infiltrated SCBB material, it had to be subjected to mechanical testing, as had the unaltered SCBB material, and the values of the respective properties compared to evaluate whether an improvement had been made. A means of testing mechanical properties on materials such as SCBB is tensile testing or compression testing, which are discussed in the following section.

6.1.1 Mechanical testing – Instron instrument

Many various material testing methods and instruments exist to compare the physical and mechanical properties of the solid materials. Strength testing is often performed on an Instron instrument or equivalent, which consists of a moveable crosshead, gripping attachments (or pressure platens for compression testing) and extensometer (external or as part of the instrument) as shown over tht page in Figure 6-1. Tensile testing involves gripping a material between crosshead and base, often machined into a "dog bone" like shape, in order to position the point of failure away from the

gripping points. A force is applied along the axis of the material by instructing the crosshead to move away from the base plate while at the same time extension is measured.

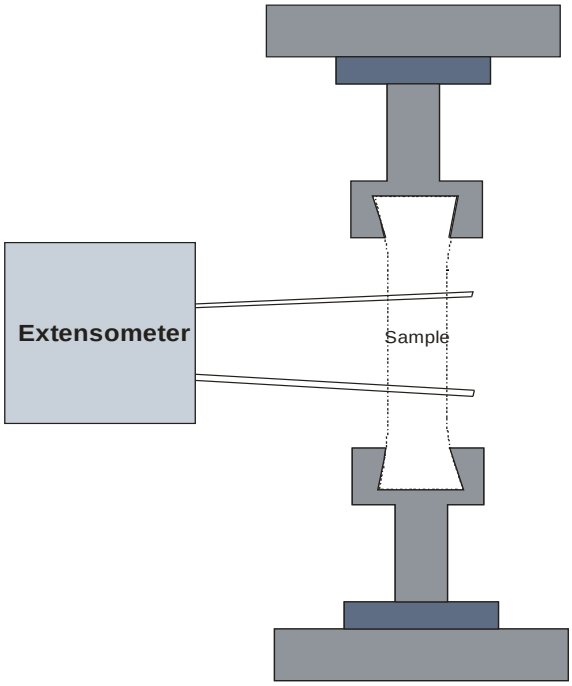

Figure 6-1 –Diagrammatic tensile strength test apparatus showing "dog-bone" shaped specimen gripped at either end with external extensometer.

To normalise measurements in order to be able to compare the strength of samples of differing dimensions, force is converted to engineering stress by factoring in the original cross-sectional area of the sample before deformation. Extension is converted to engineering strain, which is the change in length of the tested portion of the material over the original length. From a tensile test, a plot of stress versus strain is obtained, which contains mechanical information such as yield strength, tensile strength, and stiffness amongst other variables [150]. For a material such as bone, tensile testing may be employed, but samples must be precision-prepared to reproducible dimensions. This is a process which requires time, advanced machining capability, and a relatively large sample. An alternative testing method is compression testing, where samples are placed between platens attached to the crosshead and the base, after which the crosshead is moved toward the base. In this approach, stress and strain are also recorded as in tensile testing to give a stress

versus strain plot, which can be similar in appearance to a tensile test, except that, a point of comprehensive failure may not exist, especially in ductile materials. Nevertheless, in trabecular bone identical elastic modulus values are seen in both tensile and compression testing, while measured strength values are similar at lower modulus values, but diverge linearly at higher modulus values, with compression testing resulting in the calculation of higher strength values [82]. Despite its ease of use, compression testing suffers from a number of disadvantages that render values less accurate than tensile tests. If the specimen is misaligned, as is presented in Figure 6-2a below, then large stresses can be focused on one particular area which leads to an under estimation of Young's modulus, and inaccurate strain values. This factor can be accommodated for by the introduction of a spherical socket or ceramic bearing [151] to allow the top platen to swivel and align with specimen as shown in Figure 6-2b below.

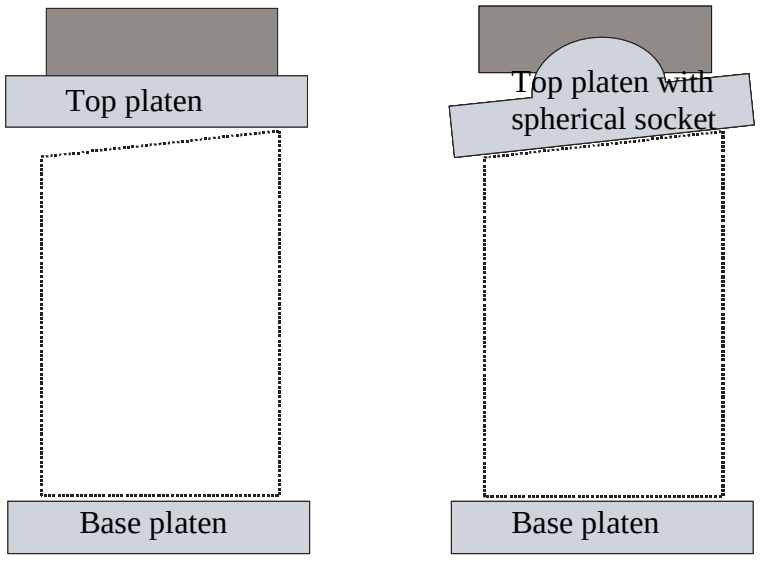

a) b)

Figure 6-2 – Diagrammatic representation of a spherical socket allowing the top platen to swivel in compression testing.

Another limitation of compression testing affects samples of bone origin in particular. This is the tendency of bone samples to be weaker at the cut ends than in the centre of the material due to the localised destruction of the intact trabecular architecture to leave exposed non-braced single weak struts of material. These collapse easily to give

exaggerated strain rates with correspondingly low stress values, which appears as a "toe-region" on a stress / strain plot. This factor can be corrected by adjusting the plot so that an extension of the linear region projects through stress and strain values = 0, as shown below in Figure 6-3.

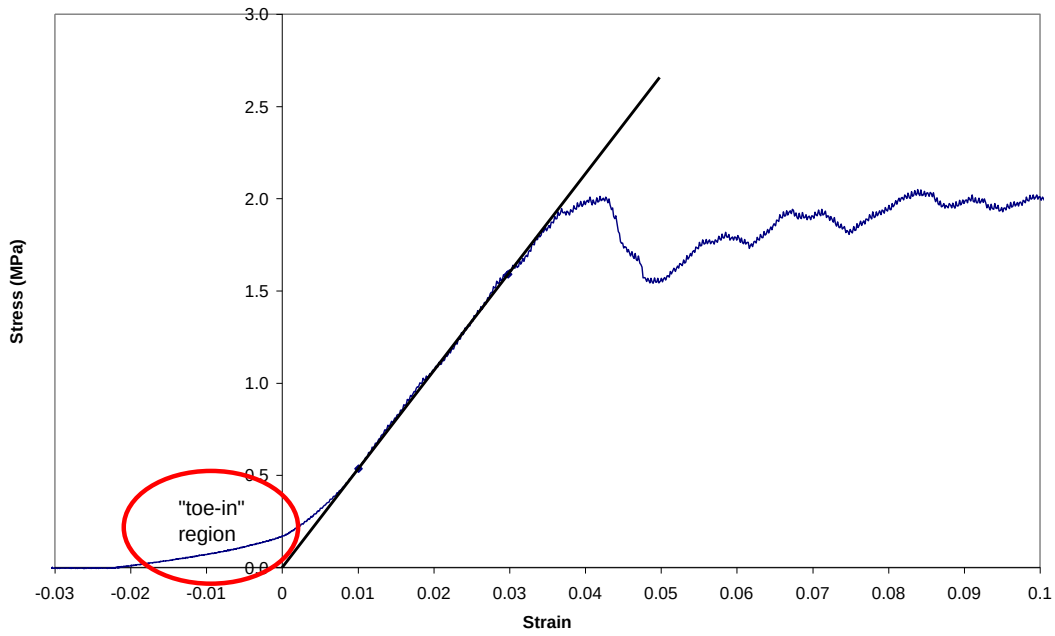

Figure 6-3 – Example of a stress vs. strain compression test plot with "toe-in" region indicated. The data have been transposed so that extrapolation of the linear region intercepts stress and strain = 0 to reduce error which would otherwise be caused by the "toe-in" region.

6.2 Materials

A mechanical testing apparatus was modelled on a system in use at the University of Otago operated by Prof. Mike Swain, the components of which are shown in Figure 6-4 opposite. A vertical push rod was designed and manufactured to fit into the attachment socket of the load cell located in the horizontal cross arm of the Instron instrument. A thread and locking nut below the socket were incorporated into the design to prevent load on the securing pin. A pivot point was created at the end of the push rod by machining a spherical cavity into the underside, and to complete the pivot, a stainless steel sphere (ball bearing) with the identical radius to that of the cavity was cut in half (insert Figure 6-4). A Teflon sheath was secured over the half ball to minimise friction on the SCBB samples.

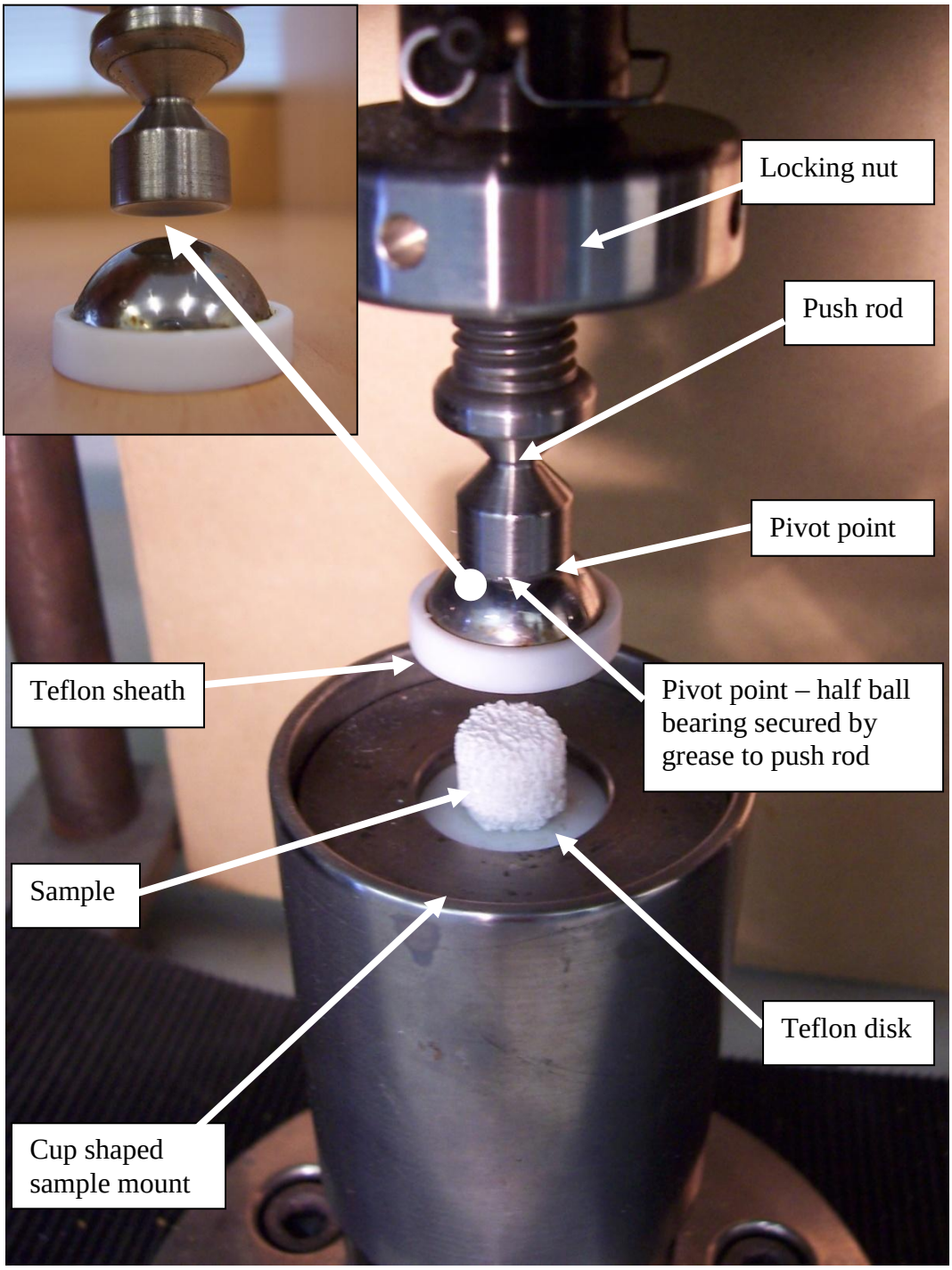

Figure 6-4 – Photograph of compression testing apparatus.

A sample mount was manufactured to complement the push rod system, and was designed to be adaptable to accommodate both dry and wet testing conditions. A "cup" shape was engineered from silversteel and hardened by heat treatment to 56-58 Rc (Rockwell Scale), as shown in Figure 6-4. Spacer disks were made to fit into the

cup, so that when testing was conducted in a dry environment, the level of the platform could be raised to provide for easier access to the platform. A Teflon disk was positioned within a metal washer on the top of the sample platform to reduce friction.

6.3 Methods

6.3.1 Instron

An Instron 5 kN load cell was secured in the Instron crosshead and the crosshead speed set to 0.5 mm / minute (0.008 mm / s) in the downward direction for compression of the samples, equating to a strain rate of 0.08 % ε / s for a 10 mm long sample. A high load limit of 4.5 kN and a maximum extension limit of 5 mm was set in the method software to protect the load cell from damage. Before a sample was subjected to compression testing each flat face of the SCBB cylinder was ground slightly with 800 grit wet & dry sandpaper to flatten the trabecular struts. Height and diameter of the samples were measured then by digital calliper, after which the sample was placed in the centre of the Teflon disk. Grease was smeared on the top of the half ball opposite the Teflon underside, allowing it to freely pivot under load and also acting as a temporary adhesive holding the half ball to the push rod between compression tests.

6.3.2 Infiltrated SCBB samples

Three different infiltrate systems were analysed by mechanical testing during this experiment. 3 groups of 15 SCBB samples were infiltrated a total of 6 times with separate infiltrations systems. These were: chitosonium chloride / $CaHPO_4$ (Infil-4), chitosonium chloride / $CaHPO_4$ / genipin (Infil-11), or PCL in THF (Infil-12) the composition of which are shown opposite in Table 4 and in comparison to other infiltrates in Table 1, p. 72. The weight increase per infiltration for each sample is shown in Appendix D. The Infil-4 infiltrate solution was immobilised between each infiltration by $NH_{3(g)}$, whereas the genipin containing infiltrate (Infil-11) after drying

was immersed in 50 mM phosphate buffer at pH 7.4. Samples were allowed to dry overnight, before being infiltrated again.

Table 4 - Concentration of infiltrate constituents for respective infiltrate systems used in mechanical testing.

	chitosan	$CaHPO_4$	genipin	PCL
Infil-4 (chitosonium chloride / $CaHPO_4$)	25 g L^{-1}	5 g L^{-1}	-	-
Infil-11 (chitosonium chloride / $CaHPO_4$ / genipin)	25 g L^{-1}	5 g L^{-1}	10 g L^{-1}	-
Infil-12 (PCL)	-	-	-	100 g L^{-1} (THF)

6.3.3 Statistical data analysis

The software package Statistica (version 8) was used to analyse the data gathered from mechanical testing, with the statistical analyses requiring that the data be transformed into linear relationships. To do this, linear transformations were made on the data, using different relationships (i.e. power, exponential) looking to see the highest r^2-values for fitted regression lines for both non-infiltrated SCBB and infiltrated samples for each mechanical property. This resulted in the following linear transformation being adopted: Log_{10} ultimate stress vs. Log_{10} apparent density, Log_{10} modulus vs. apparent density, and ln [toughness to strain = 8 %] versus ln apparent density. Natural log (ln) was used for [toughness to strain = 8 %] to maintain consistency with an exponential line of best fit being fitted to the data, see Figure 6-7 later.

Scatter plots were made of this transformed data using Statistica, to which the software applied least squares regression lines of best fit as well as 95 percent confidence intervals. In addition to this, tests of statistical significance were made for

all physical properties against apparent density with respect to infiltration status using the 'Homogeneity-of-slopes' general linear regression model. The validity of this model relies upon the respective regression lines (in this case, non-infiltrated SCBB and infiltrated SCBB) being parallel, this being what the software tests. If the regression lines are parallel within certain error limits, the y-intercept of each line may be compared and used to determine whether there is a statistically significant difference between the respective sets of data. The software returns a p-value, which indicates the probability of seeing such a difference in y-intercept values, if both sets of data were the same. Therefore, if the value of "p" is small (commonly $p < 0.05$), the probably that the result observed would occur through chance alone is very low, and we can say the sets of data are statistically different. Or when using the statistical lexicon; the "null" hypothesis that the y-intercept value is the same for both sets of data can be rejected when $p < 0.05$. However, if the lines are not parallel within statistically significant limits, this analysis cannot be employed. In this case, for this research respective scatter plots were examined for evidence of regional differences in physical property with respect to apparent density.

6.4 Results and Discussion

The employed strain rate of 0.08 % ε / s was slightly below the range recommended by Keller and Liebschner of 0.2 to 1 % ε / s for bone. However, as SCBB is a brittle material and not viscoelastic like bone, which is known to display differing stress values dependent on strain rate [152], this slight deviation was not expected to affect results. Stress / strain profiles of non-infiltrated SCBB samples tested under compression showed a high degree of variation reflecting the inherent variability in the samples themselves. For a series of SCBB samples ultimate stress varied from 0.9 MPa to 16.3 MPa. This wide-ranging variation, shown in Figure 6-5, was similar to that seen by Carter and Hayes for raw cancellous bone, while power relationship between ultimate stress and apparent density mirrors that which was derived by both Carter and Hayes and Keller [153, 154]. In the figure opoposite, error bars shown for apparent density values were calculated on the basis of error in the measurement of

sample dimensions, whilst the error bars shown for the ultimate stress values represent the error in the load cell on the Instron instrument.

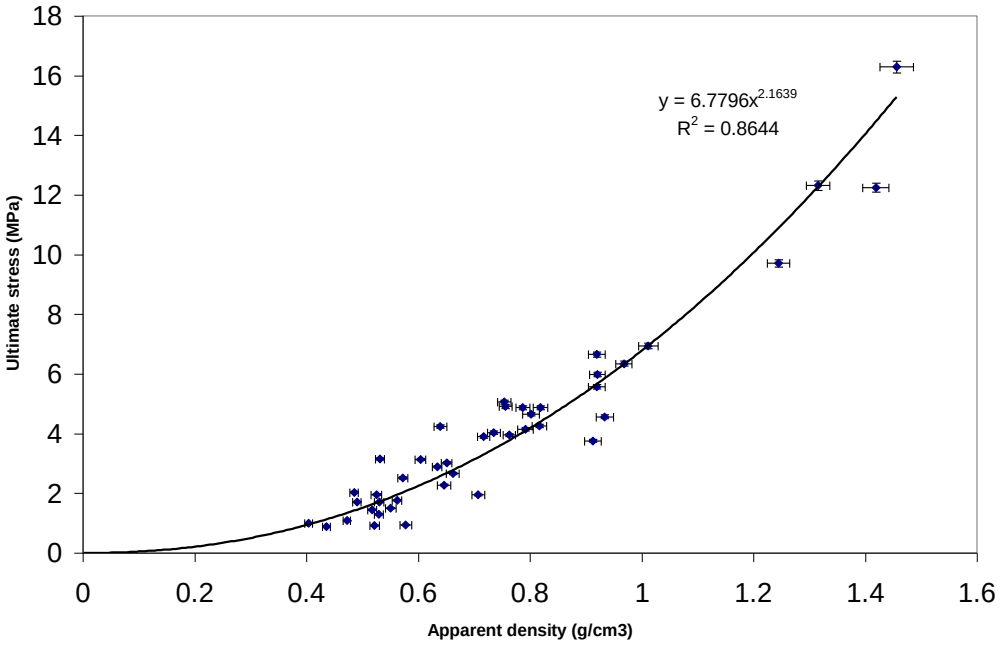

Figure 6-5 - Ultimate stress against apparent density for non-infiltrated SCBB samples.

Modulus against apparent density for non-infiltrated SCBB samples did not show the cubic relationship, which was described for raw bone by Cater and Hayes, but a power relationship for apparent density values 0.4 to 1.0 g / cm^3, as shown in Figure 6-6. Above these apparent density values, modulus values actually appeared to level out or decrease, with increasing apparent density. The reason for this was uncertain, but may have been due to a change in the basic structure of the material with increasing density. Figure 3-13 and Figure 3-14 in section 3.5.6 show the considerable differences in structure between SCBB of different densities displaying plate-like and rod-like morphology. In addition, Keller noted that theoretical analysis on trabecular bone had shown elastic modulus was proportional to the square of apparent density below 0.4 g / cm^3 and proportional to the cube above this apparent dry density value. The same effect was not seen for SCBB, but this result does show that modulus relationship can change with density. In order to compare modulus

values between non-infiltrated SCBB and infiltrated SCBB samples, only samples with apparent density values below ~ 1.0 g / cm^3 were used.

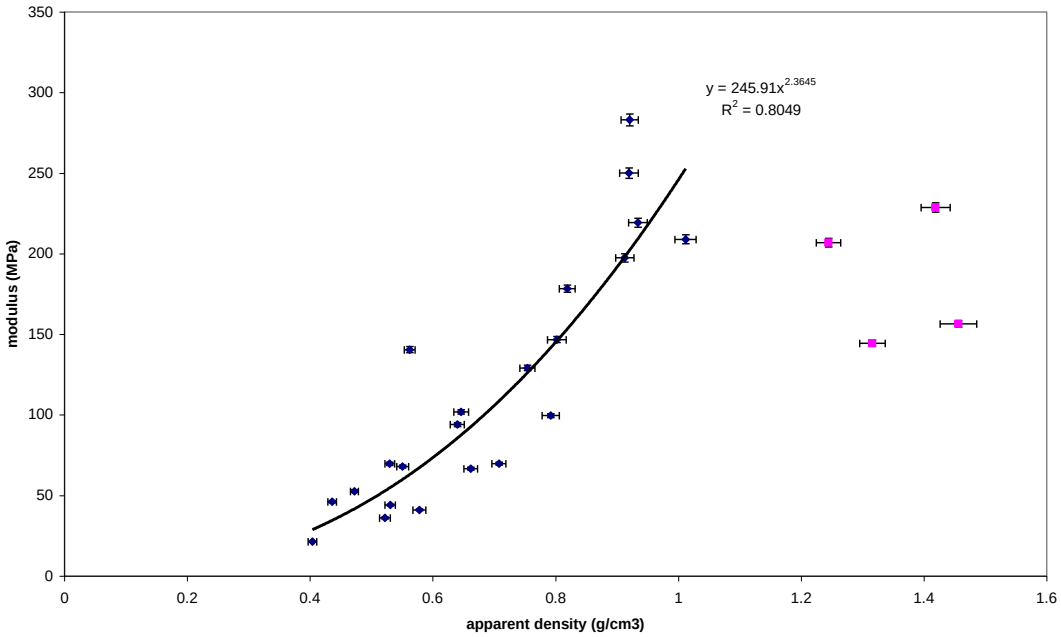

Figure 6-6 - Modulus against apparent density for non-infiltrated SCBB (control) samples. Data points above ~ 1.0 g / cm^3 apparent density appeared to show different modulus properties with respect to apparent density, therefore were not used in comparative analysis between infiltrated and non-infiltrated SCBB.

Toughness – an adaptation

Toughness is a measure of a material's ability to absorb energy before the point of fracture and can be estimated by the area under a stress / strain curve until the point of fracture [155]. With tensile testing, the point of fracture is easy to establish, because it is dramatic and complete, in compression testing this may not be so apparent, because the material can settle after an initial fracture to maintain a degree of strength.

Although displaying some variation, non-infiltrated SCBB samples under compression generally failed completely, displaying little residual strength. The infiltrated SCBB sample however showed an initial brittle material type failure, followed by a settling, which may have been due to the strength of the infiltrate or possibly because the infiltrate had bound the SCBB together in some way to maintain strength. Irrespective of the mode, the stress / strain plot shows clearly that the two

materials have different properties. However, if toughness were measured in its traditional sense to the initial point of failure, both materials would show very similar values. Therefore, in order to compare non-infiltrated SCBB and infiltrated SCBB samples, the concept of measuring the area under the curve to strain = 8 % was invoked. The value of 8 % strain was an arbitrary value chosen because it was sufficient to show the nature of the material post brittle failure, but not so long as to allow the collapsing porous structure to begin to compact upon itself, which tended to lead to increasing stress values.

The value for the area under the curve until strain = 8 % was referred to as, [toughness-to-strain = 8 %], and represents an extended measure of the material's capacity to absorb energy. The relationship between [toughness-to-strain = 8 %] and apparent density was examined for non-infiltrated SCBB and is shown below in Figure 6-7. An exponential relationship was found to be a better fit for the data rather than the power relationship, which was used for ultimate stress and modulus.

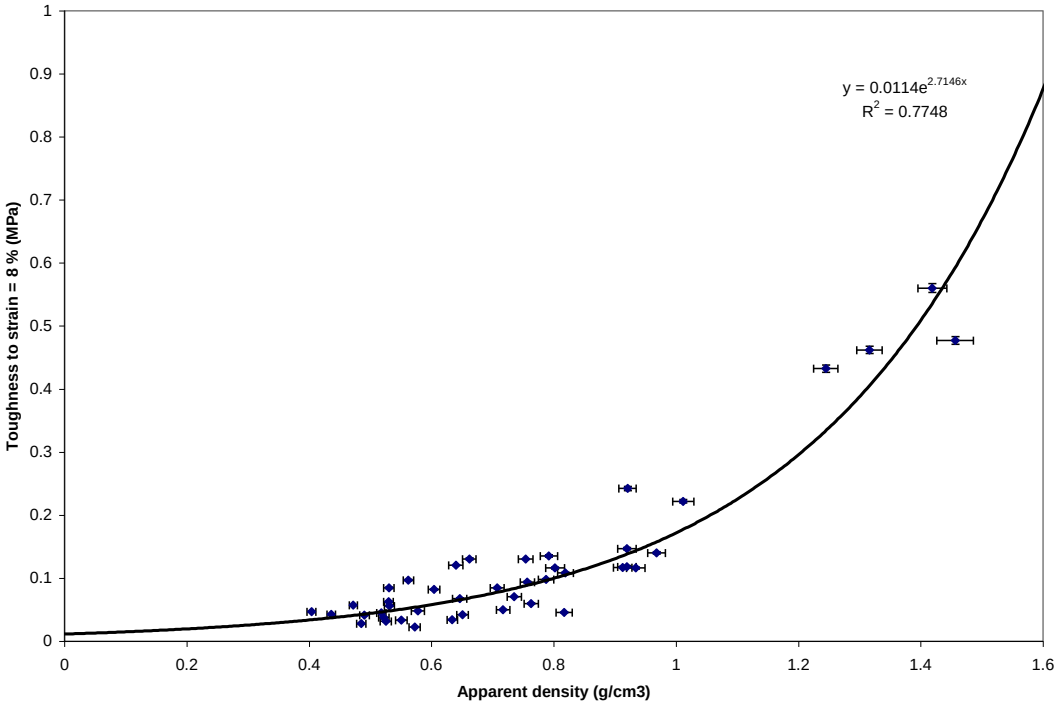

Figure 6-7 – [Toughness-to-strain = 8 %] against apparent density for non-infiltrated SCBB (control) samples.

Infiltrated SCBB samples were compression tested in the same manner as non-infiltrated SCBB samples and the data plotted together. Figure 6-8 below is illustrative of the type of plots that were obtained. Here visual inspection indicated that the infiltrated SCBB samples showed higher ultimate stress values in comparison to non-infiltrated samples at the same apparent density value especially between 0.8 and 1.0 g/cm^3. However, a statistical method was required to examine and confirm the existence of differences between various sets of data.

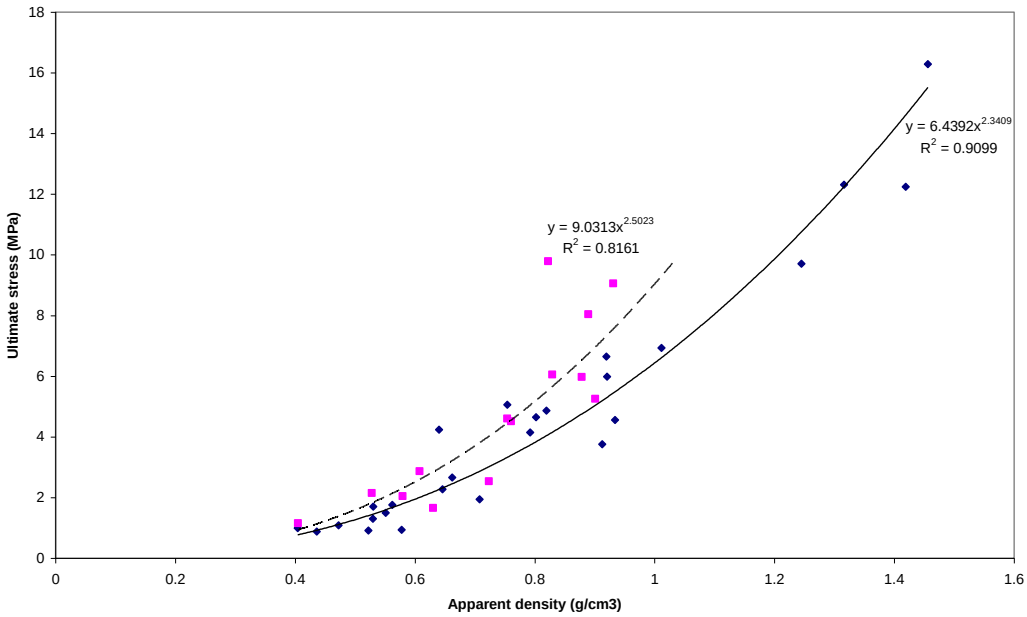

Figure 6-8 - Ultimate stress against apparent density for SCBB infiltrated with chitosan / CaP composite shown by square data points with broken trend line in comparison with non-infiltrated SCBB shown by diamond data points with solid trend line.

SCBB samples infiltrated with Infil-12 (PCL) showed no statistically significant improvement in ultimate stress values over those of non-infiltrated SCBB with p = 0.34. However, modulus values were statistically higher in the infiltrated samples with a p-value of 0.02 (for samples tested, i.e. samples under 1.0 g / cm^3 apparent density. This can be seen in Figure 6-9, where the regression line corresponding to the infiltrated samples lies above that of the regression line corresponding to the non-infiltrated SCBB samples. The dotted lines, representing 95 % confidence intervals

for each regression line, show this remains valid for a large portion of the range of apparent density values, except at higher values.

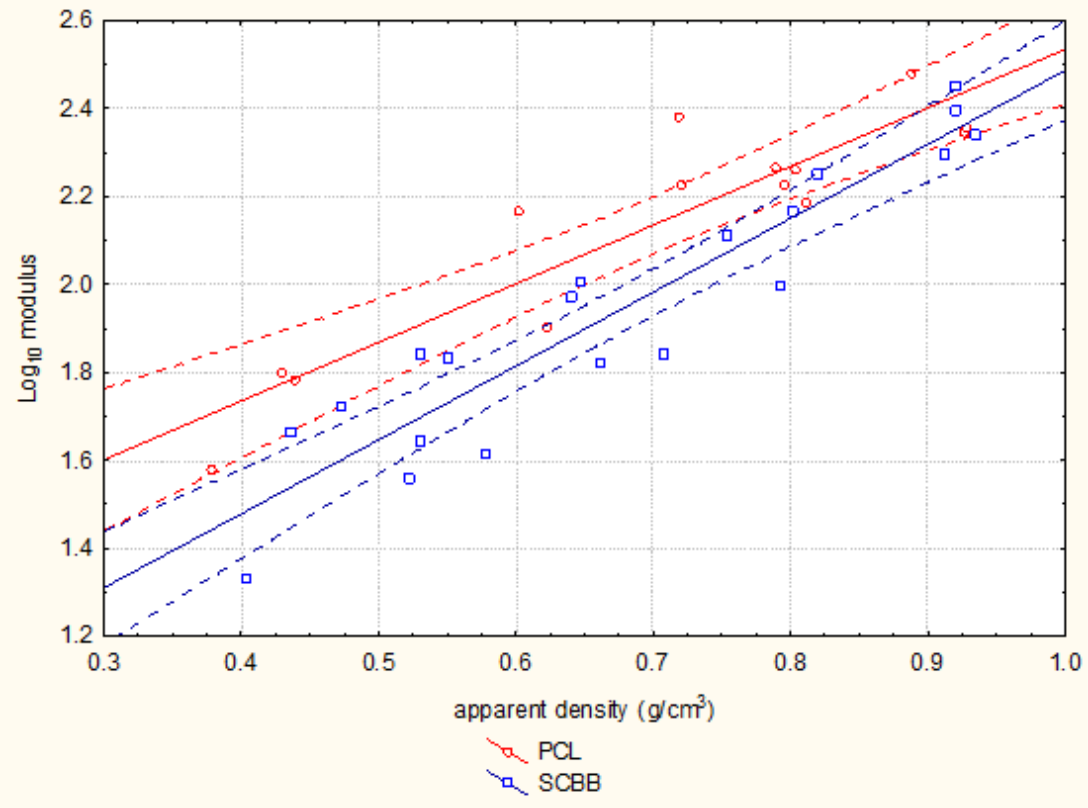

Figure 6-9 – Scatter plot of Log10 modulus versus apparent density for PCL infiltrated SCBB and non-infiltrated SCBB. Dotted lines show 95 % confidence intervals for each regression line.

[ln toughness to strain = 8 %] for PCL infiltrated SCBB samples showed no difference to non-infiltrated samples with regression lines being close to overlaid and a p-value of 0.84, see Appendix I. Ultimately, infiltration of PCL into SCBB was shown only to affect modulus.

Ultimate stress values for the Infil-11 (chitosan / $CaHPO_4$) infiltrated SCBB were shown to be greater than those for the non-infiltrated SCBB control samples, confirmed by a p-value of 0.03 in the homogeneity-of-slopes linear regression analysis. This difference can be seen in Figure 6-10 in a covariate means graph for Log_{10} ultimate stress versus treatment, where 'treatment 1' = chitosan / $CaHPO_4$ infiltrated SCBB and 'treatment 2' = non-infiltrated SCBB. Note: the term

"covariate" refers to a variable that affects the relationship between the independent variable (apparent density) and dependent variable (in this case ultimate stress). Therefore, Figure 6-10 below shows the difference in ultimate stress values due to the effect of the infiltrate.

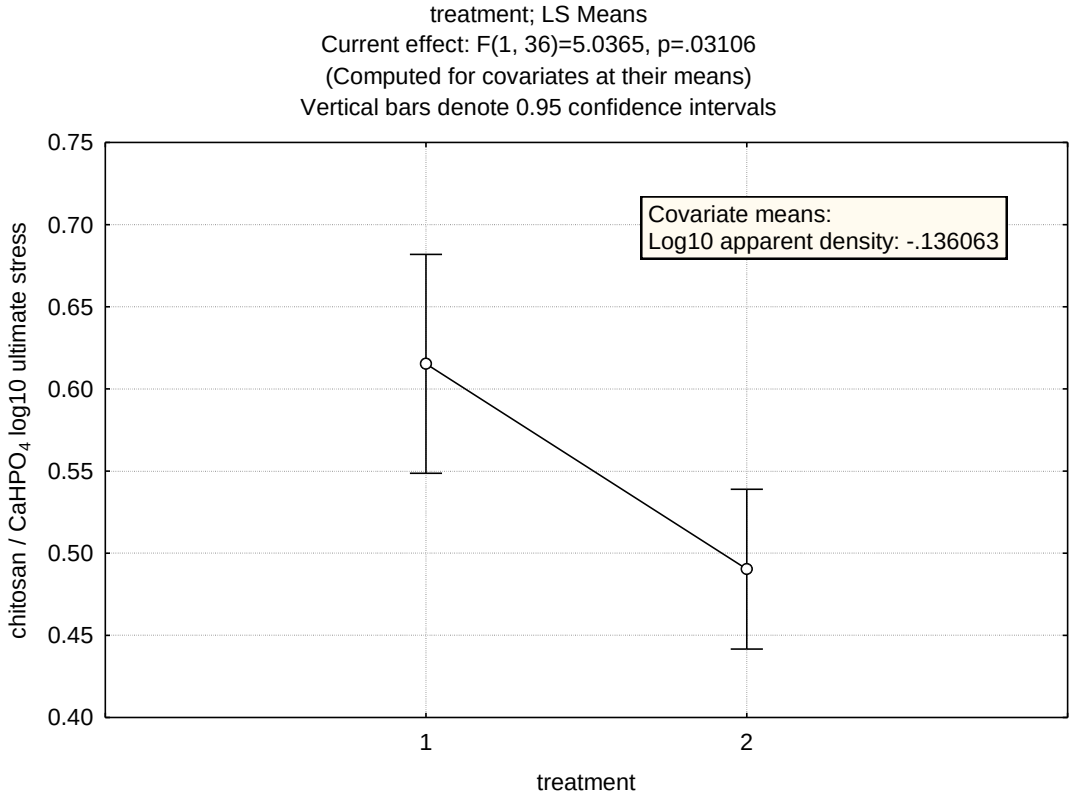

Figure 6-10 – Covariate means graph of Log_{10} ultimate stress against treatment for Infil-4 (chitosan / $CaHPO_4$) infiltrated SCBB (treatment 1) and non-infiltrated SCBB (treatment 2).

The separation in the regression lines of the Log_{10} modulus versus apparent density scatter plot shown opposite in Figure 6-11 suggested that there might be a difference between Infil-4 (chitosan / $CaHPO_4$) infiltrated SCBB and the control samples. However, this was not reflected in the regression analysis which produced a p-value of 0.19, and the null hypothesis that the treatments were the same could not be rejected.

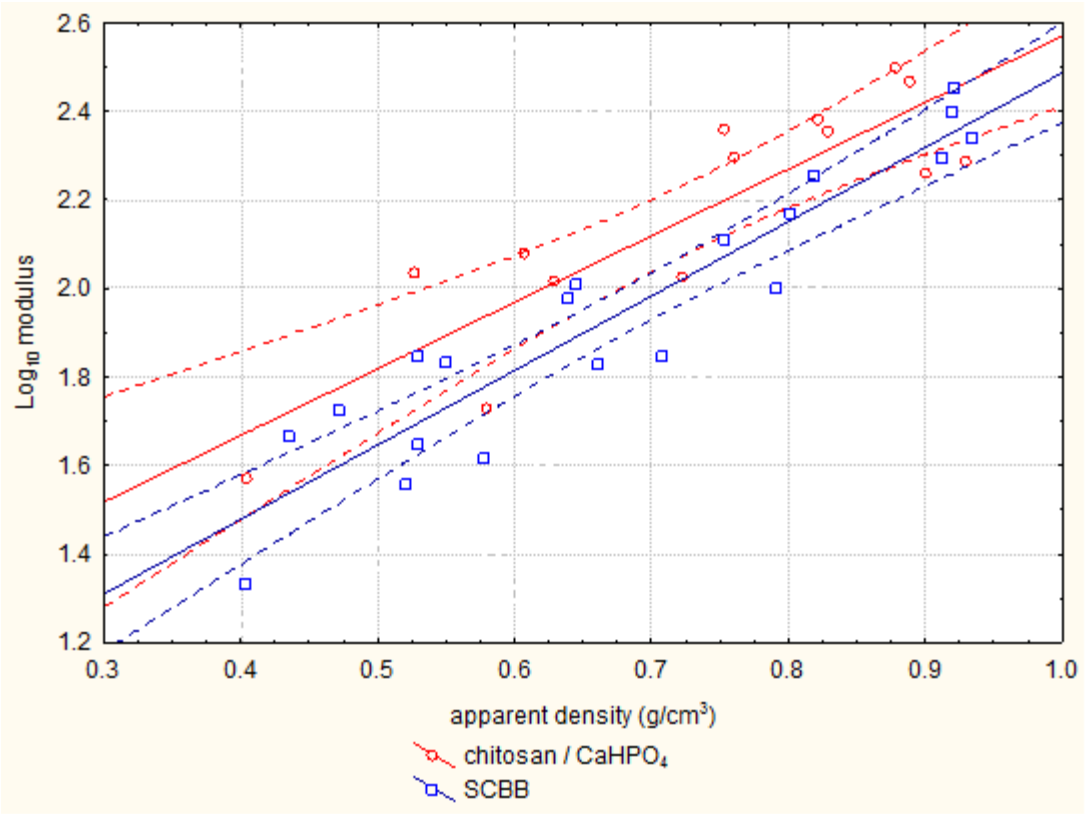

Figure 6-11 – Scatter plot of Log_{10} modulus against apparent density for Infil-4 (chitosan / $CaHPO_4$) infiltrated SCBB and control samples.

However, regression analysis using the homogeneity-of-slopes model showed that there was a statistically significant difference between [Toughness to strain = 8 %] for the Infil-4 (chitosan / $CaHPO_4$) infiltrated samples in comparison to the SCBB controls with a p-value of 0.01, see Appendix I.

The homogeneity-of-slopes regression model showed a p-value of 0.01 for the 'treatment*Log_{10}' (see Appendix I) variable with respect to Log_{10} ultimate stress against Log_{10} apparent density for comparison of infiltrated SCBB and non-infiltrated samples. The "treatment*Log_{10}" variable represents the difference in the slope of the respective regression lines. The null hypothesis for this variable is that the slopes of the respective regression lines are equivalent, but as $p < 0.05$ the null hypothesis was rejected. This meant that the homogeneity-of-slopes regression model was unsuitable for the analysis of these sets of data, while the disparity in the gradient of the slopes is evident in Figure 6-12. Significant overlap of respective 95 % confidence intervals

was also obvious making it difficult to assert that there was a difference between sets of data, except for the possibility of slightly higher Log_{10} ultimate stress values at lower Log_{10} apparent density values.

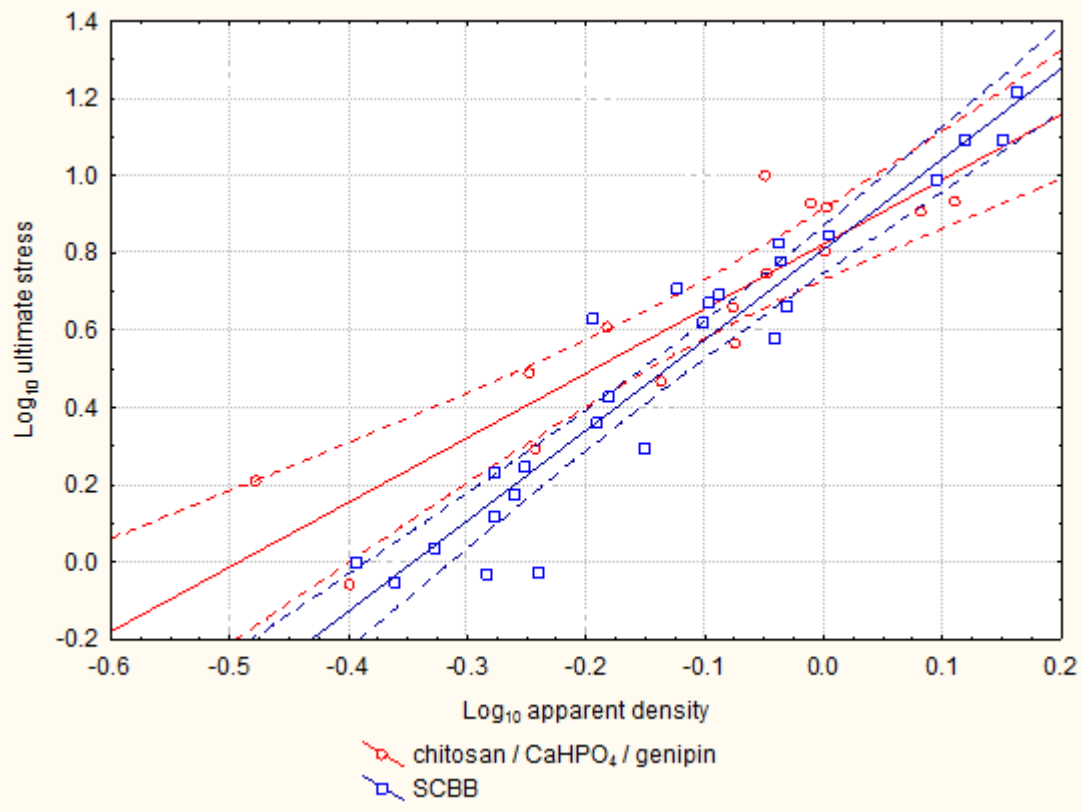

Figure 6-12 – Scatter plot of Log_{10} ultimate stress versus Log_{10} apparent density for Infil-11 (chitosan / $CaHPO_4$ / genipin) infiltrated SCBB and non-infiltrated SCBB.

The scatter plot of Log_{10} modulus against apparent density for Infil-11 (chitosan / $CaHPO_4$ / genipin) infiltrated SCBB and non-infiltrated SCBB was similar in appearance to Figure 6-12 above, with convergent lines showing a large disparity in Log_{10} modulus values at lower apparent density values and little or none at higher apparent density values. Because $p < 0.05$ for the null hypothesis that the slopes were equal, the null hypothesis was rejected, and accordingly the homogeneity-of-slopes model for this set of data was also rejected. The same pattern was repeated for the analysis of [ln toughness to strain = 8 %] against ln apparent density data where regression lines were seen to converge at higher ln apparent density values. Table 5

below provides a summary of the results for compression testing on infiltrated SCBB in comparison to non-infiltrated SCBB samples.

Table 5 – Summary of regression analysis on physical property with treatment on SCBB samples

	Infil-12 (PCL)	Infil-4 (chitosan / $CaHPO_4$)	Infil-11 (chitosan/ $CaHPO_4$ / genipin)
Ultimate stress	p = 0.34, no statistical difference between infiltrated SCBB and non-infiltrated control samples	p = 0.03, statistically higher in infiltrated samples	Inconclusive, scatter plot suggested infiltrated samples higher at lower apparent density values
Modulus	p = 0.02, statistically higher in infiltrated samples	p = 0.19, no statistical difference between infiltrated SCBB and non-infiltrated control samples	Inconclusive, scatter plot suggested infiltrated samples higher at lower apparent density values
[Toughness to strain = 8 %]	p = 0.84, no statistical difference between infiltrated SCBB and non-infiltrated control samples	p = 0.01, statistically higher in infiltrated samples	Inconclusive, scatter plot suggested infiltrated samples higher at lower apparent density values

Sarasam and Madihally observed in tensile testing that chitosan with a molecular mass between 50-190 kD (*cf.* 150 kD in this research) exhibited a modulus of ~ 2500 MPa and a breaking stress of ~ 58 MPa when tested dry. However, modulus fell significantly to ~ 6.5 MPa and breaking stress to ~ 2.5 when tested in wet conditions [104]. In addition, Ito *et al.* found that the incorporation of HAp ($CaHPO_4$ was used in this experiment) within chitosan increased tensile strength, while Hu *et al.* reported that the co-precipitate of chitosan and HAp (similar to the method by which the chitosan / $CaHPO_4$ composite was prepared in this research) led to a composite of bending strength 86 MPa and modulus of 3.4 GPa [90, 92]. By comparison, Kai *et al.* reported for PCL a modulus value for 174 kD PCL of ~ 340

MPa and a tensile yield stress of ~ 15.6 MPa[2] [66]. In spite of chitosan's inherent higher modulus in comparison to PCL, this was not reflected in the modulus of the infiltrated SCBB materials. PCL increased the modulus of the SCBB whereas the chitosan based infiltrates did not. This could have been due to differences in the specific structural integration of the infiltrates within the SCBB matrix. SEM of PCL infiltrated SCBB samples often showed the material infiltrated into the microporous structure of the SCBB. However, this phenomenon was not so prevalent in the chitosan based infiltrates, especially when pressure was not used in the infiltration process as was the case in the samples prepared for mechanical testing, cf. see section 4.4.3 pressure infiltration.

The chitosan / $CaHPO_4$ composite material may have increased the ultimate stress values through a combination of its own strength, as well as through supporting the trabecular structure of the SCBB. If one envisions a portion of the trabecular structure as a vertical beam, the overlaying infiltrate material may have reduced the tendency for the trabeculae to buckle under stress, thereby increasing the capacity of the entire material to resist stress. [Toughness to strain = 8 %] was also significantly higher in the chitosan / $CaHPO_4$ infiltrated samples than the control samples. The honeycomb structure that the infiltrate likely formed within the "mould" provided by the SCBB trabecular structure, would probably have allowed the composite to continue to absorb energy while being stressed. This was not replicated in the PCL infiltrated samples, but visual inspection of both infiltrate materials outside of the SCBB matrix suggested the deposited PCL was a more brittle material.

Testing results for the Infil-11 (chitosan / $CaHPO_4$ / genipin) infiltrated SCBB samples, on the other hand, were not conclusive. Inspection of scatter plots suggested that measures of all mechanical properties measured were improved at lower apparent density values, but that this improvement progressively diminished at higher apparent density values. The genipin cross-linked chitosan material has been shown to display

[2] In tensile testing, yield stress in PCL and breaking stress in chitosan are points at which both materials cease to behave elastically.

higher values of modulus in comparison to chitosan [125]. With a higher modulus, the cross-linked material would be expected to be more brittle than chitosan / $CaHPO_4$, and have properties more closely related to PCL. The mechanical testing appeared to show this with chitosan / $CaHPO_4$ / genipin infiltrated samples representing a middle ground between PCL and chitosan / $CaHPO_4$ infiltrates with respect to each mechanical property. The chitosan / $CaHPO_4$ / genipin infiltrate did not increase modulus at the expense of ultimate stress and [toughness to strain = 8 %] or vice versa, but resulted in a slight increase over all parameters at lower apparent density values.

6.5 Conclusion

The effect of infiltration on the mechanical properties of ultimate strength, modulus and toughness in SCBB with respect to non-infiltrated SCBB was successfully elucidated. The implementation of a statistical approach involving the use of many SCBB samples accommodated of the confounding factor of an inherent variability in the density of the starting material. SCBB infiltrated with a chitosan / $CaHPO_4$ composite material exhibited superior ultimate stress values and an adapted toughness measure in comparison to control samples. Furthermore, PCL infiltrated SCBB samples exhibited increased modulus values to the non-infiltrated SCBB material.

CHAPTER SEVEN

7 Biocompatibility testing of infiltrated SCBB

7.1 Introduction

In order for a bone replacement material to be accepted into the body, it should have zero to minimal toxicity and antigenic potential. To test these criteria, materials destined for implantation in living hosts are usually subjected to a range of *in vitro* assays before being tested in an animal or human model [156]. Animal testing can be expensive and time consuming, while materials that have not been properly screened prior to implantation have the potential to do significant damage to tissue and cause considerable discomfort to animals. An *in vitro* cytotoxicity test through the use of cell culture is a often used preliminary step in helping to determine a material's suitability to progress towards animal implantation trials [157]. These tests have advantages in that they are comparatively inexpensive to conduct, highly sensitive to the presence of cytotoxins because of the absence of biological mechanisms to remove and process toxins, quick to conduct, and due to their simple nature, readily able to be standardised [158]. A commonly used cell culture test involves culturing of an immortalised mouse fibroblast cell line known as the L929 cell line. The test sample is either placed in direct contact with a monolayer of these cells, or an extract is prepared, and added to a monolayer of the cells, with the cells being observed at subsequent time points for signs of degeneration and malformation [159].

7.2 Materials

Aldrich tetraethyl orthosilicate (TEOS), reagent grade 98 % assay; Sigma reagent grade L-ascorbic acid, SPS Medical autoclave tubing, NCTC clone 929 (ATCC

Number – CCL-1) mouse fibroblast cells, Eagles Minimum Essential Medium (MEM).

7.3 Methods

A range of infiltrated SCBB samples were prepared specifically for biocompatibility testing incorporating various infiltrate materials and immobilisation systems. As a number of these systems were specific to samples to be tested for biocompatibility, a separate labelling system (BioSCBB) from that in Table 1, p. 72 was employed and their methods of production are presented below.

7.3.1 Chitosan – (BioSCBB-1)

Infiltrate prepared as Infil-1 (1 % chitosan w / v in hydrochloric acid) in Table 1, p. 72. SCBB samples were infiltrated under vacuum with this solution, exposed to $NH_{3(g)}$ over night and then allowed to dry in the atmosphere. Three infiltrations under vacuum were made using this method.

7.3.2 Chitosan / $CaHPO_4$ – (BioSCBB-2)

1.5084 g of $CaHPO_4$ and 2.5169 g of Fluka "low viscosity" chitosan were added to 250 mL of rapidly stirred distilled water. 2.7442 g of conc. HCl was added with the solid dissolving to give a clear solution at pH 1.91. HCl was at 0.1 mol L^{-1}, a calculation of which is shown in Appendix J. 0.1 mol L^{-1} NaOH was added drop-wise to the stirred solution to increase pH to 4.10 before infiltration or storage. SCBB samples were infiltrated under vacuum with this solution, exposed to $NH_{3(g)}$ over night and then allowed to dry in the atmosphere. Three infiltrations under vacuum were made using this method.

7.3.3 Chitosan / $CaHPO_4$ / genipin – (BioSCBB-3)

The chitosan / $CaHPO_4$ solution as described in section 7.3.2 above was combined with genipin in 95% ethanol solution immediately before infiltration. This was

prepared by taking 50 mL of the chitosan / $CaHPO_4$ solution, while 0.005 g genipin was dissolved in approximately 0.5 mL 95 % ethanol. The genipin / ethanol solution was added to the chitosan / $CaHPO_4$ solution in a round bottom flask with anti-bumping granules and mixed thoroughly by manual agitation, after which the solution was subjected to vacuum, in order to remove ethanol and to degas. SCBB samples were infiltrated with this solution under vacuum, after which the sample was placed under nitrogen in an enclosed vessel and exposed to NH_3 overnight. Samples were then allowed to dry before being reinfiltrated a total of three times.

7.3.4 Chitosan / tetraethoxysilane (TEOS) – (BioSCBB-4)

A 10 g L^{-1} chitosan solution was prepared by dissolving approximately 2.5 g Fluka low viscosity chitosan in 250 mL distilled water with the addition of conc. HCl to give a solution of pH 4.5. Immediately prior to infiltration, 50 mL of this solution was degassed by vacuum and then 0.5 mL of TEOS was added. The resulting mixture was stirred rapidly by magnetic stir bar to give an emulsion of TEOS within the chitosan solution, which was subsequently infiltrated by vacuum into SCBB samples. Samples were then placed in an enclosed vessel with NH_3 overnight, allowed to dry the next day before being reinfiltrated. This was repeated to give a total of three infiltrations.

7.3.5 Chitosan /$CaHPO_4$ / genipin /urea / urease / L-ascorbic acid (BioSCBB-5)

50 mL of the chitosonium chloride / $CaHPO_4$ solution, prepared as described above in section 7.3.2, was placed in a round bottom flask. 0.005 g genipin was dissolved in approximately 0.5 mL 95 % ethanol and added to the chitosan solution, after which the solution was mixed and degassed through the application of vacuum for approximately 10 minutes. 0.2 g of urea and 0.02 g L-ascorbic acid was then added to the solution and dissolved by manual agitation of the flask. L-ascorbic acid was added as an oxygen radical scavenger to minimise genipin self-polymerisation. Immediately before infiltration into SCBB samples, 0.0033 g urease, having been

dissolved in approximately ¼ mL degassed distilled water, was added to the solution and mixed well to dissolve. After SCBB samples had been infiltrated, they were removed from the infiltration tube and individually placed in 20 mL plastic containers, which were subsequently purged with nitrogen and then had their lids screwed on. The containers were transferred to a water bath at 35°C, where they were secured in a semi-submerged state and left overnight. Samples were left overnight for the urea / urease reaction to proceed. The morning after infiltration, infiltrated SCBB samples were a slight off-white green colour and gelled material was visible within the SCBB.

Table 6 - Summary of infiltrated SCBB samples prepared for biocompatibility testing

Material	**Sample name**	**Constituents**	**pH**
no infiltrate	BioSCBB-0	(control)	-
chitosan (1 % w / v) in hydrochloric acid (chitosonium chloride)	BioSCBB-1	10 g L^{-1} chitosan, HCl	4.0 - 4.5
chitosan / $CaHPO_4$ in hydrochloric acid	BioSCBB-2	10 g L^{-1} chitosan, 6 g L^{-1} $CaHPO_4$, HCl	4.0 - 4.5
chitosan / $CaHPO_4$ / genipin	BioSCBB-3	10 g L^{-1} chitosan, 6 g L^{-1} $CaHPO_4$, HCl, 0.005 g L^{-1} genipin	4.0 - 4.5
chitosan / tetraethoxysilane (TEOS)	BioSCBB-4	10 g L^{-1} chitosan, HCl, 1 % TEOS v / v	4.0 – 4.5
chitosan / $CaHPO_4$ / genipin / urea / urease / L-ascorbic acid	BioSCBB-5	10 g L^{-1} chitosan, 6 g L^{-1} $CaHPO_4$, HCl, 0.005 g L^{-1} genipin / 4 g L^{-1} urea / 0.066 g L^{-1} urease	4.0 – 4.5

7.3.6 Sample washing

After infiltration and immobilisation, all samples were washed in distilled water at a volume of 400 mL per sample for 2 hours, with the water then replaced and the samples washed a further 2 hours, a process that was repeated a total of three times. Samples containing genipin were washed with degassed distilled water, which was continually purged with nitrogen gas during washing to prevent the samples being exposed to oxygen.

7.3.7 Protocol for cell culture test on infiltrated SCBB samples

Infiltrated SCBB samples as prepared and described above were too large (approximately 10 mm height x 10 mm diameter) to be tested in the 15 mm diameter wells used in this cell culture test. Therefore, sub-samples were produced by cutting cores in the main sample by means of a hole cutter with a 5 mm internal diameter, as shown in Figure 7-1 over the page. Sub-samples were 5 mm in diameter, between 1 and 2 mm in height, and generally between 0.02 and 0.04 g in weight. To prevent contamination of the cell culture with bacteria or fungi, all samples (infiltrated and non-infiltrate SCBB) were before use, which was accomplished through autoclaving. Samples were placed in individual autoclave bags created by cutting sections of a length of SPS Medical autoclave tubing. Autoclaving was carried out in an industrial autoclave designed for hospital use for 30 minutes, a process that consisted of a steam treatment for 20 minutes and then dry heat for 10 minutes.

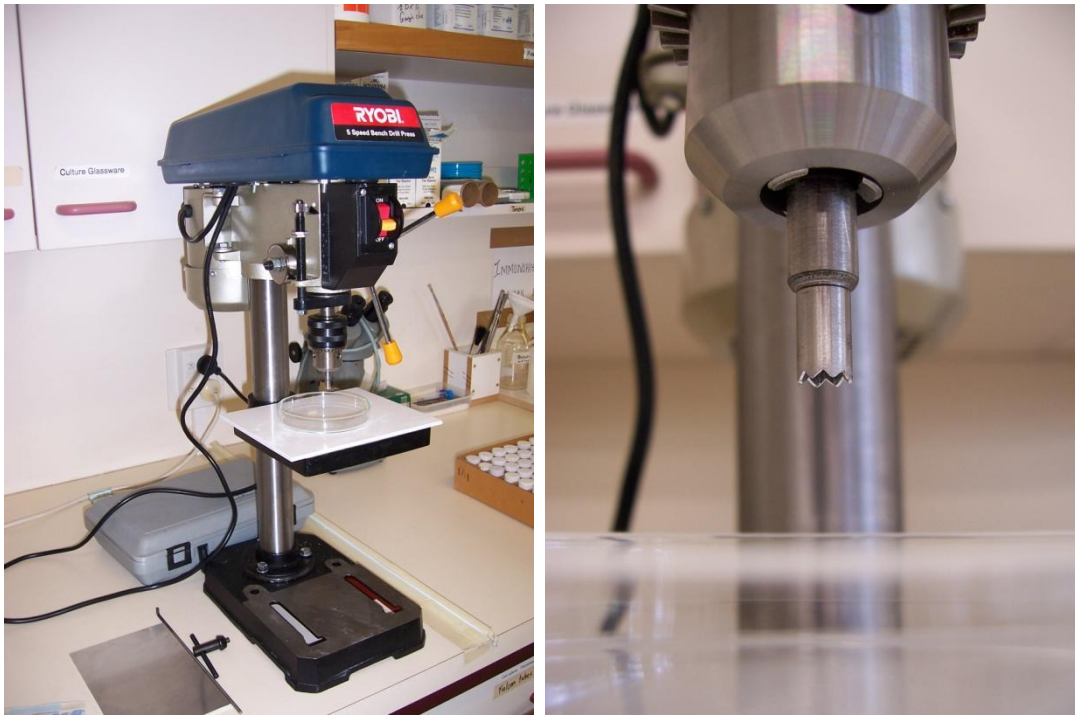

Figure 7-1 – Photograph of drill set containing hole-cutter (left) and close-up of hole-cutter with 5 mm internal diameter (right).

7.3.8 Preparation of L929 cell line for cell culture testing

All L929 culture work was carried out at the Department of Anatomy and Structural Biology at the University of Otago. NCTC clone 929 (ATCC Number – CCL-1) mouse fibroblast cells were removed from liquid nitrogen storage and reanimated in Minimum Essential Medium (MEM), containing 2 mM L-glutamine, 10% Foetal Calf Serum (FCS) v / v and 1 % v / v penicillin/streptomycin and amphotericin-B solution. The L929 cells were plated out in 10 mL of the aforementioned media in Petri dishes and incubated at 37°C in a 5 % CO_2 atmosphere. At approximately 90 % confluency[3], cells were passaged[4], re-suspended in 10 mL fresh media, of which 1 mL was removed and plated out onto a new Petri dish. 10 mL fresh media was added on top of the cells to give a cell concentration of approximately 10 % of the original. Cells

[3] Confluency is an estimation of the extent to which cells cover the bottom of the culturing dish. Therefore , 100 % confluency equates to not being able to see the Petri dish beneath the cells in practice.

[4] "Passaging" is the process of subculturing cells, and involves removing a portion of cells from one culturing dish and plating them out onto a new dish with fresh media.

were passaged a minimum of 4 times before being used in the proceeding cell culture cytotoxicity tests.

7.3.9 Direct contact cell culture test

This biocompatibility test was carried out in accordance with the method described in the International Standard BS EN ISO 10993-5 (1999) Biological evaluation of medical devices – Part 5: Test for cytotoxicity: in vitro methods [160]. This test measures the cytotoxicity induced by direct contact with the test material, and in addition, any leachates stemming from the test material. L929 cells were removed from culture dishes by the application of trypsin / EDTA solution and re-suspended in MEM. A sample was transferred by micro-pipette to a haemocytometer, so that cells could be counted in order to calculate cell concentration. The number of cells required per each 16 mm diameter well in the 24 well plates that were used in the study, was calculated from a previous experiment conducted by SafePharm Laboratories in accordance with the abovementioned ISO test. Here 2 ml of 1 x 10^5 cells / mL were transferred to 35 mm diameter wells equating to 208 cells / mm^2 of well. This cell count was converted to the 16 mm diameter wells used in this study, which equated to 41,796 (~ 40,000) cells per well. Therefore, from the haemocytometer cell count ~ 40,000 cells were transferred to each well of a 24 well plate and then 0.4 mL fresh media added on top. The plate was placed in the incubator and incubated for 24 hours at 37°C in a 5 % CO_2 atmosphere. After 24 hours, plates were removed from the incubator and examined under an inverted microscope.

Direct Contact Biocompatibility Test – Protocol 1

At approximately 90 % confluency, cells were ready for the experiment, at which point, the media was aspirated from the cells and replaced with 0.4 mL fresh media. 5 mm diameter infiltrated SCBB samples were soaked in fresh media before being gently placed on the monolayer of L929 cells. This was carried out in triplicate for each sample. Positive controls were prepared by dissolving 20 mg digitonin in 1 mL

DMSO, which was further diluted with distilled water to give a 300 µg / mL solution of digitonin. 5 mm diameter filter paper "dots" (polypropylene) were prepared and 10 µL of the digitonin solution was pipetted onto the surface of the dots, being rapidly absorbed and dispersed throughout the material. Negative controls were prepared from filter paper dots soaked in cell culture medium. In addition, a media control was implemented during the test in which cells within wells were exposed to media only. All controls were performed in triplicate as per samples.

Cell monolayers were examined by inverted microscope at time intervals, t = 1, 24, 48 and 72 hours, while photographs were taken to examine for signs of cellular degradation and malformation. Cytotoxic response was evaluated according to the scale presented below in Table 7.

Table 7 – Cytotoxicity / Reactivity Grading Scale

Grade	Cytotoxicity/Reactivity	Description of Cytotoxicity/Reactivity Zone
0	None	No detectable zone around or under specimen
1	Slight	Some malformed or degenerated cells
2	Mild	Zone limited to area under specimen and less than 0.5 cm beyond the specimen
3	Moderate	Zone extends 0.5 to 1.0 cm beyond specimen
4	Severe	Zone extends greater than 1.0 cm beyond specimen but does not involve entire dish

(From Safepharm Laboratories Limited, Derbyshire, UK in accordance with ISO 10993-5 Tissue Culture Cytotoxicity Test Using L929 Cells – Direct Contact Method)

Direct Contact Biocompatibility Test – Protocol 2

Due to the less than desirable results of the initial cell culture test, a second cell culture test was undertaken with modifications to the way samples were prepared. After the 5 mm sub-samples had been cut from the original 10 mm diameter by 10 mm height cylinders, each ~ 0.03 g sub-sample was soaked in 10 mL PBS (phosphate buffered saline) for 24 hours with periodic swirling and then soaked in 10 mL distilled water for 6 hours with periodic swirling. These samples were then autoclaved in steam for 20 minutes and a 10 minute drying cycle as per the 1st cell

culture test. Before samples were placed on the L929 fibroblast cells, they were soaked in media (Eagles MEM) for 10-15 minutes, in contrast to being simply dipped in the media with the previous method. In addition, all infiltration variations listed in Table 6 above were tested.

HET-CAM test

Fertilised hen's eggs were placed in an incubator at 37°C and turned every day to replicate the action of the mother. After 6 days the eggs were removed from the incubator and transported to an aseptically maintained laminar flow cabinet, where the egg shell over the air-sack was removed along with the air-sack membrane to expose the CAM. Samples were placed in duplicate (within different eggs) on a prominent blood vessel and then photographs taken at 0.5, 2 and 5 minutes after exposure. A single drop of 0.1 mol L^{-1} NaOH was placed on the CAM surface as a positive control and a ~ 5 mm x 5 mm x 2 mm square of agarose gel was used as a negative control. The opening into the egg was then covered by a polyethylene plastic cling wrapping to prevent foreign matter from entering the cavity. Samples were returned to the incubator and then photographed at 24, 48 and 72 hours post exposure to gauge the long term effects of the solid samples.

7.4 Results and Discussion

The first cell culture test (Protocol-1) involved testing samples BioSCBB-0, BioSCBB-1, BioSCBB-2 and BioSCBB-4. Control samples at t = 1 hour showed fibroblast cells with extended fibrils indicating a low level or no cytotoxicity, an example of which is shown in Figure 7-2. However, several balled cells were also apparent suggesting some stress, which may have been the result of physical trauma during transport of the samples. Digitonin positive controls were no different in appearance from negative controls for all time points, indicating that the positive controls as prepared were not appropriate for this experimental technique. As is presented further on, SCBB samples themselves were shown to impact on the L929 fibroblast cells, in effect acting as positive controls.

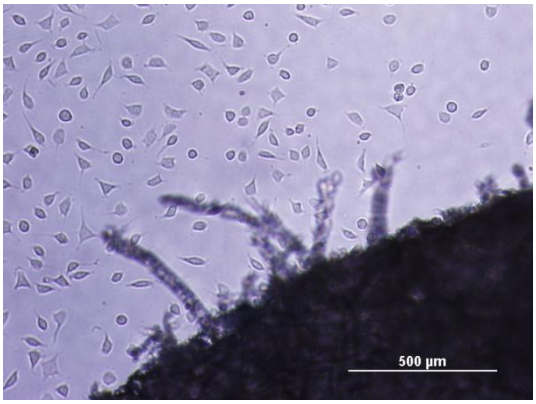

Figure 7-2 – Negative control (paper dot soaked in media) at t = 1 hour showing fibroblasts in close proximity, but several with several balled cells suggesting a level of stress.

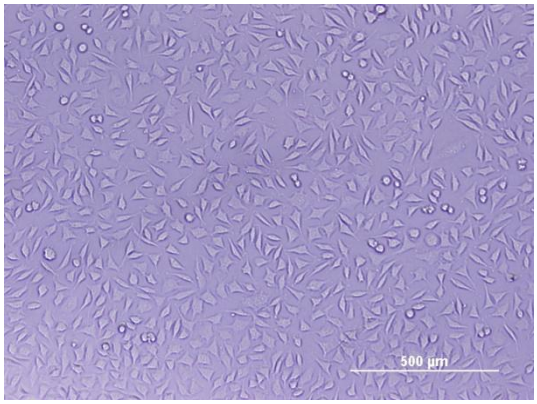

Figure 7-3 – Media only control

By contrast, the media only control showed fibroblasts displaying a healthy splayed morphology with extended fibrils as shown above in Figure 7-3.

7.4.1 Non-infiltrated SCBB

Figure 7-4 below shows one example of the effect the non-infiltrated SCBB sample had on the L929 cells that lay in close proximity to the sample. The dark shadow in the upper right hand corner is a portion of the 5 mm diameter SCBB sample. Degradation and malformation in cells similar to this were seen in the immediate vicinity around large portions of each of the triplicate samples. However, this effect was restricted to well within 0.5 cm beyond the sample to give a "mild" cytotoxic response according to the scale in Table 7 above.

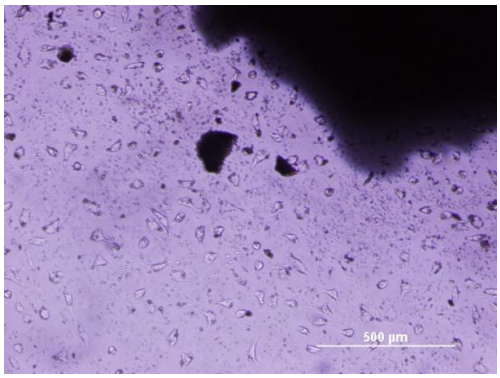

Figure 7-4 – SCBB without infiltrate, t = 1, immediate proximity to sample. Image showing balled cells, cell fragments from lysis (small particles) and recession of cells from sample due to cell degradation.

Figure 7-5a below shows cells after 24 hours in close proximity to the sample with some cells maintaining a non-balled fibroblast like structure. However, the extent of degradation and malformation is apparent when compared against healthy cells in Figure 7-5b, which shows the state of the cells further from the sample, but less than 0.5 cm away. At 24 hours, there were also some regions around the SCBB samples that showed very little degradation as shown in Figure 7-5c, and moderate degradation as shown in Figure 7-5d.

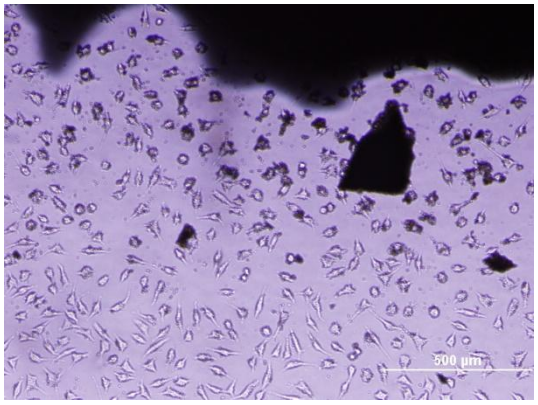

a) Immediate proximity to SCBB sample. Image showing balled cells, cell fragments from lysis (small particles) and recession of cells from sample due to cell degradation. However, some cells appeared to still be viable although somewhat malformed.

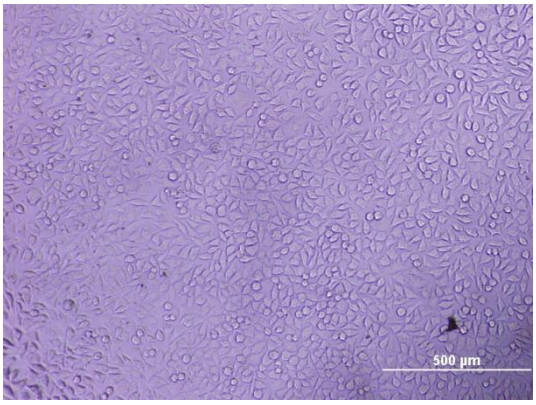

b) Midway between sample and edge of well (approximately 2.5 mm from sample) showing high confluency of cells. Some cells are balled, but it is not possible to say whether this was due to mitosis, contact inhibition processes or cytotoxic effects. In general the cells look healthy and viable.

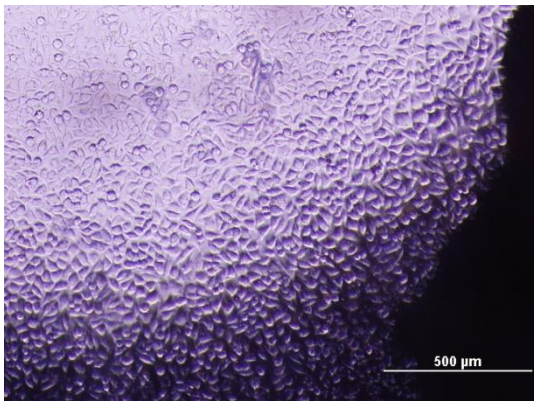

c) Immediate proximity to SCBB sample. Image showing cells in high confluency, some with a balled appearance but limited if any degradation.

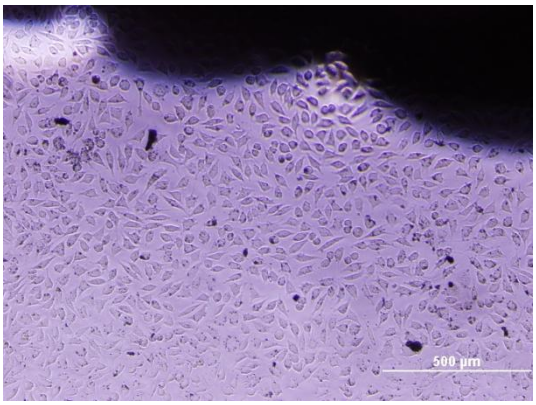

d) Immediate proximity to SCBB sample showing a reduction in the density of cells in comparison to areas distant to the sample as shown above in b).

Figure 7-5 – Non-infiltrated SCBB at t = 24 hours

Images taken at 48 hours and 72 hours showed the same trend as seen at 24 hours with damage to cells in immediate proximity to the SCBB sample, but not to an increased extent in comparison to 24 hours, while cells 2-3 mm away appeared unaffected. Overall, the data showed that non-infiltrated SCBB sample prepared according to Protocol-1 elicited a "mild" cytotoxic response (2 on the scale) for all time points, which is shown in Table 8, p. 173.

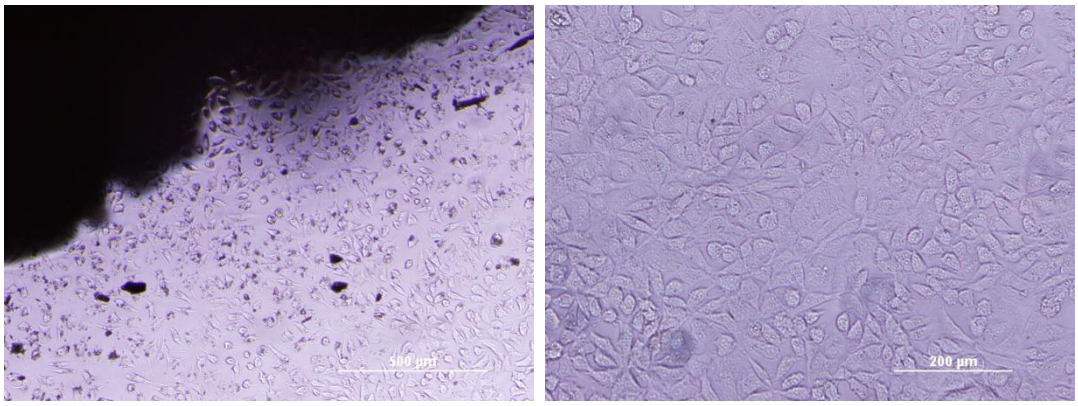

a) Immediate proximity to SCBB sample. Image showing recession of cells from the sample.

b) Cells 2-3 mm from the sample showing 100 % confluency and balling of cells.

Figure 7-6 – Non-infiltrated SCBB at t = 72 hours

The positive control consisting of 10 µL of 300 µg/mL digitonin on a paper dot of filter paper approximately 5 mm in diameter proved to have only limited relevance with a limited amount of balling of cells in close proximity to the material. The negative control of a filter paper dot showed no inhibition of the cells. The non-infiltrated SCBB samples prepared according to Protocol-2 displayed reduced cytotoxic response in comparison to those prepared by Protocol-1. Figure 7-7 opposite shows the appearance of L929 cells after approximately 1 hour in the presence of non-infiltrated SCBB samples. In contrast to Protocol-1 samples, destruction of cells in proximity to the material as a result of lysis was not apparent. Cells did however have a less than optimal fibroblast appearance, which is normally characterised by a flattened morphology with widely extended fibrils. Considering the high confluency of the cells, even at this early stage, it is possible that this appearance was due to cell-to-cell contact induced morphological changes rather than cytotoxic effects. This appraisal was supported by the appearance of L929 cells at t = 48 hours,

where areas of reduced L929 density, probably caused by movement of the SCBB sample during transport scraping cells off the well surface, were seen to be repopulated by L929 cells now with the necessary space to display classic fibroblast morphology, see Figure 7-9a. Adding weight to this concept was the fact that the media only control wells displayed the same balling effect due to the high confluency. Nevertheless, this high level of confluency made the evaluation of cytotoxic response values between 0 None and 1 Slight (some malformed or degraded cells) more challenging. Note: the shadow seen around the black shape of the SCBB sample in the microscope image is an illumination effect and not related to the morphology of the L929 cells.

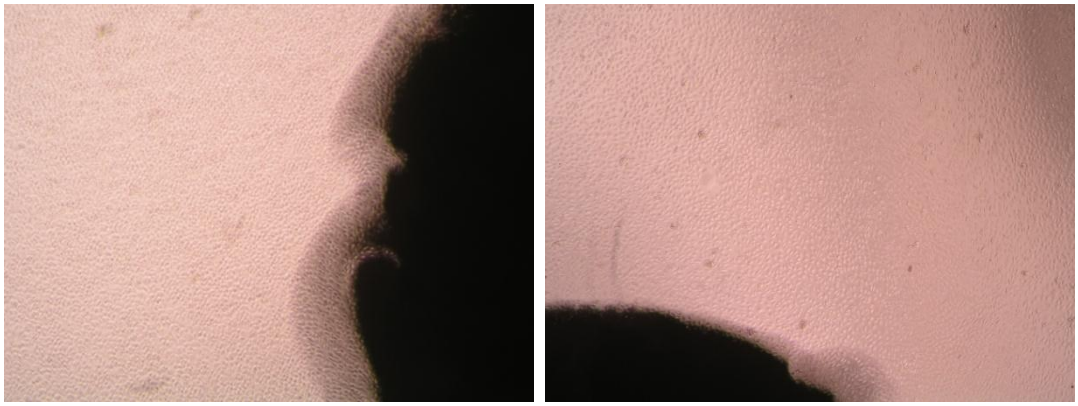

Figure 7-7 – Microscope images of non-infiltrated SCBB at t = 1 hour showing a monolayer of L929 cells right up to the edge of the sample.

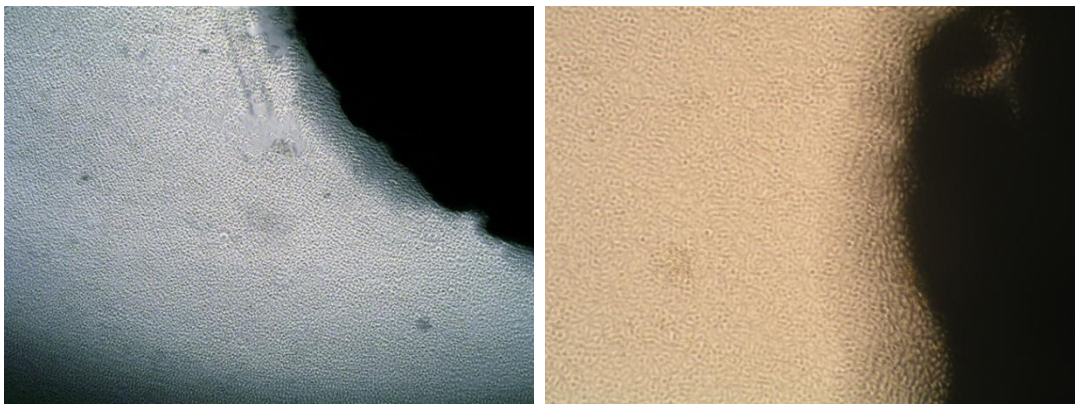

a) Non-infiltrated SCBB at 24 hours. b) Non-infiltrated SCBB at 48 hours.

Figure 7-8 – Microscope images of L929 cells at t = 24 (a) and t = 48 (b) hours after being exposed to non-infiltrated SCBB.

a) Non-infiltrated SCBB at 48 hours showing L929 fibroblast cells flattened and extended in close proximity to the sample where space allows.

b) Non-infiltrated SCBB at 48 hours, edge of well.

Figure 7-9 – Microscope images of L929 cells at t = 48 hours after being exposed to non-infiltrated SCBB, a) displaying the expansive morphology of cells when provided sufficient space and b) showing 100 % confluency of L929 cells at the periphery of the well showing balling but with no signs of degradation.

Recession of cells from the sample and cell lysis were not apparent in t = 24 hours or in t = 48 hours as shown in Figure 7-8. This was a consistent phenomenon occurring close to the sample as well as at the edge of the wells as shown in Figure 7-9b. Table 9 (p. 173) gives a summary of cytotoxic responses at each time point. These results were an improvement from Protocol-1 in which cytotoxic responses of 2 were seen for all time points (Table 8, p. 173).

7.4.2 Infiltrated SCBB samples

All infiltrated SCBB samples from Protocol-1, namely BioSCBB-1, BioSCBB-2 and BioSCBB-4 showed near identical results in cytotoxicity testing. At t = 1 hours cells in the immediate vicinity to the sample showed signs of recession from the sample and balling as shown in Figure 7-10. However, signs of lysis were not as apparent when compared against the non-infiltrated SCBB sample (see Figure 7-4 above).

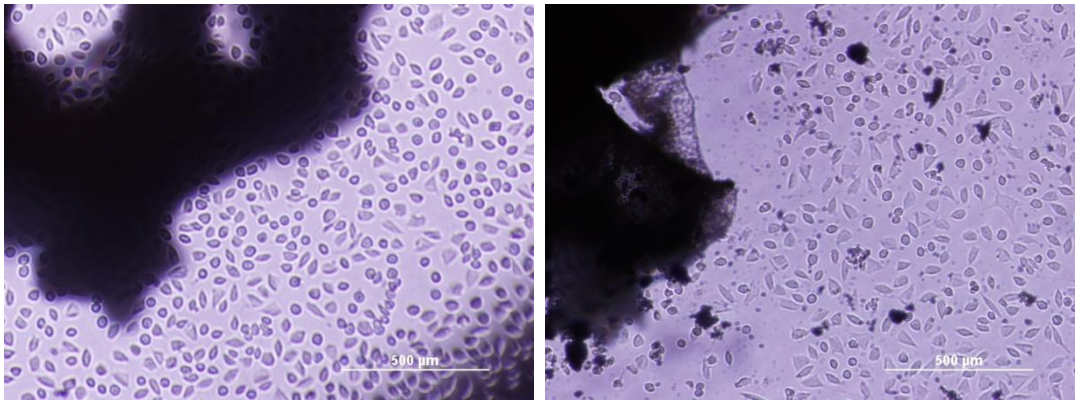

a) BioSCBB-1 (SCBB infiltrated with chitosan)

b) BioSCBB-2 (SCBB infiltrated with chitosan / $CAHPO_4$)

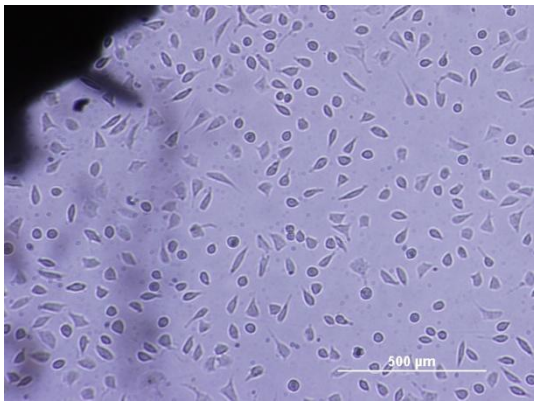

c) BioSCBB-4 (SCBB infiltrated with chitosan / TEOS)

Figure 7-10 – Microscope images of infiltrated SCBB samples at t = 1 hour.

Signs of cell degradation and malformation were apparent up to approximately 2-3 mm from the edge of the sample indicating a mild cytotoxic response at t = 1 hour. By contrast, at t = 24, 48 and 72 hours after the samples had been placed on the monolayer of cells, there was considerable cell degradation across the entire area of the 16 mm diameter wells. This is shown in Figure 7-9 where the edge of the wells for each sample is presented showing significant cell degradation and malformation for the time point t = 24 hours. This must be considered as a moderate cytotoxic response, although because the wells did not extend beyond 0.5 cm from the sample and it was therefore not possible to differentiate between a moderate and a severe

reaction. Time points t = 48 and 72 hours showed similar results but with a decreasing presence of intact cells (generally balled cells) with increasing time.

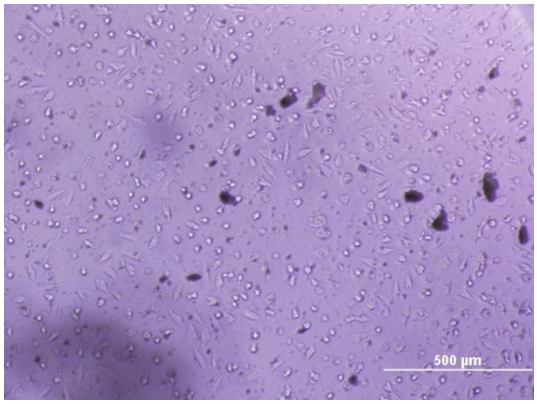

a) BioSCBB-1 (SCBB infiltrated with chitosan)

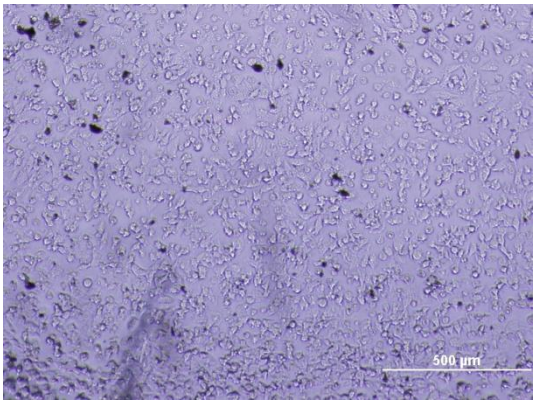

b) BioSCBB-2 (SCBB infiltrated with chitosan / $CAHPO_4$)

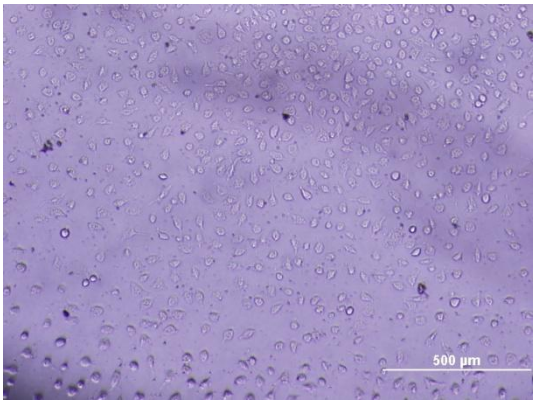

c) BioSCBB-4 (SCBB infiltrated with chitosan / TEOS)

Figure 7-11 – The edge of the 16 mm diameter wells infiltrated SCBB samples at t = 24 hours showing cellular degradation and malformation.

A summary of the cytotoxicity grades for each sample type is given below in Table 8, which shows explicitly that the samples, and in particular the infiltrated SCBB samples, were toxic with respect to the L929 cells.

Table 8 – Cytotoxicity grade per sample and time point for Protocol-1.

Time point (hours)	Non-infiltrated SCBB	Chitosan infiltrated SCBB	Chitosan/$CaHPO_4$ infiltrated SCBB	Chitosan/TEOS infiltrated SCBB
1	2	2	2	2
24	2	3-4	3-4	3-4
48	2	3-4	3-4	3-4
72	2	3-4	3-4	3-4

Photographic results of Protocol-2 biocompatibility testing are presented in Appendix K. Significantly, the finding of the Protocol-2 cell culture test was that all cytotoxic responses were significantly reduced with respect to those seen in Protocol-1. This can be seen by comparing cytotoxic response results for Protocol-1 presented in Table 8 above and Protocol-2 presented in Table 9 below. Mild reactions were seen almost immediately (t = 1 hour) for infiltrated samples in Protocol-1, whereas very little reaction was seen in Protocol-2 until 48 hours after sample exposure to the cells. Moderate to severe reactions were not seen in Protocol-2 until t = 48 hours for infiltrated samples, by contrast these responses were seen within 24 hours in Protocol-1.

Table 9 - Cytotoxicity grade per sample and time point for Protocol-2.

Time point (hours)	Non-Infiltrated SCBB	Chitosan infiltrated SCBB	Chitosan/ $CaHPO_4$ infiltrated SCBB	Chitosan/ TEOS infiltrated SCBB	Chitosan/Ca HPO_4 /genipin infiltrated SCBB	Chitosan/$CaHPO_4$ /genipin /urea/urease/ ascorbic acid infiltrated SCBB
1	0-1	0-1	0-1	0-1	0-1	0-1
24	0-1	0-1	0-1	0-1	0-1	0-1
48	0-1	3	3	3	3	0-1

The results obtained in the L929 cell culture test showed levels of toxicity in both the non-infiltrated and infiltrated SCBB samples that was considered high. During preparation infiltrated samples were washed repeatedly with copious quantities of distilled water in a fashion shown to remove a large proportion of by-product ammonia, ammonium and chloride. In theory, these compounds / ions should be the

only soluble by-products of the infiltration and immobilisation processes. In an effort to account for the toxic effect of the SCBB samples, a calculation was made as a means of estimating the concentration of NH_3 / NH_4^+ in a culture well with 0.4 mL media as used in the study. This resulted in a value of approximately 12 mmol L^{-1} (12,000 µmol L^{-1}) NH_3 / NH_4^+ (see Appendix L).

As discussed in section 5.7, NH_3 / NH_4^+ concentrations as low as 2 – 3 mmol L^{-1} have been seen to inhibit cell growth in cell cultures, while levels from 5 – 50 mmol L^{-1} have been seen to cause apoptosis and necrosis [149]. More particular to the intended end use of the material, compared to a typical arterial NH_3 / NH_4^+ concentration in the human body of ~100 µmol L^{-1}, this level must be considered extremely high. However, it should also be remembered that the human body has the capacity to rapidly metabolise large quantities of NH_3 / NH_4^+, as Lockwood *et al.* observed when injecting "^{13}N-ammonia" (pH 7.2 phosphate buffered NaCl solution) into the blood stream. They observed that all ^{13}N was metabolised and seen only in metabolites at 10 minutes after injection [171]. The complex biological mechanisms required for such metabolic processing of foreign chemicals are unlikely to be available to a monolayer of fibroblast cells, whose primary function is to lay down collagenous connective tissue.

Alternatively, or in combination with NH_3 / NH_4^+, the presence of $Ca(OH)_2$ in the SCBB may have been responsible for the cytotoxicity seen in the samples. Barbosa *et al.* showed that $Ca(OH)_{2(aq)}$ was highly toxic to L929 cells at a concentration of 13 mmol L^{-1} possibly due in part to an increase in pH. Concentrations of 5 mmol L^{-1} and below however showed no signs of cytotoxicity [161]. Figure 4-27, section 3.5.9, p. 97 shows that placing SCBB under autoclave conditions (heat and steam) reduces the level of alkalinity of the surfaces of material. Presumably this occurs through steam condensing on the material to give hot water capable of dissolving and carrying away quantities of $Ca(OH)_2$. As the samples used in biocompatibility testing were autoclaved in steam permeable bags, a similar process may have occurred. Condensing steam that formed during autoclaving may have dissolved quantities of

$Ca(OH)_2$ from the non-infiltrated SCBB samples, which could have been drawn away by soaking into the permeable autoclave bag. In combination with this, more $Ca(OH)_2$ could have been washed away or neutralised by the buffer solution during the subsequent soaking in MEM media before samples were placed on the cell monolayer. In contrast, infiltrated SCBB samples had a layer of chitosan (or chitosan composite) material covering most surfaces of the SCBB. This chitosan material is permeable to water (and steam), but could act to slow down the removal of $Ca(OH)_2$. If steam permeated through the chitosan layer during autoclaving to dissolve $Ca(OH)_2$ from the surface of the SCBB, this material would require significantly more time to diffuse through the chitosan layer. This concept of the $Ca(OH)_2$ (aqueous or solid) being trapped beneath and/or within the chitosan layer is shown below in Figure 7-12.

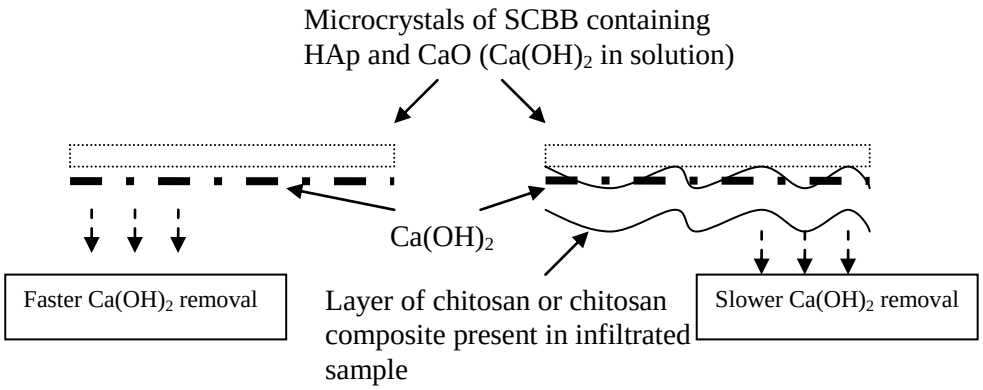

Figure 7-12 - Diagrammatic representation of chitosan coated SCBB samples due to infiltration and the trapping of $Ca(OH)_2$ beneath.

The disparity in the toxicity results for non-infiltrated SCBB in comparison to infiltrated samples supports this concept. Non-infiltrated SCBB samples proved to be cytotoxic to cells in close proximity to the sample immediately after introduction to the same extent, or an even greater extent, than the infiltrated samples, compare Figure 7-4 to Figure 7-10 (a-c) above. However, non-infiltrated SCBB samples were never exposed to $NH_{3(g)}$, therefore cytotoxicity could not be attributed to NH_3 / NH_4^+ presence and therefore more likely to be $Ca(OH)_{2(aq)}$. By contrast, the surface of the

infiltrated SCBB samples were protected by infiltrate that would have limited the removal of $Ca(OH)_2$ by autoclaving and soaking in MEM. Accordingly, infiltrated samples showed a slow increase in cytotoxicity over the 72 hours indicating a continuous leaching of soluble toxic material from within the sample. Whereas, non-infiltrated SCBB showed a rapid but overall less toxic effect indicating the presence of readily available toxic material but less of it. It should be noted however, that this theory does not preclude the presence of NH_3 / NH_4^+ as the cause of the cytotoxicity seen particularly in samples produced under Protocol-1.

TEOS

The concept of combining TEOS with the chitosan infiltrating solution has not been discussed previously in the thesis, but it was considered as a possible infiltrating system. As biocompatibility testing was undertaken at another university, (University of Otago, New Zealand) the opportunity to test potential infiltrates was also taken. TEOS and chitosan have been combined before in research designed to develop a pH sensitive drug delivery membrane [162], as well as a potential sorbent for liquid chromatography [163]. The following method is an adaptation of that described by Rashidova *et al.* for the reaction of chitosan with tetraethoxysilane (TEOS) using a sol-gel method [163]. Al-Sagheer and Muslim characterised the product of the reaction between chitosan and TEOS by FT-IR concluding that a combination of covalent and ionic bonds were formed, seen in Figure 7-13 [164].

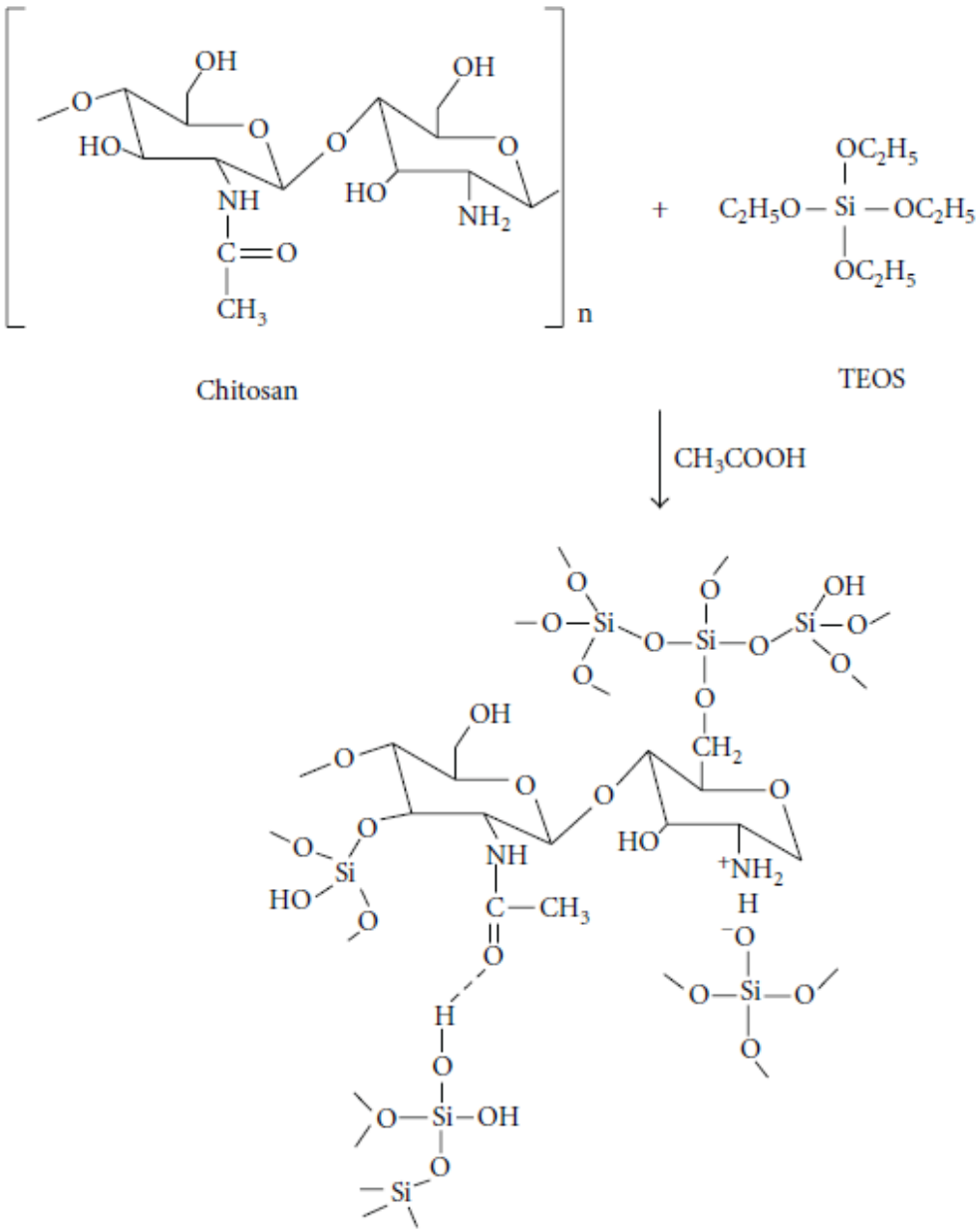

Figure 7-13 – Reaction scheme between TEOS and chitosan

HET-CAM

The HET-CAM test was carried out using a modified method from that described by Luepke [165]. According to the original method, fertilised hen's eggs were incubated for 9 days and on the 10th day the chorioallantoic membrane (CAM) of the developing embryo, which is a vascularised respiratory membrane, was exposed by removal of a portion of shell [165]. The CAM (blood vessels and albumen) at the site

of contact was examined at specific end-point times (0.5, 2 and 5 minutes) for three specific indicators of tissue damage [166]. Luepke used hyperaemia (increased blood flow), haemorrhage and coagulation of the albumen as end-points; however, further studies have suggested that blood vessel lysis, haemorrhage and coagulation are more reproducible end-points [167]. Scores for each of the time points and signs of irritation were tallied to give an irritation score (IR). However, in the research presented here the HET-CAM test was used as an initial trial to give a qualitative indication of the response of tissue to the presence of the solid material. A more comprehensive study could involve examination of the CAM under microscope, histological evaluation and viewing under SEM as described by Valdes *et al.* [168].

No evidence was seen of blood vessel degradation (lysis or haemorrhage) or albumen coagulation on any of the samples at the 0.5, 2 and 5 minute periods. This contrasted strongly with the positive control, i.e. a single drop of 0.1 mol L^{-1} NaOH placed on the CAM which showed significant blood vessel lysis and haemorrhage increasing over the 5 minutes of contact, as shown in Figure 7-14. The negative control of agarose gel showed, in contrast, no response over the same period of exposure. Over the three days, a wide range of effects were seen from the death of the embryo to disappearance (submergence from view) of the sample into the albumen. These effects appeared to be random, as duplicates tended not to be affected together. If not caused by the presence of the sample, embryo death and CAM degradation could have been the result of infection, which would not be unexpected given the significant breach in the defensive barrier protecting the embryo through the removal of a portion of shell.

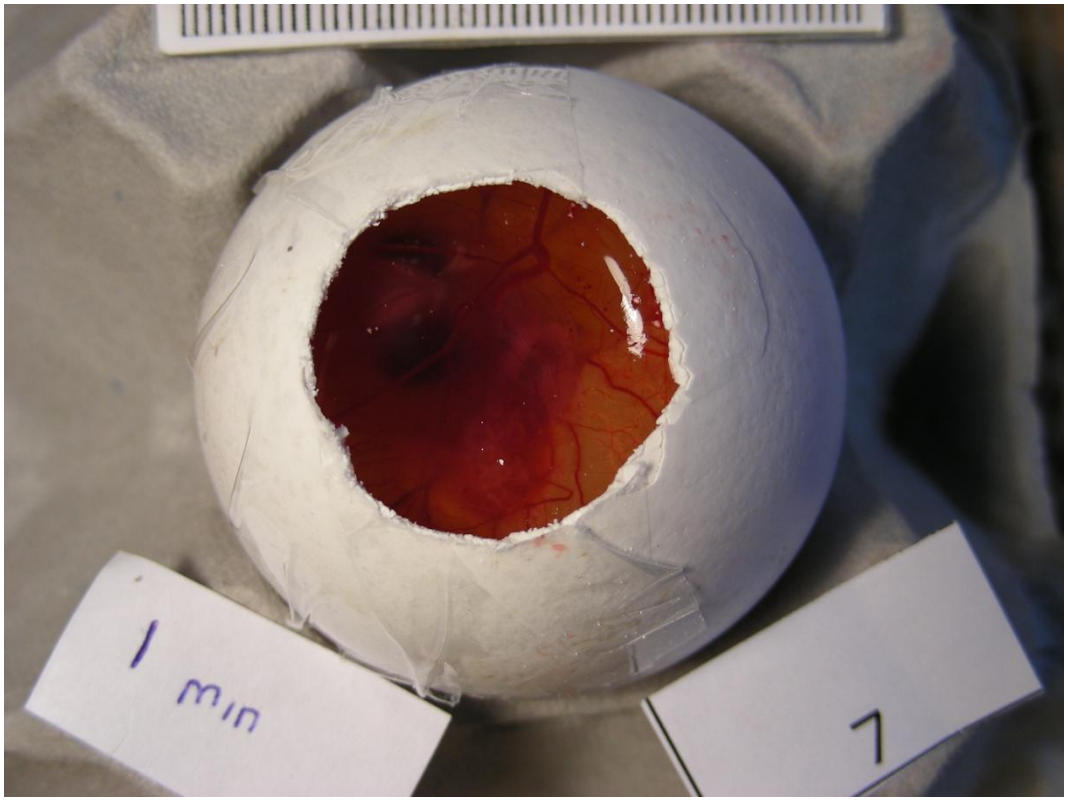

Figure 7-14 – HET-CAM test positive control showing CAM surface dispersed blood due to broken blood vessels caused by the application of 0.1 mol L^{-1} NaOH.

Another factor that could have affected the health of the embryos was the transfer of eggs from incubator to platform each day for photography. This factor was borne out of an observation on one occasion, where embryos were subjected to a significant physical trauma during handling. Therefore, it was not possible with this duplicate sample test to ascertain whether effects were dependent on the materials or as a result of random effects such as infection or shock.

Figure 7-15 shows the typical progression in the appearance of the exposed CAM after being presented with a sample, (BioSCBB-1). The sample was not pre-soaked in a buffer or saline solution, (which would have been a preferable pre-conditioning of the sample, as it would have reduced the possibility of the sample drawing moisture from the CAM tissue), so that tissue damage could have been caused. Despite this, all photographs for the SCBB sample infiltrated with chitosan displayed no visually

discernible signs of blood vessel degradation or albumen coagulation over the 72 hours.

Physical responses to the presence of all test samples are shown below in Table 10 and Table 11 and reveal that there was no visibly noticeable effect, by all the samples on the CAM within the first 5 minutes. In retrospect, this was not surprising as the sample was in solid form, requiring that toxic compounds, if present, be first solubilised or leached out of the material, before they could affect the CAM tissue. Later time points also showed no obvious signs of any of the materials causing coagulation of the albumen, haemorrhage or lysis of the blood vessels, except in one of the BioSCBB-2 samples where a ring of blood was seen to form around the periphery of the sample at t = 24 hours shown in Figure 7-16 below. This could have indeed been due to cytotoxin-induced haemorrhage, or alternatively, this could have been the result of the sharp edge of the sintered bone cutting through a blood vessel as it proceeded to submerge into the albumen.

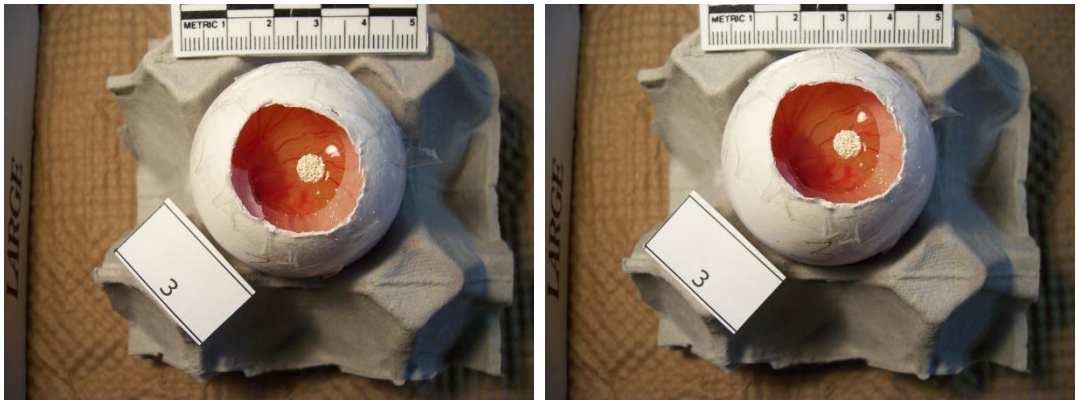

a) 0.5 minutes

b) 2 minutes

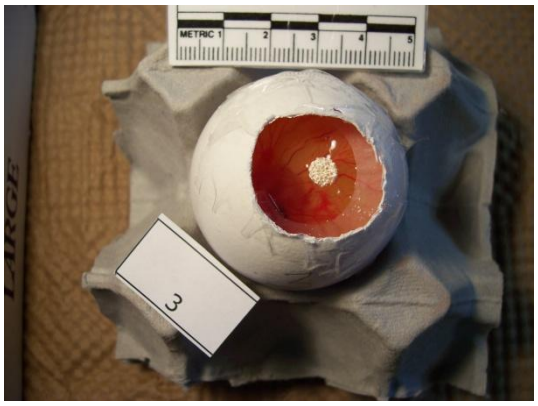

c) 5 minutes

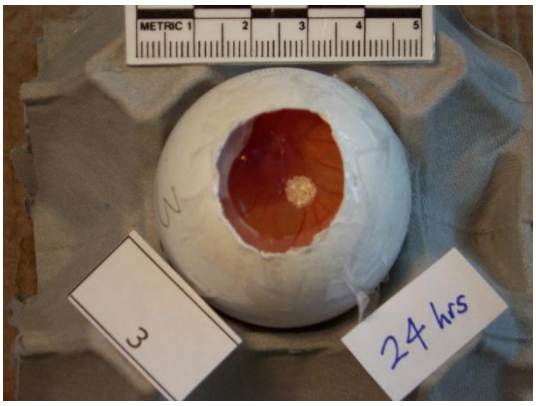

d) 24 hours

e) 48 hours

f) 72 hours

Figure 7-15 - Images of HET-CAM test on SCBB sample infiltrated with chitosan from 0.5 minutes to 72 hours exposure.

Table 10 – Description of the physical response to the presence of sample at respective time points.

Time	BioSCBB-0		BioSCBB-1		BioSCBB-2		BioSCBB-4	
0.5 min	No reaction, sample on surface of CAM	No reaction, sample on surface of CAM	No reaction, sample on surface of CAM	No reaction, sample on surface of CAM	No reaction, sample on surface of CAM	No reaction, sample on surface of CAM	No reaction, sample on surface of CAM	No reaction, sample on surface of CAM
2 min	No reaction, sample submerging into albumen	No reaction, sample on surface of CAM	No reaction, sample on surface of CAM	No reaction, sample on surface of CAM	No reaction, sample on surface of CAM	No reaction, sample on surface of CAM	No reaction, sample on surface of CAM	No reaction, sample on surface of CAM
5 min	No reaction, sample submerged into albumen	No reaction, sample on surface of CAM	No reaction, sample on surface of CAM	No reaction, sample on surface of CAM	No reaction, sample on surface of CAM	No reaction, sample on surface of CAM	No reaction, sample on surface of CAM	No reaction, sample on surface of CAM
24 hours	Few blood vessels visible. Embryo appears dead.	Sample submerged into albumen. No blood vessel degradation.	Sample submerged into albumen. No blood vessel degradation.	Sample submerged into albumen. No blood vessel degradation.	Sample submerged into albumin. Blood around sample periphery.	Few blood vessels. Yellow of egg dispersed throughout albumen. Embryo appears dead.	Sample submerged into albumen. No blood vessel degradation.	Sample submerged into albumen. No blood vessel degradation.
48 hours	-	Sample submerged further into albumen, ~ 10 mm. No blood vessel degradation.	Sample submerged into albumen. No blood vessel degradation.	Sample submerged into albumen. No blood vessel degradation.	Sample submerged into albumen. Blood around sample periphery penetrating into sample.	Continued evidence of decaying embryo indicated by hardening of yellow and albumen.	Sample submerged into albumen. No blood vessel degradation.	Sample submerged into albumen. No blood vessel degradation.
72 hours	-	Sample disappeared into albumen. No blood vessel degradation.	Sample submerged into albumen. No blood vessel degradation.	Sample submerged into albumen. No blood vessel degradation.	Sample submerged deeply into albumen, barely visible. Embryo still living.	Contents solid indicating embryo death.	Sample submerged into albumen. No blood vessel degradation.	Sample submerged into albumen. No blood vessel degradation.

Table 11 - Description of the physical response to the presence of sample at respective time points.

Time	BioSCBB-3		BioSCBB-5		Positive Control 0.1 M NaOH		Negative Control Agarose Pellet	
0.5 min	No reaction, sample on surface of CAM	No reaction, sample on surface of CAM	No reaction, sample on surface of CAM	No reaction, sample on surface of CAM	Coagulation of albumen and complete lysis of blood vessels at point of contact.	Coagulation of albumen and complete lysis of blood vessels at point of contact.	No reaction, sample on surface of CAM	No reaction, sample on surface of CAM
2 min	No reaction, sample submerging into albumen	No reaction, sample on surface of CAM	No reaction, sample on surface of CAM	No reaction, sample on surface of CAM	Coagulation of albumen and complete lysis of blood vessels at point of contact.	Coagulation of albumen and complete lysis of blood vessels at point of contact.	No reaction, sample on surface of CAM	No reaction, sample on surface of CAM
5 min	No reaction, all sample submerged into albumen	No reaction, sample on surface of CAM	No reaction, sample on surface of CAM	No reaction, sample on surface of CAM	Coagulation of albumen and complete lysis of blood vessels at point of contact.	Coagulation of albumen and complete lysis of blood vessels at point of contact.	No reaction, sample on surface of CAM	No reaction, sample on surface of CAM
24 hours	Embryo damaged during transfer. Loss of contents. Embryo dead.	Sample submerged into albumen. No blood vessel degradation.	Sample submerged into albumen. No blood vessel degradation.	Embryo damaged during transfer. Loss of shell contents. Embryo dead.	Point of contact not obvious. Albumen somewhat cloudy	Point of contact not obvious. Albumen somewhat cloudy	No reaction, sample on surface of CAM	Albumen somewhat cloudy
48 hours	-	Sample submerged into albumen. No blood vessel degradation.	Sample submerged into albumen. No blood vessel degradation.	-	Albumen clearer.	Albumen clearer.	No reaction, sample on surface of CAM	Albumen very cloudy, contents firm. Embryo dead.
72 hours	-	Sample submerged into albumen. No blood vessel degradation.	Sample submerged into albumen. No blood vessel degradation.	-	Albumen clear with large dark red blood vessels.	Albumen clear with large dark red blood vessels.	No reaction, sample on surface of CAM	-

Figure 7-16– Photograph of BioSCBB-2 sample on CAM after 24 hours showing a ring of blood around the sample.

Death of the embryos appeared to be random, as death did not occur in both duplicates for any of the samples. Therefore, embryo death was more likely to be caused by external factors such as physical trauma during movement, dehydration or infection. In embryos that survived the prolonged exposure experiment (72 hours), there was little physical change on the CAM and within the embryo, except for a general reduction in the opacity in the space around the embryo (prevalence of egg yellow appeared to decrease) and a slight thickening and reddening of blood vessels. As dilation of blood vessels and hyperemia (increased blood flow) have been used as indicators of irritancy in previous HET-CAM studies, this appearance change must be considered a possible indicator of cytotoxic response. However, the growth and expansion of blood vessels are just as likely to be the result of natural embryonic maturation processes.

This HET-CAM test was initiated with the goal that it should serve as a preliminary study on the feasibility of testing the SCBB materials by HET-CAM, while providing qualitative data on the response of a complete living organism to the presence of the materials. The fundamental problem with testing an opaque solid such as this is that the site of direct contact between material and tissue is not apparent unless the test sample is removed before examination, and it is this area that gives the most information over the nature of the tissue response. Commonly, the test material is washed away at specific time points revealing the contact area (Luepke), but the attempt to combine short term time points and long term time points, with low sample numbers prevented such a method in this experiment. Ultimately, the HET-CAM experiment revealed incidences where each of the samples could be accommodated within the tissue and circulatory system of the chicken embryos for up to three days after placement, while no dramatic destruction of tissue (rupture of blood vessels, coagulation, haemorrhage) occurred, in stark contrast to the case with the NaOH 0.1 mol L^{-1} positive control.

Ultimately, biocompatibility testing revealed (through the L929 cell culture test) that the SCBB and infiltrated SCBB samples contained a leachable cytotoxic substance or substances. However, comparison in cytotoxicity between Protocol-1 and Protocol-2 samples showed a marked reduction in cytotoxicity after the samples were exposed to PBS for 24 hours. This revealed that cytotoxic materials could be neutralised or flushed out by PBS. Of the Protocol-2 produced samples, the BioSCBB-5 sample proved to have the least cytotoxic effect. This result supports the argument that the cytotoxicity was due to the presence of NH_3 / NH_4^+, because the preparation method did not involve the exposure of the samples to $NH_{3(g)}$, but relied on the conversion of urea to ammonia by the action of the enzyme urease. The catalysis reaction is inhibited as pH approaches 8, meaning the pH of the infiltrate components could not have approached the pH values 10-11 seen in samples exposed to $NH_{3(g)}$. Ultimately, this would have determined that there was less free NH_3 / NH_4^+ present in this sample to be washed away or neutralised. Another factor that could have contributed to BioSCBB-5's lower level of cytotoxicity was the crosslinking effect of genipin.

Crosslinking of chitosan with genipin has been shown to reduce swelling in the material [94], which would have reduced the permeability of the material to water, thereby trapping any putative cytotoxic byproducts (e.g. NH_3, NH_4Cl) within the matrix.

Alternatively, cytotoxicity may have been in part due to remnant $Ca(OH)_2$ in the SCBB. Soaking with PBS could have neutralised $Ca(OH)_2$ present on the surface (surfaces available to liquid contact) of the SCBB sample without infiltrate, however with the samples that had been infiltrated, the layer of infiltrate may not have been permeable enough to allow complete neutralisation during soaking in PBS. Although, the layer of infiltrate may have been permeable enough to allow $Ca(OH)_2$ to slowly leach out during the cell culture test. The results of the Protocol-2 cell culture test in particular, where obvious cytotoxic effects were not seen until 48 hours after cells were exposed to the samples, are compatible with this hypothesis. When considering samples containing genipin, as mentioned above, crosslinking action would be anticipated to reduce swelling, thereby reducing the rate of water permeation and accordingly reducing the rate that $Ca(OH)_2$ would be released into the surroundings.

7.5 Conclusion

Biocompatibility testing revealed that infiltrated SCBB samples, that had been treated with $NH_{3(g)}$ required longer washing and buffer treatment than was initially undertaken. This was highlighted by the reduction of cytotoxicity effects with Protocol-2 samples in comparison to Protocol-1 samples. The earlier were buffered in PBS for 24 hours on top of the Protocol-1 samples 3 x 1-hour washings in distilled water and 15 minute buffer treatment. HET-CAM testing showed signs that SCBB samples (infiltrated and non-infiltrated) were compatible with a living system, as illustrated by the lack of the pronounced signs of irritation as seen in the positive control 0.1 mol L^{-1} $NaOH_{(aq)}$.

CHAPTER EIGHT

8 Summary and conclusions

The central concept of this research was inspired by the appearance of the macroscopic and microscopic structure of SCBB, leading to the notion of infiltrating a biocompatible organic reinforcing material into one or both of these void spaces to mimic the mineral / organic bio-composite from which natural bone is composed.

A comprehensive SCBB sample production system was developed allowing for the rapid manufacture of large quantities of samples suited to mechanical compression testing. To do this, raw bovine femoral bone was sectioned perpendicular to the primary load-bearing axis of the femoral shaft through the knee joint condyles at one end and the femoral head at the other. Three repetitions of a 2-hour long autoclaving cycle in water at 2 atm pressure led to the removal of large portions of fatty material, in addition to a quantity of gelatinous material assumed to be proteinaceous. Sintering at 1000°C for 3 hours led to the production of a material shown by IR to be devoid of organic content, while XRD in addition to IR analysis confirmed the material to consist almost exclusively of crystalline hydroxyapatite in combination with low levels of CaO.

CaO was an undesirable by-product of the sintering process because upon implantation into an aqueous environment, such as in the human body, it would produce a pH increase that could result in cell dysfunction or death. Therefore, methods of processing the SCBB were developed to minimise the presence of CaO on the surface of the material. To reiterate what has been stated earlier, because the SCBB is a porous material, the term “surface” used throughout this thesis, unless otherwise stated, refers to all surfaces of the hydroxyapatite material available for

contact on and inside the SCBB material, including the external bulk surface, the surface of the macropores and the surface of the crystallites within the microporous structure. Repeated washing of the SCBB material in water proved to be effective in progressively removing surface alkalinity, while washing in carbonated water proved to more rapidly and significantly reduce the alkalinity induced by the presence of CaO. As an alternative, it was found that exposure to the steam within an autoclave was capable of reducing surface alkalinity present in the SCBB material. Although it was expected that none of these methods would be capable of reducing the CaO trapped within the solid crystallites of hydroxyapatite, it was reasoned that lowering of surface alkalinity would mitigate any sudden pH changes in media in which the SCBB was immersed, after which the body's metabolic processes could accommodate the gradual release of low levels of CaO.

Two primary infiltrate materials were selected as candidates to be infiltrated into SCBB. PCL was chosen because of its proven biocompatibility and bioresorbability, while also showing excellent processing properties such as thermoplasticity and solubility in certain organic solvents. The potential of PCL to be melted and then forced into the SCBB material by vacuum was tested, but proved unsuccessful because of the highly viscous nature of the melted material. Therefore, PCL was dissolved in THF and successfully infiltrated at room temperature under vacuum though a process that was simple and reproducible. IR and SEM analysis on sub-samples taken from all regions of the infiltrated SCBB samples showed comprehensive infiltration of PCL, with SEM often showing infiltration of PCL in the microporous structure of the SCBB. Under this system, repeated infiltrations could be applied in order to deposit the desired quantity of PCL within the SCBB.

The potential of chitosan as an infiltrating material was also investigated. With its global abundance, along with the presence of extensive research into biomedical applications related to chitosan and its ability to dissolve in various acids to produce a liquid infiltrate, chitosan was considered a very appropriate material to infiltrate into SCBB. Fluka 'low viscous' chitosan with a molecular mass of approximately 150 kD

was used for all experimental work within this research, but this was done for sake of consistency and should not preclude the notion of using other chitosans of different chain length and/or degree of deacetylation. Chitosan was dissolved in HCl, because the HCl allowed the co-dissolution of mineral compounds such as HAp and $CaHPO_4$ which could be ultimately co-deposited with the chitosan inside the SCBB during immobilisation.

With an aim to improving the mechanical properties of chitosan upon deposition through the action of a composite effect, combination solutions of chitosan and calcium phosphate (HAp and brushite ($CaHPO_4$)) were prepared. Literature reviews also suggested that a composite of these compounds would reduce the uptake of water in aqueous environments which would help maintain mechanical strength. It was found that at a 1 : 1 w / w chitosan to HAp ratio, a maximum concentration of 6 g L^{-1} for both compounds could be dissolved in ~ 0.12 mol L^{-1} HCl.. Additional types of infiltrating solutions were prepared with the incorporation of the natural chitosan cross-linking agent genipin in order to alter the physical and thereby mechanical properties of the deposited infiltrate material.

Several immobilisation strategies and methods were trialled during the course of this research. The simplest method of depositing chitosan, or a combination of chitosan and other materials within the SCBB matrix, was firstly to prepare a suspension by raising the pH of a solution, through the addition of NaOH or $NH_{3(aq)}$ for example, and then infiltrating this suspension into the SCBB. Due to the relatively large macropores of the SCBB (~ 0.2 - 0.7 mm), the suspension could be infiltrated by vacuum into all internal regions of the material. The infiltrate then became immobilised upon drying. However, due to the particulate nature of the suspension, this process completely eliminated the possibility of infiltrating chitosan into the microporous structure of the SCBB. To enable the possibility of achieving this goal, the infiltrate had to be infiltrated as a liquid and then immobilised (i.e. converted to a solid) *in situ*, within the SCBB.

Internal immobilisation was achieved by increasing the pH of the infiltrating solution with several means of doing this investigated. One such means was to use the effect of an electric current to induce the migration of basic anions in solution via the freshly infiltrated SCBB material. A phenolphthalein pH indicator added to the infiltrate proved that the method successfully increased the pH of the solution within the SCBB above 8.0 causing precipitation of solids from the infiltrate solutions. However, the method also appeared to cause the migration of the protonated chitosan molecule within the SCBB material leaving some extremities of the SCBB without infiltrate. In another pH-increasing method, urea was added to the infiltrating solution, which upon heating under pressure to ~ 120°C in an autoclave caused urea to undergo a thermal hydrolysis reaction leading to the release of $NH_{3(aq)}$ and a consequent increase in pH. This caused the precipitation of chitosan and any accompanying mineral component, but did have the undesirable effect of causing browning of the chitosan if the process was repeated more than 2 or 3 times. A means to circumvent this problem was to use the enzyme urease in place of heat to effect the hydrolysis reaction at room temperature. When the appropriate quantity of urease and urea was added to an infiltrate solution, precipitation was seen to occur after approximately two hours. Although urease is a very toxic compound, due to its ability to catalyse urea to ammonia within the body it can be easily denatured by heating above 70°C, and accordingly deactivated.

Cross-linking chitosan with the natural cross-linker genipin was an alternative non-pH raising strategy to immobilise chitosan within the SCBB. It was found that if 0.5 % w / w genipin to chitosan was added to the chitosan infiltrate solution this was sufficient to yield an insoluble infiltrate after ~ 14 hours. Measures were taken during the preparation of solutions containing genipin to remove oxygen from the solution by degassing, storing under nitrogen and minimising exposure to the atmosphere, because the presence of oxygen led to a blue / green colouration caused by genipin self polymerisation. The method could also be combined with a pH-raising method of immobilisation, in which the synergies of using the pH increasing ability of urease

with urea, and the cross-linking ability of genipin, were combined with chitosan and calcium phosphate, to achieve immobilisation within the SCBB pores.

Ultimately, the action of ammonia gas was determined to be the most practical method of precipitating and immobilising infiltrate within the SCBB material. Because ammonia is gaseous, it could penetrate rapidly into an infiltrated SCBB sample, reaching all areas of a 10 mm diameter x 10 height sample within 30 minutes. As an added advantage, it was shown by IR spectroscopic analysis that ammonia gas could penetrate several millimetres into solid chitosonium chloride / HAp infiltrate composite over a period of 24 hours exposure. This penetrative property of ammonia gas made possible a method that involved repeated infiltrations followed by one final immobilisation step at the end.

Exposure of infiltrated samples to ammonia gas led, however, to high levels of ammonia within the material that could be highly toxic to living tissue upon implantation. Therefore, the infiltrated / ammonia-immobilised samples were washed in distilled water and the efficacy thereof studied. Levels of ammoniacal-N (NH_3 / NH_4^+) and chloride in the washing water and that remaining within the samples were measured at 1 hour intervals. A significant proportion of ammoniacal-N was removed from within the sample after 4 x 1 hour washes in distilled water, but remnants were still present even after 6 x 1 hour washes. Chloride levels were reduced to control levels (chloride in SCBB) after 5 x 1 hour washes. Information gained from biocompatibility testing showed that prolonged buffer treatment (at least 24 hours) was required after washing in distilled water to generate a material with low cyto-toxicity.

A fundamental objective of this research was to infiltrate organic material into the microporous structure of the SCBB. SEM showed that infiltration into the microporous structure was achieved for PCL and chitosan when vacuum processes were used for the infiltration, but probably only during the first infiltration step because an overlaying barrier of infiltrate was formed after the first infiltration. To

enable the tracing of chitosan through separate infiltration steps, the chitosan molecule was labelled with FITC using a method described by Qaqish. Fine particles of infiltrated SCBB were removed from the samples by scraping with a scalpel, and when viewed under fluorescence microscope. The characteristic patterns of fluorescence revealed whether the FITC-labelled chitosan was present within the microporous structure, or only lying on the surface of the microporous structure.

As discussed infiltration of chitosan and calcium phosphate infiltrating solution under vacuum proved sufficient to deposit infiltrate into the microporous structure of the SCBB, but only at the first infiltration stage. A previous layer of infiltrate was seen to act as a barrier to further infiltration into the microporous structure. To overcome this limitation, a hydrostatic pressure vessel was designed and built in cooperation with the engineering company Tamaterau Engineering Ltd. With up to 90 atm of pressure, FITC labelled chitosan and HAp infiltrating solution could be forced into the microporous structure of the SCBB following a previous infiltrating step. Proof of infiltration into the microporous structure was then able to be made through fluorescence microscopy.

Mechanical strength measurements in the form of compression testing were used to determine the effect infiltration had on the mechanical properties of the SCBB material. Initially, testing was carried out on non-infiltrated SCBB samples to establish a correlation between mechanical properties and apparent (bulk) density. This was done because of the variable nature of SCBB samples. After this was confirmed, these results were used to act as control values against which infiltrated samples were compared. Mechanical properties that were used to compare samples were ultimate stress, modulus and a modified toughness value. This modified toughness value was calculated from the area under the stress / strain curve to a specific strain value (8 % strain), as a means of accounting for the ability of certain infiltrated samples to maintain a degree of strength after an initial point of failure. Linear transformations were performed on the data, which allowed the data to be subjected to linear regression analysis.

Results showed that SCBB samples infiltrated with Infil-4 (chitosan / $CaHPO_4$) displayed superior ultimate stress and [toughness to strain = 8 %] values in comparison to non-infiltrated SCBB samples, while Infil-12 (PCL) infiltrated samples showed increased modulus values only. Samples infiltrated with chitosan / $CaHPO_4$ in combination with the cross-linking agent genipin (Infil-11) showed no overall statistically significant change in mechanical properties. However, visual examination of scatter plots showing regression lines and 95 % confidence intervals, suggested that this infiltrate increased all mechanical properties, but only in SCBB samples possessing lower apparent density. By contrast, at higher apparent density values, no effect was noted for samples infiltrated with Infil-11.

In vitro and in vivo testing were also carried out on the SCBB samples. SCBB samples subjected to a range of infiltration protocols were prepared to be tested for biocompatibility through a direct contact L929 mouse fibroblast cell culture test and a modified HET-CAM test. Samples were washed in distilled water for a total 6 hours and then treated with a phosphate buffer at pH 7.4 for 15 minutes. This was system of washing was named Protocol-1 and samples treated in this way showed significant cytotoxic response, but more so for samples that had been infiltrated in comparison to non-infiltrated SCBB. This response was attributed to inadequate washing and/or buffering of the samples to remove sufficient quantities of infiltration by-products to render the samples non-toxic. Accordingly, samples were treated with phosphate buffer for a further 24 hours (Protocol-2) and a 2^{nd} cell culture test carried out. Results from this test showed significantly less cytotoxic response, especially at earlier stages of the test (0 to 24 hours) where almost no response was noted. At 48 hours some cytotoxic response was noted for infiltrated samples, which may have been due to the leaching of deeply buried infiltration by-products or $Ca(OH)_2$. These results indicated that a more extensive period of washing and buffering process was required than that initially used in the preparation of these samples, but results also showed that longer buffering and washing processes were effective in reducing the cytotoxicity of the samples.

HET-CAM was used to observe the reaction of a living system to the presence of the materials. While it is commonly conducted as only a short 5-minute test to observe the irritancy of liquid samples on living tissue, the solid nature of the samples under investigation necessitated an extension of exposure time to 72 hours after samples were placed on the CAM. No samples caused obvious immediate degradation (within 5 minutes) of the CAM as would have been indicated by blood vessel lysis, haemorrhage, or coagulation of the albumin. Over the subsequent three days, deaths were observed for various embryos, but these appeared to occur due to random causes and not ostensibly because of exposure to the SCBB samples. In general, the deaths only occurred in one of a duplicate pair of samples.

8.1 Conclusions

Several aims set out at the beginning and developed during the course of the research were realised and include:

- A system was developed enabling the mass production of SCBB samples of suitable dimensions to be later tested by compression testing.

- SCBB was shown to be a material conducive to infiltration with an organic matrix, confirming the potential to alter its mechanical and biological properties.

- Infiltration systems involving vacuum, vacuum and pressure and pressure alone were developed to successfully infiltrate PCL and chitosan / calcium phosphate composites into the macro- and microporous structure of the SCBB.

- An immobilisation process was developed to make the infiltrated material insoluble so that it remained in place within the SCBB.

- Washing and buffering process were instigated and shown capable of removing and/or neutralising the toxic effects of by-products generated during the immobilisation process.

- Despite the inherent variability in the SCBB starting material a mechanical testing system incorporating statistical analysis was developed enabling meaningful comparison between non-infiltrated and infiltrated samples.

- The infiltration system consisting of chitosan and $CaHPO_4$ was shown to increase the ultimate stress and a modified extended toughness measure of infiltrated SCBB samples, while infiltration with PCL tended to increase modulus values.

The following contributions to science were made:

- This research had contributed knowledge and thinking into the possibilities, challenges and limitations of infiltrating organic material, or organic material in combination with a mineral to produce a composite, into SCBB. Infiltration into the relatively large macropores of the material was uncomplicated and accomplished through vacuum. However, repeated infiltration into the microporous structure of SCBB required a gradual increase in the pressure of the infiltrate to allow the solubilisation and propulsion of overlaying infiltrate into the micropores.

- It was shown that methods previously used to increase the pH of solutions without the physical addition of a basic compound, such as the thermal hydrolysis of urea and urease catalysis of urea, were able to be successfully applied within the SCBB matrix to immobilise chitosan and calcium phosphate composite infiltrate.

- A novel system for increasing the pH of a solution containing ions capable of conducting an electrical current was developed. This was made possible through the electric field induced migration of basic ions from one electrode placed in a basic salt solution to another separated by a semi-permeable membrane and the infiltrated SCBB (through which the current travelled by diffusion).

- It was demonstrated overall that an organic material could be successfully infiltrated into the porous SCBB matrix to yield a potential bone replacement material with altered physical properties to that of the starting SCBB material and possessing (upon instigation of the correct washing and buffering protocols) a low bio-toxicity response.

8.2 Further work

Although many possibilities with respect to the processing techniques and materials used in the manufacture of the infiltrated SCBB material were investigated, there remain a number of parameter modifications with the potential to improve the product.

- The annealing of chitosan (~ 100-120°C for periods of an hour or more) has been shown to cause cross-linking reactions within the compound [197, 198]. This process has been shown to reduce the uptake of water, increase mechanical strength and increase biocompatibility [95, 144]. Experimentation with annealing was not carried out in this research, as the focus was towards optimising infiltration processes and *in situ* immobilisation systems. It is the opinion of this author, that the chitosan / calcium phosphate systems described here within this body of work may show significant improvements in mechanical strength, particularly in a moist environment, with an annealing treatment. The cross-linking reaction should reduce the propensity of the chitosan material to absorb water, which is a fundamental reason for the reduction in mechanical strength of chitosan in an aqueous environment.

- Very early in this research, it was established that a suspension of chitosan and calcium phosphate could be produced and infiltrated repeatedly into the macropores of the SCBB material under vacuum. If the concept of infiltrating chitosan / calcium phosphate into SCBB was to be commercialised to produce bone replacement material for the market, and the idea of infiltrating the material into the microporous structure was deemed unnecessary, there seems little reason to use any other system apart from this simple suspension infiltration system. Therefore, for infiltration into the macroporous structure of the SCBB alone, the author recommends continued investigation into the potential of suspension production, modification (e.g. cross-linked with genipin) and infiltration.

- The co-deposited 1:1 chitosan / HAp composite material was particularly attractive as an infiltrate material, because of its visual resemblance to bone, largely due to the quantity of white HAp in the material. It is recommended that further work with co-precipitated chitosan as an infiltrate focus around this concept material, possibly in combination with genipin to cross-link the material and then a final annealing step.

- A fundamental limitation to co-depositing chitosan and calcium phosphate is the amount of each material the can be simultaneously dissolved in solution. For example, for the 1 : 1 chitosan / HAp solution, a limit of 6 g L^{-1} for each when dissolved in $HCl_{(aq)}$ was established. This dictates that many iterations of infiltration must be made to build up a significant quantity of material within the SCBB. As a resolution to this problem, each of the components could be infiltrated individually in an alternating pattern. This would enable higher concentrations of each to be used, and it is likely that upon infiltration the chitosan solution would encapsulate the deposited calcium phosphate crystals to form a composite material.

- In following the suggested mode of alternating chitosan and calcium phosphate infiltrations, it may also be possible to form a molecularly layered form of chitosan and calcium phosphate. When protonated (in solution) chitosan is a positively charged molecule, whereas the phosphate ion is negatively charged ranging from -3 to -1. Alternate infiltrations with a chitosan solution and a calcium phosphate solution of the appropriate anionic species, perhaps with washing steps between, may enable a molecularly layered composite to be formed. If successful, this approach would be predicted to have greater success in more comprehensively filling the microporous voids in the SCBB. However, this approach would very likely require many, many iterations of infiltration. Combinations of layers of chitosan, calcium phosphate and genipin could also be trialled.

- The potential of PCL was not explored to its full potential in this research. PCL is a thermoplastic and early attempts were made to utilise this property by melting the material and forcing it into the SCBB material. Unfortunately, PCL at and slightly above its melting temperature is highly viscous, which in combination with the lack of appropriate apparatuses in a chemistry laboratory for forcing a hot viscous liquid into a porous material, made attempts at infiltration fraught with difficulty, dangerous and ultimately unsuccessful. PCL is routinely injection moulded by heating the material and forcing it into a mould to give specific shapes. There appears no reason why PCL could not be heated and injected into the porous SCBB material. It is possible that the force of the viscous liquid could crush the SCBB matrix, which could be countered by thinning the PCL with a solvent such as THF. In fact, thinning with a volatile solvent would be preferable, because after infiltration the solvent would evaporate causing the PCL to shrink back, effectively opening up the macroporous structure of the SCBB.

8.3 Publications

- Patent – "A Medical Preparation"
    - Abstract: A bone matrix, including: a bone matrix material, which has had organic material removed, and a replacement material that has replaced the organic material, the bone matrix characterised in that the bone matrix is formed from a single piece of bone.
    - Inventors
        - D. F. Laird
        - M. R. Mucalo
        - G. Dias
    - Pub. No.: WO/2008/069686
    - International Application No.: PCT/NZ2007/000354
    - Publication Date: 12.06.2008

- International Filing Date: 06.12.2007
- Chapter 2 Demand Filed: 12.06.2008

- Annual Conference of the Australasian Society for Biomaterials and Tissue Engineering (ASBTE) , 2007, Melbourne, Australia; “Reinforced Sintered Cancellous Bovine Bone as a Potential Bone Implant Material”, D. F. Laird, M. R. Mucalo and G. Dias. (Oral presentation).

- NZBio Conference, 22-24 March, 2007, Auckland, New Zealand, “Reinforced Sintered Cancellous Bovine Bone as a Potential Implant Material”, D. F. Laird, M. R. Mucalo and G. Dias, (Poster Presentation – third prize).

- Schrock Symposium, April, 2008, Auckland, New Zealand, “Novel Bone Replacement Material from Reinforced Sintered Bovine Bone.” D. F. Laird, M. R. Mucalo and G. Dias, (oral presentation)

References

1. Georgiade, N., et al., *The use of particulate hydroxyapatite and plaster of Paris in aesthetic and reconstructive surgery.* Aesthetic Plastic Surgery, 1993. **17**(2): p. 85-92.
2. Bloemers, F.W., et al., *Autologous bone versus calcium-phosphate ceramics in treatment of experimental bone defects.* Journal of Biomedical Materials Research Part B: Applied Biomaterials, 2003. **66B**(2): p. 526-531.
3. Hing, K.A., *Bioceramic Bone Graft Substitutes: Influence of Porosity and Chemistry.* International Journal of Applied Ceramic Technology, 2005. **2**(3): p. 184-199.
4. Tuominen, T., et al., *Bovine bone implant with bovine bone morphogenetic protein in healing a canine ulmar defect.* International Orthopaedics, 2001.
5. Yao, C.-H., et al., *Calvarial bone response to a tricalcium phosphate-genipin crosslinked gelatin composite.* Biomaterials, 2005. **26**(16): p. 3065-3074.
6. Trentz, O.A., et al., *Osteroblasts response to allogenic and xenogenic solvent dehydrated cancellous bone in vitro.* Biomaterials, 2003. **24**(20): p. 3417-3426.
7. Pinchuk, N.D. and L.A. Ivanchenko, *Making Calcium Phosphate Biomaterials.* Powder Metallurgy and Metal Ceramics, 2003. **42**(7): p. 357-371.
8. Hench, L.L. and J. Wilson, *An Introduction to Bioceramics*, in *An Introduction to Biocermics*, L.L. Hench and J. Wilson, Editors. 1993, World Scientific: Singapore.
9. Taniguchi, Y., et al., *Sintered Bone Implantation for the Treatment of Benign Bone Tumours in the Hand.* J Hand Surg [Br], 1999. **24**(1): p. 109-112.
10. Doi, Y., et al., *Sintered carbonate apatites as bioresorbable bone substitutes.* Journal of Biomedical Materials Research, 1998. **39**(4): p. 603-610.
11. Joschek, S., et al., *Chemical and physicochemical characterization of porous hydroxyapatite ceramics made of natural bone.* Biomaterials, 2000. **21**(16): p. 1645-1658.
12. Barralet, J., et al., *Thermal decomposition of synthesised carbonate hydroxyapatite.* Journal of Materials Science: Materials in Medicine, 2002. **13**: p. 529-533.
13. Foster, D.L., *Studies on Calcium Phosphates Derived from New Zealand Animal Bone*, in *Chemistry*. 2001, University of Waikato: Hamilton. p. 250.
14. Albrektsson, et al., *Osteoinduction, osteoconduction and osseointegration.* European Spine Journal, 2001. **10**(0): p. S96-S101.
15. Matsumoto, T., et al., *Effects of sintered bovine bone on cell proliferation, collagen synthesis, and osteoblastic expression in MC3T3-E1 osteoblast-like cells.* Journal of Orthopaedic Research, 1999. **17**(4): p. 586-592.
16. Minamide, A., et al., *The use of sintered bone in spinal surgery.* European Spine Journal, 2001. **10**: p. S185-S188.
17. Johnson, G.S., *Characterisation and Processing of Biological Hydroxyapatite*, in *Chemistry*. 1998, University of Waikato: Hamilton.

18. Mucalo, M.R., et al., *The novel use of waste animal bone from New Zealand agricultural sources as a feedstock for forming plasma sprayed hyroxyapatite coatings on biomedical implant materials.* Journal of Applied Biomaterials & Biomechanics, 2004. **2**: p. 96-104.
19. Johnson, G.S., M.R. Mucalo, and M.A. Lorier, *The processing and characterization of animal-derived bone to yield materials with biomedical applications. Part I: Modifiable porous implants from bovine condyle cancellous bone and characterization of bone materials as a function of processing`*. Journal of Materials Science: Materials in Medicine, 2000. **11**: p. 427-441.
20. Johnson, G.S., et al., *The processing and characterization of animal-derived bone to yield materials with biomedical applications. Part II: milled bone powders, reprecipitated hydroxyapatite and the potential used of these materials.* Journal of Materials Science: Materials in Medicine, 2000. **11**: p. 725-741.
21. Martini, F.H., *Fundamentals of Anatomy & Physiology*. 2001, New Jersey: Prentice Hall.
22. Salma, B., *Xenogeneic Bone Grafting in Humans.* Clinical Orthopaedics, 1983. **174**: p. 113-121.
23. Worth, A., et al., *The evaluation of processed cancellous bovine bone as a bone graft substitute.* Clinical Oral Implant Research, 2005. **16**: p. 379-386.
24. Worth, A.J., et al., *Combined xeno/auto-grafting of a benign osteolytic lesion in a dog, using a novel bovine cancellous bone biomaterial.* New Zealand Veterinary Journal, 2007. **55**(3): p. 143-148.
25. Ma, J., R. Wollmann, and S. Lindquist, *Neurotoxicity and Neurodegeneration When PrP Accumulates in the Cytosol.* Science, 2002. **298**(5599): p. 1781-1785.
26. Casolari, A., *Heat resistance of prions and food processing.* Food Microbiology, 1998. **15**(1): p. 59-63.
27. Thomas Raul Appel, D.R.F.v.R.M.H., *Safety of oleochemical products derived from beef tallow or bone fat regarding prions.* European Journal of Lipid Science and Technology, 2001. **103**(11): p. 713-721.
28. Brown, P., et al., *New Studies on the Heat Resistance of Hamster-Adapted Scrapie Agent: Threshold Survival after Ashing at 600 degrees C Suggests an Inorganic Template of Replication.* Proceedings of the National Academy of Sciences of the United States of America, 2000. **97**(7): p. 3418-3421.
29. Sutter, B., et al., *Bovine Dowels for Anterior Cervical Fusion: Experience in 66 Patients with a Note on Postoperative CT and MRI Appearance.* Acta Neurochir (Wien), 1995. **137**: p. 192-198.
30. Guo, X.E., *Mechanical Properties of Cortical Bone and Cancellous Bone Tissue*, in *Bone Mechanics Handbook*, S.C. Cowin, Editor. 2001, CRC Press: Boca Raton.
31. Jee, W.S.S., *Integrated Bone Tissue Physiology: Anatomy and Physiology*, in *Bone Mechanics Handbook*, S.C. Cowin, Editor. 2001, CRC Press: Boca Raton.
32. Rey, C., et al., *Hydroxyl groups in bone mineral.* Bone, 1995. **16**(5): p. 583-6.

33. Arends, J. and W.L. Jongebloed, *Apatite single crystals. Formation, dissolution and influence of CO_3^{2-} ions.* Journal of the Royal Netherlands Chemical Society, 1981. **100**(1): p. 3-9.
34. Liao, S., et al., *The preparation and characteristics of a carbonated hydroxyapatite/collagen composite at room temperature.* Journal of Biomedical Materials Research Part B: Applied Biomaterials, 2005. **74B**(2): p. 817-821.
35. Meneghini, C., et al., *Rietveld Refinement on X-Ray Diffraction Patterns of Bioapatite in Human Fetal Bones.* Biophys. J., 2003. **84**(3): p. 2021-2029.
36. Judex, S., et al., *Combining High-resolution Micro-computed Tomography with Material Composition to Define the Quality of Bone Tissue.* Current Osteoporosis Rerports, 2003. **1**: p. 11-19.
37. Keaveny, T.M., et al., *Application of the Tsai--Wu Quadratic Multiaxial Failure Criterion to Bovine Trabecular Bone.* Journal of Biomechanical Engineering, 1999. **121**(1): p. 99-107.
38. Saxena, R. and T.S. Keller, *Computer Modeling for Evaluating Trabecular Bone Mechanics,* in *Mechanical Testing of Bone and the Bone-Implant Interface*, Y.H. An and R.A. Draughn, Editors. 2000, CRC Press: Boca Raton. p. 407-435.
39. Rapillard, L., M. Charlebois, and P.K. Zysset, *Compressive fatigue behavior of human vertebral trabecular bone.* Journal of Biomechanics, 2006. **39**(11): p. 2133-2139.
40. Keller, T.S. and M.A.K. Liebschner, *Tensile and Compression Testing of Bone,* in *Mechanical Testing of Bone and the Bone-Implant Interface*, H.A. Yuehuei and R.A. Draughn, Editors. 2000, CRC Press. p. 175-205.
41. Keaveny, T.M., et al., *Biomechanics of trabecular bone.* Annual review of biomedical engineering, 2001. **3**: p. 307-333.
42. Elliot, J.C., *Structure and Chemistry of the Apatites and Other Calcium Orthophosphates"*. 1994, Amsterdam: Elsevier.
43. Zahn, D., *Mechanisms of Calcium and Phosphate Ion Association in Aqueous Solution.* Zeitschrift für anorganische und allgemeine Chemie, 2004. **630**(10): p. 1507-1511.
44. Hashizume, H., et al., *Changes in the extracellular matrix on the surface of sintered bovine bone implanted in the femur of a rabbit: An immunohistochemical study* Journal of Orthopaedic Science, 1998. **3**(1): p. 42-53.
45. Akazawa, T., et al., *Osteoinduction by Functionally Graded Apatites of Bovine Origin Loaded with Bone Morphogenetic Protein-2.* Journal of the American Ceramic Society, 2005. **88**(12): p. 3545-3548.
46. Kawakami, T., et al., *Regenerative Medicine of Bone and Teeth - with special references to biological principles, problems and their indicators.* Journal of Hard Tissue Biology, 2007. **16**(3): p. 95-113.
47. Bignon, A., et al., *Effect of micro- and macroporosity of bone substitutes on their mechanical properties and cellular response.* Journal of Materials Science: Materials in Medicine, 2003. **14**(12): p. 1089-1097.

48. Taniguchi, Y., et al., *Sintered bone implantation for the treatment of benign bone tumours in the hand.* The Journal of Hand Surgery: Journal of the British Society for Surgery of the Hand, 1999. **24**(1): p. 109-112.
49. Basle, M.F., et al., *Cellular reponse to calcium phosphate ceramics implanted in rabbit bone.* Journal of Materials Science: Materials in Medicine, 1993. **4**: p. 273-280.
50. Artzi, Z., et al., *Biomaterial Resorption Rate and Healing Site Morphology of Inorganic Bovine Bone and -Tricalcium Phosphate in the Canine: A 24-month Longitudinal Histologic Study and Morphometric Analysis*
The International Journal of Oral & Maxillofacial Implants, 2004. **19**(3): p. 357-368.
51. Rumpel, E., et al., *The biodegradation of hydroxyapatite bone graft substitutes in vivo.* Folia Morphologica, 2006. **65**(1): p. 43-48.
52. Anderson, J.M., *Inflammation, Wound Healing, and the Foreign-Body Response*, in *Biomaterials Science*, B.D. Ratner, et al., Editors. 2004, Elsevier Academic Press: Amsterdam.
53. Park, J.B. and Y.K. Kim, *Metallic Biomaterials*, in *Biomaterials: Principles and Applications*, J.B. Park and J.D. Bronzino, Editors. 2003, CRC Press: Boca Raton. p. 1-20.
54. Long, et al., *Titanium alloys in total joint replacement : a materials science perspective*. Vol. 19. 1998, Oxford, ROYAUME-UNI: Elsevier.
55. Breme, J. and V. Biehl, *Metallic Biomaterials*, in *Handbook of Biomaterials Properties*, J. Black and G. Hastings, Editors. 1998, Chapman & Hall: London.
56. Lee, H.B., G. Khang, and J.H. Lee, *Polymeric Biomaterials*, in *Biomaterials: Principles and Applications*, J.B. Park and J.D. Bronzino, Editors. 2003, CRC Press: Boca Raton. p. 55-77.
57. Silver, F.H. and D.L. Christiansen, *Biomaterials Science and Biocompatibility*. 1999, New York: Springer.
58. Hu, Y., et al., *Development of a porous poly(L-lactic acid)/hydroxyapatite/collagen scaffold as a BMP delivery system and its used in healing canine segmental bone defect.* Journal of Biomedical Materials Research Part A, 2003. **67A**(2): p. 591-598.
59. Higashi, S., et al., *Polymer-hydroxyapatite composites for biodegradable bone fillers.* Biomaterials, 1986. **7**: p. 183-187.
60. Lee, J.H., et al., *Interaction of Different Types of Cells on Polymer Surfaces with Wettability Gradient.* Journal of Colloid and Interface Science, 1998. **205**(2): p. 323-330.
61. Li, J. and G.W. Hastings, *Oxide bioceramics: inert ceramic materials in medicine and dentistry*, in *Handbook of Biomaterial Properties* J. Black and G. Hastings, Editors. 1998, Chapman & Hall: London.
62. Oonishi, H. and K. Oomaniuda, *Degradation/resorption in bioactive ceramics in orthopaedics*, in *Handbook of Biomaterial Properties*, J. Black and G. Hastings, Editors. 1998, Chapman & Hall: London.
63. Wu, C.-S., *A comparison of the structure, thermal properties, and biodegradability of polycaprolactone/chitosan and acrylic acid grafted polycaprolactone/chitosan.* Polymer, 2005. **46**(1): p. 147-155.

64. Pitt, C.G., *Poly(ε-caprolactone) and its copolymers*, in *Biodegradable polymers as drug delivery systems*, M. Chasin and R. Langer, Editors. 1990, Dekker: New York. p. 77-119.
65. Gardyne, S.J., *Use of Poy(ε-caprolactone) as a Platform for the Delivery of Bioactive Compounds via the Vaginal Mucosa of Cattle.*, in *Chemistry*. 2005, University of Waikato: Hamilton. p. 0-160.
66. Kai, W., et al., *Thermal and mechanical properties of a poly(epsi-caprolactone)/graphite oxide composite.* Journal of Applied Polymer Science, 2008. **107**(3): p. 1395-1400.
67. Calandrelli, L., et al., *Natural and Synthetic Hydroxyapatite Filled PCL: Mechanical Properties and Biocompatibility Analysis.* Journal of Bioactive and Compatible Polymers, 2004. **19**(4): p. 301-313.
68. Goldberg, D., *A review of the biodegradability and utility of poly(caprolactone).* Journal of Environmental Polymer Degradation, 1995. **3**(2): p. 61-67.
69. Sun, H., et al., *The in vivo degradation, absorption and excretion of PCL-based implant.* Biomaterials, 2006. **27**(9): p. 1735-1740.
70. Chen, D.R., J.Z. Bei, and S.G. Wang, *Polycaprolactone microparticles and their biodegradation.* Polymer Degradation and Stability, 2000. **67**: p. 455-459.
71. Galed, G., et al., *N-Deacetylation and depolymerization reactions of chitin/chitosan: Influence of the source of chitin.* Carbohydrate Polymers, 2005. **62**(4): p. 316-320.
72. Shepherd, R., S. Reader, and A. Falshaw, *Chitosan functional properties.* Glycoconjugate Journal, 1997. **14**: p. 535-542.
73. Ravi Kumar, M.N.V., *A review of chitin and chitosan applications.* Reactive and Functional Polymers, 2000. **46**(1): p. 1-27.
74. Harish Prashanth, K.V. and R.N. Tharanathan, *Chitin/chitosan: modifications and their unlimited application potential--an overview.* Trends in Food Science & Technology, 2007. **18**(3): p. 117-131.
75. Baxter, A., et al., *Improved method for i.r. determination of the degree of N-acetylation of chitosan.* International Journal of Biological Macromolecules, 1992. **14**(3): p. 166-169.
76. Brugnerotto, J., et al., *An infrared investigation in relation with chitin and chitosan characterization.* Polymer, 2001. **42**(8): p. 3569-3580.
77. Sabnis, S. and L.H. Block, *Improved infrared spectroscopic method for the analysis of degree of N-deacetylation of chitosan.* Polymer bulletin, 1997. **39**(1): p. 67-71.
78. Schatz, C., et al., *Typical Physicochemical Behaviors of Chitosan in Aqueous Solution.* Biomacromolecules, 2003. **4**(3): p. 641-648.
79. Cheng, M., et al., *Study on physical properties and nerve cell affinity of composite films from chitosan and gelatin solutions.* Biomaterials, 2003. **24**(17): p. 2871-2880.
80. Zhang, Y., et al., *Calcium Phosphate-Chitosan Composite Scaffolds for Bone Tissue Engineering.* Tissue Engineering, 2003. **9**(2): p. 337-345.

81. Mi, F.-L., et al., *In vitro evaluation of a chitosan membrane cross-linked with genipin.* Journal of Biomaterials Science -- Polymer Edition, 2001. **12**(8): p. 835-850.
82. Keaveny, T.M., *Strength of Trabecular Bone*, in *Bone Mechanics Handbook*, S.C. Cowin, Editor. 2001, CRC Press: Boca Raton.
83. Hua, Y., et al. *Natural hydroxyapatite/chitosan composite for bone substitute materials*. in *Engineering in Medicine and Biology 27th Annual Conference*. 2005. Shanghai, China.
84. Ito, M., *In vitro properties of a chitosan-bonded hydroxyapatite bone-filling paste.* Biomaterials, 1991. **12**: p. 41-45.
85. Manjubala, I., et al., *Biomimetic mineral-organic composite scaffolds with controlled internal architecture.* Journal of Materials Science: Materials in Medicine, 2005. **16**: p. 111-119.
86. Khor, E. and L.Y. Lim, *Implantable applications of chitin and chitosan.* Biomaterials, 2003. **24**: p. 2339-2349.
87. Morimoto, M., H. Saimoto, and Y. Shigemasa, *Control of Functions of Chitin and Chitosan by Chemical Modification.* Trends in Glycoscience and Glycotechnology, 2002. **14**(78): p. 205-222.
88. Berger, J., et al., *Structure and interactions in covalently and ionically crosslinked chitosan hydrogels for biomedical applications.* European Journal of Pharmaceutics and Biopharmaceutics, 2004. **57**: p. 19-34.
89. Mi, F.-L., et al., *Synthesis and characterization of biodegradable TPP/genipin co-crosslinked chitosan gel beads.* Polymer, 2003. **44**(21): p. 6521-6530.
90. Ito, M., et al., *Effect of hydroxyapatite content on physical properties and connective tissue reactions to a chitosan-hydroxyapatite composite membrane.* Journal of Biomedical Materials Research, 1999. **45**(3): p. 204-208.
91. Matsuda, A., et al., *Preparation and mechanical property of core-shell type chitosan/calcium phosphate composite fiber.* Materials Science and Engineering: C, 2004. **24**(6-8): p. 723-728.
92. Hu, Q., et al., *Preparation and characterization of biodegradable chitosan/hydroxyapatite nanocomposite rods via in situ hybridization: a potential material as internal fixation of bone fracture.* Biomaterials, 2004. **25**(5): p. 779-785.
93. Ding, S.-J., *Biodegradation behavior of chitosan/calcium phosphate composites.* Journal of Non-Crystalline Solids, 2007. **353**(24-25): p. 2367-2373.
94. Mi, C.F.-L., S.-S. Shyu, and C.-K. Peng, *Characterization of ring-opening polymerization of genipin and pH-dependent cross-linking reactions between chitosan and genipin.* Journal of Polymer Science Part A: Polymer Chemistry, 2005. **43**(10): p. 1985-2000.
95. Ramos, R., V. Carvalho, and M. Gama, *Novel hydrogel obtained by chitosan and dextrin-VA co-polymerization.* Biotechnology Letters, 2006. **28**(16): p. 1279-1284.
96. Choudhari, S.K., et al., *Development of novel blocked diisocyanate crosslinked chitosan membranes for pervaporation separation of water-*

isopropanol mixtures. Journal of Membrane Science, 2007. **302**(1-2): p. 197-206.
97. Mi, F.-L., H.-W. Sung, and S.-S. Shyu, *Synthesis and characterization of a novel chitosan-based network prepared using naturally occurring crosslinker.* Journal of Polymer Science Part A: Polymer Chemistry, 2000. **38**(15): p. 2804-2814.
98. Koo, H.-J., et al., *Antiinflammatory effects of genipin, an active principle of gardenia.* European journal of pharmacology 2004. **495**(2-3): p. 201-208.
99. Mi, F.L., et al., *In vivo biocompatibility and degradability of a novel injectable-chitosan-based implant.* Biomaterials, 2002. **23**: p. 181-191.
100. Yin, Y., et al., *Preparation and characterization of macroporous chitosan-gelatin/?-tricalcium phosphate composite scaffolds for bone tissue engineering.* Journal of Biomedical Materials Research Part A, 2003. **67A**(3): p. 844-855.
101. Kim, C.H., et al., *Improvement of the Biocompatibility of Chitosan Dermal Scaffold by Rigorous Dry Heat Treatment.* Macromolecular Research, 2004. **12**(4): p. 367-373.
102. VandeVord, P.J., et al., *Evaluation of the biocompatibility of a chitosan scaffold in mice.* Journal of Biomedical Materials Research, 2002. **59**(3): p. 585-590.
103. Chung, T.-W., et al., *Growth of human endothelial cells on photochemically grafted Gly-Arg-Gly-Asp (GRGD) chitosans.* Biomaterials, 2002. **23**: p. 4803-4809.
104. Sarasam, A. and S.V. Madihally, *Characterization of chitosan-polycaprolactone blends for tissue engineering applications.* Biomaterials, 2005. **26**: p. 5500-5508.
105. Howling, G.I., et al., *The effect of chitin and chitosan on the proliferation of human skin fibroblasts and keratinocytes in vitro.* Biomaterials, 2001. **22**: p. 2959-2966.
106. Rao, S.B. and C.P. Sharma, *Use of chitosan as a biomaterial: Studies on its safety and hemostatic potential.* Journal of Biomedical Materials Research, 1997. **34**(1): p. 21-28.
107. Muzzarelli, R.A.A., *Human enzymatic activities related to the therapeutic administration of chitin derivatives.* Cellular and Molecular Life Sciences (CMLS), 1997. **53**(2): p. 131-140.
108. Francis Suh, J.K. and H.W.T. Matthew, *Application of chitosan-based polysaccharide biomaterials in cartilage tissue engineering: a review.* Biomaterials, 2000. **21**(24): p. 2589-2598.
109. Jiang, T., C.M. Pilane, and C.T. Laurencin. *Fabrication of Novel Porous Chitosan Matrices as Scaffolds for Bone Tissue Engineering*. in *Materials Research Society Symposium Procedings Volume 845*. 2005.
110. Dorozhkin, S., *Calcium Orthophosphates in Nature, Biology and Medicine.* Materials, 2009. **2**(2): p. 399-498.
111. van Ruijven, L.J., et al., *The effect of bone loss on rod-like and plate-like trabeculae in the cancellous bone of the mandibular condyle.* Bone, 2005. **36**(6): p. 1078-1085.

112. Gao, Y., et al., *Characterization and osteoblast-like cell compatibility of porous scaffolds: bovine hydroxyapatite and novel hydroxyapatite artificial bone.* Journal of Materials Science: Materials in Medicine, 2006. **17**(9): p. 815-823.
113. Rhee, S.-H., et al., *Effect of Heat-Treatment Temperature on the Osteoconductivity of the Apatite Derived from Bovine Bone.* Key Engineering Materials, 2006. **309-311**: p. 41-44.
114. Herliansyah, M.K., et al., *Preparation and Characterization of Natural Hydroxyapatite: A Comparative Study of Bovine Bone Hydroxyapatite and Hydroxyapatite from Calcite.* Materials Science Forum, 2007. **561-565**: p. 1441-1444.
115. Rodrigues, C.V.M., et al., *Characterization of a bovine collagen-hydroxyapatite composite scaffold for bone tissue engineering.* Biomaterials, 2003. **24**(27): p. 4987-4997.
116. Silverstein, R.M. and F.X. Webster, *Spectrometric Identification of Organic Compounds*. Sixth Edition ed. 1998: John Wiley & Sons Inc. 482.
117. Gallagher, W., *FTIR Analysis of Protein Structure*. 2005.
118. Rey, C., et al., *Resolution-enhanced Fourier transform infrared spectoscopy study of the environment of phosphate ion in the early deposits of a solid phase of calcium phosphate in bone and enamel and their evolution with age: 2. Investigations in the ϖ3 PO_4 Domain.* Calcified Tissue International, 1991. **49**: p. 383-388.
119. Hsu, C.-P.S., *Infrared Spectroscopy*, in *Handbook of Instrumental Techniques for Analytical Chemistry*, F. Settle, Editor. 1997, Prentice-Hall: London.
120. Rey, C., et al., *The carbonate environment in bone mineral: a resolution-enhanced fourier transform infrared spectroscopy study.* Calcified Tissue International, 1989. **45**: p. 157-164.
121. Kanno, T., et al., *Adsorption properties of acidic and basic proteins on the surface of carbonate-containing hydroxyapatite.* Phosphorus Research Bulletin, 2007. **21**: p. 25-30.
122. Xu, G., I.A. Aksay, and J.T. Groves, *Continuous Crystalline Carbonate Apatite Thin Films. A Biomimetic Approach.* Journal of the American Chemical Society, 2001. **123**: p. 2196-2203.
123. Shi, J., et al., *Thermal behavior of dental enamel and geologic apatite: An infrared spectroscopic study.* American Mineralogist, 2003. **88**: p. 1866-1871.
124. *CRC Handbook of Chemistry and Physics*. 80th ed, ed. D.R. Lide. 2000, Boca raton: CRC Press.
125. Butler, M.F., Y.-F. Ng, and P.D.A. Pudney, *Mechanism and kinetics of the crosslinking reaction between biopolymers containing primary amine groups and genipin.* Journal of Polymer Science Part A: Polymer Chemistry, 2003. **41**(24): p. 3941-3953.
126. Qaqish, R.B. and M.M. Amiji, *Synthesis of a fluorescent chitosan derivative and its application for the study of chitosan-mucin interactions.* Carbohydrate Polymers, 1999. **38**(2): p. 99-107.
127. Elovaara, E., P. Pfäffli, and H. Savolainen, *Burden and Biochemical Effects of Extended Tetrahydrofuran Vapour Inhalation of Three Concentration Levels.* Acta pharmacologica et tocicologica, 1984. **54**: p. 221-226.

128. Lin-Vien, D., et al., *The Handbook of Infrared and Raman Characteristic Frequencies of Organic Molecules*. 1991, Boston: Academic Press Inc.
129. Pedroni, V.I., et al., *Chitosan structure in aqueous solution.* Colloid & Polymer Science, 2003. **282**(1): p. 100-102.
130. Lamarque, G., et al., *Physicochemical Behavior of Homogeneous Series of Acetylated Chitosans in Aqueous Solution: Role of Various Structural Parameters.* Biomacromolecules, 2005. **6**(1): p. 131-142.
131. Chang, R., *Chemistry*. 5th ed. 1994, New York: McGraw - Hill Inc.
132. Rahimpour, M.R., *A non-ideal rate-based model for industrial urea thermal hydrolyser.* Chemical Engineering and Processing, 2004. **43**(10): p. 1299-1307.
133. González-Marcos, M.P., et al., *Effect of thermal treatments on surface chemical distribution and catalyst activity in nickel on silica systems.* Journal of Molecular Catalysis A: Chemical, 1997. **120**(1-3): p. 185-196.
134. AI-Mayouf, A.M. and A.O. McDougall, *Factors Affecting Diffusion Coefficient of the Hydroxide Ion.* Journal of King Saud University, 1994. **6**(2): p. 305-315.
135. Tuckerman, M.E., D. Marx, and M. Parrinello, *The nature and transport mechanism of hydrated hydroxide ions in aqueous solution.* Nature, 2002. **417**(6892): p. 925-929.
136. Fernandes, R., et al., *Electrochemically Induced Deposition of a Polysaccharide Hydrogel onto a Patterned Surface.* Langmuir, 2003. **19**: p. 4058-4062.
137. Kobayashi, T., S. Nakamura, and K. Yamashita, *Enhanced osteobonding by negative surface charges of electrically polarized hydroxyapatite.* Journal of Biomedical Materials Research, 2001. **57**(4): p. 477-484.
138. Nagai, M., et al., *Electrical conductivity of calcium phosphate ceramics with various Ca/P ratios.* Journal of Materials Science, 1991. **26**: p. 2949-2953.
139. Nakamoto, K., *Infrared and Raman Spectra of Inorganic and Coordination Compounds*. Fourth Edition ed. 1986, New York: John Wiley & Sons.
140. Osman, Z. and A.K. Arof, *FTIR studies of chitosan acetate based polymer electrolytes.* Electrochimica Acta, 2003. **48**(8): p. 993-999.
141. Magnin, D. and S. Dumitriu, *Interactions between polysaccharides and polypeptides*, in *Polysaccharides: Structural Diversity and Functional Versatility*, S. Dumitriu, Editor. 2004, CRC Press.
142. Yi, H., et al., *Biofabrication with Chitosan.* Biomacromolecules, 2005. **6**(6): p. 2881-2894.
143. Payne, G.F. and S.R. Raghavan, *Chitosan: a soft interconnect for hierarchical assembly of nano-scale components.* Soft Matter, 2007. **3**(5): p. 521-527.
144. Pop, V., A. Kriza, and M. Ilis, *Synthesis and stability studies in physiological-like conditions of two urea complexes of copper (II) and manganese (II).*
145. Gorin, G., C. Chin, and S. Wang, *Dissociation of urease in acetate buffer of pH 3.5 with retention of the enzymatic activity.* Cellular and Molecular Life Sciences (CMLS), 1968. **24**(7): p. 685-687.
146. Howell, S.F. and J.B. Sumner, *The Specific Effects of Buffers upon Urease Activity.* J. Biol. Chem., 1934. **104**(3): p. 619-626.
147. Daily Med, *Current Medication Information* 2006, Daily Med.

148. Lockwood, A.H., et al., *The dynamics of ammonia metabolism in man. Effects of liver disease and hyperammonemia.* The Journal of Clinical Investigation, 1979. **63**(3): p. 449-460.
149. Schneider, M., I.W. Marison, and U. von Stockar, *The importance of ammonia in mammalian cell culture.* Journal of Biotechnology, 1996. **46**(3): p. 161-185.
150. Askeland, D.R., *The Science and Engineering of Materials*. 1996, London: Chapman & Hall.
151. Speirs, A.D., et al., *Calcium phosphate cement composites in revision hip arthroplasty.* Biomaterials, 2005. **26**: p. 7310-7318.
152. An, Y.H., W.R. Barfield, and R.A. Draughn, *Basic Concepts of Mechanical Property Measurement and Bone Biomechanics*, in *Mechanical Testing of Bone and the Bone-Implant Interface*, H.A. Yuehuei and R.A. Draughn, Editors. 2000, CRC Press: Boca Raton.
153. Carter, D.R. and W.C. Hayes, *The compressive behavior of bone as a two-phase porous structure.* J Bone Joint Surg Am, 1977. **59**(7): p. 954-962.
154. Keller, T.S., *Predicting the compressive mechanical behavior of bone.* Journal of Biomechanics, 1994. **27**(9): p. 1159-1168.
155. Higgins, R.A., *Properties of Engineering Materials*. 2nd ed. 1994, London: Edward Arnold.
156. Hanks, C.T., J.C. Wataha, and Z. Sun, *In vitro models of biocompatibility: A review.* Dental Materials, 1996. **12**(3): p. 186-193.
157. Kirkpatrick, C.J., et al., *Review Paper:current Trends in Biocompatibility Testing.* Proceedings of the Institution of Mechanical Engineers -- Part H -- Journal of Engineering in Medicine, 1998. **212**(2): p. 75-84.
158. Wallin, R.F. and E.F. Arscott, *A Practical Guide to ISO 10993-5: Cytotoxicity.* MDDI, 1998. **20**: p. 96-98.
159. SafePham, L., *Tissue culture cytotoxicity test using L929 cells -direct contact method*.
160. ISO, *Biological evaluation of medical devices-Part 5: Tests for in vitro cytotoxicity*. 1999.
161. Barbosa, S.V., C.M.S. Barroso, and P.A. Ruiz, *Cytotoxicity of endodontic irrigants containing calcium hydroxide and sodium lauryl sulphate on fibroblasts derived from mouse L929 cell line.* Brazilian Dental Journal, 2009. **20**: p. 118-121.
162. Park, S.-B., et al., *A novel pH-sensitive membrane from chitosan -- TEOS IPN; preparation and its drug permeation characteristics.* Biomaterials, 2001. **22**(4): p. 323-330.
163. Rashidova, S.S., et al., *Bionanocompositional chitosan-silica sorbent for liquid chromatography.* Journal of Chromatography B, 2004. **800**(1-2): p. 49-53.
164. Al-Sagheer, F. and S. Muslim, *Thermal and mechanical properties of chitosan / SiO_2 hybrid composites.* Journal of Nanomaterials, 2010. **2010**.
165. Luepke, N.P., *Hen's egg chorioallantoic membrane test for irritation potential.* Food and Chemical Toxicology, 1985. **23**(2): p. 287-291.

166. Schlage, W.K., H. Bulles, and B. Kurkowsky, *Use of the HET-CAM Test for the Determination of the Irritant Potential of Cigarette Sidestream Smoke.* Toxicology in Vitro, 1999. **13**: p. 829-835.
167. NICEATM-ICCVAM. *In Vitro Test Methods for Detecting Ocular Corrosives and Severe Irritants - Background Review Document for Hen's Egg Test - Chorioallantoic Membrane (HET-CAM) Test*. 2006 [cited 2009; Available from: http://iccvam.niehs.nih.gov/methods/ocutox/ivocutox/ocu_brd_hetcam.htm.
168. Valdes, T.I., D. Kreutzer, and F. Moussy, *The chick chorioallantoic membrane as a novel <I>in vivo</I> model for the testing of biomaterials.* Journal of Biomedical Materials Research, 2002. **62**(2): p. 273-282.
169. Kurtz, J., et al., *Gender differences and individual variation in the immune system of the scorpionfly Panorpa vulgaris (Insecta: Mecoptera).* Developmental & Comparative Immunology, 2000. **24**(1): p. 1-12.
170. Hayama, M., et al., *Optimum dialysis membrane for endotoxin blocking.* Journal of Membrane Science, 2003. **219**(1-2): p. 15-25.
171. Mchedlov-Perossyan, N.O., et al., *Acid-base Behavior of Flourescein Isothiocyannate in Aqueous Media and in Micellar Surfactant Solutions.* CPS.
172. Ajioka, M., et al., *The basic properties of poly(lactic acid) produced by the direct condensation polymerization of lactic acid.* Journal of Polymers and the Environment, 1995. **V3**(4): p. 225-234.
173. Otake, K., et al., *One-Step Preparation of Chitosan-Coated Cationic Liposomes by an Improved Supercritical Reverse-Phase Evaporation Method.* Langmuir, 2006. **22**(9): p. 4054-4059.
174. King, M.B., et al., *The Mutual Solubilities of Water with Supercritical and Liquid Carbon Dioxide.* Journal of Supercritical Fluids, 1992. **5**(4): p. 296
175. Tassaing, T., et al. *Water-carbon dioxide mixtures at high temperatures and pressures as studied by infrared and Raman spectroscopies*. in *14th International Conference of the Properties of Water and Steam in Kyoto*. 2004. Japan.

Appendix A – Molar solubility of $Ca(OH)_2$

	$K_{sp}\ Ca(OH)_2$	=	$5.02 \times 10^{-6}\ mol^3\ L^{-3}$
	$[Ca^{2+}][OH^-]^2$	=	$5.02 \times 10^{-6}\ mol^3\ L^{-3}$
	let s	=	$[Ca^{2+}]$
	$\therefore$ K_{sp}	=	$4s^3$
	s	=	$1.08 \times 10^{-2}\ mol\ L^{-1}$
$\therefore$	molar solubity $Ca(OH)_2$	=	$3 \times (1.08 \times 10^{-2}\ mol\ L^{-1})$
		=	$3.24 \times 10^{-2}\ mol\ L^{-1}$

Note: This is an estimate because a pH electrode responds to the activity of H^+ in solution, which varies in its relationship to the concentration of H^+ according to the ionic strength of the solution.

Appendix B – Concentration of HCl and urea in chitosan solutions

The following is an example of the preparation of a chitosan solution with urea:

- 0.5080 g of Fluka low viscosity chitosan was sprinkled into 50 mL rapidly stirred distilled water
- 0.2926 g of concentrated $HCl_{(aq)}$ was added dropwise to dissolve the chitosan to give a solution at pH 2.45.

○	density $HCl_{(conc.)}$)	=	$1.179\ g\ mL^{-1}$ [124]
○	$\therefore$ $V(HCl_{(conc.)})$	=	$0.2926\ g / 1.179\ g\ mL^{-1}$
		=	0.2482 mL
○	n(HCl)	=	$11.64\ mol\ L^{-1} \times 0.0002482\ L$
		=	0.002887 mol

- c(HCl) = 0.002887 mol / 0.05 L
  = 0.0577 mol L^{-1}

- Weight of the same number of moles of urea to HCl from above:
  - g(urea) required = 60.06 g mol^{-1} x 0.002887 mol
    = 0.1734 g urea in 50 mL water

The 0.1734 g of urea was added to the stirred chitosan solution first before the pH was increased to between 4.0 – 4.5 by the addition of 0.1 mol L^{-1} NaOH. However, in other preparations urea was added after pH was increased by addition of NaOH and did not cause solute precipitation, i.e. either method is acceptable. The result of the addition of urea to the chitosan solution was a slight increase in pH from 2.45 to 2.48, which was subsequently increased to 4.52 by the dropwise addition of 0.1 mol L^{-1} NaOH. This chitosan / urea solution was stored at 4°C until required for infiltration into the SCBB samples.

Appendix C - Purification of FITC labelled chitosan

To ensure that the appearance of fluorescence within the SCBB samples when examined under fluorescence microscope could not be attributed to the presence of remnant unreacted free FITC in solution, the FITC labelled chitosan was subjected to a purification procedure. 1 g of the FITC labelled chitosan precipitate was redissolved in 100 mL water with 0.7993 g conc. HCl. When all chitosan had been dissolved to form a solution at pH 1.35, 1 mol L^{-1} $NaOH_{(aq)}$ was added until all solid had precipitated at a pH of ~ 9.5. The solid was filtered from the liquid over a Buchner funnel and the liquid collected to be run on a Cary 300 UV-Vis spectrometer to evaluate for the presence of free FITC.

The precipitate was subsequently washed 4 times with 100 mL distilled water, once with 100 mL 0.1 mol L^{-1} NaOH and then once again with 100 mL distilled water. The washing liquid was collected each time and analysed on a Cary 300 UV-Vis at

479 nm. Maximum absorbance of FITC commonly occurs at 494 nm [169, 170], but samples showed a maximum closer to 479 nm. However, as FITC can exist in the protonated form, the neutral species, as well as forming mono- and di-anionic species (H_3R^+, H_2R, HR^-, and R^{2-}) each with specific pK_a values and each possessing significantly different absorbance spectra, pH can alter the observed maximum absorbance [171].

A standard curve was generated by running standard solutions of FITC on the Cary 300 UV at 479 nm. Initially, a stock solution of FITC in water was generated by dissolving 0.00069 g FITC in 1 L of water with 1 drop of 0.01 mol L^{-1} NaOH added to give a solution of FITC at a concentration of 1.772 x 10^{-6} mol L^{-1} and a pH of 8.56. NaOH was added to emulate the matrix of the water used for washing, because the FITC labelled chitosan had been exposed to NaOH during precipitation. Serial dilutions were made of the stock solution to give the concentrations shown below in Table A - 1. Errors were calculated from the error in weighing FITC as well as volumetric errors in pipettes and volumetric flasks.

Table A - 1 – Concentration of standard FITC solutions and associated error.

Solution	Concentration	µmol	% error	absolute error (µmol)
"Stock"	1.772 x 10^{-6}	1.77	1.47	0.03
"1/2"	8.860 x 10^{-7}	0.89	1.60	0.01
"1/4"	4.430 x 10^{-7}	0.443	1.75	0.008
"1/8"	2.215 x 10^{-7}	0.222	1.89	0.004
"1/16"	1.108 x 10^{-7}	0.111	2.03	0.002

The supernatant and subsequent washing waters (and NaOH wash solution) run on the Cary 300 showed concentrations as presented in Figure A – 1. Washing with 100 mL 0.1 mol L^{-1} NaOH as the 4^{th} wash liberated more FITC from the precipitated chitosan that was not removed by washing with water alone, showing that the acidic FITC molecule was more soluble in an alkaline solution. Figure A -1 shows both the concentrations in µmol for the standard solutions and washing water concentrations. This serves as a reference for comparison in the fluorescence microscopy images of

SCBB samples infiltrated with FITC labelled chitosan and SCBB samples infiltrated with the FITC standard solutions, which is presented in the following section.

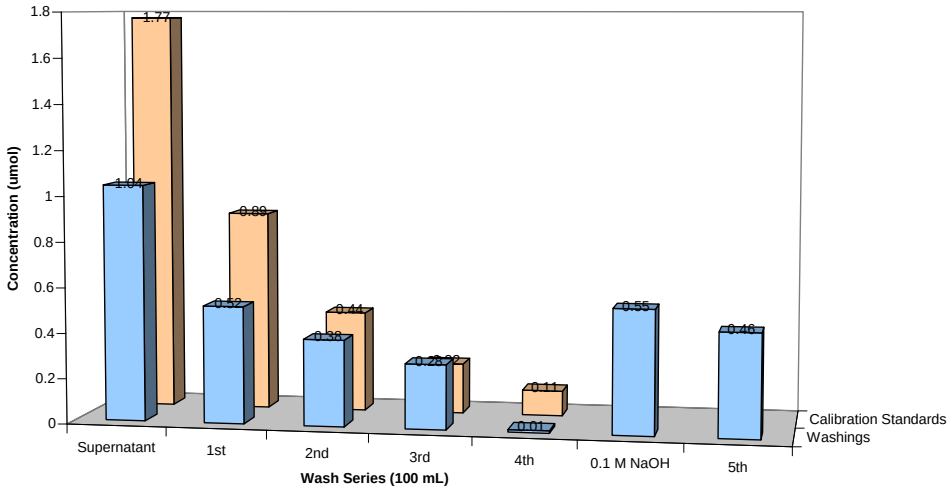

Figure A - 1 – Concentrations of FITC in standard solutions (behind) and concentrations of FITC in succesive washings (+ $NaOH_{(aq)}$) (in front) calculated on Cary 300 UV-Vis from calibration curve of standard solutons.

Evaluation of the potential of fluorescence in SCBB to be the result of "free" FITC

This experiment was conducted to confirm that fluorescence observed in SCBB samples infiltrated with FITC labelled chitosan was due to the infiltrate and not free unreacted FITC in solution. It was possible that remnant free FITC molecules, bound to the FITC labelled chitosan when liberated in solution, could penetrate regions of the SCBB matrix, for example the microporous structure, independent of the bulk chitosan solution. This can be imagined by evoking a reverse osmotic effect, where the microporous structure of the SCBB acts as a semi-permeable membrane allowing smaller molecules such as water and dissolved FITC to pass, but not larger dissolved chitosan molecules.

Method

To examine the fluorescence that free FITC in solution would generate after being infiltrated into SCBB samples, samples were infiltrated under vacuum with each of the FITC in alkaline water standard solutions as described above. After infiltration, samples were prepared by sectioning and then scraping the cut surface with a scalpel over a glass microscope slide to collect the small fragments that were produced. Samples were examined on a Leica DML fluorescence microscope running a 50 Watt mercury arc lamp. For fluorescence images, samples were illuminated using a Leica I3 blue filter / reflector system (excitation filter BP 450-490 nm), commonly with a HC PL FLUOTAR 10x / 0.30 objective lens. An initial image showing the position and size of the fragments was captured by illuminating the sample from above (or below) with an incandescent light source. Digital photographs were taken of all fluorescence images at a 1/5 second exposure time and a digital sensitivity of ISO 1600. Fluorescence intensity and dispersion throughout the SCBB samples was visually compared against examples of samples having been infiltrated with FITC labelled chitosan.

Results

Figure A - 2b opposite shows the extent of fluorescence in a SCBB sample infiltrated with the "stock" solution of FITC dissolved in alkaline water, see Table A -1 above for concentration. On close inspection, fluorescence was detectable in most fragments (difficult to see in image), especially the larger fragments some of which are indicated by arrows in Figure A - 2b. The area designated as "significant fluorescence" could have been formed by the concentration of the FITC solution in one particular volume of SCBB as the solvent evaporated. Further fluorescence images were taken of various regions of the sample, showing similar overall levels of fluorescence to that seen in Figure A - 2b, with similar sporadic regions of higher fluorescence intensity.

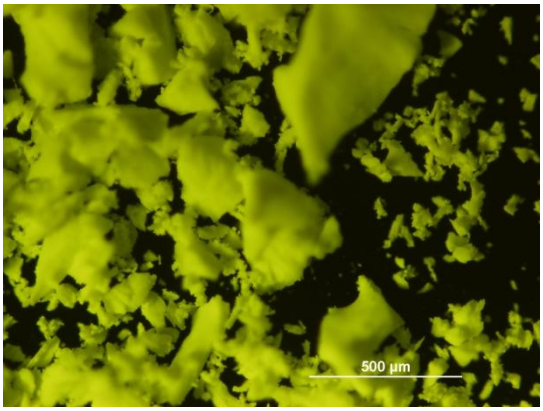

a) Microscope image of SCBB fragments infiltrated with "stock" FITC solution in alkaline solution illuminated from above by incandescent light. No fluorescence is visible under this system.

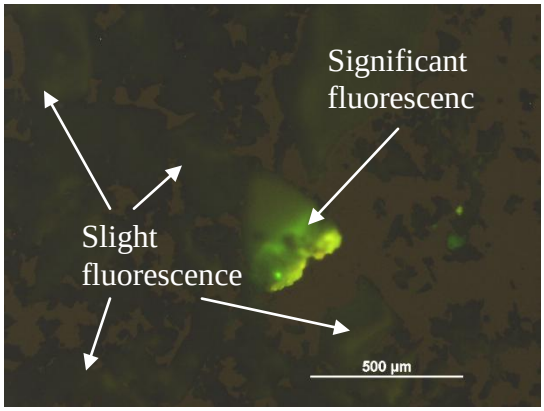

b) Fluorescence microscope image of the same sample shown in a) excited by blue light (450-490 nm).

Figure A -2 – Microscope images of SCBB sample having been infiltrated with the "stock" solution of FITC in alkaline water showing the position of fragments a), and the fluorescence emanating from those fragments b).

The same procedure as outlined above was repeated for a SCBB sample infiltrated with the "1/2" FITC in alkaline solution. In this case, fluorescence was at a level barely visible under the same illumination and sensitivity conditions to those in the "stock" solution, as shown below in Figure A – 3 where the only visible sign of fluorescence is indicated by an arrow.

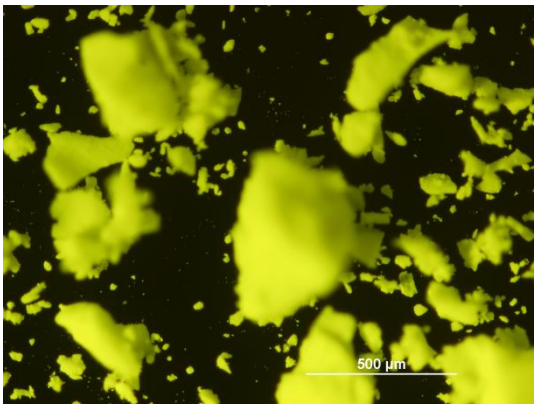

a) Microscope image of SCBB fragments having been infiltrated with "1/2" FITC in alkaline standard solution illuminated from above by incandescent light. No fluorescence is visible under this system.

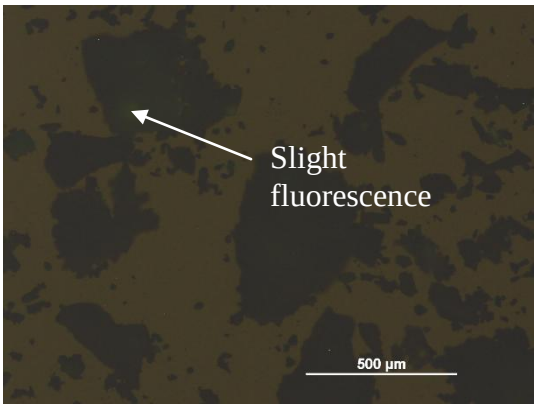

b) Fluorescence microscope image of the same sample shown in a) excited by blue light (450-490) nm). Only one small area of fluorescence is just distinguishable.

Figure A - 3 - Microscope images of SCBB sample having been infiltrated with the "1/2" standard solution of FITC in alkaline water showing the position of fragments a), and the fluorescence emanating from those fragments b).

Figure A – 3 showed the level of fluorescence generated by the "1/2" standard solution was practically undetectable under the conditions samples were tested, and the FITC concentration of this solution was higher than any of those seen in the waters used to wash the re-precipitated FITC-labelled chitosan. Therefore, significant levels of fluorescence in the images above could not be attributed to free FITC in solution, but must show the presence of FITC-labelled chitosan. The obvious uneven distribution of the FITC-labelled chitosan on the broken fragments of SCBB in Figure 4-29 (p. 100) showed that the visible appearance of fluorescent material lying on the microporous structure was different and discernible from fluorescence emanating from within the microporous structure.

Appendix D - SCBB weight increase per infiltration

Table A - 2 - Weight increase in SCBB samples when repeatedly infiltrated with Infil-4 (chitosonium chloride and $CaHPO_4$).

Sample	Initial Weight	1st Infiltration	2nd Infiltration	3rd Infiltration	4th Infiltration	5th Infiltration	6th Infiltration	Apparent density (g / mL)	Bulk volume (mL)
1	1.4356	1.4435	1.4597	1.4773	1.4923	1.5083	1.5195	0.8896	1.6137
2	0.4873	0.4989	0.511	0.5252	0.5374	0.55	0.5599	0.4049	1.2035
3	0.7636	0.7753	0.7889	0.8048	0.8183	0.8322	0.8435	0.5278	1.4469
4	0.8131	0.8216	0.8352	0.8498	0.8621	0.8754	0.8850	0.6301	1.2904
5	1.5580	1.5707	1.5872	1.6073	1.624	1.6426	1.6551	0.8784	1.7737
6	1.3424	1.353	1.371	1.392	1.4089	1.4274	1.4402	0.7542	1.7800
7	1.0871	1.0933	1.104	1.1181	1.1298	1.1422	1.1521	0.8290	1.3113
8	1.2046	1.2118	1.2246	1.2415	1.2565	1.2722	1.2829	0.8225	1.4645
9	0.8919	0.9036	0.9176	0.9347	0.9482	0.9636	0.9752	0.6078	1.4674
10	1.1223	1.1245	1.1362	1.1494	1.16	1.1719	1.1805	0.9010	1.2456
11	1.0229	1.032	1.0483	1.0665	1.0805	1.0958	1.1079	0.7232	1.4144
12	1.7677	1.7711	1.7858	1.8023	1.8151	1.8298	1.8400	1.1819	1.4957
13	1.2767	1.2811	1.2961	1.3126	1.3248	1.3381	1.3481	0.9307	1.3717
14	1.0408	1.0423	1.0571	1.0754	1.0884	1.1033	1.1141	0.7606	1.3684
15	1.0092	1.0188	1.0347	1.0553	1.0724	1.0907	1.1049	0.5796	1.7412

Table A - 3 - Weight increase in SCBB samples when repeatedly infiltrated with Infil-11 (chitosonium chloride, $CaHPO_4$ and genipin).

Sample	Initial Weight	1st Infiltration	2nd Infiltration	3rd Infiltration	4th Infiltration	5th Infiltration	6th Infiltration	Apparent density (g / mL)	Bulk volume (mL)
1	0.4528	0.4695	0.5674	0.5016	0.5244	0.5457	0.5587	0.3992	1.1342
2	0.7667	0.7844	0.8845	0.8193	0.8443	0.8689	0.8838	0.3338	2.2972
3	2.3530	2.3817	2.4476	2.4319	2.453	2.4784	2.4931	1.2895	1.8247
4	1.3966	1.4257	1.5971	1.4705	1.4945	1.5197	1.5362	0.8982	1.5549
5	1.4228	1.4497	1.588	1.4979	1.5234	1.5516	1.5675	0.8950	1.5898
6	1.5390	1.5685	1.6033	1.6147	1.6357	1.6591	1.674	1.0036	1.5336
7	0.8576	0.8761	0.9035	0.9144	0.9328	0.9545	0.9694	0.7303	1.1743
8	0.9623	0.9805	1.009	1.0186	1.035	1.054	1.0671	0.8449	1.1389
9	0.7063	0.7315	0.778	0.7702	0.7937	0.8153	0.8305	0.5653	1.2494
10	1.6058	1.6297	1.7124	1.6845	1.7109	1.7381	1.7541	1.0083	1.5926
11	1.3475	1.3677	1.3992	1.4117	1.433	1.4525	1.4611	1.2082	1.1153
12	1.0304	1.0555	1.1345	1.1077	1.1354	1.1628	1.1798	0.6590	1.5636
13	1.6719	1.6999	1.8168	1.7599	1.7892	1.8246	1.8389	0.9763	1.7125
14	0.9210	0.9507	1.2173	1.0011	1.0371	1.0762	1.0974	0.5734	1.6061
15	1.2206	1.2437	1.2883	1.2913	1.3168	1.3362	1.3532	0.8397	1.4536

Table A - 4 - Weight increase in SCBB samples when repeatedly infiltrated with Infil-12 (PCL).

Sample	Initial Weight	1st Infiltration	2nd Infiltration	3rd Infiltration	4th Infiltration	5th Infiltration	6th Infiltration	Apparent density (g / mL)	Bulk volume (mL)
1	1.2935	1.3772	1.4189	1.4578	1.5124	1.5245	1.5141	0.9259	1.3971
2	0.7173	0.8311	0.8735	0.9475	1.0345	1.0672	1.0689	0.4288	1.6726
3	1.2150	1.3202	1.3827	1.4458	1.5207	1.5591	1.5515	0.7186	1.6907
4	1.3830	1.461	1.5053	1.5478	1.6079	1.637	1.6106	0.9282	1.4900
5	1.1870	1.2747	1.3192	1.3602	1.4288	1.4595	1.4462	0.7957	1.4919
6	1.4910	1.5885	1.66	1.7299	1.8268	1.8579	1.8656	0.8884	1.6783
7	0.6050	0.7064	0.766	0.8354	0.9235	0.9567	0.9738	0.4395	1.3765
8	0.5015	0.5943	0.659	0.7342	0.8378	0.8784	0.9011	0.3789	1.3236
9	0.7447	0.832	0.8798	0.9428	1.0338	1.0634	1.0766	0.6227	1.1959
10	0.9879	1.1032	1.1822	1.2654	1.3751	1.4164	1.4374	0.6028	1.6389
11	1.1355	1.2374	1.3189	1.3931	1.4405	1.483	1.4952	0.8028	1.4145
12	0.9454	1.044	1.1245	1.1998	1.2464	1.2892	1.3056	0.7206	1.3120
13	0.8845	0.9703	1.0402	1.1032	1.1424	1.1825	1.1975	0.7885	1.1218
14	2.0580	2.1291	2.1907	2.2339	2.2639	2.306	2.3155	1.3635	1.5094
15	1.0546	1.1474	1.2186	1.2741	1.2940	1.3455	1.3577	0.8116	1.2995

Appendix E - Chitosonium migratory effect

The migratory effect of chitosan was observed in an experiment designed to provide visual evidence of chitosan precipitation by electric field induced OH^- migration as follows.

Method

A V shaped tube with internal diameter ~ 5 mm was mounted with each end pointing upwards as shown opposite in Figure A - 4. Approximately 2 mL chitosonium chloride solution was introduced to the bottom of the V through a needle attached to a syringe. Thereafter, each side of the tubing was filled slowly and simultaneously with 0.1 mol L^{-1} NaOH to the levels seen in the photograph. After allowing the apparatus to sit for 12 minutes, a 12 V DC current was applied through platinum electrodes for 3 hours, after which the apparatus was allowed to sit overnight.

Results

Precipitation of white chitosan was immediately visually evident at the interface between chitosonium chloride and 0.1 mol L^{-1} NaOH after the addition of the NaOH. Within 2-3 minutes, no more precipitation was observed with the precipitate appearing to act as a barrier between the $NaOH_{(aq)}$ and chitosonium chloride. However, when a DC current of 12 V was applied through platinum electrodes, a front of precipitating chitosan was observed to move from the negative electrode towards the positive electrode as captured in successive photographs and presented in Figure A – 4 and Figure A - 5. The progression of the precipitation front was believed to be caused by the electric field induced migration of $OH^-_{(aq)}$ through the precipitated chitosan.

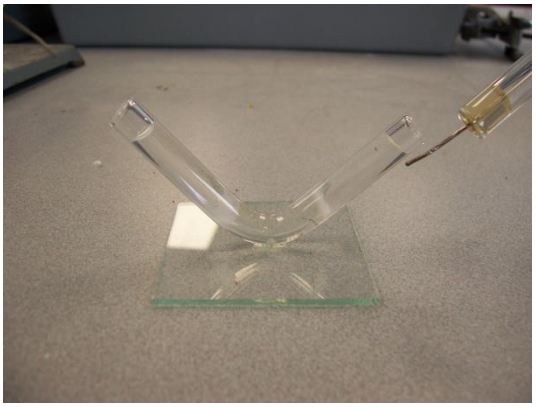

a) 1 minute

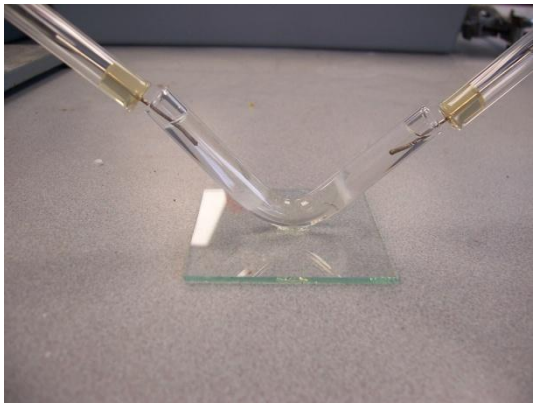

b) 12 minutes (current on)

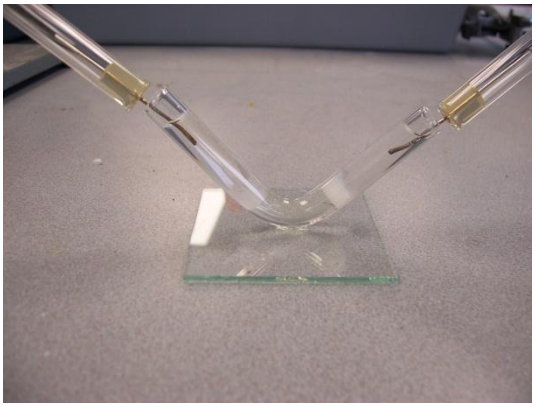

c) 19 minutes

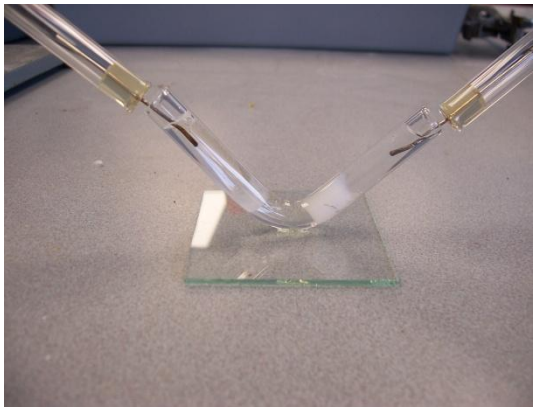

d) 32 minutes

Figure A - 4 - Photographs showing the progression of a chitosan precipitation front from a chitosan chloride solution as a result of a current applied through adjacent NaOH solution.

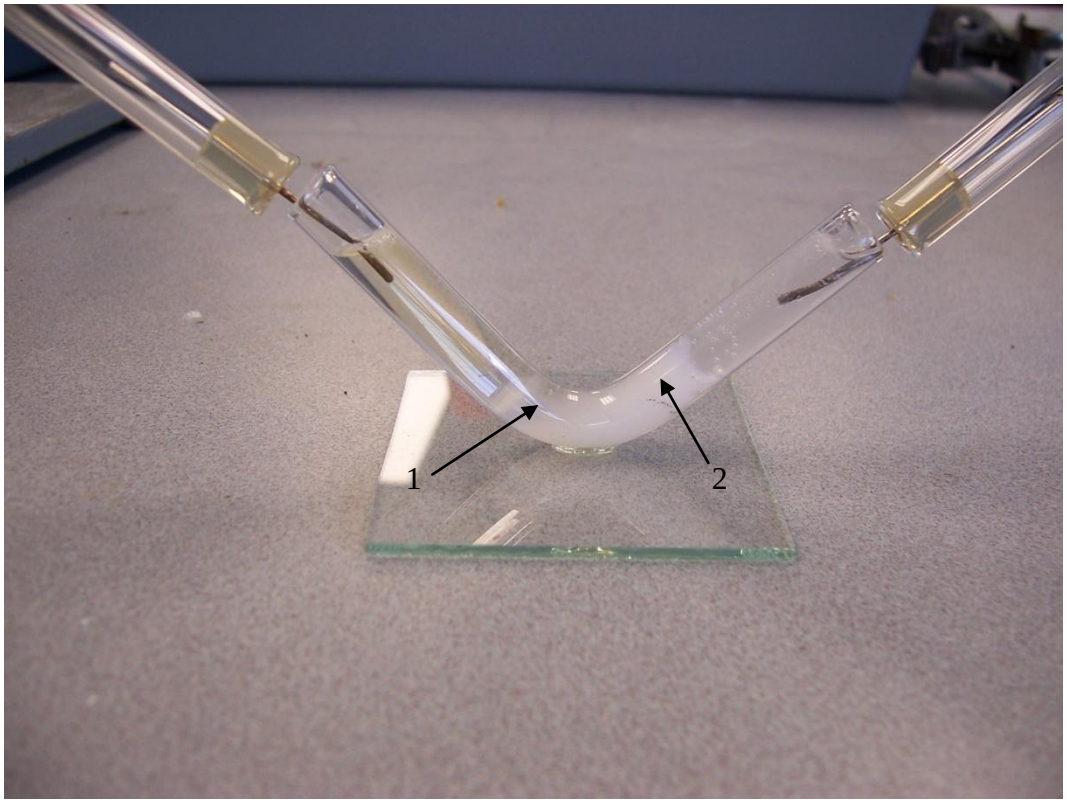

Figure A – 5 - Photograph showing the progression of a chitosan precipitation front from a chitosonium chloride solution at 70 minutes as a result of a current applied through adjacent NaOH solution.

However, at approximately 70 minutes no further precipitation was observed which remained the situation for the next 2 hours that voltage was applied. On close examination of the region of chitosan precipitate, there was a decreasing quantity of material towards the positive electrode, as indicated by arrow 1) on Figure A - 5. Conversely, a greater quantity of white precipitate was observed at the negative electrode side as shown by arrow 2). The appearance of the precipitate remained unchanged after voltage was deceased and the apparatus left overnight. This suggested that all chitosan had indeed precipitated, and that the region showing less precipitate at the positive electrode end (arrow 1) could be explained by the migration of the positively charged chitosonium ion toward the negative electrode. In addition to this, a white suspension was observed in the $NaOH_{(aq)}$ at the negative electrode end and not the positive end $NaOH_{(aq)}$ again indicating chitosonium ion movement towards the positive electrode.

Appendix F - Calculation of the volume of air that can be dissolved in water with pressure

The theoretical volume of air able to be solubilised in water at atmospheric and higher pressures may be calculated using Henry's law relating partial pressure of gases to concentration of that gas in solution as shown below:

$$p = k_H c$$

Where p is the partial pressure of the gas above the solution, k_H is the Henry's law constant for that gas, and c is the concentration of the gas in solution. In this calculation, only oxygen and nitrogen were considered as other gases in air are of low concentration, and for the purposes of this estimate calculation their contribution to the total gas dissolved in water was considered negligible. Henry's law constants for 25°C were taken from Atkins' Physical Chemistry and converted from Torr to atm. Actual experiments were carried out at room temperature (~ 20°C), which would have introduced some error into the following calculations.

Concentration of oxygen in water at 25°C and 1 atm (Henry's law constant, k_H = 4.34 x 10^4 atm):

$$c_O = (1 atm \, x \, 0.21) \div \frac{4.34 \, x 10^4 \, atm}{55.56 \, mol \, L^{-1}}$$

$$= 2.69 \, x 10^{-4} \, mol \, L^{-1}$$

(0.21 = fraction of oxygen in air)
(55.56 mol L^{-1} = concentration of water in l L)

Concentration of nitrogen in water at 25°C and 1 atm (Henry's law constant k_H = 8.57 x 10^4 atm):

$$c_N = (1 atm \, x \, 0.79) \div \frac{8.57 \, x 10^4 \, atm}{55.56 \, mol \, L^{-1}}$$

$$= 5.12 \, x 10^{-4} \, mol \, L^{-1}$$

(0.79 = fraction of nitrogen in air)

Therefore the total number of mol of "air" (nitrogen and oxygen) in 1 L of water at 1 atm is:

n(gas dissolved in 1 L of water) = 2.69 x 10^{-4} mol + 5.12 x 10^{-4} mol

= 7.81 x 10^{-4} mol

If the ideal gas equation, PV = nRT, is applied a value for the volume of gas within 1 L of water may then be calculated with the assumption that the gases behave ideally. Volume of air soluble in 1 L of water at 25°C:

V("air") = (7.81 x 10^{-4} mol x 0.082058 (L atm mol^{-1} K^{-1}) x 298 K) /1 atm

= 0.019 L, or 19 mL air / 1 L of water.

At higher pressures significantly higher concentrations of air can be dissolved in water, equating to higher volume equivalents at atmospheric pressure which are displayed in Table A - 5 below.

Table A - 5 – Volume of air able to be dissolved in 1 L of water at different pressures.

Pressure (atm)	Air volume (mL) equivalent at 1 atm / 1L water
1	19
10	190
50	950
100	1900

Therefore, when considering the standard volume of infiltrating liquid inside the pressure vessel of 30 mL (and assuming that the volume of air that can be dissolved

in such a liquid is similar to that of water) 0.57 mL of air will dissolve at 1 atm, 28 mL at 50 atm, and 57 mL at 100 atm.

Appendix G - Methods for the analysis of total ammoniacal-N and Cl^-

Samples were prepared as 100 mL aqueous solutions, refrigerated at 4°C and submitted to Hill Laboratories, 1 Clyde Street, Private Bag 3205, Hamilton 3240, New Zealand for analysis. Samples were analysed for total ammoniacal-N and chloride using the following instrument and methods.

Table A - 6 – Analysis methods and parameters for total ammoniacal-N and chloride

Substance Type	Water
Parameter Method Used	Detection Limit
Sample filtration for general testing	Sample filtration through 0.45µm membrane filter
Method – (Total Ammoniacal-N Filtered sample)	Phenol/hypochlorite colorimetry.
	Discrete Analyser. (NH_4-N = NH_4^+-N + NH_3-N) APHA 4500-NH_3 F (modified from manual analysis) 21st ed. 2005
Detection Limit	0.01 g m^{-3}
Method – (Chloride Filtered sample)	Ferric thiocyanate colourimetry.
	Discrete Analyser. APHA 4500-Cl^- E (modified from continuous-flow analysis) 21st ed. 2005.
Detection Limit	0.5 g m^{-3}

Appendix H – Calculation of the concentration of residual Cl^- and NH_3 / NH_4^+ after 3 x 1-hour washes

For the calculation, the number of mol of Cl^- after wash 3 was regarded as the total number of mol of NH_4Cl. The concept of an "average SCBB sample" was used for the calculation with dimensions of: 10 height mm x 10 mm diameter, therefore a bulk volume of ~ 0.8 mL, apparent density = 0.8 g mL^{-1}, and void volume of 75 % (corresponding to apparent density from Figure 3-12, p. 50. From Figure 5-29 (p. 134) the average mol Cl^- in the SCBB samples after the third 1-hour wash was 4.8 x 10^{-6} mol, therefore the concentration of Cl^- may be calculated by using the mol value, the bulk volume and the void space percentage as shown below in Equation 6.

Equation 6

$$[Cl^-] = \frac{4.8\ x\ 10^{-6}\ mol}{0.00080\ L\ (0.80\ mL)\ x\ 0.75\ (75\ \%\ void\ space)}$$

$$= 0.008\ mol\ L^{-1}$$

The same estimation calculation was made for total ammoniacal-N, by taking the level for total ammoniacal-N from Figure 5-28 (p. 134) for wash 3. This value was 2 orders of magnitude higher than Cl^-, corresponding to a concentration of approximately:

Equation 7

$$[NH_3 / NH_4^+] = \frac{1.57\ x\ 10^{-4}\ mol}{0.00080\ L\ (0.80\ mL)\ x\ 0.75\ (75\ \%\ void\ space)}$$

$$= 0.26\ mol\ L^{-1}$$

Appendix I -Statistical analysis on compression testing

Ultimate stress

Infil-12 (PCL)

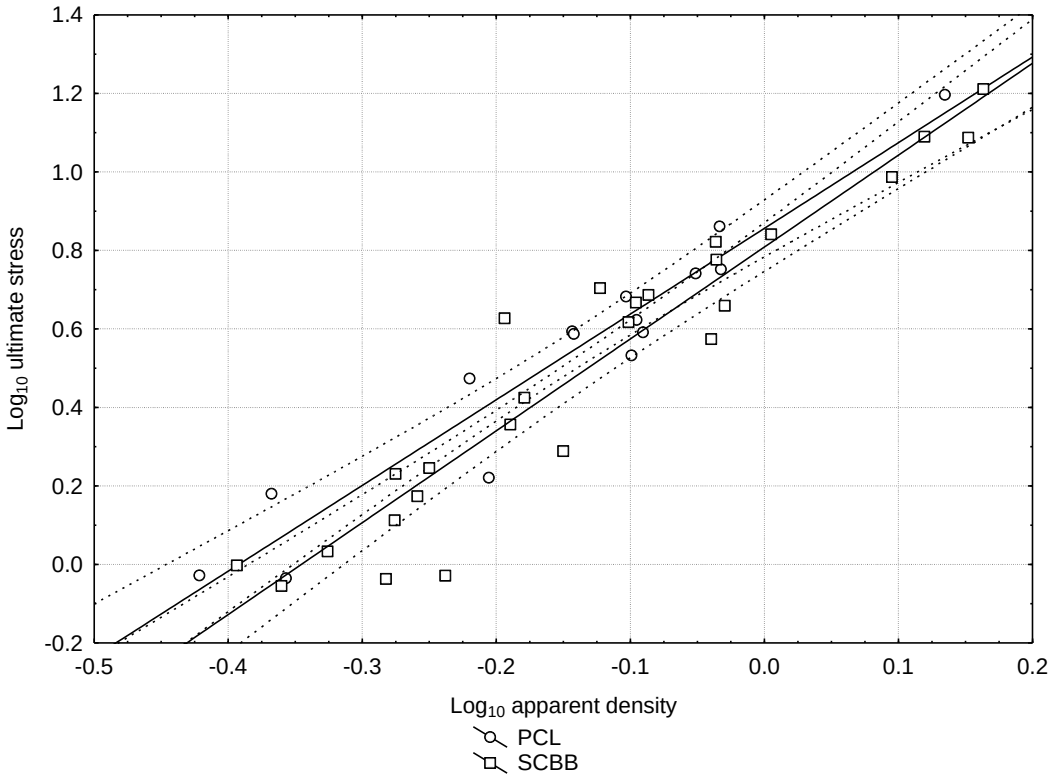

Regression lines

Log10 apparent density:PCl Log10 ultimate stress: $y = 0.8564 + 2.1834*x$; $r = 0.9647$, $p = 0.00000$; $r^2 = 0.9307$

Log10 apparent density:PCl Log10 ultimate stress: $y = 0.8088 + 2.3409*x$; $r = 0.9539$, $p = 0.0000$; $r^2 = 0.9099$

Homogeneity-of-slopes model

Effect	Univariate Results for Each DV (Spreadsheet1.sta) Sigma-restricted parameterization Effective hypothesis decomposition				
	Degr. of Freedom	PCl Log10 ultimate stress SS	PCl Log10 ultimate stress MS	PCl Log10 ultimate stress F	PCl Log10 ultimate stress p
Intercept	1	13.46649	13.46649	1129.593	0.000000
treatment	1	0.01097	0.01097	0.920	0.343603
Log10 apparent density	1	4.14284	4.14284	347.508	0.000000
treatment*Log10 apparent density	1	0.00502	0.00502	0.421	0.520275
Error	37	0.44110	0.01192		
Total	40	5.26107			

For 'treatment*Log_{10} apparent density' $p > 0.05$, therefore the null hypothesis that the regression lines have the same slope could not be rejected and the model was appropriate. $p > 0.05$ for 'treatment' showed that there was no statistical difference between the PCL infiltrated SCBB and non-infiltrated SCBB samples with regard to ultimate stress.

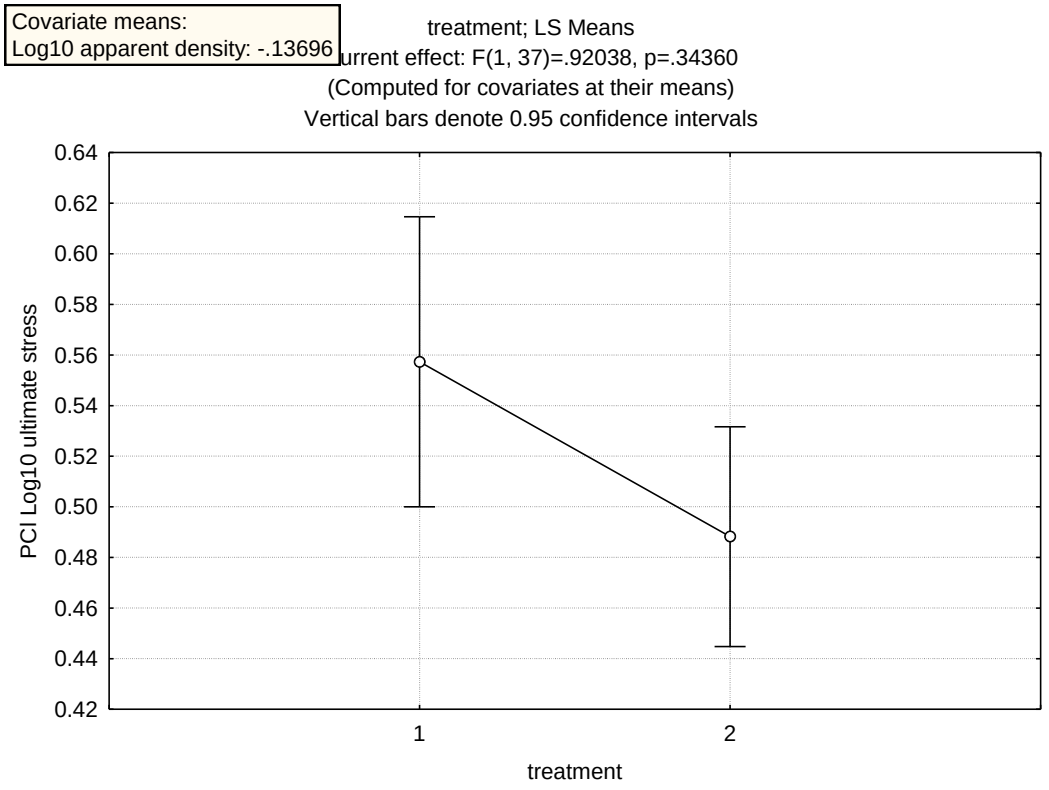

'Treatment 1' represents Log_{10} ultimate stress values of PCL infiltrated SCBB and 'treatment 2' represents non-infiltrated SCBB samples while incorporating the effect of apparent density.

Infil-4 (chitosan / $CaHPO_4$)

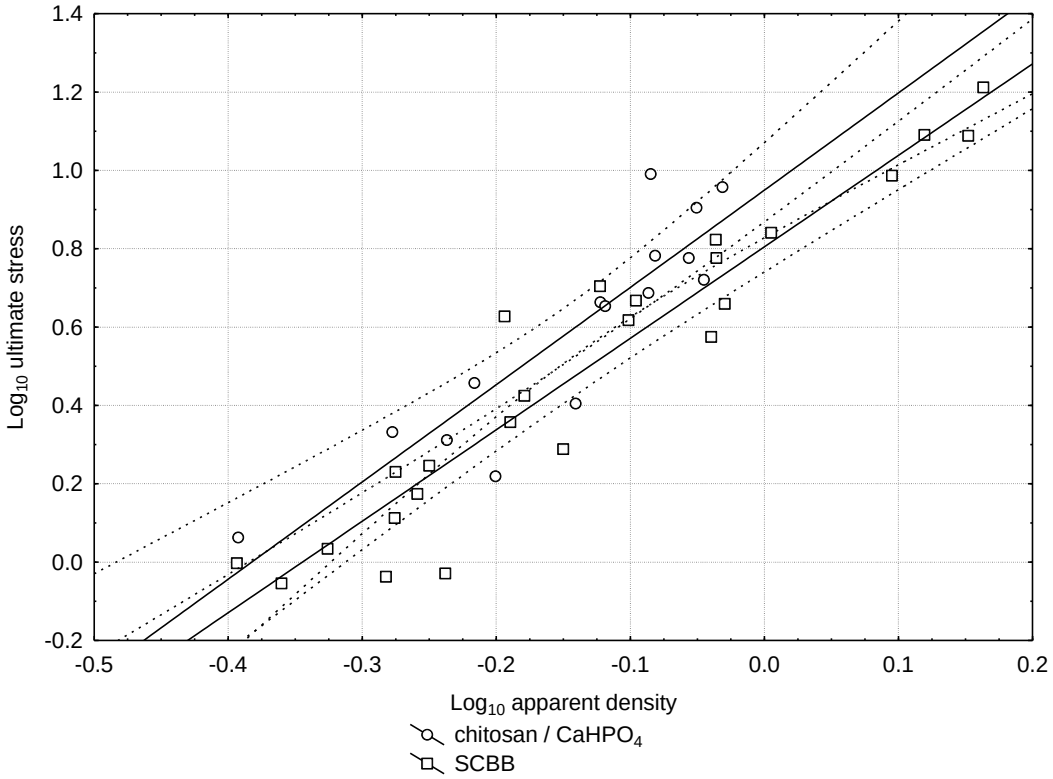

Regression lines

Log10 apparent density:chitosan / $CaHPO_4$ log10 ultimate stress: $y = 0.9557 + 2.5023*x$;
$r = 0.9034$, $p = 0.00001$; $r^2 = 0.8161$

Log10 apparent density:chitosan / $CaHPO_4$ log10 ultimate stress: $y = 0.8048 + 2.3349*x$; $r = 0.9544$, $p = 0.0000$; $r^2 = 0.9110$

Homogeneity-of-slopes model

Effect	Univariate Results for Each DV (Spreadsheet1.sta) Sigma-restricted parameterization Effective hypothesis decomposition				
	Degree. of Freedom	Chitosan / $CaHPO_4$ Log10 ultimate stress SS	Chitosan / $CaHPO_4$ Log10 ultimate stress MS	Chitosan / $CaHPO_4$ Log10 ultimate stress F	Chitosan / $CaHPO_4$ Log10 ultimate stress p
Intercept	1	10.84088	10.84088	726.5572	0.000000
treatment	1	0.07515	0.07515	5.0365	0.031059
Log10 apparent density	1	2.73714	2.73714	183.4434	0.000000
treatment*Log10 apparent density	1	0.00304	0.00304	0.2036	0.654575
Error	36	0.53715	0.01492		
Total	39	4.87886			

For 'treatment*Log_{10} apparent density' $p > 0.05$, therefore the null hypothesis that the regression lines have the same slope could not be rejected and the model was appropriate. $p < 0.05$ for 'treatment' showed that there was a statistically significant difference between the chitosan/HAp infiltrated SCBB and non-infiltrated SCBB samples with regard to ultimate stress.

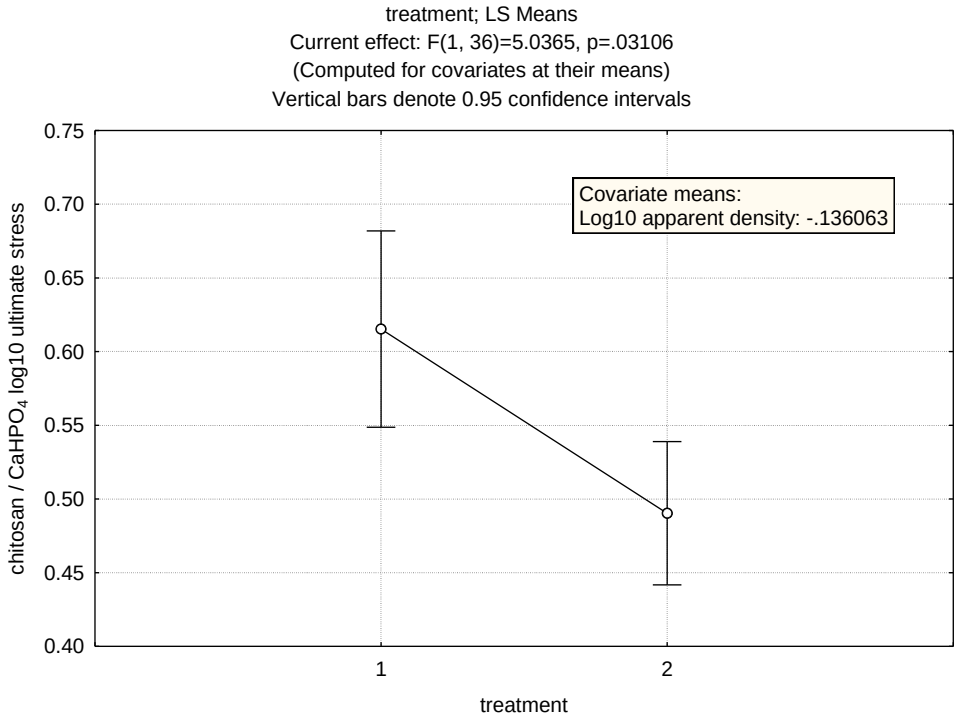

'Treatment 1' represents Log_{10} ultimate stress values of chitosan / $CaHPO_4$ infiltrated SCBB and 'treatment 2' represents non-infiltrated SCBB samples while incorporating the effect of apparent density.

Infil-11 (chitosan / $CaHPO_4$ / genipin)

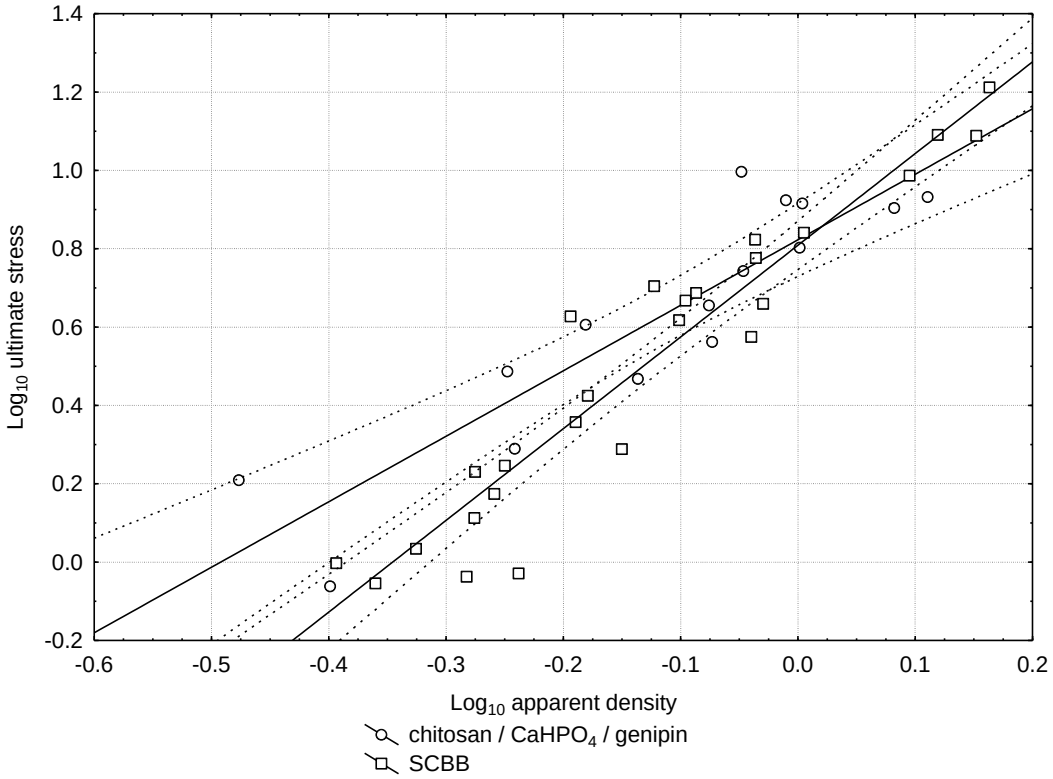

Regression lines

Log10 apparent density:chitosan / $CaHPO_4$ /genipin Log10 ultimate stress: $y = 0.8228 + 1.6718*x$; $r = 0.9040$, $p = 0.00000$; $r^2 = 0.8173$

Log10 apparent density:chitosan / $CaHPO_4$ / genipin Log10 ultimate stress: $y = 0.8088 + 2.3409*x$; $r = 0.9539$, $p = 0.0000$; $r^2 = 0.9099$

Homogeneity-of-slopes model

Effect	Univariate Results for Each DV (Spreadsheet1.sta) Sigma-restricted parameterization Effective hypothesis decomposition				
	Degree. of Freedom	Chitosan / $CaHPO_4$ / genipin Log10 ultimate stress SS	Chitosan / $CaHPO_4$ / genipin Log10 ultimate stress MS	Chitosan / $CaHPO_4$ / genipin Log10 ultimate stress F	Chitosan / $CaHPO_4$ / genipin Log10 ultimate stress p
Intercept	1	15.93194	15.93194	1019.935	0.000000
treatment	1	0.00116	0.00116	0.075	0.786401
Log10 apparent density	1	3.84753	3.84753	246.312	0.000000
treatment*Log10 apparent density	1	0.10698	0.10698	6.849	0.012772
Error	37	0.57796	0.01562		
Total	40	5.19335			

For 'treatment*Log_{10} apparent density' $p < 0.05$, therefore the null hypothesis that the regression lines have the same slope was rejected and the model was not appropriate. Examination of the scatter plot suggested that Log_{10} ultimate stress values were significantly different (higher) at lower apparent density values as shown by the lack of overlap of 95 % confidence intervals in this region.

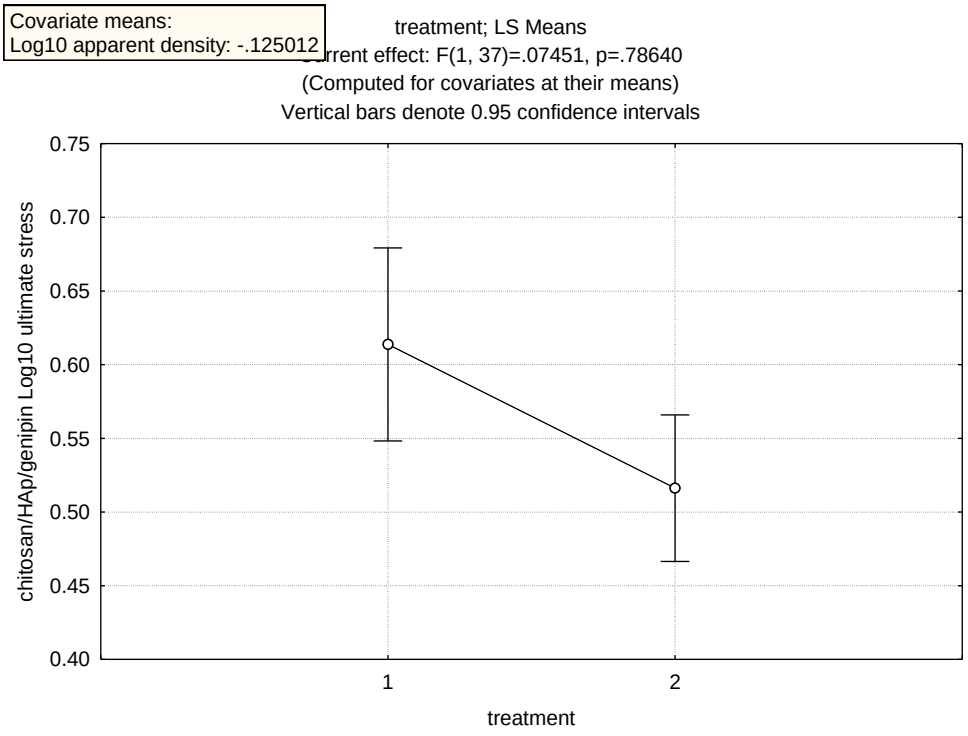

Toughness to strain = 8 %

Infil-12 (PCL)

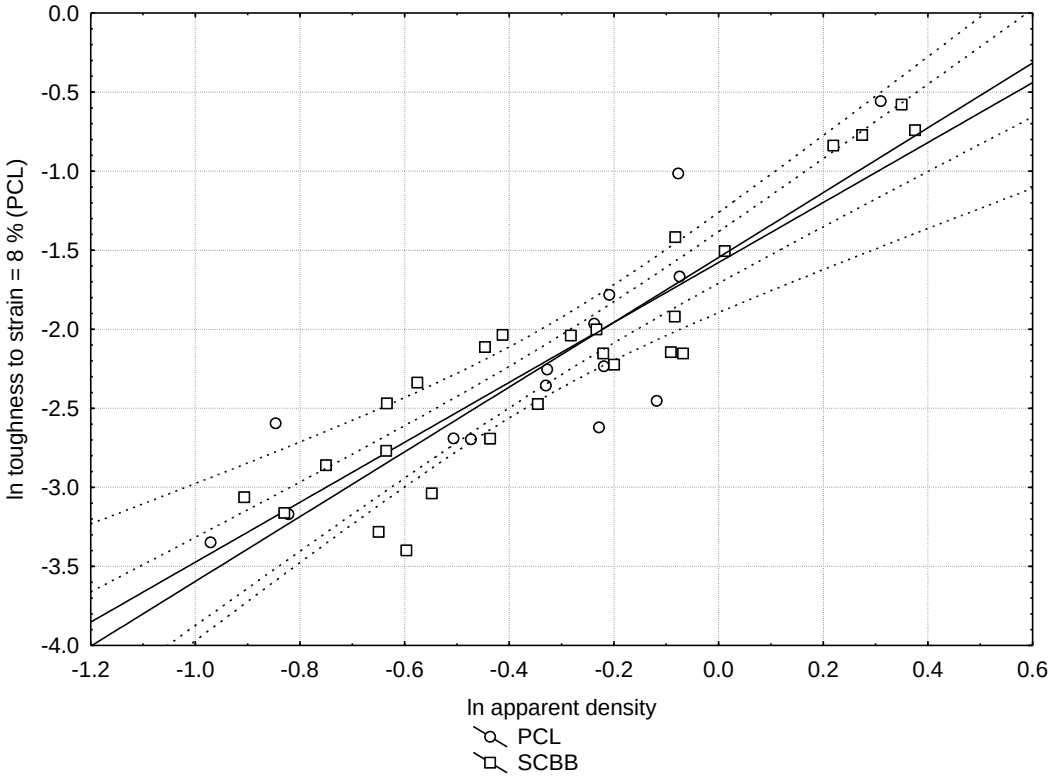

Regression lines

ln apparent density:ln toughness to strain = 8 % (PCL): y = -1.5777 + 1.8955*x; r = 0.8592, p = 0.00004; r^2 = 0.7382

ln apparent density:ln toughness to strain = 8 % (PCL): y = -1.546 + 2.049*x; r = 0.9247, p = 0.0000; r^2 = 0.8552

Effect	Univariate Results for Each DV (Spreadsheet2.sta) Sigma-restricted parameterization Effective hypothesis decomposition				
	Degree. of Freedom	ln toughness to strain = 8 % (PCL) SS	ln toughness to strain = 8 % (PCL) MS	ln toughness to strain = 8 % (PCL) F	ln toughness to strain = 8 % (PCL) p
Intercept	1	47.38672	47.38672	402.2049	0.000000
treatment	1	0.00490	0.00490	0.0416	0.839462
ln apparent density	1	16.69610	16.69610	141.7118	0.000000

Effect	Univariate Results for Each DV (Spreadsheet2.sta) Sigma-restricted parameterization Effective hypothesis decomposition				
	Degree. of Freedom	ln toughness to strain = 8 % (PCL) SS	ln toughness to strain = 8 % (PCL) MS	ln toughness to strain = 8 % (PCL) F	ln toughness to strain = 8 % (PCL) p
treatment*ln apparent density	1	0.02528	0.02528	0.2146	0.645898
Error	37	4.35924	0.11782		
Total	40	23.85405			

For ‘treatment*ln apparent density’ $p > 0.05$, therefore the null hypothesis that the regression lines have the same slope could not be rejected and the model was appropriate. $p > 0.05$ for ‘treatment’ showed that there was no statistical difference between the PCL infiltrated SCBB and non-infiltrated SCBB samples with regard to [ln toughness to strain = 8 %].

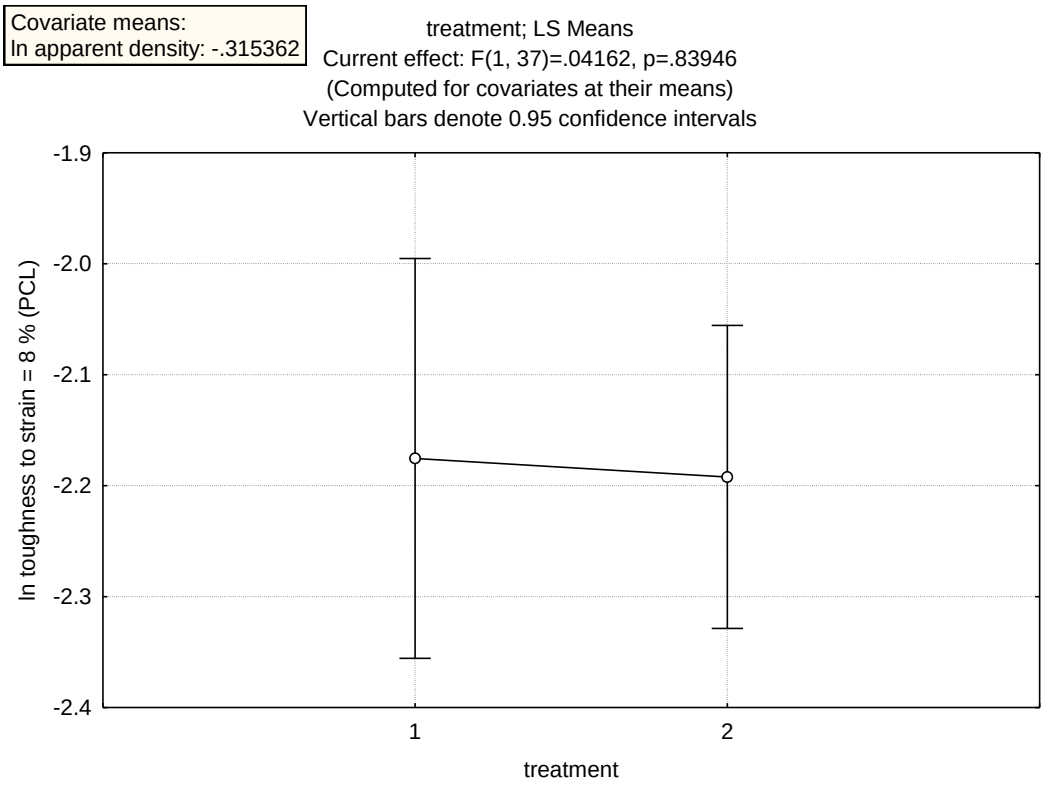

‘Treatment 1’ represents [ln toughness to strain = 8 %] values of PCL infiltrated SCBB and ‘treatment 2’ represents non-infiltrated SCBB samples while incorporating the effect of apparent density.

Infil-4 (chitosan / $CaHPO_4$)

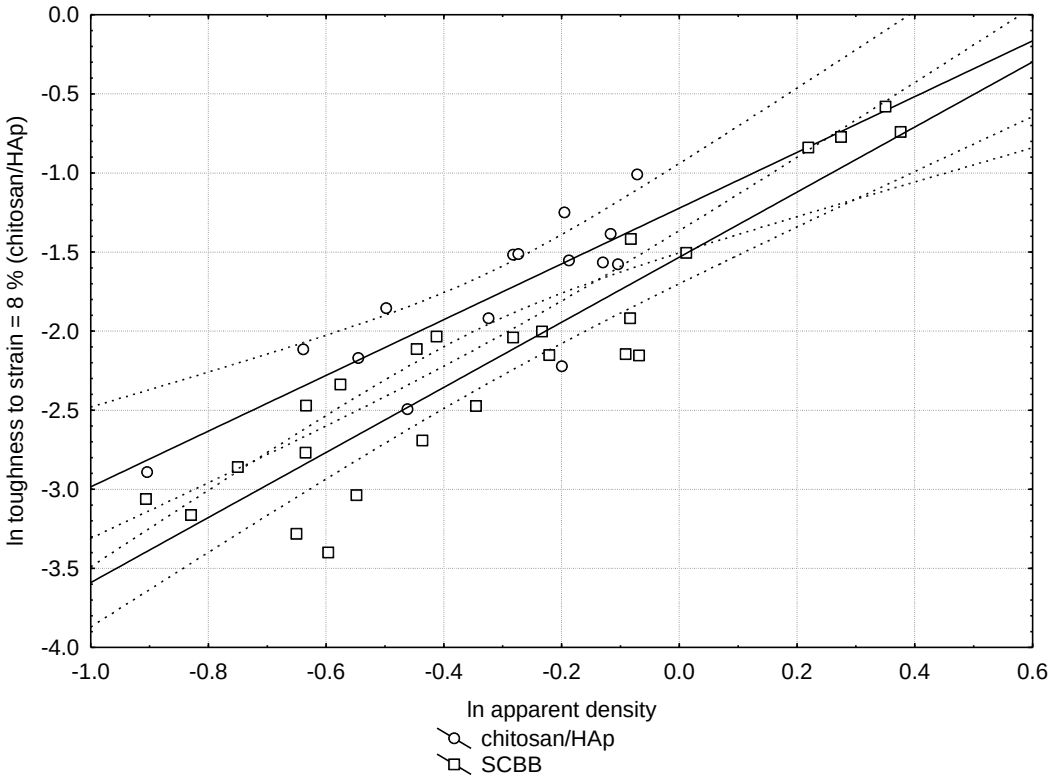

Regression lines

ln apparent density:ln toughness to strain = 8 % (chitosan / $CaHPO_4$): y = -1.1362 + 1.8805*x; r = 0.8986, p = 0.00001; r^2 = 0.8075

ln apparent density:ln toughness to strain = 8 % (chitosan / $CaHPO_4$): y = -1.5326 + 2.0576*x; r = 0.9273, p = 0.0000; r^2 = 0.8598

Effect	Univariate Results for Each DV (Spreadsheet2.sta) Sigma-restricted parameterization Effective hypothesis decomposition				
	Degree. of Freedom	ln toughness to strain = 8 % (chitosan / $CaHPO_4$) SS	ln toughness to strain = 8 % (chitosan / $CaHPO_4$) MS	ln toughness to strain = 8 % (chitosan / $CaHPO_4$) F	ln toughness to strain = 8 % (chitosan / $CaHPO_4$) p
Intercept	1	25.04621	25.04621	304.0045	0.000000
treatment	1	0.58461	0.58461	7.0958	0.011485
ln apparent density	1	9.55295	9.55295	115.9513	0.000000
treatment*ln apparent density	1	0.01758	0.01758	0.2133	0.646944
Error	36	2.96595	0.08239		

Effect	Univariate Results for Each DV (Spreadsheet2.sta) Sigma-restricted parameterization Effective hypothesis decomposition				
	Degree. of Freedom	ln toughness to strain = 8 % (chitosan / $CaHPO_4$) SS	ln toughness to strain = 8 % (chitosan / $CaHPO_4$) MS	ln toughness to strain = 8 % (chitosan / $CaHPO_4$) F	ln toughness to strain = 8 % (chitosan / $CaHPO_4$) p
Total	39	20.74995			

For ‘treatment*ln apparent density’ $p > 0.05$, therefore the null hypothesis that the regression lines have the same slope could not be rejected and the model was appropriate. $p < 0.05$ for ‘treatment’ showed that there was a statistically significant difference between the chitosan / $CaHPO_4$ infiltrated SCBB and non-infiltrated SCBB samples with regard to [ln toughness to strain = 8 %].

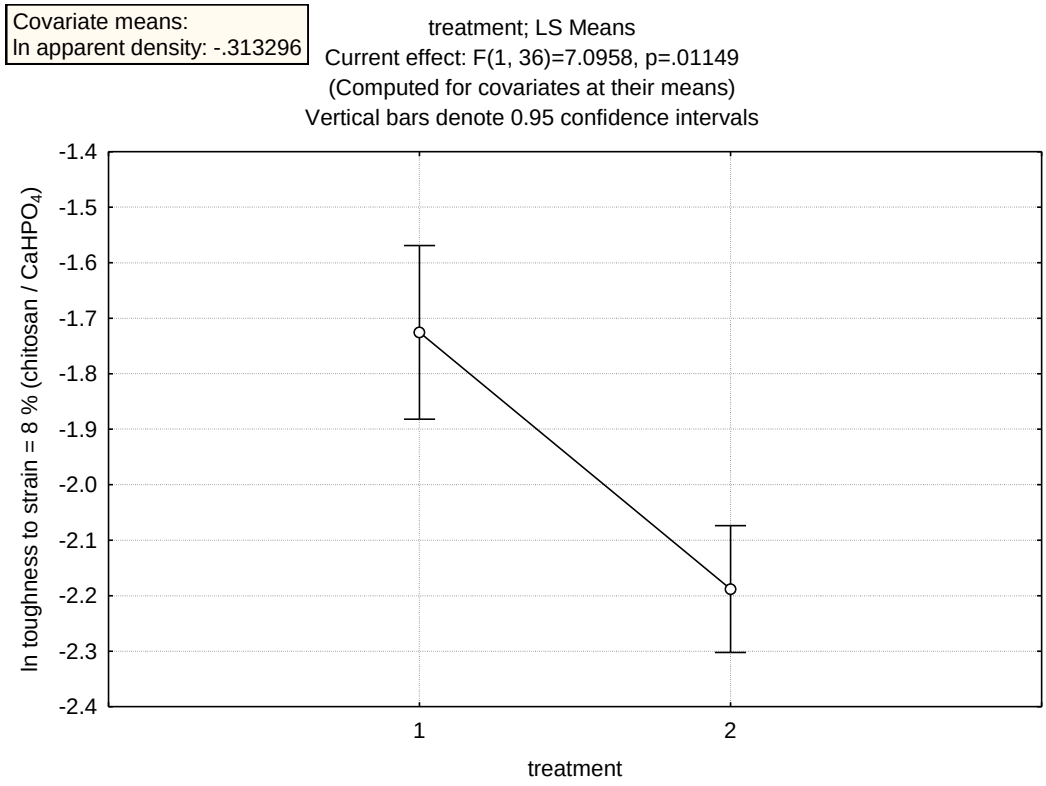

'Treatment 1' represents [ln toughness to strain = 8 %] values of chitosan / $CaHPO_4$ infiltrated SCBB and 'treatment 2' represents non-infiltrated SCBB samples while incorporating the effect of apparent density.

Infil-11 (chitosan / $CaHPO_4$ / genipin)

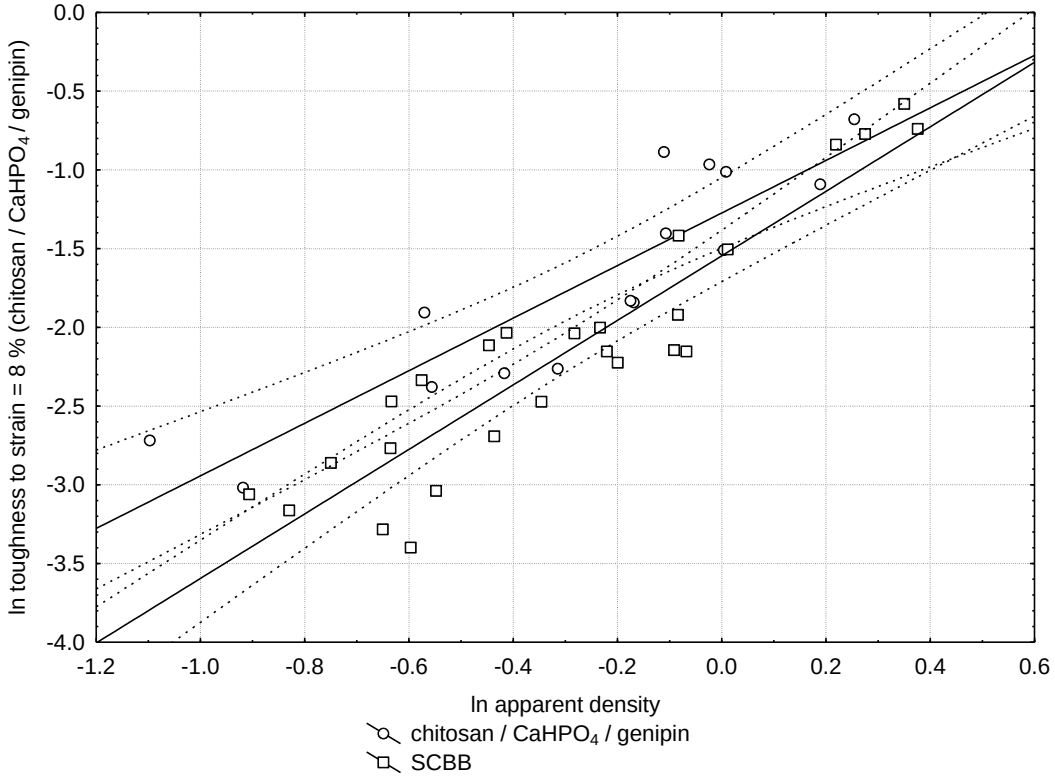

Regression lines

ln apparent density:ln toughness to strain = 8 % (chitosan / $CaHPO_4$ / genipin): $y = -1.2737 + 1.6696*x$; $r = 0.8959$, $p = 0.00001$; $r^2 = 0.8027$

ln apparent density:ln toughness to strain = 8 % (chitosan / $CaHPO_4$ / genipin): $y = -1.546 + 2.049*x$; $r = 0.9247$, $p = 0.0000$; $r^2 = 0.8552$

Effect	Univariate Results for Each DV (Spreadsheet2.sta) Sigma-restricted parameterization Effective hypothesis decomposition

	Degree of Freedom	ln toughness to strain = 8 % (chitosan / $CaHPO_4$ / genipin) SS	ln toughness to strain = 8 % (chitosan / $CaHPO_4$ / genipin) MS	ln toughness to strain = 8 % (chitosan / $CaHPO_4$ / genipin) F	ln toughness to strain = 8 % (chitosan / $CaHPO_4$ / genipin) p
Intercept	1	47.58027	47.58027	470.6640	0.000000
treatment	1	0.44359	0.44359	4.3880	0.043097
ln apparent density	1	17.51839	17.51839	173.2919	0.000000
treatment*ln apparent density	1	0.18237	0.18237	1.8041	0.187405
Error	37	3.74040	0.10109		
Total	40	25.07280			

For 'treatment*ln apparent density $p > 0.05$, therefore the null hypothesis that the regression lines have the same slope could not be rejected and the model was appropriate. $p < 0.05$ for 'treatment' showed that there was statistical difference between the chitosan / $CaHPO_4$ / genipin infiltrated SCBB and non-infiltrated SCBB samples with regard to [ln toughness to strain = 8 %].

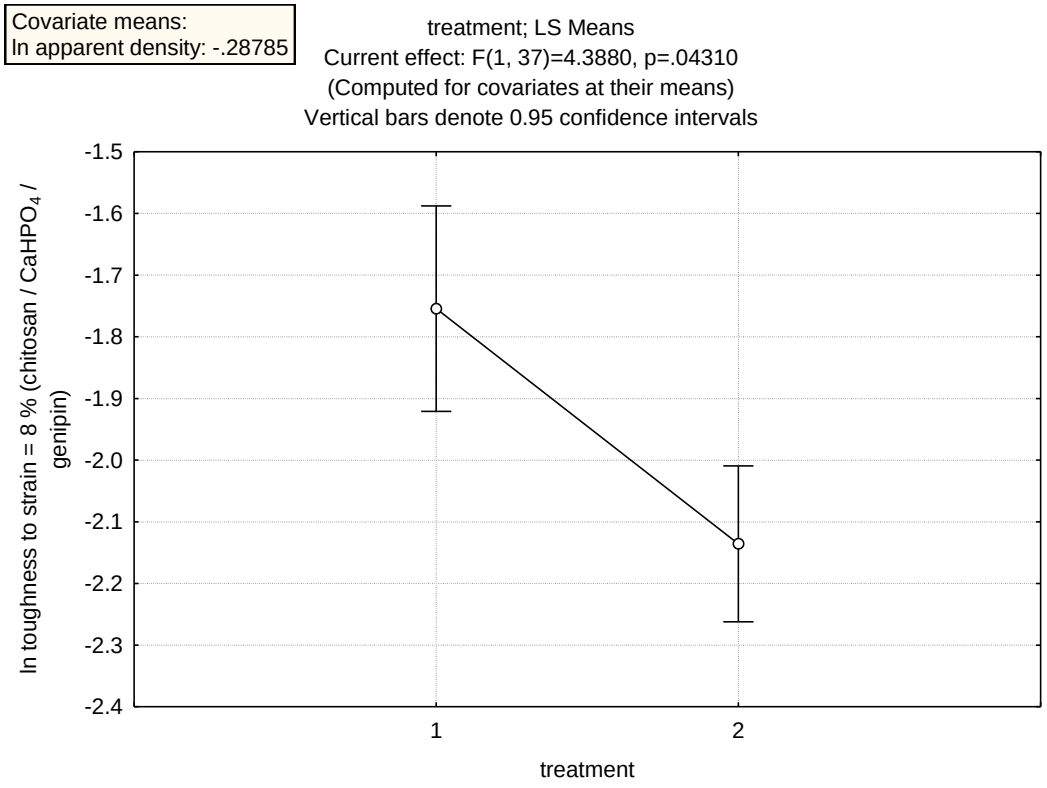

'Treatment 1' represents [ln toughness to strain = 8 %] values of chitosan / $CaHPO_4$ / genipin infiltrated SCBB and 'treatment 2' represents non-infiltrated SCBB samples while incorporating the effect of apparent density.

Modulus

Infil-12 (PCL)

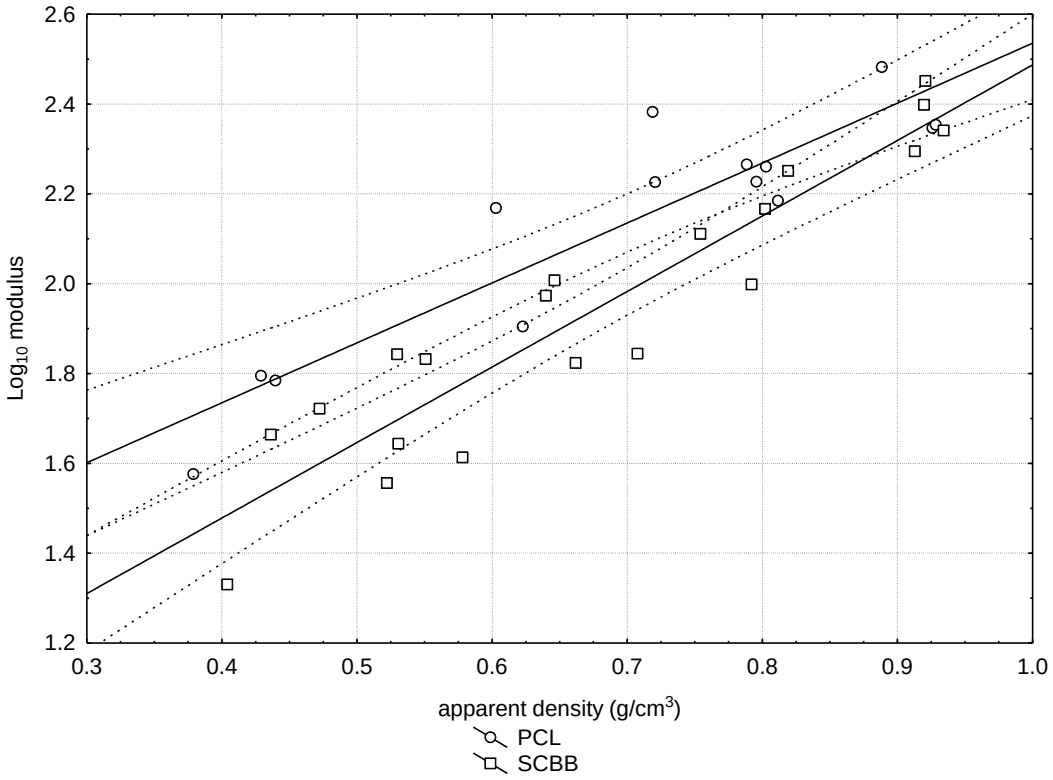

Regression lines

apparent density (g/cm^3):PCL Log10 modulus: $y = 1.2012 + 1.3343*x$; $r = 0.9161$, $p = 0.00000$; $r^2 = 0.8392$

apparent density (g/cm^3):PCL Log10 modulus: $y = 0.8058 + 1.6813*x$; $r = 0.9360$, $p = 0.00000$; $r^2 = 0.8760$

Effect	Univariate Results for Each DV (Spreadsheet10.sta) Sigma-restricted parameterization Effective hypothesis decomposition				
	Degree of Freedom	PCL Log10 modulus SS	PCL Log10 modulus MS	PCL Log10 modulus F	PCL Log10 modulus p
Intercept	1	1.956096	1.956096	156.0751	0.000000
treatment	1	0.075925	0.075925	6.0580	0.019815

Effect	Univariate Results for Each DV (Spreadsheet10.sta) Sigma-restricted parameterization Effective hypothesis decomposition				
	Degree of Freedom	PCL Log10 modulus SS	PCL Log10 modulus MS	PCL Log10 modulus F	PCL Log10 modulus p
apparent density (g/cm3)	1	2.247865	2.247865	179.3550	0.000000
treatment*apparent density (g/cm3)	1	0.029761	0.029761	2.3746	0.133808
Error	30	0.375991	0.012533		
Total	33	3.075475			

For 'treatment*apparent density' $p > 0.05$, therefore the null hypothesis that the regression lines have the same slope could not be rejected and the model was appropriate. $p < 0.05$ for 'treatment' showed that there was statistical difference between the PCL infiltrated SCBB and non-infiltrated SCBB samples with regard to modulus.

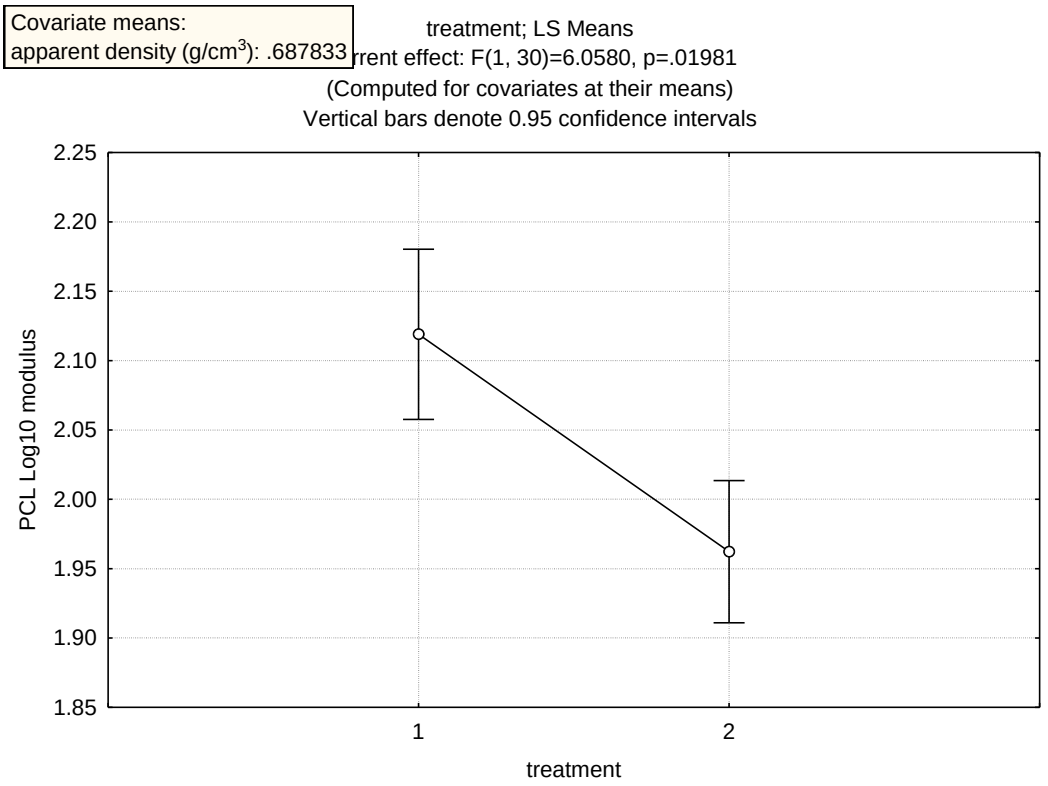

'Treatment 1' represents Log_{10} modulus values of PCL infiltrated SCBB and 'treatment 2' represents non-infiltrated SCBB samples while incorporating the effect of apparent density.

Infil-4 (chitosan / $CaHPO_4$)

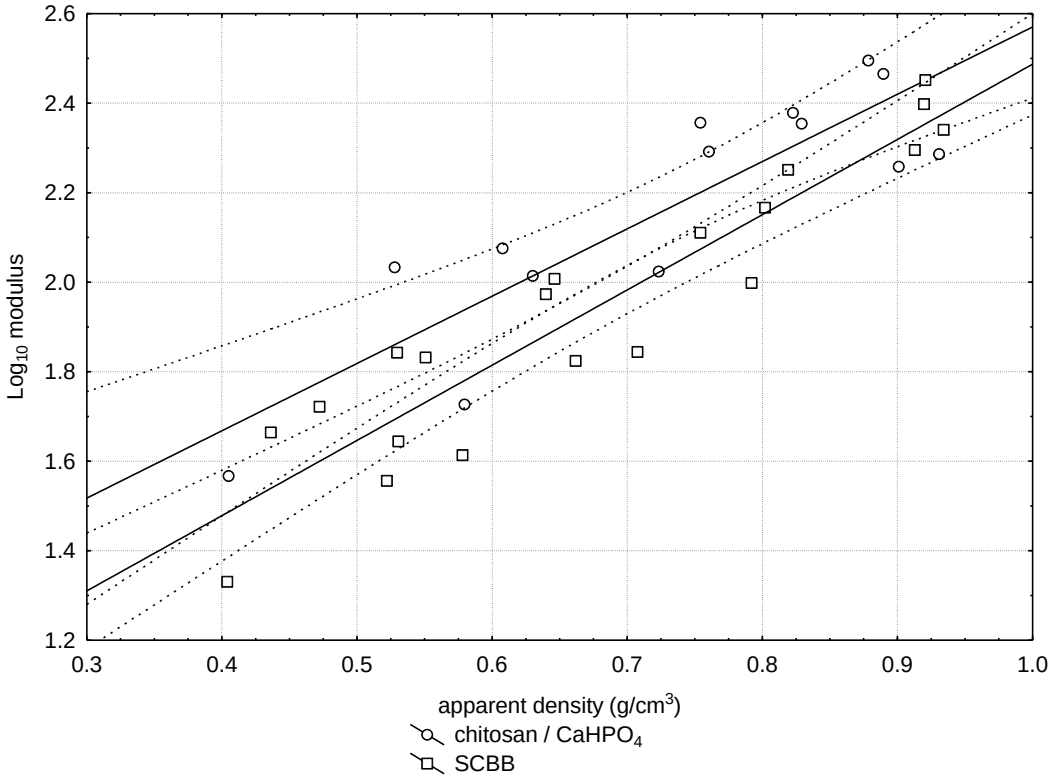

Regression lines

Apparent density (g/cm^3):chitosan / $CaHPO_4$ Log10 modulus: $y = 1.0663 + 1.504*x$; $r = 0.8768$, $p = 0.00004$; $r^2 = 0.7689$

Apparent density (g/cm^3):chitosan / $CaHPO_4$ Log10 modulus: $y = 0.8058 + 1.6813*x$;
$r = 0.9360$, $p = 0.00000$; $r^2 = 0.8760$

Effect	Univariate Results for Each DV (Spreadsheet10.sta) Sigma-restricted parameterization Effective hypothesis decomposition				
	Degree of Freedom	Chitosan / $CaHPO_4$ Log10 modulus SS	Chitosan / $CaHPO_4$ Log10 modulus MS	Chitosan / $CaHPO_4$ Log10 modulus F	Chitosan / $CaHPO_4$ Log10 modulus p

Effect	Univariate Results for Each DV (Spreadsheet10.sta) Sigma-restricted parameterization Effective hypothesis decomposition				
	Degree of Freedom	Chitosan / $CaHPO_4$ Log10 modulus SS	Chitosan / $CaHPO_4$ Log10 modulus MS	Chitosan / $CaHPO_4$ Log10 modulus F	Chitosan / $CaHPO_4$ Log10 modulus p
Intercept	1	1.376168	1.376168	91.4633	0.000000
treatment	1	0.026659	0.026659	1.7718	0.193185
apparent density (g/cm3)	1	2.118855	2.118855	140.8239	0.000000
treatment*apparent density (g/cm3)	1	0.006565	0.006565	0.4363	0.513938
Error	30	0.451384	0.015046		
Total	33	3.208340			

For 'treatment*apparent density' $p > 0.05$, therefore the null hypothesis that the regression lines have the same slope could not be rejected and the model was appropriate. $p > 0.05$ for 'treatment' showed that there was no a statistical difference between the chitosan / $CaHPO_4$ infiltrated SCBB and non-infiltrated SCBB samples with regard to modulus.

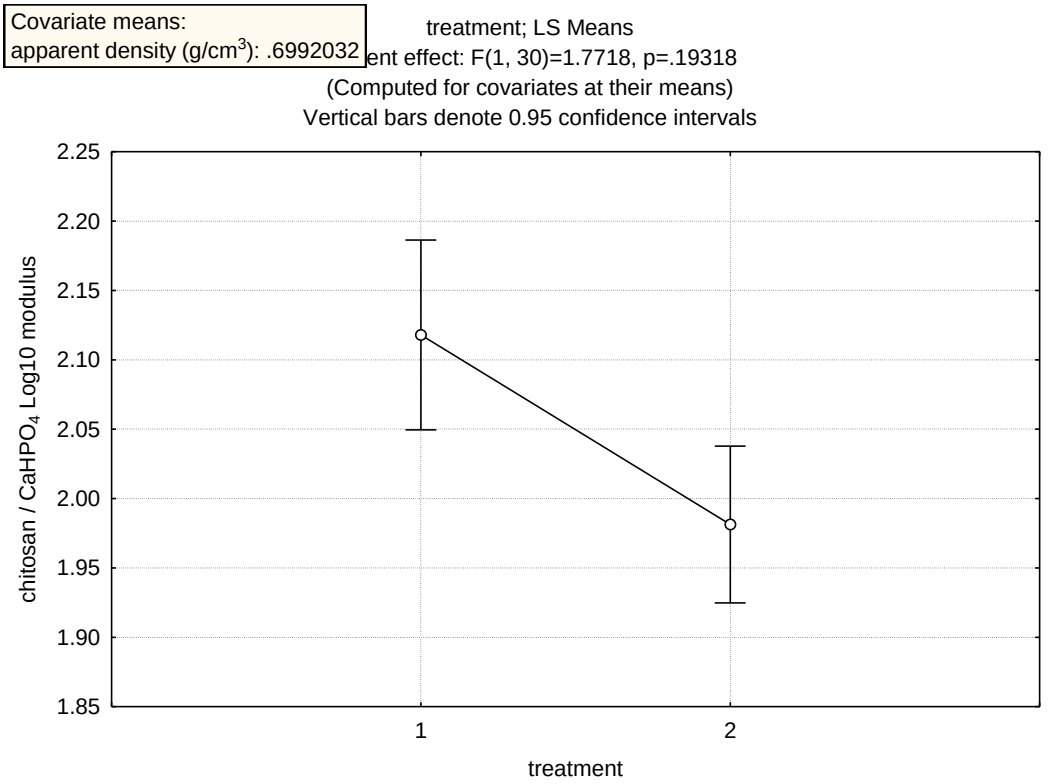

'Treatment 1' represents modulus values of chitosan / $CaHPO_4$ infiltrated SCBB and 'treatment 2' represents non-infiltrated SCBB samples while incorporating the effect of apparent density.

Infil-11 (chitosan / $CaHPO_4$ / genipin)

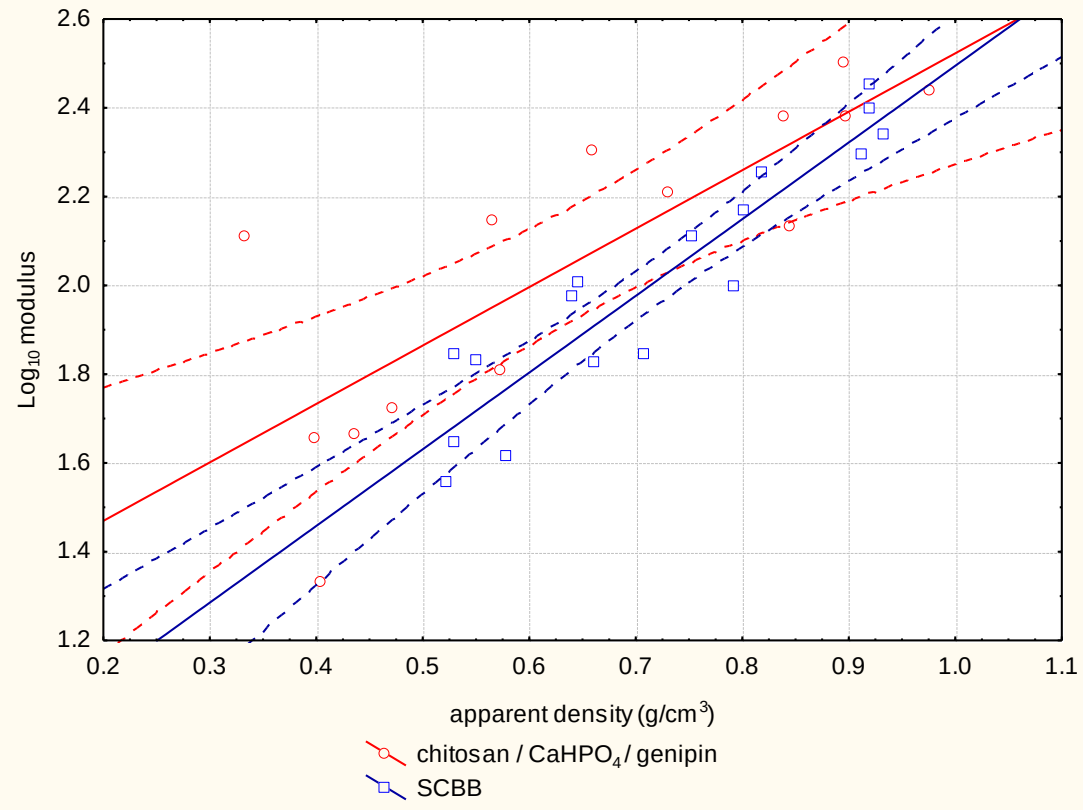

Regression lines

Apparent density (g/cm^3):chitosan / $CaHPO_4$ / genipin Log 10 modulus: $y = 1.5348 + 0.9297*x$; $r = 0.7589$, $p = 0.0068$; $r^2 = 0.5759$

Apparent density (g/cm^3):chitosan / $CaHPO_4$ / genipin Log 10 modulus: $y = 0.7669 + 1.7278*x$; $r = 0.9293$, $p = 0.00000$; $r^2 = 0.8635$

Effect	Univariate Results for Each DV (Spreadsheet10.sta) Sigma-restricted parameterization Effective hypothesis decomposition

	Degree of Freedom	Chitosan / $CaHPO_4$ / genipin Log 10 modulus SS	Chitosan / $CaHPO_4$ / genipin Log 10 modulus MS	Chitosan / $CaHPO_4$ / genipin Log 10 modulus F	Chitosan / $CaHPO_4$ / genipin Log 10 modulus p
Intercept	1	2.698031	2.698031	141.1397	0.000000
treatment	1	0.261731	0.261731	13.6917	0.000973
apparent density (g/cm3)	1	1.720075	1.720075	89.9808	0.000000
treatment*apparent density (g/cm3)	1	0.142551	0.142551	7.4572	0.010993
Error	27	0.516133	0.019116		
Total	30	2.928988			

For 'treatment*apparent density' $p < 0.05$, therefore the null hypothesis that the regression lines have the same slope was rejected and the model was not appropriate. Nonetheless, examination of the scatter plot showed higher Log_{10} modulus values for infiltrated samples at lower apparent density values.

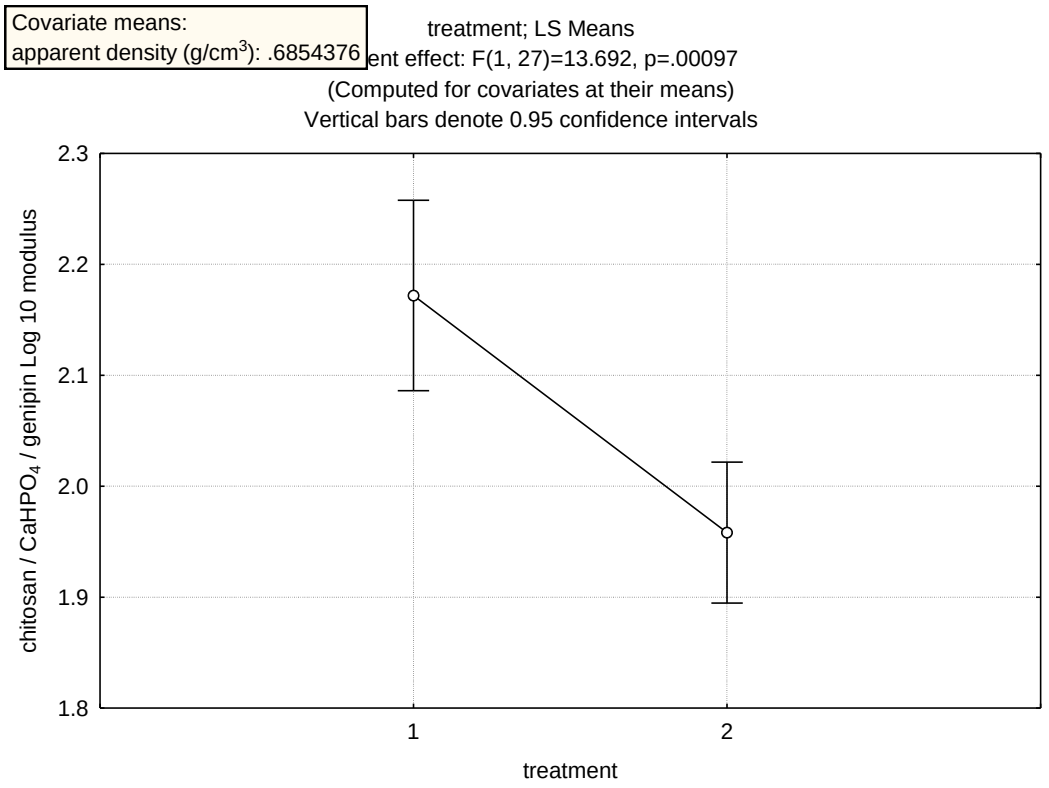

Appendix J - Concentration of HCl in chitosan / $CaHPO_4$ infiltrating solution

Conc. HCl has a density of 1.18 g/mL and molarity of 11.65 mol L^{-1} which enables the calculation of the concentration of HCl in the Infil-4 (chitosan / $CaHPO_4$) solution shown below:

Number of mL of HCl conc.

2.7442 g HCl conc. ÷ 1.18 g mL^{-1} = 2.33 mL

Number of moles of HCl

11.65 mol L^{-1} x 0.00233 mL = 0.0271 mol

Concentration of HCl in 250 mL solution

0.0271 mol ÷ 0.025 L = 0.108 mol L^{-1}

0.1 M NaOH was added drop-wise to the stirred solution to increase pH to 4.10 before infiltration or storage.

Appendix K – Protocol-2 L9292 biocompatibility testing

BioSCBB-1 / Protocol-2 (SCBB infiltrated with chitosan)

Figure A – 6 shows that at t = 1 hour and t = 24 hours there was little indication of cytotoxic response (balling of cells possibly due to high confluency), whereas at t = 48 hours there was obvious degradation of cells (made apparent by the marked reduction in density) and malformation. An explanation of this seemingly delayed

and extensive cytotoxic effect is that the leaching of the cytotoxin from within the samples into the media was slower than the subsequent diffusion through the media. This would result in the cytotoxin concentration increasing at near uniform rate across the range of the well until a level was attained that began to damage all cells.

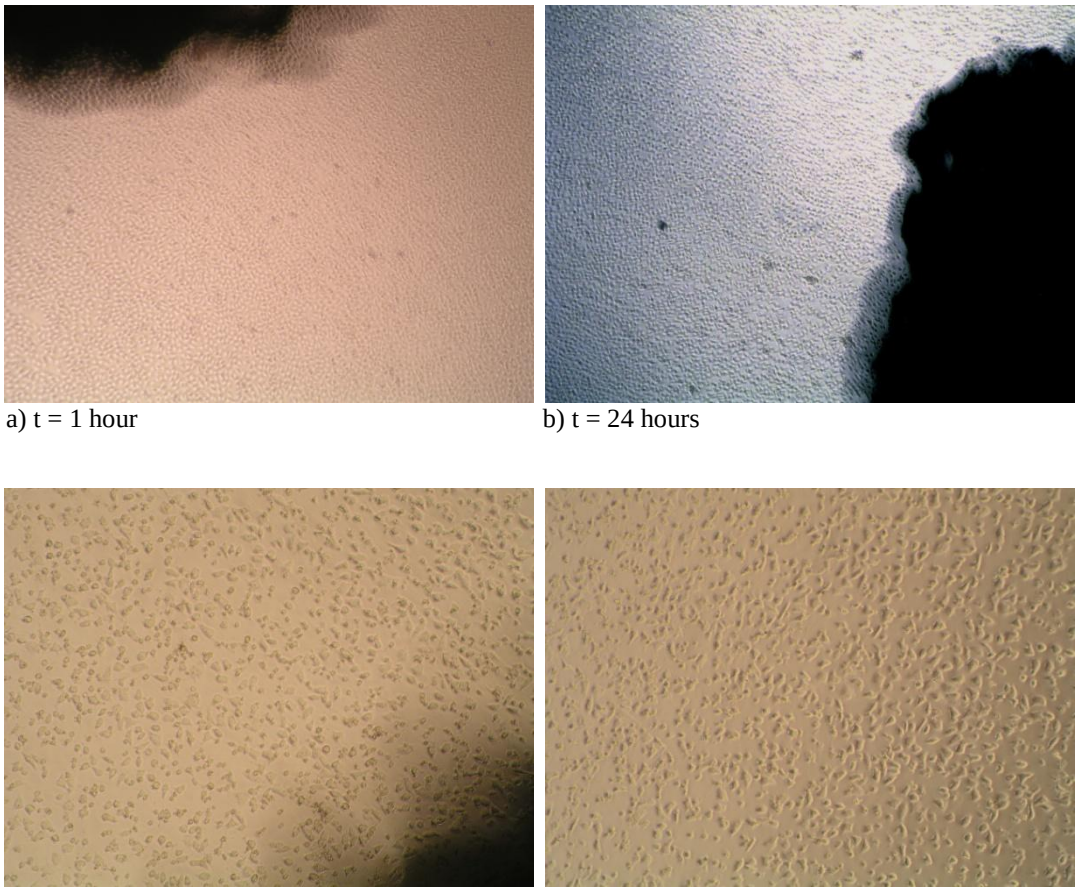

a) t = 1 hour

b) t = 24 hours

c) t = 48 hours

d) t = 48 hours, well edge

Figure A - 6 – Microscope images of L929 cells response to BioSCBB-1 at t = 1 hour, t = 24 and t = 48 hours.

Table A - 7 - Cytotoxic response to BioSCBB-1

Time (hours)	t = 1	t = 24	t = 48
Cytotoxic Response	0-1	0-1	3

BioSCBB-2 / Protocol-2 (SCBB infiltrated with chitosan / $CaHPO_4$)

Results of this test were similar to those seen above for SCBB infiltrated with chitosan as can be seen below in Figure A - 7, where a pronounced cytotoxic effect was seen at t = 48 hours.

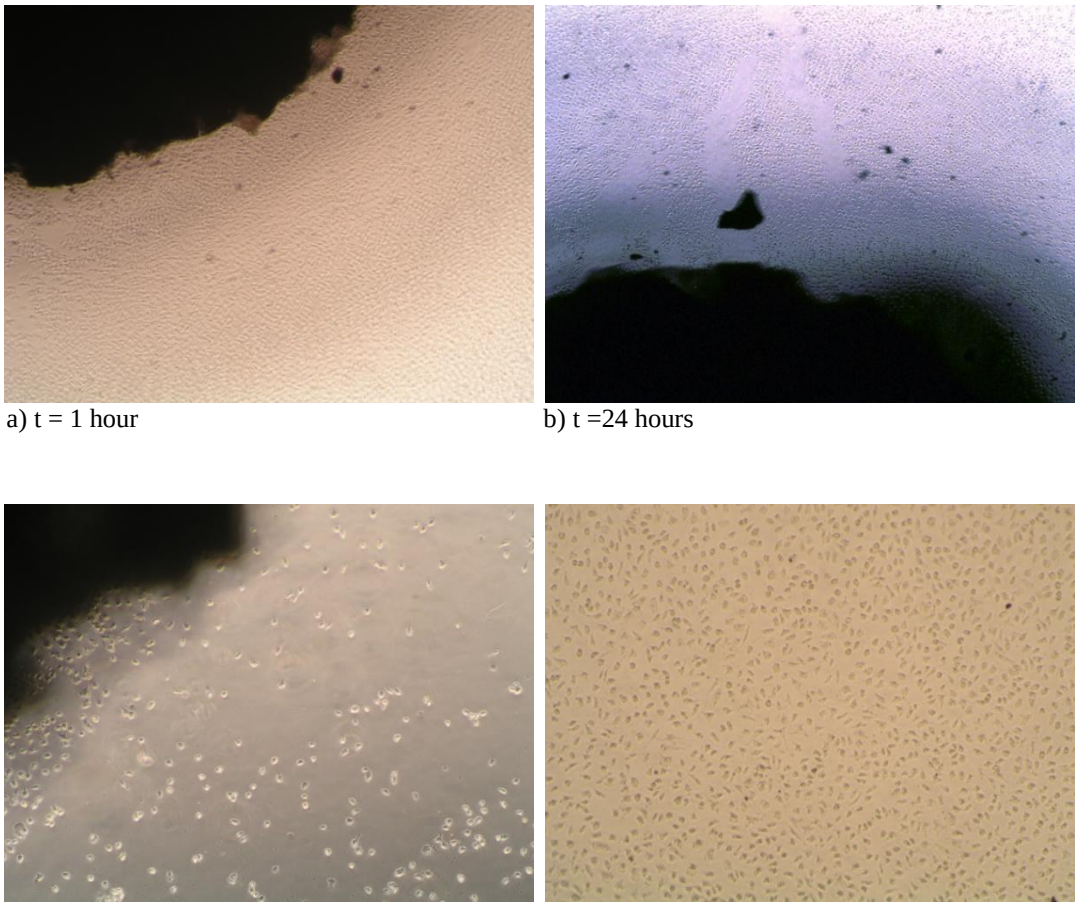

a) t = 1 hour

b) t =24 hours

c) t = 48 hours

d) t = 48 hours, edge of well

Figure A - 7 – Microscope images of L929 cells response to SCBB infiltrated with chitosan / $CaHPO_4$ at t = 1, t =24 and t = 48 hours.

Table A - 8 - Cytotoxic response to BioSCBB-2

Time (hours)	t = 1	t = 24	t = 48
Cytotoxic Response	0-1	0-1	3

BioSCBB-4 (SCBB infiltrated with chitosan / TEOS)

BioSCBB-4 samples again showed similar results to BioSCBB-2 samples, except for the t = 48 hours images which showed a slightly less intense cytotoxic reaction to the presence of the material. As with the previous samples, at t = 48 hours there was a decrease in density of L929 cells indicating cell degradation, however as Figure A - 8d below shows, there were also a number of cells displaying healthy morphology with an elongated flattened structure and fibril extensions at 48 hours. This was the same phenomenon that occurred in the BioSCBB-0 (non-infiltrated SCBB) samples at t = 48 hours.

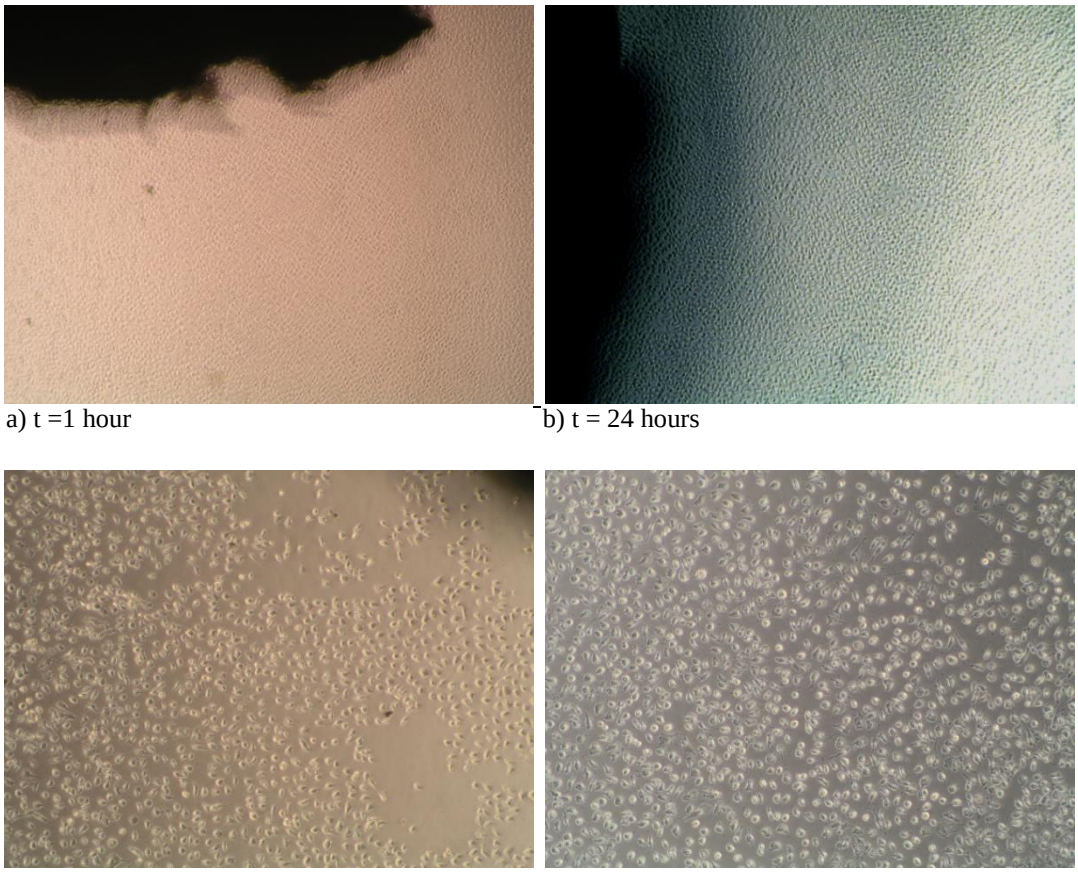

a) t =1 hour b) t = 24 hours

c) t =48 hours d) t = 48 hours, edge of well

Figure A - 8 - Microscope images of L929 cells response to SCBB infiltrated with chitosan / TEOS at t = 1 hour, t =24 and t = 48 hours.

Table A - 9 - Cytotoxic response to BioSCBB-4

Time (hours)	t = 1	t = 24	t = 48
Cytotoxic Response	0-1	0-1	3

BioSCBB-3 (SCBB infiltrated with chitosan / $CaHPO_4$ / genipin)

BioSCBB-3 samples displayed a comparable cytotoxic response as that shown by BioSCBB-4 infiltrated samples, the results of which are presented above. At t = 1 hour and t = 24 hours cell degradation was not apparent although partially balled cells indicated a degree of stress, again possibly due to the presence of a cytotoxin or due to the high level of confluence. By t = 48 hours a pronounced reduction in confluence was apparent indicating the degradation of cells, in addition to more obvious balling immediately adjacent to the sample and at the edge of the culture well.

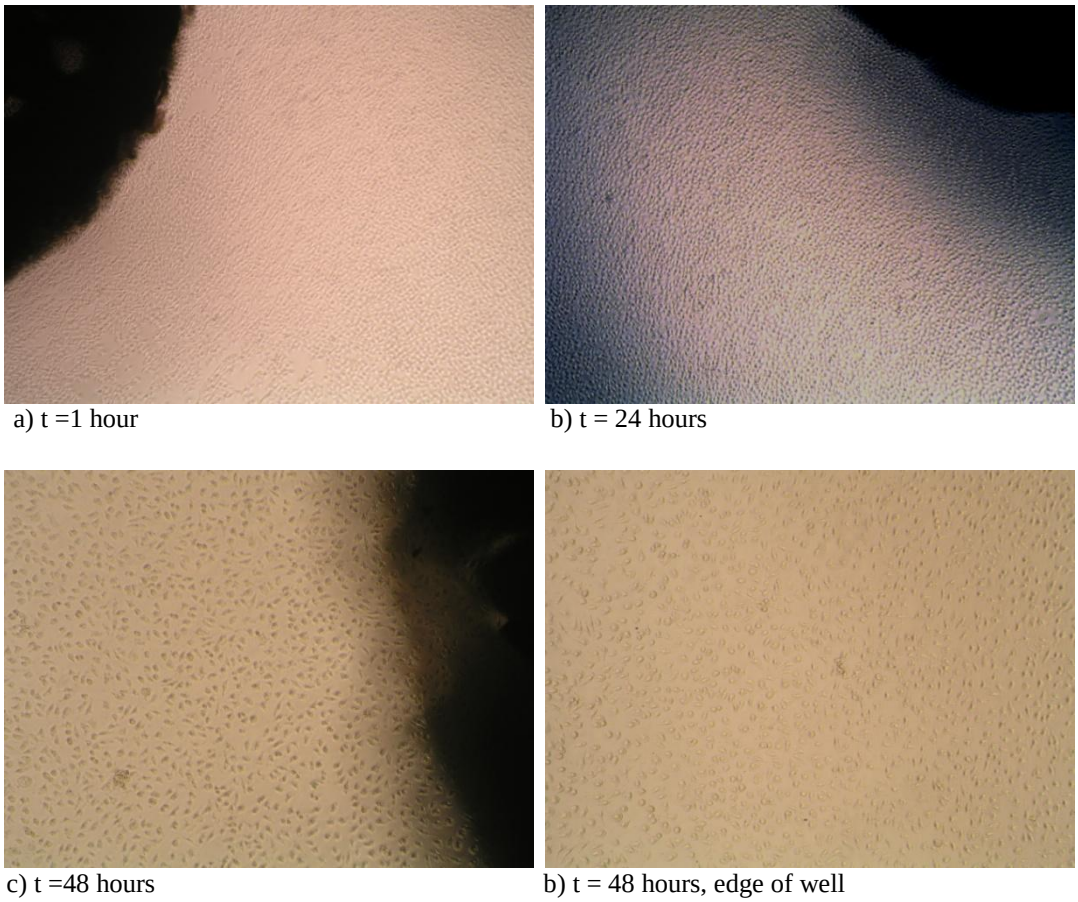

a) t =1 hour

b) t = 24 hours

c) t =48 hours

b) t = 48 hours, edge of well

Figure A - 9 - Microscope images of L929 cells response to SCBB infiltrated with chitosan / $CaHPO_4$ / genipin at t = 1 hour, t =24 and t = 48 hours.

Table A - 10 - Cytotoxic response to BioSCBB-3

Time (hours)	t = 1	t = 24	t = 48
Cytotoxic Response	0-1	0-1	3

BioSCBB-5 (SCBB infiltrated with chitosan / $CaHPO_4$ / genipin / urea / urease / ascorbic acid)

No recession of L929 cells from the sample was seen to occur at any time point as shown below in Figure A - 10.

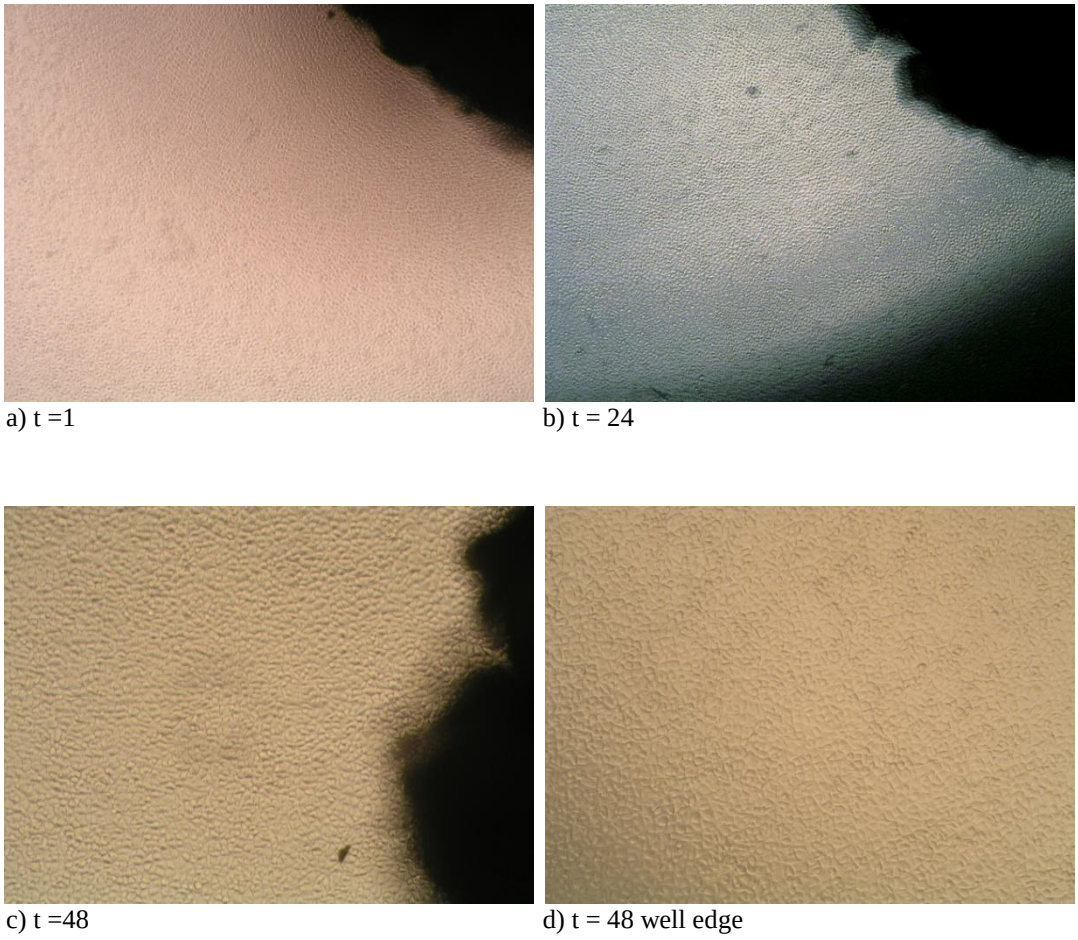

a) t =1 b) t = 24

c) t =48 d) t = 48 well edge

Figure A - 10 - Microscope images of L929 cells response to SCBB infiltrated with chitosan / $CaHPO_4$ / genipin / urea / urease at t = 1, t =24 and t = 48 hours.

Table A - 11 - Cytotoxic response to BioSCBB-5

Time (hours)	t = 1	t = 24	t = 48
Cytotoxic Response	0-1	0-1	0-1

Appendix L – Estimation of NH_3 / NH_4^+ in cell culture well

Figure 5-28 (p. 134) shows the average level of ammoniacal-N in two samples remaining after having undergone successive 1-hour washes in distilled water, with the water being replaced between washes. After 3 x 1 hour washes (cf. 3 x 2 hours washes for samples in this study), the average number of moles of ammoniacal-N in two samples with an average weight of 1.0 g was:

Mol ammoniacal-N / 1 g sample = 1.57×10^{-4} mol.

If this level of ammoniacal-N is comparable to the level in the 0.03 g average samples used in this biocompatibility study, then the concentration of NH_3 / NH_4^+ in the 0.4 mL testing wells could approach:

1.57×10^{-4} mol (/ 1 g sample) x 0.03 g = 4.71×10^{-6} mol

$[NH_3/NH_4^+]$ in 0.4 mL media = 4.71×10^{-6} mol / 0.0004 L

= 0.0118 mol L^{-1}

= <u>11,800 µmol L^{-1}</u>

Appendix M - Attempt to infiltrate chitosan into SCBB by supercritical carbon dioxide and water

Throughout this research a constant search was made towards an ideal way of infiltrating a solid material into the SCBB material, with particular attention to achieving infiltration into the microporous structure of the SCBB. Conceptually, the ideal process should be continuous, as the infiltration of a mass of material, with a

subsequent deposition stage would likely block the micropores and render them resistant to further infiltration. This has been demonstrated throughout this research, with the construction of a pressure vessel (section 4.4.2) designed to overcome the problem. However, at the outset of this research other potential solutions not yet discussed were considered; vapour transportation of a solid into the SCBB material and then deposition was an appealing concept, as was an *in situ* polymerisation reaction of monomer units progressively introduced into the SCBB. The direct condensation polymerisation of lactic acid as described by Ajioka *et al.* to form poly(lactic acid) but undertaken *in situ* was considered a possible candidate for such a process [172]. Equally appealing was the idea of a molecular-layering of material, for example, by exposing the SCBB to HPO_4^{2-}, then chitosonium chloride (which would react with the basic anion and deposit), then more HPO_4^{2-}, eventually leading to the construction of a tightly packed layered solid.

With a continuous process in mind, the idea of using supercritical CO_2, or pressurised CO_2 dissolved in water to carry chitosan into the SCBB material was conceived. Otake *et al.* described a process of using pressurised CO_2 in water to dissolve chitosan in a process to produce chitosan coated cationic liposomes. Solubility rates were not high, with 50 mg L^{-1} of chitosan dissolving at 100 bar [173], cf. 10 g L^{-1} easily achieved when chitosan is dissolved in acids such as acetic or hydrochloric. However, if a system capable of producing repeated depositions of chitosan could be developed, this low-level solubility may be acceptable from a practical viewpoint.

Method

This experiment was carried out at the supercritical CO_2 facility at SCION, Rotorua, NZ with the kind permission of Dr. Robert Franich. 0.5 g of low viscosity chitosan (Fluka) was introduced into a supercritical CO_2 pressure vessel of volume 120 cm^3 on top of a magnetic stirrer. A previously weighed sample of SCBB was suspended by a wire cage attached to the CO_2 down pipe and lowered into the pressure vessel, as shown opposite in Figure A - 11. 1 mL of distilled water was introduced into the vessel by pipette, the vessel sealed and then evacuated for 2 minutes to remove air. CO_2 was then pumped into the evacuated vessel and the vessel heated until 150 bar

and 40°C was achieved. The magnetic stirrer was activated, while this temperature and pressure was maintained for 1 hour. Afterwards, the vessel was cooled with ice water to approximately 20°C; this is below the critical temperature of CO_2 and was done to reduce the solubility of chitosan to cause precipitation on and within the SCBB sample. The pressure was then slowly released to atmospheric pressure on the pressure vessel. The SCBB sample was removed and placed in a fume cupboard and exposed to the maximum amount of airflow, in order to promote drying. After an hour, the sample was reintroduced into the supercritical CO_2 apparatus and the process as described above repeated, after which the sample was allowed to dry and then weighed.

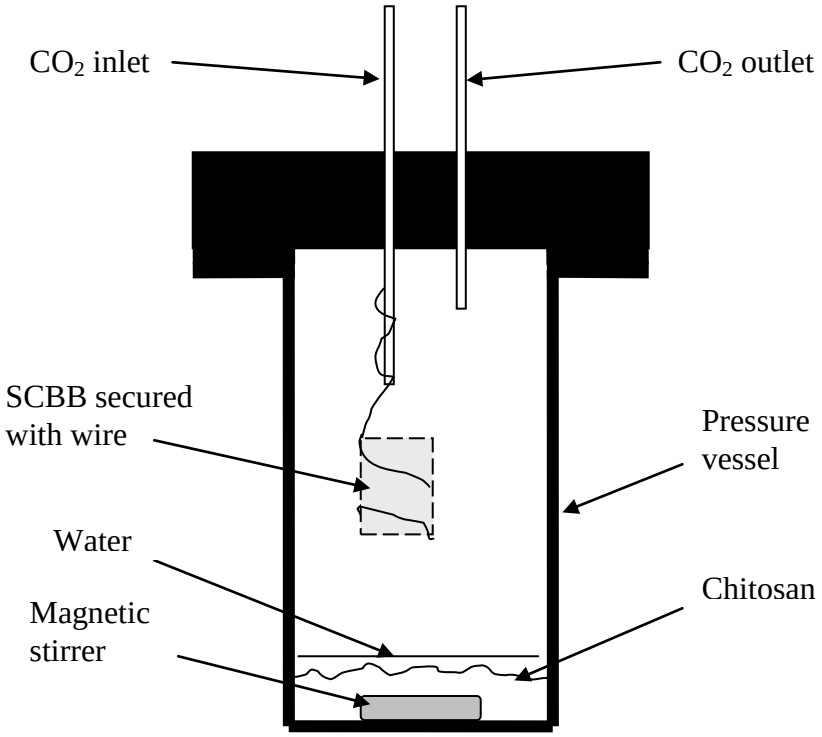

Figure A - 11 - Diagrammatic representation (not to scale) of supercritical CO_2 pressure vessel with SCBB sample suspended from CO_2 feed tube.

Results

When the pressure vessel was opened, it was noted that chitosan powder was present around the opening of the pressure cylinder as seen below in Figure A - 12. This was confirmation that the chitosan had been dispersed within the supercritical CO_2 water mixture. However, it was not proof that the chitosan had dissolved, as it could have been distributed simply as a particulate suspension by the action of the magnetic stirrer on the fluid.

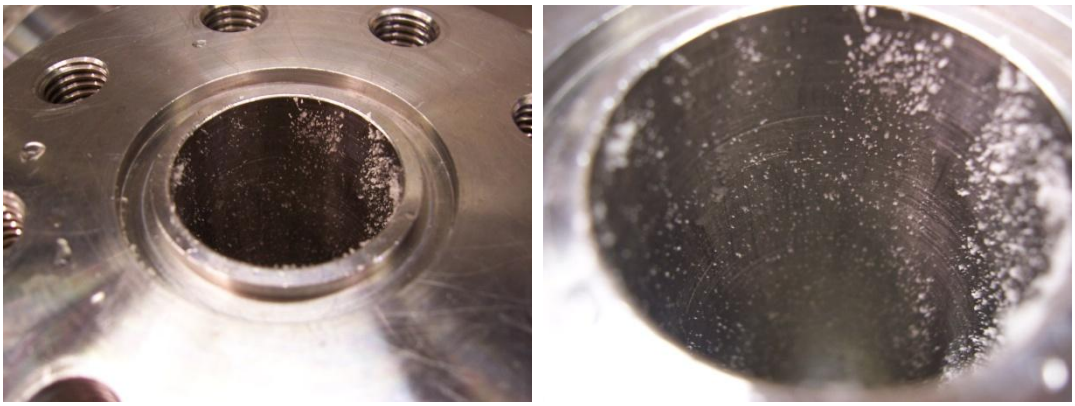

Figure A - 12 – Photographs of the opening of the supercritical CO_2 pressure vessel showing chitosan powder.

Moreover, weights of the SCBB before and after it had been placed in the supercritical CO_2 apparatus did not show an increase that would have indicated the deposition of chitosan. Additionally, the presence of chitosan was not detected in an IR spectrum of the treated SCBB material or in SEM images. Over the short time (1 day) that this experimental method was explored, chitosan was not detected within the SCBB sample. The overall aim was that chitosan would dissolve in the water / $CO_{2(aq)}$ mix in the bottom of the vessel to form a saturated solution, which would result in the transfer of chitosan into an overlying supercritical CO_2 / water level, ultimately transferring chitosan to the sample. Although, relatively low, mutual solubilities exist between water and supercritical CO_2 (and liquid CO_2) [174, 175], there was a theoretical possibility that the experiment could work. However, chitosan transfer from the bottom of the pressure vessel to sample was not seen to occur in this experiment. In a separate experiment chitosan was seen to dissolve in $CO_{2(aq)}$ (generated by a commercial soda drink maker) at atmospheric pressure at the rate of 0.60 g L^{-1}, suggesting that solubility in the water in the bottom of the vessel was not

an issue. Despite the lack of success in this experimental trial, the supercritical fluid method was still regarded as having potential and would have been explored further outside of limitations in apparatus availability. It could be reserved for future investigations on the SCBB / infiltrated chitosan system.